A SCANNING TUNNELLING MICROSCOPY INVESTIGATION OF THE INTERACTION OF SULPHUR WITH SEMICONDUCTOR SURFACES

A thesis for the degree of Ph.D.

Presented to Dublin City University
by

Philip Moriarty, B.Sc.
School of Physical Sciences
Dublin City University

Research Supervisor
Dr. Greg Hughes

December 1993

ACKNOWLEDGEMENTS

Firstly, my sincere thanks to Dr. Greg Hughes for his continued guidance, support, encouragement, and helpful and interesting discussions over the last three years. I must also express my gratitude to Dr. Ludger Koenders, PTB, Braunschweig for similar guidance, discussion, patience, and the use of (and help with) the Omicron STM for extended periods of time! A big debt of gratitude also to the rest in Labor. 5.13, especially; H. Wolff, for all his expert technical assistance, S. Schmidt for her etching of the tungsten tips used for all the STM work presented here, and R.Köning for help with the STM system. Finally, in PTB, I must thank Dr. Gunter Wilkening who initiated the STM project, Uwe Braasch for both his help with regard to accomodation, expenses etc. and his hospitality, and Dieter and Brigitte Schwohnke (and family!) who made me feel very much at home in Germany. The German-Irish Scientific Collaboration (specifically, EOLAS and GKSS) supplied funding for my visits to PTB which is gratefully acknowledged. Dr. David Woolf, University of Wales, Cardiff kindly provided the As capped GaAs(100),(111)B and Si(111) samples.

My thanks to everybody in the NML, EOLAS who've helped make my time there interesting. For all his expert help over the last three years in producing high quality prints of STM images, and particularly for all his effort involving this thesis, I must sincerely thank Al Devine. All the Physics (and Biology) postgrads and undergrads who made my time in DCU enjoyable, Dr. Liam Roberts for all his help - and conversation through the small hours - at Daresbury SRS, Dr. Tony Cafolla for the curve fitting software used to fit the spectra in Chapter 5 and his advice on photoemission, STM and surface science in general. Also at Daresbury, I must gratefully acknowledge the assistance of both Dr. Paul Bailey and Dave Teehan.

Many thanks to: my family and relatives; Dr. Aidan Fitzsimons, Dr. Susan O' Donovan, Steve, Pete, Mick, Sean and Kerry for reminding me that there is a life outside of UHV and STM; Marie's family for all their help; and finally, and most importantly, Marie for all her support, and tolerance of me rarely being at home over the last three years!!

DECLARATION

I hereby certify that this material, which I now submit for assessment on the programme of study leading to the award of Ph.D. is entirely my own work and has not been taken from the work of others save and to the extent that such work has been cited and acknowledged within the text of my work.

Signed: P. Moriarty Date: 28-01-94

Candidate

ABSTRACT

UHV and ambient Scanning Tunnelling Microscopy (STM) have been used to investigate the interaction of sulphur with Si and GaAs (100) and (111) surfaces. The adsorption of group VI elements on GaAs and other III-V semiconductor surfaces is well known to passivate the surface, that is, reduce the number of mid-gap surface states. We find that *in situ* room temperature adsorption of sulphur on both Si(100)-(2x1) and Si(111)-(7x7) surfaces, using an electrochemical cell, does not produce an ideal bulk terminated (1x1) phase. Thermal desorption of the S overlayer from the Si(100) surface at 325°C leads to the creation of a c(4x4) reconstruction coexisting with the (2x1) reconstruction of the clean surface. High resolution filled- and empty-state images have led to the proposal of a missing dimer defect model for this reconstruction. Following sulfur desorption, at 375°C, from the Si(111) surface, monolayer deep holes in the (7x7) terraces are clearly visible. Near the edges of these holes, surface atoms are found in either a disordered phase, or forming small areas of other metastable reconstructions. A coalescence of surface vacancies, following defect creation due to sulfur desorption leads to the monolayer etching mechanism.

Use of As capped GaAs samples made a characterisation of the clean surface, before sulfur deposition, possible. Room temperature adsorption of sulphur on both GaAs(100) and GaAs(111)B surfaces leads to the appearance of a (1x1) LEED pattern.We find no evidence from STM imaging of a well ordered surface corresponding to this (1x1) phase. Instead, the (1x1) LEED pattern arises through an amorphous S overlayer saturating dangling bonds. Annealing of the S covered GaAs(100) surfaces to temperatures above 350°C promotes the formation of a (2x1) reconstruction. STM data, coupled with Auger electron and synchrotron radiation photoelectron core-level spectroscopy studies, suggest that the (2x1) surface most likely consists of both As and S dimers with sulfur also diffusing into the bulk GaAs crystal. For the GaAs(111)B surface, after annealing, a similar situation involving both As and S termination, occurs. Fermi level movement due to sulfur adsorption and subsequent annealing on both (100) and (111)B surfaces is discussed.

Ambient STM and tunnelling spectroscopy measurements on $P_2S_5/(NH_4)_2S_x$ treated GaAs(100) samples indicate that, with regard to surface homogeneity, they are topographically, chemically and electrically much superior to etched, untreated samples. The subsequent oxidation of these surfaces has been investigated using the real time 3-dimensional imaging capabilities of the STM. Tunnelling spectroscopy results show a considerable reduction in band bending for the passivated surface, with evidence to suggest that the Fermi level is unpinned.

Dedicated to Marie

CHAPTER I: A GENERAL INTRODUCTION TO SCANNING TUNNELLING MICROSCOPY

Some fundamental Scanning Tunnelling Microscopy concepts and theories are detailed within the following chapter leading to a discussion of the application of the technique to the study of semiconductor surfaces. The related tunnelling spectroscopy method is also briefly described.

1.1 The STM Experiment

Scanning Tunnelling Microscopy (STM)[1] is based on the observation that electrons, because of their wave-like nature, can tunnel through the potential barrier established when two surfaces (biased appropriately) are brought to within a few atomic diameters (5-20 Å) of each other. In the STM context, a very sharp metal tip - tungsten, gold or a platinum-iridium alloy are most commonly used - is positioned above the sample surface of interest so that a vacuum gap or barrier of comparable width to that noted above is formed. At this distance the wave functions of the sample and tip which are decaying exponentially in the vacuum barrier region overlap. When a small bias voltage (typically 10mV - 4 V) is applied, electrons quantum-mechanically tunnel across the gap with a probability that increases exponentially as the tip approaches the surface. The solution of Schrödinger's equation inside a rectangular barrier in one dimension (i. e. the planar tunnelling situation) is of the form :

$$\psi = A \exp(\pm \kappa z) \qquad (1.1)$$

Here κ represents the exponential decay of the wavefunctions into the vacuum and is normally termed the *inverse decay length*.

$$\kappa = (h/2\pi)^{-1} (2m(\phi - E))^{1/2} \qquad (1.2)$$

Where ϕ is the *effective barrier height* (or effective work function - simply the average of the tip and sample surface work functions) as shown in the energy level diagram of Figure 1.1. (The tip is assumed to have a constant density of states). E is the energy measured with respect to the Fermi level. If the sample and tip are in thermodynamic equilibrium, as illustrated in Fig 1.1 (a), then their Fermi levels must be equal. Electrons attempting to pass from sample to tip (or vice versa) encounter a barrier that is approximately trapezoidal in shape. When a bias voltage V is applied to the sample, its energy levels will be shifted upward or downward (dependent on bias polarity) by an amount eV. At positive bias, tunnelling occurs from occupied electronic states of the tip into unoccupied states of the sample (Fig 1.1(b)). Conversely, at negative bias (Fig

1.1(c)), electrons tunnel from occupied states of the sample into unoccupied states of the tip.

The tunnelling current decays exponentially with barrier width d according to:

$$I \propto \exp(-2\kappa d) \qquad (1.3)$$

It is found that , typically, 2κ is approximately 2Å^{-1}. Thus, the tunnelling current drops by nearly an order of magnitude for every 1 angstrom of vacuum between the tip and sample. Tunnelling, therefore, can only be observed in practice for very small separations. Furthermore, even moderate stability of the tunnelling current requires the isolation of the tunnelling device from sub-angstrom magnitude vibrations.

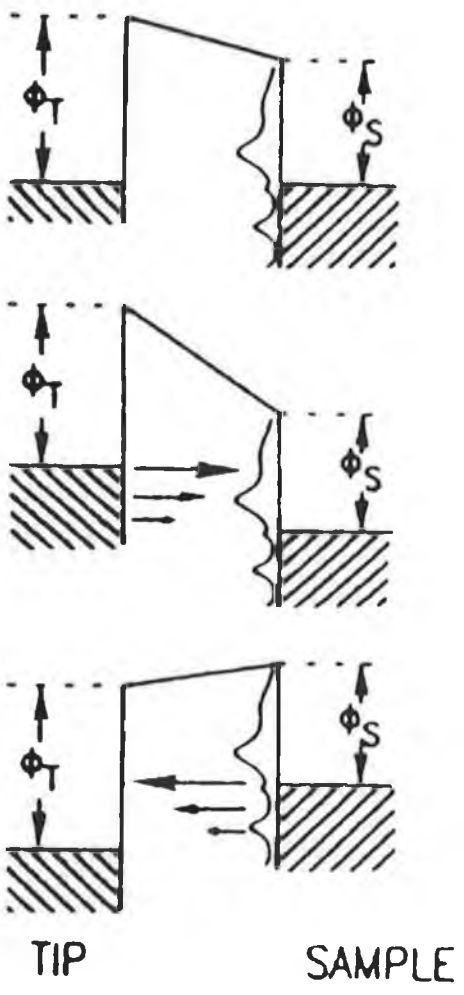

Fig 1.1 *Schematic energy level diagram of tip-sample system (a) at thermodynamic equilibrium, (b) positive sample bias and (c) negative sample bias.* ϕ_S *,*ϕ_T *are the sample and tip work functions, respectively.*

It was not until the 1970's that the first reports of the direct observation of vacuum tunnelling came[2], with Binnig *et al.*[1] of the IBM research laboratory in Zürich, Switzerland ultimately applying the tunnelling phenomenon to achieve atomically resolved images using the STM in 1982. (Binnig and Rohrer subsequently received the Nobel prize in 1986 for their efforts). Fig 1.2 is a schematic diagram of the principle of operation of the IBM group's STM. Piezoelectric drives, Px and Py, scan the metal tip over the sample surface with the control unit (which, in all STM's, is either an analogue or digital feedback loop) applying the necessary voltage to the Pz piezodrive to maintain a constant current by adjusting the tip height. The "electronic topography" of the surface is then inferred directly from the voltage applied to the z-direction piezodrive. Alternatively it is possible to use a much looser feedback for the tip so that its height remains approximately constant over the surface and tunnelling current rather than tip height is detected by the control unit. The former mode of operation is referred to as *constant current* with the latter as *constant height*. A resolution of better than two angstroms in the lateral plane is possible with 0.1Å in the vertical plane achievable.

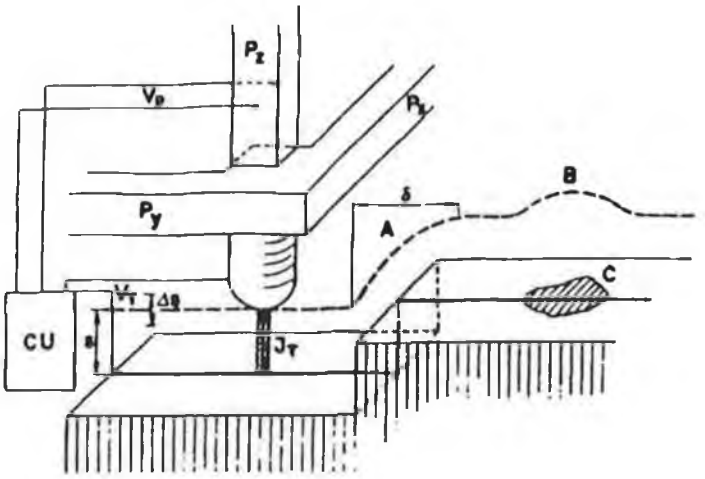

Figure 1.2 *Schematic diagram of the principle of operation of the STM.(From Ref .1).*

1.2 STM as a Surface Probe

Until recently, surface geometry and surface electronic structure have been investigated using different experimental methods. Those techniques used to determine the geometrical nature of a surface (that is the symmetry of the unit cell or the positions of individual surface atoms) do not provide information on the energy distribution of the electron states. Electron diffraction, atom and ion scattering all fall within this category.

Photoelectron spectroscopy (both X-Ray and Ultra-Violet), inverse photoelectron spectroscopy and electron energy loss spectroscopy, for instance, are sensitive electronic structure probes but achieve no direct measure of the geometry of the surface. The development of STM has bridged the gap between such geometric and electronic structure analysis techniques.

It is important to note the benefit of using STM to examine surface structure as opposed to diffraction methods such as Low Energy Electron Diffraction (LEED) or Reflection High Energy Electron Diffraction (RHEED). Such methods yield an inverse space pattern dependent on the long range periodicity of the surface. STM, by virtue of it being a real space technique, does not require the presence of long range order and can thus examine both well ordered and highly disordered surface regions or overlayers. Furthermore, STM is a local, atomistic probe - it is possible to map out surface states with angstrom resolution. Therefore we essentially can have a spectroscopic analysis of a single atom. Compare this to, roughly, the 10^{10} - 10^{11} atomic sites typically encompassed by the spot size used in photoemission or LEED studies. Unlike photoemission, however, it is - at present - impossible to determine the chemical nature of a surface species using STM alone. Indeed, an STM image contains a strong convolution of topographic, chemical and electronic features which must be correctly interpreted. The interpretation of the STM image is the subject of the following sections.

1.3 Theoretical aspects

It has been stated in section 1.1 that the tunnelling current is exponentially related to the product of the barrier width and the inverse decay length (Eqn 1.3). This equation holds only for voltages $V << \phi$. At higher bias voltages the effective barrier height becomes a function of the applied voltage. Also, in the case of non-free electrons and non-planar barriers (i. e. when a full 3-dimensional analysis of the problem is adopted) the total current can no longer be expressed in such a simple form.

1.3.1 Tunnelling Hamiltonian Treatment

Most three dimensional treatments of the tunnelling current are based on Bardeen's tunnelling Hamiltonian formalism[3]. Here the tip-surface interaction is assumed as being weak, with the unperturbed wavefunctions of the sample (Ψ_s) and the tip (Ψ_t) used in the tunnelling current calculation. Using first order perturbation theory, the tunnelling current is given by:

$$I = 2\pi(h/2\pi)^{-1} e^2 V \sum | M_{t,s} |^2 \delta(E_t - E_F)\delta(E_s - E_F) \qquad (1.4)$$

Where the summation is over all tip and sample states, V is the applied voltage, $M_{t,s}$ is the tunnelling matrix element between states Ψ_s and Ψ_t and E_s, E_t are the energies of Ψ_s

and Ψ_t. It is the evaluation of the tunnelling matrix that poses the greatest problem. Bardeen[3] showed that the tunnelling matrix may be written in the form:

$$M_{t,s} = (h/2\pi)^2 (2m)^{-1} \int dS \cdot (\Psi_s^* \nabla \Psi_t - \Psi_t \nabla \Psi_s^*) \qquad (1.5)$$

Therefore, to accurately calculate the tunnelling current it is first necessary to know explicitly the wave functions of both surface and tip. However, the actual atomic structure of the tip is never well defined. Tersoff and Hamann[4] have described the tip by assuming the simplest possible model - as this leads to a particularly simple and useful interpretation of the tunnelling image it is worth describing it in a little detail.

1.3.2. The s-wave Model

To derive the simplest model for the tip Tersoff and Hamann[4] considered what would be the ideal STM. There are two important considerations with regard to atomic resolution imaging:

i) The maximum possible resolution and thus, the smallest possible tip is desirable.

ii) The properties of the surface and not the more complex surface-tip interaction are required to be measured.

Therefore, the ideal STM tip would consist of a point source of current and we can write:

$$I \propto \sum |\Psi_s(r_t)|^2 \delta(E_s - E_F) \equiv \rho(r_t, E_F) \qquad (1.6)$$

That is, the ideal STM simply measures the local density of states at the Fermi level at the position of the tip. In their paper Tersoff and Hamann[4] also show that equation 1.6 above remains valid regardless of tip size, as long as the tunnelling matrix may be approximated by that of an s-wave tip wave function. The tip position r_t must then be interpreted as the centre of the tip, that is, the origin of the s-wave. That the STM image does indeed correspond to a map of $\rho(r_t, E_F)$ for a realistic model of a one atom tip has been confirmed by Lang[5] using first principles calculations.

1.4 Tip Effects

The most important part of the STM apparatus is the tip which probes the structure of the sample surface. However, in general, the tip geometry and electronic structure are unknown and, furthermore, may change during the course of an experiment. This can have quite drastic effects on both STM imaging and tunnelling spectroscopy measurements (discussed in Section 1.6).

As the STM measures a "convolution" of sample and tip states the lateral resolution of the image will be dependent on both the sharpness of the tip and its charge densities. When atomically resolved images are possible, tunnelling must involve a single or , at most, a couple of tip atoms. Metallic clusters (such as Au, W or Pt-Ir) will most likely have s-wave character extending out into the vacuum. Adsorption of a foreign atom onto the tip can significantly modify this charge density behaviour (Fig.1.3), yielding distorted images showing the presence of tip-, and not sample-, related features. Tromp *et al.* [6] have witnessed a degradation in resolution for tunnelling into filled states of the Ag/Si(111) surface but not for the empty states. This effect was attributed to a rearrangement of tip atoms.

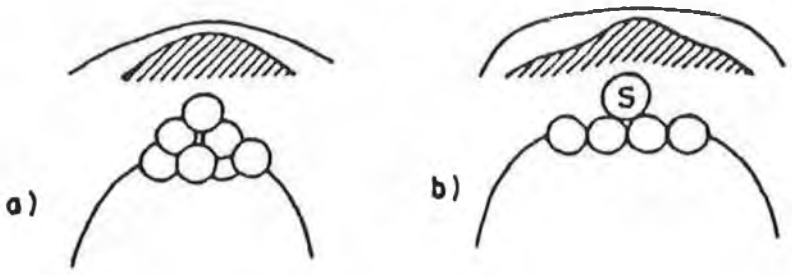

Fig.1.3 *Adsorption of a foreign atom onto the tip. The contours of the filled and empty charge densities are represented by the shaded area and line, respectively (From ref. 7)*

The presence of clusters of sample atoms on the end of the tip which may be present after "crashing" can produce a number of effects as detailed by Demuth *et al.* [7] For example, silicon atoms adsorbed on the tip may produce an adatom or dimer cluster - Figs 1.4 (a) and (b) respectively. The former case would lead to the creation of a highly localised state and thus ultra-high resolution. The dimer cluster, on the other hand, will lead to both a non-surface dependent asymmetry and, due to a larger spatial difference between filled and empty states of the tip, an offset between filled and empty states of the sample.

When imaging is at the micron or sub-micron, as opposed to the atomic scale, the macroscopic shape of the tip is most important. A tip that is blunt or that has more than one protrusion will lead to tunnelling shifting from one position to another and will produce a total image that is a collection of different surface region images. The tip cone angle plays a vital role in the apparent slope of vertical walls. As Griffith *et al.* [8] have recently discussed, knowledge of the cone angle is not enough to determine the true wall shape as the image is not a linear convolution and thus the effect of tip shape cannot be

deconvolved from the image. Tip shape - surface contour mixing is a non-linear process at either the micron or angstrom level.

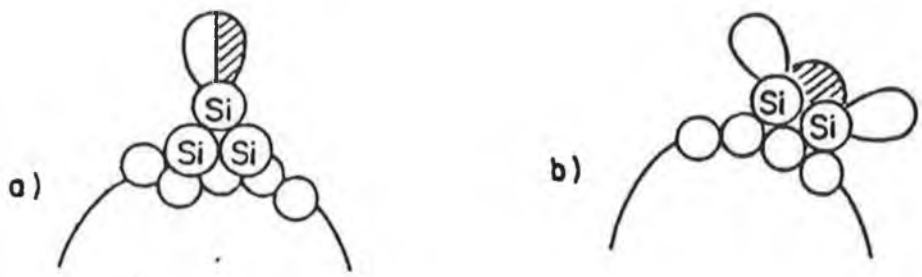

Fig 1.4 *Adsorbed adatom (a), and dimer (b) tip clusters. (From ref. 7)*

1.5 Application of STM to Semiconductor Surfaces

The atoms in the bulk of a periodic crystalline solid are arranged in a well ordered structure so that the net force on each is zero. Consequently, at a surface of such a solid interatomic forces in the uppermost atomic layer will be significantly modified due to the absence of neighbouring atoms on one side. This leads to a condition of equilibrium at the surface which will differ from that of the bulk. In tetrahedrally bonded semiconductors (such as Si, GaAs, InP etc.), the high directionality of the chemical bond leads to a strong distortion of atomic positions at the surface when these bonds are broken. There are two ways in which the atomic configuration at the surface of a semiconductor may vary from that of the bulk.

1.5.1 Relaxation and Reconstruction

Relaxation of the surface is said to occur when the periodicity parallel to the surface is the same as the bulk periodicity but the interlayer separation within the first few atomic layers has changed. A well understood example of surface relaxation is the clean GaAs(110) surface. GaAs cleaves along the 110 plane exposing a non-polar (i. e. equal numbers of gallium and arsenic atoms) face. Compared with their bulk positions the As atoms of the topmost layer are raised, whereas the Ga atoms are lowered . This condition is also referred to as buckling and is illustrated schematically for III-V semiconductors in Fig 1.5.

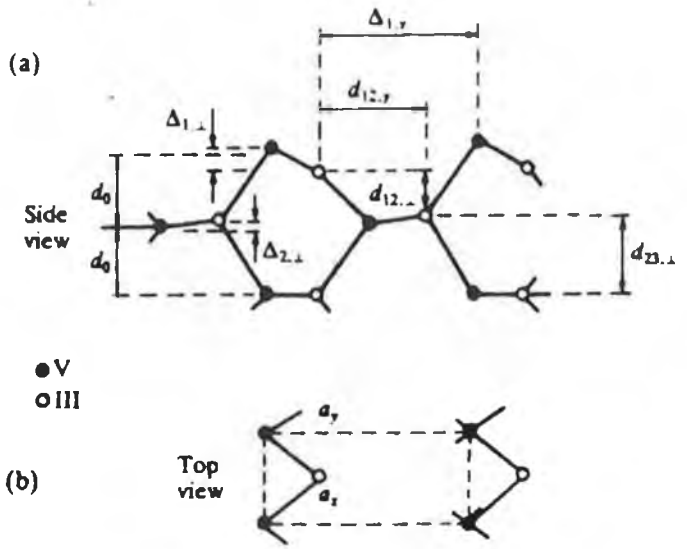

Fig 1.5 *Relaxation of a III-V semiconductor (110) surface. (a) side view, (b) top view with unit cell outlined (From "Metal-Semiconductor Contacts", E. H. Rhoderick and R. H. Williams, Oxford Science Publications, 1988)*

It should be emphasised that not only a structural but also an electronic modification occurs. The creation of the (110) surface leaves two half-filled or "dangling" bonds per unit cell directed out of the surface. These dangling bonds introduce electronic states within the semiconductor band gap. Relaxation causes these states to be "shifted" out of the band gap. The surface atoms with dangling bonds directly after cleavage form a half filled band of surface states. Relaxation causes charge transfer from one bond to the other (one atom to the other) and thus splits the surface state band into a filled and empty band which are removed from the gap. This charge transfer has interesting implications for STM studies of the GaAs(110) surface. Surface relaxation, as described, results in filled states localised on As sites and empty states localised on Ga sites. Therefore, tunnelling out of filled states yields an image of As atoms and tunnelling into empty states will produce an image representative of the Ga atomic positions[9].

A more dramatic change of the atomic configuration at a semiconductor surface is termed *reconstruction*. In this case the symmetry in the surface plane differs from that in the bulk. The surface unit mesh will therefore have dimensions different from a projected bulk unit cell. Again, this process is due to the unsatisfied nature of the semiconductor surface bonds and the resulting large free energy present. In order to diminish the dangling bond density the surface atoms rearrange themselves or reconstruct. It is normal to describe the surface unit cell in terms of bulk lattice vectors in a 2D Miller indices terminology. That is, a (2x2) surface reconstruction refers to a surface unit cell with lattice vectors twice the magnitude of those of the bulk terminated plane. Reconstruction,

like relaxation, is not strictly limited to the first atomic surface layer but can extend several layers into the crystal. The first semiconductor surface imaged with the STM was the Si(111)-(7x7) reconstruction. This particular reconstruction is described in depth in Chapter 4, suffice to say that STM real space images of the (7x7) surface structure were instrumental in confirming the currently well accepted model of Takayanagi *et al.* [10] after considerable debate spanning a number of decades.

1.5.2 Steps and Overlayers

On a real surface defects are always present. The most important and common one-dimensional line defect is the step which separates two terraces from each other. The first STM images of this fundamental surface defect were illustrated by Becker *et al* .[11] on the Si(111)-7x7 surface where they noted a strong correlation between the position of the step edge and the 7x7 unit cell orientation at the edge. So-called vicinal surfaces, where there is a miscut from the nominal surface direction (for example, 2° from the (001) direction for a Si(001) surface) will display a distance between steps dependent on the miscut angle. Atomic resolved STM has improved our knowledge of how step behaviour is dependent on annealing, contamination, growth conditions etc. STM topographs have been recently produced by O'Mahony *et al.* [12] of vicinal Si(111) surfaces (miscut 4° towards (112)) after thermal annealing followed by rapid quenching to room temperature. These topographs illustrated a temperature dependent transition from wide irregular terraces separated by clusters of double steps to evenly spaced terraces separated by single monatomic steps. That study was preceeded by an investigation of structural disorder on vicinal surfaces by Swartzentruber *et al.* [13] where disorder along step edges at room temperature was attributed to the cooling rate.

As has been mentioned previously, STM is an ideal tool to study not only ordered "perfect" surfaces but also aperiodic or localized surface structures. One important consideration is that STM cannot be expected to give atomic resolution on rough surfaces. Therefore, extreme care must be taken during sample preparation to provide atomically flat sample surfaces if atomic resolution imaging is required. During the course of this work it was found that surfaces yielding a clear Low Energy Electron Diffraction (LEED) pattern possibly signifying a well ordered surface reconstruction produced STM images where only an amorphous overlayer was visible. This can be accounted for by the fact that STM is particularly sensitive to the very first atomic surface layer whereas LEED probes a number of surface layers. An amorphous layer such as that observed in the STM images would lead to only an increase in the diffuse background of the LEED pattern. So, in some senses, STM is at its best when looking at surfaces with well ordered coverages of a monolayer (ML) or less. As a result, the vast majority of adsorbate-on-semiconductor systems studied to date have dealt with different ordered reconstructions.

The STM images of the Al/Ga/In/Sn - Si(111) ($\sqrt{3}$ x $\sqrt{3}$) R30° (where the R refers to the angle of rotation of the overlayer lattice with respect to the bulk) surfaces were consistent with existing models that had both experimental and theoretical support[14,15]. The observation of phase boundaries between the clean and metal-covered surface allowed the determination of the metal adatom bonding sites. In the early stages of overlayer growth (i. e. at submonolayer coverages) STM is a powerful technique to study the formation of clusters[16], nucleation[17], and the bonding of isolated atoms[18]. All of these phenomena are inherently spatially localized and therefore mostly impossible to study by other surface science probes. A considerable amount of work to date has been published on the reaction of metals with both the Si(111) and Si(100) surfaces.

Study of the interaction of metals with the GaAs surface has concentrated on the (110) face. Martensson and Feenstra[19] have shown that Sb atoms on the GaAs(110) surface occupy positions close to those expected by an extension of the bulk lattice. Deposition of Sb at room temperature produced large flat terraces exhibiting a (1x1) reconstruction. Antimony, when adsorbed on the GaAs surface, is one of a number of species known as a surface passivant. Sulphur has been shown to also act as a passivating overlayer on the GaAs surface and a discussion of this passivation effect is given in the following chapter. Gold on GaAs(110), at a few tenths of a monolayer coverage, was investigated by Feenstra[20]. It was found that the gold atoms are located equidistant between four As atoms and about 1.4 Å away from surface Ga atoms which indicated the presence of a Au-Ga bond. Finally, the Fe-GaAs(110) system when studied by STM[21], illustrated that iron has a tendency to form 3D clusters which if greater than about 35 atoms in size begin to exhibit metallic behaviour.

1.6 Tunnelling Spectroscopy

Spectroscopic information relies on changing the bias voltage applied to the sample but can be obtained in a number of ways depending on which variables are held constant and which are actually measured. Voltage-dependent STM imaging is the simplest way of obtaining spectroscopic information, by simply acquiring tunnelling images at different bias magnitudes and at either polarity. With a voltage V applied to the sample only states lying between E_F and E_F+eV (or E_F-eV) contribute to the tunnelling current. Changes in the spatial symmetry of STM constant current images as a function of bias can thus provide information about the symmetry of electron states at various energies.

The acquisition of full I(V) tunnelling spectra across a bias range (eg -3V to +3V) can provide more detailed information on the density of electronic surface states. In practice, an I(V) spectrum is obtained after freezing the tip position - by opening the feedback loop at a pre-set stabilisation voltage and tunnelling current- and thus ramping the voltage applied to the sample while monitoring the magnitude of the tunnel current. (A description of the acquisition of I(V) spectra in this manner using the Nanoscope STM may be found in section 3.2). Atomically resolved I(V) measurements were first

performed by Hamers *et al.* [22] by acquiring I(V) curves while simultaneously scanning the tip position. This technique was used to map out the complete electronic structure of the Si(111)-7x7 unit cell and is known as *Current Imaging Tunnelling Spectroscopy (CITS)* . Use of a sample-and-hold circuit gating the feedback control system on and off is the normal method of producing CITS data (and is used by the Omicron UHV STM system, also described in Chapter 3).

This type of local tunnelling spectroscopy was used by Hamers and Köhler[23] to study the electronic properties of atomic sized defects on the Si(001) surface. Their results were directly presented as plots of tunnelling current versus voltage since, as they state, this is often the most straight-forward way of demonstrating the semiconducting or metallic nature of a surface (or surface region). In their spectroscopic plots, presented in Fig.1.6, current at negative sample bias is due to tunnelling from filled sample states - i.e. valence band states (if no filled surface states exist within the band gap). Current at positive bias arises from tunnelling into empty (conduction band) states. A surface state band gap of 0.9 eV is observable in this spectrum. For spectra taken above various defects on the Si(100) surface, however, there are variations in the amount of current flowing from states within the band gap region (Figs.1.6(b) and 1.6(c)). In fact,above a particular type of surface defect Hamers and Köhler found metallic behaviour with the absence of a band gap in the tunnelling spectrum - Fig 1.6(d).

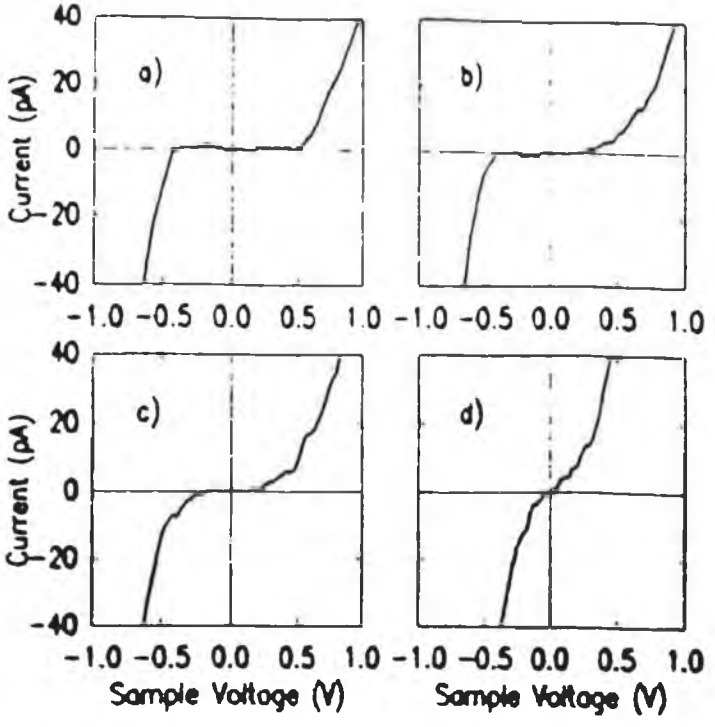

Fig. 1.6 *Local tunnelling spectroscopy on the Si(001) surface. (From Ref. 23)*

The identification of particular surface states at various energies related to different atoms within the Si(111)-7x7 unit cell was carried out by measuring the spatial variation in the surface differential conductivity[24]. This was then compared to the (simultaneously) acquired tunnelling image in order to locate density of states features in the unit cell. However, Feenstra *et al* .[25] have noted that there is a large dependence of such spectra on tip height due to the exponential relationship between tip-sample separation and barrier transmission. A plot of normalized conductance ((dI/dV)/(I/V)) provides a measure of the normalised density of states (i. e. the tip-sample separation no longer significantly affects the spectrum).

Tunnelling spectroscopy has recently been shown to apply to determining the nature of the tunnelling tip. Hockett and Creager[26] have shown that for electrochemically etched tungsten tips exposed to air for extended periods without treatment in hydroflouric (HF) acid, a tunnelling spectrum representative of a semiconductor is found due to the formation of tungsten oxide. HF acid removes the oxide - tungsten metal being inert to attack from this acid - producing a spectrum that is without the presence of a band gap, i. e. is metallic in nature.

References

1. G. Binnig, H. Rohrer, C. H. Gerber and E. Weibel, *Phys. Rev. Lett.* **49** 57 (1982)
2. R. Young, J. Ward and F. Scire, *Phys. Rev. Lett* . **27** 922 (1971)
3. J.Bardeen, *Phys. Rev. Lett.* **6** 57 (1991)
4. J. Tersoff and D. R. Hamann, *Phys. Rev. B* **31** 805 (1985)
5. N. D. Lang, *Phys. Rev. Lett.* **56** 1164 (1986)
6. R.M. Tromp, E. J. Van Loenen, J.E. Demuth and N.D. Lang, *Phys. Rev. B* **37** 9042 (1988)
7. J. E. Demuth, U. Köhler and R. J. Hamers, *Journ. of Microscopy* **152(2)** 299 (1988)
8. J.E. Griffith, D. A. Grigg, M. J. Vasile, P. E. Russell and E. A. Fitzgerald, *Journ. Vac. Sci. Technol. A* **10(4)** 674 (1992)
9. R. M. Feenstra, J. A. Stroscio, J. Tersoff and A. P. Fein, *Phys. Rev. Lett* **58** 1192 (1987)
10. K. Takayanagi, Y. Tanishiro, M. Takahashi and S. Takahashi, *Journ. Vac. Sci. Technol. A* **3** 1502 (1985)
11. R. S. Becker, J. A. Golovchenko, E. G. McRae and B. S. Swartzentruber, *Phys. Rev. Lett.* **55** 2028 (1985)
12. J. D. O' Mahony, J. F. McGilp, F. M. Leibsle, P. Weightman and C. F. J. Flipse, *Semicond. Sci. Technol.* **8** 495 (1993)
13. B. S. Swartzentruber, Y. -W. Mo, M. B. Webb and M. G. Lagally, *Journ. Vac. Sci. Technol. A* **3** 1502 (1989)
14. R. J. Hamers and J. E. Demuth, *Phys. Rev. Lett.* **60** 2527 (1988)
15. J. Nogami, S. Park and C.F. Quate, *Surf. Sci.* **203** L631 (1988)
16 P. N. First, J. A. Stroscio, R. A. Dragoset, D. T. Pierce and R. J. Celotta, *Phys. Rev. Lett.* **63** 1416 (1989)
17. U. K. Köhler, J. E. Demuth and R. J. Hamers, *Phys. Rev. Lett.* **60** 2499 (1988)
18. U. K. Köhler, J.E. Demuth and R. J. Hamers, *Journ. Vac. Sci. Technol.A* **7** 2860 (1989)
19. P. Martensson and R. M. Feenstra, *Phys. Rev. B.* **39** 7744 (1989)
20. R. M. Feenstra, *Journ. Vac. Sci. Technol. B* **7** 925 (1989)
21. J. A. Stroscio, P. N. First, R. A. Dragoset, L. J. Whitman, D. T. Pierce and R. J. Celotta, *Journ. Vac. Sci. Technol. A* **8** 284 (1990)
22. R. J. Hamers, R. J. Tromp, J. E. Demuth, *Phys. Rev. Lett.* **56** 1972 (1986)
23. R. J. Hamers and U. K. Koehler, *Journ. Vac. Sci. Technol. A* **7(4)** 2854 (1989)
24. R. S. Becker, J. A. Golovchenko, D. R. Hamann and B. S. Swartentruber, *Phys. Rev. Lett.* **55** 2032 (1985)
25. R. M. Feenstra, J. A. Stroscio and A. P. Fein,*Surf. Sci.* **181** 295 (1987)
26. L. A. Hockett and S. E. Creager, *Rev. Sci. Instrum.* **64(1)** 263 (1993)

CHAPTER II: SULPHUR PASSIVATION OF III-V SEMICONDUCTOR SURFACES

The importance of preparing and maintaining oxide-free, electrically homogeneous III-V semiconductor surfaces with a low density of surface states ("passivation") is discussed. A variety of ultra high vacuum surface treatments and wet chemical methods using group VI elements, primarily sulphur, have been developed by a number of research groups to this end; a review of such passivation methods is presented.

2. 1 Band Bending and Fermi Level Pinning

The bulk electronic structure of the elemental and III-V compound semiconductors has been extensively studied, both experimentally and theoretically, and is thought to be well understood (see Refs 1 and 2, for example). Termination of the lattice at a surface leads to electronic states which differ from those in the bulk, as described in the preceeding chapter. These *surface states* are determined by the chemical bonding environment and geometric arrangement (reconstruction or relaxation) of the surface atoms and often have energies within the bulk energy band gap. States such as these, existing on a free surface, are termed *intrinsic states*.

Consider, for example, the cleaved Si(111) surface. Each surface atom has an unpaired electron due to termination of the bulk periodicity. This electron is in a localized orbital directed away from the surface which may act as either a donor or acceptor. Such an orbital is referred to as a *dangling bond*. A neutral level, φ_0, may be defined that represents the Fermi level position for an electrically neutral surface. Clean, cleaved Si(111) 2x1 surfaces have a high density of surface states which fall into two bands. Filled surface states lie within the bulk valence band with the empty surface states falling within the bulk band gap. Here φ_0 would lie between these bands of surface states. If the position of the Fermi level does not coincide with that of φ_0, a net charge will exist at the surface causing the production of an electric field in the semiconductor which leads to *band bending*. The energy bands bend upwards for a net negative charge and downward for net positive charge (for an n-type semiconductor). Upward band bending on the Si(111) cleaved surface is illustrated in Fig 2.1. The area over which the bands are bent is termed the *depletion region.*. For downward band-bending the carrier concentration in the region over which the bands are bent is increased and this region is said to be *accumulated.*

To explain the concept of *Fermi level pinning,* it is first necessary to describe the mechanism underlying the formation of a metal-semiconductor contact or a *Schottky Barrier*. We will take the case of a Schottky barrier formed between an n-type semiconductor and a metal with work function (ϕ_m) greater than the work function of the semiconductor (ϕ_s) (Fig.2.2(a))(χ_s is the semiconductor electron affinity). In this situation, electrons will flow from the semiconductor to the metal upon contact.

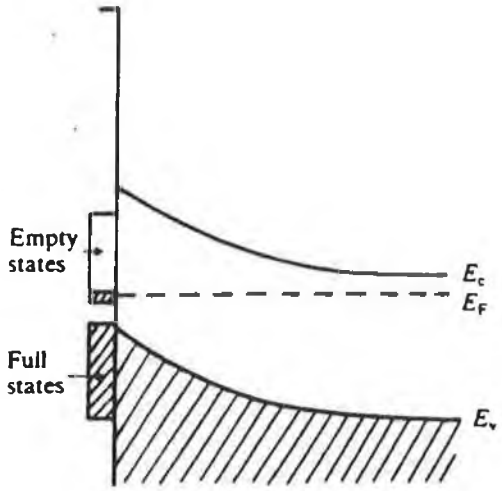

Fig 2. 1 *Band bending on the clean, cleaved Si(111) surface. (From Ref.3)*

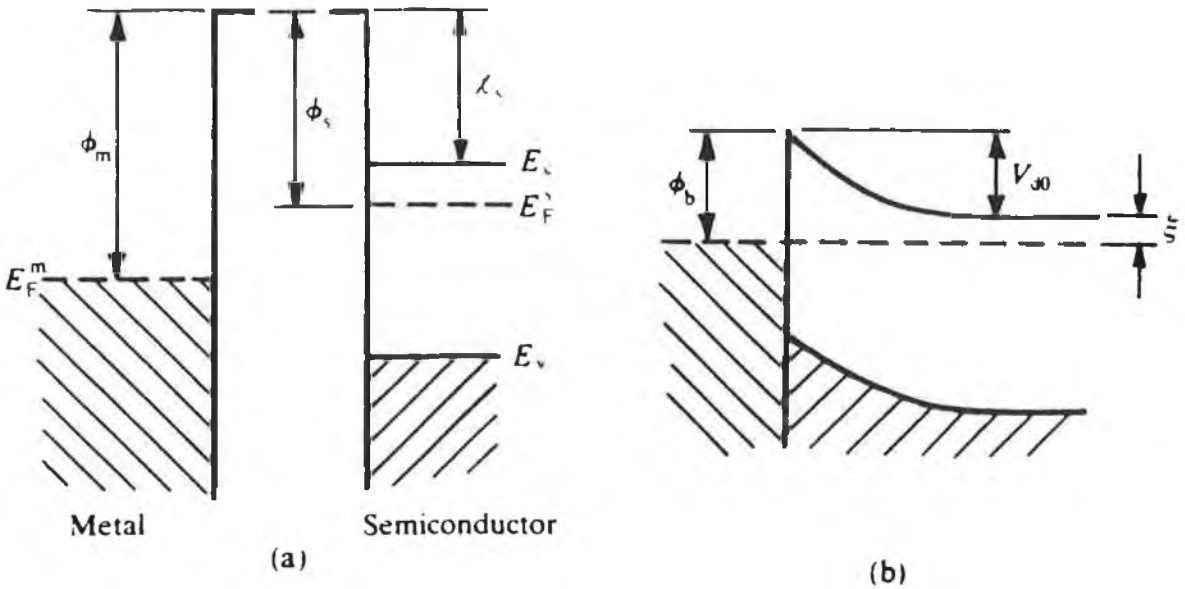

Fig 2. 2 *Formation of a Schottky barrier between an n-type semiconductor and metal of work function greater than the semiconductor electron affinity.* **(a)** *Metal and semiconductor separated* **(b)** *Metal and semiconductor in contact with concommital band-bending in the semiconductor. (From Ref 3)*

This electron flow continues until the metal and semiconductor Fermi levels come to equilibrium. As the semiconductor is n-type, positive charge due to uncompensated donors will reside in the near surface region that has been depleted of electrons, giving rise to band bending (of magnitude V_{d0}) within a region of depletion width W (Fig. 2.2(b)). Thus, in the absence of prior semiconductor surface states (the*flat-band condition*), there will be a linear relationship between the barrier height (ϕ_b) of the metal-semiconductor contact and the metal work function. Bardeen[4] first explained the deviation of experimental barrier height data from the linear relationship predicted by the Schottky model. In the presence of a sufficient density of surface states - which is, in fact, quite low in terms of surface atom density (about a thousandth) - charge transfer on deposition of a metal will only occur to, or from, these surface states. Therefore, the interior of the semiconductor is effectively screened from the metal. In this case, the Fermi level is effectively *pinned* near the surface states. Any rectification properties of the metal-semiconductor junction thus formed are due entirely to surface state induced band-bending and not the creation of a barrrier due to Fermi level equalisation. Subsequent deposition of metals on a pinned semiconductor surface will yield barrier heights that are almost independent of the metal work function.

Only in the case of the cleavage (110) face of III-V semiconductors is a flat band condition for the clean surface observed (provided the surface has a low density of defects). Deposition of thin metal layers leads to band bending with the Fermi level becoming pinned mid-gap. Feenstra[5] has investigated the geometric structure and electronic states of Au atoms on the GaAs(110) surface using STM and STS. On the clean surface, neglecting dopant states (discussed in Chapter 6), a band-gap region of width 1.4 eV is observed. After deposition of 0.1 ML of gold, small clusters of gold atoms are seen in the STM images. STS data taken above these clusters indicated the presence of a state within the upper part of the band-gap and an increase in spectral intensity in the valence band (close to the Valance Band Maximum (VBM)). It should be stressed that at the coverages used, the gold clusters exhibited non-metallic behaviour. After ascertaining that the Au adsorbates bond to Ga atoms (from the STM images), Feenstra[5] developed a model to explain the appearance of the STS spectra. Au donates one electron to the Ga dangling bond, thus forming a filled state. This state was associated with the spectral features in the valence band. The Au-Ga bond can *accommodate* a second electron in an empty state (i. e. an electron from the STM tip may tunnel into this state). This empty level was associated with the state observed in the upper part of the band gap. The consistency of the results just discussed with similar STM studies of the Sb/GaAs(110) system by Feenstra and Mårtensson[6] and the Fe/GaAs(110) system by First *et al.* [7] indicates that a "*Metal Induced Gap States*" [8] model of metal/GaAs(110) surface interaction is most likely. Therefore, the metal-GaAs(110) bonds at the interface must be replaced by some other bond to produce an unpinned surface. With regard to the Sb/GaAs(110) surface at submonolayer Sb

coverage, the metal adsorbates formed ordered (1x1) islands having a band gap in their I(V) spectra. States within this band gap were found to exist at the *edges* of the adsorbate terrace. A complete saturation of bonds at a full 1 ML Sb coverage leads to a Femi level free to move within the band gap.

A number of recent STM and STS studies have shown that on the clean GaAs(100) surface the Fermi level is pinned mid-gap by surface states coincident with the bulk valence and conduction band edges. (UHV Tunnelling spectra on the clean GaAs(100) surface acquired in the course of this work are presented in Chapter 5). Pashley *et al.*[9] have attributed the Fermi level pinning to surface acceptor states (due to Si doping) on the n-type surface. STS data indicated that there was no peak in state density at the pinned Fermi level, but rather gap states extending in from the band edges were observed.

In the above, we have considered the ideal, clean semiconductor surface prepared under Ultra High Vacuum conditions. As mentioned, the clean Si(111) surface has a relatively high density of surface states that pin the Fermi level. The electronic properties of this surface are considerably improved by the formation of a thermal oxide[10]. Silicon based devices have achieved their dominance over other semiconductor based technologies due to the high quality of this stable oxide. In contrast, the formation of oxides on GaAs results in a high density of surface states and subsequent Fermi level pinning. The presence of oxygen on the GaAs surface leads to the formation of both gallium and arsenic oxides. The enhanced thermodynamic stability of gallium oxides over arsenic oxides leads to the gradual reduction of arsenic oxides by neighbouring gallium resulting in the segregation of arsenic atoms. It has been proposed by Lee[11] that the segregation of arsenic atoms following this reaction sequence results in a high surface state density and limits the performance of GaAs based electronic and optoelectronic devices. Absence of a stable GaAs/Oxide phase has also prevented the development of a GaAs Metal-Insulator-Semiconductor technology. Clearly, a method of treating *(passivating)* the GaAs surface that reduces the surface state density, decreases the band-bending and, at best, unpins the Fermi level would be invaluable. Attempts to date at achieving this goal are reviewed in the following sections.

2. 2 Sodium Sulphide and Ammonium Sulphide Based Passivation.

Ideally, a passivating adsorbate must perform three functions; prevent surface oxidation or reaction with another chemical species, eliminate surface state density, and prevent interfacial state formation. In 1987, Sandroff *et al.* [12] illustrated an increase in current gain of a heterojunction bi-polar transistor from 30 to 2000 after spin coating a thin film of $Na_2S{\cdot}9H_2O$ onto the device. Furthermore, the same solution used to treat the GaAs(100) surface has been reported to increase the photoluminescence (PL) intensity 60-fold[13]. Since these initial reports, a considerable effort has been applied to the study of aqueous sulphide treated GaAs, and to a lesser extent, InP surfaces.

Both Yablonovitch *et al.* [14] and Nottenburg *et al.*[15] found that improvements in the surface recombination velocity (SRV) of $Na_2S\cdot 9H_2O$ treated GaAs surfaces approach those of the AlGaAs/GaAs interface. The beneficial effects of such a treatment were attributed to the removal of states within the band gap by Fan *et al.* [16] making the metal-GaAs barrier highly sensitive to the metal work function[17]. One limitation of these sodium sulphide treatments is aging. Sandroff *et al.*[12] noted that improvements in transistor gain persisted only for 1-2 days. An ambient STM investigation of the GaAs(100) surface passivated in an aqueous Na_2S solution by Berkovits *et al.*[18] reported stable imaging of the treated surface for several hours in air. The untreated surface yielded irreproducible images. Current-voltage characteristics indicated that the passivation strongly reduced the density of band-gap states. However, a reduction in the number of mid-gap states does not necessarily mean the unpinning of the Fermi level, as argued by Spindt *et al.* [19] from a photoemission study of sodium sulphide treated GaAs(100) surfaces. They observed the characteristic increase in photoluminescence intensity but found that the surface Fermi level was near mid-gap. One possible explanation for these results, as put forward by the authors, was in terms of the *Advanced Unified Defect Model (AUDM)* of Spicer *et al.*[20]. In that model, interface states are associated with anti-site defects i. e. As atoms on Ga sites or vice-versa. The Fermi level position in the gap will thus be determined by the relative densities of these two types of defect. Spindt *et al.* [19] proposed that excess arsenic near the surface of the untreated wafer caused the Fermi level to lie at about 0.75 eV from the VBM. They then suggested that the Na_2S treatment removed excess As, allowing the Ga_{As} defect state sites to pull the Fermi level closer to the VBM. This predicts an increase in band-bending on n-type GaAs after sodium sulphide treatment. Interestingly, very recent STM and STS studies of Feenstra *et al.*[21] using low temperature grown GaAs(110) containing about $10^{20}\,cm^{-3}$ arsenic related point defects, have revealed a band of donor states (located 0.5 eV above the Fermi level) arising from the defects. The structure of the defect, as determined from STM images, was found to be consistent with that of an isolated As anti-site defect in a tetrahedral environment.

An investigation of Schottky barriers formed on ammonium sulphide treated n- and p-type GaAs[22] found an order of magnitude reduction in surface state density compared to an untreated surface. The Schottky diodes showed no apparent aging after several months of room air exposure. An X-Ray Photoelectron Spectroscopy (XPS) study of similarly treated $(NH_4)_2S$ surfaces[23] indicated that an approximate 0. 6 ML coverage was obtained. The chemical state of the sulphur did not change with long exposure to air and the sulphide layer was not lost as the GaAs surface became oxidised. It has been reported[24] that the effects of ammonium sulphide surface treatment are more durable that those of sodium sulphide. Richter and Hartnagel[25] have used STM to characterize the ambient oxidation of NH_4OH etched and $(NH_4)_2S$ passivated GaAs(100) surfaces. They reported a considerable increase in the electrical homogeneity of the sulphur passivated

surface when compared with the NH_4OH etched surface. Fan *et al.*[26] have reported the increased passivating effects of an $(NH_4)_2S_x$ solution when compared with an $(NH_4)_2S$ solution due to the etching behaviour of a reactive sulphur species only present in the former. Nannichi *et al.* [27] have proposed that this is due to the more complete removal of the residual surface oxides by the $(NH_4)_2S_x$ treatment. An etch rate of 2-3 nm/hr at a temperature of 45°C has been estimated[28]. Oigawa *et al.*[28] have extended this ammonium polysulphide treatment to the <100> faces of a number of other III-V semiconductors. Schottky barrier diodes were fabricated by evaporating various metals onto chemically etched and $(NH_4)_2S_x$ treated surfaces. They found a strong dependence of barrier height on metal work function for all sulphur treated surfaces. These results contradicted the earlier reports of both Spindt *et al.*[19] and Besser and Helms[29] that the Fermi level is merely re-pinned at a new gap position and provided considerable evidence to support the claim that the sulphur treatments do unpin the Fermi level.

Although there are still some discrepancies in the literature regarding the chemistry of sulphide passivation, all the authors agree that under aqueous sulphide treatment the native oxide layer is removed and a thin layer consisting of sulphur atoms covalently bound to the GaAs surface is formed. According to Synchrotron Radiation Photoemission Spectroscopy (SRPES) studies, three bonding states - Ga-S, As-S and S-S are observed for the room temperature (RT) $(NH_4)_2S_x$ treated GaAs(100) surface[30]. After a 360°C anneal in vacuum, which removes the amorphous sulphur overlayer, only Ga-S bonds were observed. Band bending was seen to be relaxed with a Fermi level shift of about 0.3 eV towards the CBM. A Reflection High Energy Electron Diffraction (RHEED) and XPS study of $(NH_4)_2S_x$ treated GaAs(100) surfaces[31] reported that for room temperature adsorption a (1x1) RHEED pattern was observed- attributed to sulphur adsorption on Ga bridge sites - with no second peak at higher binding energy in the As 2p XPS spectrum, as was observed for an untreated sample. This would indicate that in the $(NH_4)_2S_x$ treated case, As oxidation did not occur. After annealing in the 260°C-420°C temperature range, a (2x1) RHEED pattern was observed. No obvious chemical shift was observed in either Ga 2p or As 2p XPS peaks which the authors suggested was an indication of Ga-S bond formation. An As-S bond would lead to charge transfer from As to S and thus a larger chemical shift would occur. The (1x1) RHEED pattern observed by this group has been shown by Ohno[32], using first principles pseudopotential calculations, to be also most likely due to S atoms adsorbed on the bridge site of both Ga and As terminated (100) surfaces.

Further to this work, Ohno and Shiraishi[33] carried out a complementary theoretical study of the electronic properties of the S/GaAs(100) - (1x1) surface. For the Ga terminated surface the adsorption of S causes a marked reduction in the density of gap states which is not observed on the As terminated surface due to the appearance of an As-S anti-bonding state within the gap. The (2x1) structure observed after annealing was explained in terms of sulphur dimer formation, with the observation of only Ga-S bonds

after this anneal accredited to the Ga-S bonding energy being larger by 0.61 eV than that of the As-S bond. By performing total energy calculations within an empirical tight-binding model Ren and Chang[34] found that by forming a S induced (2x1) reconstruction on the As terminated GaAs(100) surface it was possible to yield a surface with no states mid-gap. They considered a number of possible geometries for the (2x1) reconstruction occuring on an As rich (2x4) GaAs(100) surface. (A detailed description of this reconstruction is given in Chapter 5, its most important feature being that the (2x4) periodicity is due to an ordering of As dimers and missing dimers). Every arsenic dimer may be bridged by either a sulphur atom or disulphur molecule, or one of the two As dimer atoms may be substituted by a sulphur atom. For the bridging sulphur atom or dimer geometries a lower total unit cell energy than that of the As dimer reconstruction was found. Difficulties in determining the total energy of the substitution model unit cell meant that it was impossible to decide if this structure was also lower in energy.

In an optical study of sulphur passivated GaAs(001) by Na_2S solutions, Berkovits and Paget[35] demonstrated that after annealing at a temperature of 440°C the S-treated surface was covered by As and S dimers aligned along the [110] direction. After annealing at 580°C sulphur desorbed from the surface, resulting in the appearance of a line in the reflectance anisotropy spectra indicative of the formation of Ga dimers aligned along [110]. There was little change in the S-Ga bond as a function of annealing temperature. However, after annealing at 530°C S-As bonds were broken allowing the formation of As dimers. Sandroff *et al.*[36] have also investigated this system and have concluded that no significant amount of reaction product forms between surface atoms and sulphide solutions as they observed no high energy shoulder on the Ga 3d XPS peak. They proposed a model whereby disulphur molecules bridge adjacent As atoms in a way which nearly preserves the tetrahedral bonding geometry of bulk As. AES measurements of Geib *et al.*[37] indicate that $(NH_4)_2S$ treatment results in 0.5 to 1 monolayer (ML) of sulphur on the GaAs(100) surface. As the substrate temperature increases from RT to 350°C As was found to evaporate from the surface while the concentration of sulphur remained unchanged. They explained these results in terms of a two step H_2S (dissolved in the $(NH_4)_2S$ solution) dissociation model. For substrate temperatures less than approximately 110°C, H_2S dissociates into H+HS and the HS molecule then bonds to As sites. At higher temperatures, these HS molecules dissociate to form AsH_3 and a stronger As-S bond. The AsH_3 evaporates reducing the surface As concentration. At even higher temperatures the surface becomes void of As and only Ga-S bonds are formed.

A recent analysis of GaAs(100) surface prepared with various wet and *in situ* sample treatments by Wang*et al.*[38] demonstrated that $(NH_4)_2S$ reduced the carbon contamination found on acid etched surfaces. The proposed sulphur monolayer formed a (2x1) superstructure after annealing to 575°C to remove residual oxides. This group also

found that sulphur desorption, probably in elemental form, occured at about 600°C, leading to the appearance of the clean GaAs(100) surface (4x1) reconstruction.

Sugiyama *et al.*[39] have investigated the structure of $(NH_4)_2S_x$ passivated GaAs(111) surfaces using soft X-ray standing waves. They proposed that on the GaAs(111)A (Ga) surface, S atoms are located on top of the first layer Ga atoms, while on the GaAs(111)B (As) surface, S atoms replace the first layer As atoms. The structure models presented were consistent with previous photoemission results[40]. Ohno[41] has calculated the S-Ga bond energies for S atoms on GaAs(111)A and B surfaces by the pseudopotential method. He found a value of 6.1eV for the S-Ga bond on S/GaAs(111)B, much larger than the the 4.3 eV value determined for the S/GaAs(111)A surface. Therefore the S/GaAs(111)B surface is predicted to be more stable than the S/GaAs(111)A.

Similar passivation of InP(100) surfaces using $(NH_4)_2S_x$ solutions has been studied by a number of groups. These investigations will be briefly described to highlight similarities with GaAs(100) work. Tao *et al.* [42] observed a (1x1) LEED pattern after RT $(NH_4)_2S_x$ treatment that persisted even after several days exposure to air. High resolution XPS studies showed that the InP(100) - (1x1) surface is terminated by S which bonds only to In. X Ray Adsorption Near Edge Structure (XANES)[43] was also employed to determine the structure of this surface. S was found to form a bridge bond with two In atoms along the [011] direction. After annealing at 200-350°C, the sulphur passivated (1x1) surface forms a (2x1) reconstruction[44]. This was attributed to an exchange between phosphorous and sulphur and a subsequent dimerisation of sulphur atoms. However, a (2x1) unit cell with one monolayer of sulphur leads to a surface charge imbalance. The existence of both S-S and P-P dimers with the same surface concentration was described as the only possibility to define an ideal surface free from electronic states.

A major problem affecting the long term stability of the sulphur passivated GaAs surfaces as described above is the inherent thermodynamic instability of Ga and As sulphides with respect to the corresponding oxides[45]. Lee *et al.*[11] reported a five-fold increase in the photoluminescence (PL) intensity when the GaAs(100) surface was passivated using a P_2S_5 / NH_4OH solution, with the PL intensity remaining constant over 10 days exposure to air. They suggested that the significant advantage offered by the addition of phosphorous compounds to the passivation treatment is the enhanced thermodynamic stability of phosphorous oxide over gallium oxide. This would mean that a surface phosphorous oxide could not be reduced by gallium, thereby inhibiting the reaction sequence which leads to arsenic segregation. Wang *et al.* [46] have used a wide range of techniques to characterise GaAs(100) surfaces passivated in $P_2S_5/(NH_4)_2S$ solutions both with and without additions of free sulphur. XPS studies of the passivated surfaces revealed evidence of the presence of sulphur bound to both Ga and As surface atoms. An increase of PL intensity up to 23 times the signal for the freshly etched surface

was observed for surfaces passivated in $P_2S_5/(NH_4)_2S/S_x$. This treatment also yielded the surface with the slowest PL intensity degradation rate on exposure to air.

A comprehensive analysis of $P_2S_5/(NH_4)_2S$ treated GaAs(100) has recently been described by Dagata *et al.*[47-49] with the ultimate objective of preparing a surface which is topographically and chemically uniform. They have also reported an improved passivation due to the $P_2S_5/(NH_4)_2S$ treatment as compared with $(NH_4)_2S$ alone and have adapted the former treatment so as to make it compatible with STM imaging (as described in Chapter 6). Time-of-flight Secondary Ion Mass Spectrometry (TOF SIMS) and XPS studies carried out on these passivated surfaces suggested that the stability of the $P_2S_5/(NH_4)_2S$ passivated surface was as a result of the formation of an ordered ultrathin oxide and not due to sulphur termination. More recent XPS and AES studies by this group[50] have indicated that S is buried between the oxide overlayer and the GaAs substrate. The oxide contains a variety of As and Ga bonding configurations.

2. 3 UHV Exposure of GaAs Surfaces to S_2 and H_2S.

Chemical treatments using *in situ* dry processes are inherently superior to wet chemical processing in terms of contamination levels and homogeneity. Although S is used as a dopant in GaAs (in the form of H_2S in vapour phase epitaxy) , there have been relatively few studies dealing with H_2S adsorption on GaAs. Ranke *et al.*[51] investigated the interaction between H_2S and different GaAs surfaces by core level photoelectron spectroscopy combined with AES. Use of a cylindrically shaped GaAs single crystal enabled six inequivalent orientations to be studied. Sulphur uptake was found to depend on both crystal orientation and temperature. Low temperature adsorption (< 150K) leads to changes in the As 3d peak whereas for higher adsorption temperatures (280°C-450°C) the Ga 3d peak is mainly affected (for all orientations). Two peaks shifted by 0.45 and 0.8 eV towards higher binding energy were found which were attributed to Ga atoms with one and two sulphur ligands. The adsorption of H_2S onto GaAs(100) surfaces at 425°C as investigated by Massies *et al.*[52], was found to change the surface structure from the well-known c(2x8) reconstruction (as described in Chapter 5) to a well-defined 2x1 structure. The authors also noted a dramatic decrease in the As (33eV) Auger line intensity as a function of H_2S exposure while the Ga line remained constant. This effect and the associated change in surface structure were associated with an exchange reaction between S and As atoms in the surface layer. Tiedje *et al.*[53] have similarly determined, from high resolution photoemission studies, that a treatment of the GaAs(100) surface with H_2S at room temperature followed by annealing at 400°C passivates the surface through removal of the As atoms and the formation of GaS_x chemical species. They found that the Fermi level at the passivated surface is located slightly above mid-gap (by 0.15 eV) and that the surface is stable for some time in both air and water.

In an XPS study of the influence of S and Se on the Schottky barrier height and interface chemistry of Au contacts to GaAs, Waldrop[54] used a vapour stream of

elemental S from a heated quartz ampule as a sulphur source. He found that exposure of clean GaAs(100) surfaces to elemental S or Se resulted in the formation of a 5 angstroms thick layer of Ga and As chalcogenides. The Schottky barrier height for Au contacts to these S- or Se- treated surfaces had a 0.2 eV variation centred about the 0.89eV barrier for ideal contacts. Koenders *et al.*[55] have investigated the interaction of molecular sulphur, obtained from a solid state electrochemical cell (see Section 3.8.2), with cleaved GaAs(110) surfaces. Using a Kelvin probe and UPS they found that adsorption of sulphur causes an increase in band-bending and a pinning of the Fermi level at 0.3 eV above the VBM for both n- and p- type GaAs(110). This they attributed to charge transfer from substrate to adsorbate due to S being more electronegative than either Ga or As. A comparison of the reaction of molecular sulphur from an electrochemical cell and gaseous H_2S with the GaAs(100) surface by Mokler and Watson[56] indicated that H_2S adsorption led to at most 1 ML of sulphur at the surface, whereas S_2 adsorption yielded coverages as high as 5 ML. For that study a Ga rich c(8x2) surface was exposed to both sulphur sources. For an S_2 saturated surface, thermal desorption spectra (TDS) had peaks due to GaS_2 and AsS_2 centred at 150°C. Monitoring the monosulphides (GaS, AsS) also yielded a peak at 150°C, and the start of a peak at 550°C. After the adsorption of S_2 to 20% of saturation, only monosulphide peaks were observed at 550°C, with a 3:1 AsS:GaS ratio. TDS of the H_2S saturated surface revealed AsS and GaS desorption (no disulphides) with AsH_3 and GaH desorbing at 100°C.

Roberts *et al.*[57] have studied the surface chemistry resulting from the interaction of S_2 with the decapped GaAs(100) surface using SRPES. They found that sulphur adsorption characteristics are critically dependent on the composition (i. e. As/Ga ratio) of the GaAs surface. Their core level vacuum UPS studies indicate that, for RT adsorption, sulphur bonds to both Ga and As atoms, with two separate bonding configurations observed for the S-As reaction. After annealing the As rich sulphur covered surface to 150°C, one As-sulphur component disappeared. No significant change in the Ga 3d core level was observed after annealing. Sugahara *et al*.[58] have also studied the adsorption of S_2 on the GaAs(100) surface using a "sulphur annealing" technique where the surface is exposed to sulphur at elevated temperatures. SRPES measurements indicated that Ga-S bonds were formed after oxide removal. (4x1)(after annealing at temperatures in excess of 480°C) and (2x1) (> 360°C) reconstructions were observed with an average sulphur layer thickness of 1.5 Å and 2.4 Å respectively. Band bending for the n-type S-annealed surfaces was found to be reduced by 0.2 - 0.3 eV.

In summary, there remains some controversy over the exact nature of chemical bonding of sulphur adsorbates on III-V semiconductor surfaces and the degree to which band bending is affected. As described, some results suggest a complete unpinning of the Fermi level whereas others have indicated a mere shift of the pinning position. While it is widely accepted that sulphur adsorption (whether in aqueous sulphide, H_2S, S or S_2

form) causes a notable improvement in the electronic properties of the GaAs surface, the precise form of the interaction is still not well understood

References

1. S. M. Sze, *Physics of Semiconductor Devices,* 2nd Ed. (Wiley, 1981)
2. M. L. Cohen and T. L. Bergstresser, *Phys. Rev.* **141** 789 (1966)
3. E. H. Rhoderick and R. H. Williams, *Metal-Semiconductor Contacts*, 2nd Ed., (Oxford Science Publications, 1988)
4. J. Bardeen, *Phys. Rev.* **71** 717 (1947)
5. R. M. Feenstra, *Phys. Rev. Lett.* **63** 1412 (1989)
6. R. M. Feenstra and P. Martensson, *Phys. Rev. Lett.* **61** 447 (1988)
7. P. N. First, J. A. Stroscio, R. A. Dragoset, D. T. Pierce and R. J. Celotta, *Phys. Rev. Lett.* **63** 1416 (1989)
8. J. Tersoff, *Phys. Rev. Lett.* **52** 465 (1984)
9. M. D. Pashley, K. Haberern, R. M. Feenstra and P. D. Kirchner, *Phys. Rev. B* **48** 4612 (1993)
10. P.Balk in *The Si-SiO_2 System,* Materials Science Monographs No. 32, (Elsevier Publishers B. V., The Netherlands). (1988)
11. H. H. Lee, R. J. Raciot and S. H. Lee, *Appl. Phys. Lett.* **54** 724 (1989)
12. C. J. Sandroff, R. N. Nottenburg, T. C. Bischoff and R. Bhat, *Appl. Phys. Lett.* **51** 33 (1987)
13. C. J. Sandroff, M. S. Hedge, L. A. Farrow, C.C. Chang and J. P. Harbison, *Appl. Phys. Lett.* **54** 362 (1989)
14. E. Yablonovitch, B.J. Skromme, R. Bhat, J. P. Harison and T. J. Gmitter, *Appl. Phys. Lett.* **54** 555 (1989)
15. R. N. Nottenburg, C. J. Sandroff, D. A. Humphrey, T. H. Hollenbeck and R. Bhat, *Appl. Phys. Lett.* **52** 118 (1988)
16. J. Fan, H. Oigawa and Y. Nannichi, *Jpn. Journ. Appl. Phys.* **27** L1331 (1988)
17. M. S. Carpenter, M. R. Melloch and T. E. Dungan, *Appl. Phys. Lett.* **53** 66 (1988)
18. V. L. Berkovits, L. F. Ivantson, I. V. Makarenko, T. V. L' Vora, R. V. Khasieva and V. I. Safarov, *Sov. Phys. Semicond.* **25(3)** 231 (1991)
19. C. J. Spindt, R. S. Besser, R. Cao, K. Miyano, C. R. Helms and W. E. Spicer, *Journ. Vac. Sci. Technol. A* **7(3)** 2466 (1989)
20. W. E. Spicer, Z. Lilienthal - Weber, E. R. Weber, N. Newman and T. Kendelewizc, *Journ. Vac. Sci. Technol. B* **6** 1245 (1988)
21. R. M. Feenstra, J. M. Woodall and G. D. Petit, *Phys. Rev. Lett.* **71** 1176 (1993)
22. J. E. Samaras and R. B. Darling, *Journ. Appl. Phys.* **172(1)** 168 (1992)
23. B. A. Cowans, Z. Dardas, W. N. Delgalss, M. S. Carpenter and M. R. Melloch, *Appl. Phys. Lett.* **54** 365 (1989)
24. K. C. Hwang and S. S. Li, *J. Appl. Phys.* **67** 2162 (1990)
25. R. Richter and H. L. Hartnagel, *J. Electrochem. Soc.* **137** 2879 (1990)
26. J. Fan, H. Oigawa and Y. Nannichi, *Jpn. Journ. Appl. Phys.* **27** L2125 (1988)

27. Y. Nannichi, J. Fan, H. Oigawa and A. Koma, *Jpn. Journ. Appl. Phys.* **27** L2367 (1988)
28. H. Oigawa, J. Fan, Y. Nannichi, H. Sugahara and M. Oshima, *Jpn. Journ. Appl. Phys.* **30** L322 (1991)
29. R. S. Besser and C. R. Helms, *Appl. Phys. Lett.* **52** 20 (1988)
30. H. Sugahara, M. Oshima, H. Oigawa, H. Shigekawa and Y. Nannichi, *Journ. Appl. Phys.* **69** 4349 (1991)
31. H. Hirayama, Y. Matsumoto, H. Oigawa and Y. Nannichi, *Appl Phys. Lett.* **54** 2565 (1989)
32. T. Ohno, *Surf. Sci.* **255** 229 (1991)
33. T. Ohno and K. Shiraishi, *Phys. Rev. B* **42** 11194 (1990)
34. S. -F. Ren and Y. -C. Chang, *Phys. Rev. B* **41** 7705 (1990)
35. V. L. Berkovits and D. Paget, *Appl. Phys. Lett.* **61** 1835 (1992)
36. C. J. Sandroff, M.S. Hedge and C. C. Chang, *Journ. Vac. Sci. Technol. B* **7** 841 (1989)
37. K. M. Geib, J. Shin and C. W. Wilmsen, *Journ. Vac. Sci. Technol. B* **8** 838 (1990)
38. X. -S. Wang, K. W. Self, R. Maboudian, C. Huang, V. Bressler-Hill and W. H. Weinburg, *Journ. Vac. Sci. Technol. A* **11(4)** 1089 (1993)
39. M. Sugiyama, S. Maeyama, M. Oshima, H. Oigawa, Y. Nannichi and H. Hashizume, *Appl. Phys. Lett.* **60** 3247 (1992)
40. T. Scimeca, Y. Muramatsu, M. Oshima, H. Oigawa and Y. Nannichi, *Phys. Rev. B* **44** 12927 (1991)
41. T. Ohno, *Phys. Rev. B.* **44** 6306 (1991)
42. Y. Tao, A. Yelon, E. Sacher, Z. H. Lu and M. J. Graham, *Appl. Phys. Lett.* **60** 2669 (1992)
43. Z. H. Lu, M. J. Graham, X. H. Feng and B. X. Xang, *Appl. Phys. Lett.* **60** 2773 (1992)
44. D. Gallet and G. Hollinger, *Appl. Phys. Lett.* **62** 982 (1993)
45. O. Kubaschewski and C. B. Alcock, *Metallurgical Thermochemistry*, 5th Ed. (Pergamon, New York) (1979)
46. Y. Wang, Y. Darici and P. H. Holloway, *Journ. Appl. Phys.* **71** 2746 (1992)
47. J. A. Dagata, W. Tseng, J. Bennett, J. Schneir and H. H. Harary, *Appl. Phys. Lett.* **59** 3288 (1991)
48. J. A. Dagata, J. Schneir, H. H. Harary, J. Bennett and W. Tseng, *Journ. Vac. Sci. Technol. B* **9** 1384 (1991)
49. J. A. Dagata, W. Tseng, J. Bennett, E. Dobisz, J. Schneir and H. H. Harary, *Journ. Vac. Sci. Technol. A* **10** 2105 (1992)
50. M. J. Chester, T. Jach and J. A. Dagata, *Journ. Vac. Sci. Technol. A* **11(3)** 474 (1993)

51. W. Ranke, J. Finster and H. J. Kuhr, *Surf. Sci.* **187** 112 (1991)
52. J. Massies, F. Dezaly and N.T. Linh, *Journ. Vac. Sci. Technol.* **17** 1134 (1980)
53. T. Tiedje, K. M. Colbow, D. Rogers, Z. Fu and W. Eberhardt, *Journ. Vac. Sci. Technol. B* **7** 837 (1989)
54. J. R. Waldrop, *Journ. Vac. Sci. Technol. B* **2** 445 (1984)
55. L. Koenders, M. Bloemacher and W. Monch, *Journ. Vac. Sci. Technol. B* **6** 1416 (1988)
56. S. M. Mokler and P. R. Watson, *Journ. Vac. Sci. Technol. A* **9** 1374 (1991)
57. L. Roberts, G. Hughes, B. Fennema and M. Carbery, *Journ. Vac. Sci. Technol. B* **10** 1862 (1992)
58. H. Sugahara, M. Oshima, H. Oigawa and Y. Nannichi, *Thin Solid Films* **23** 1 (1992)

CHAPTER III: EXPERIMENTAL SYSTEMS AND TECHNIQUES

The following chapter details the experimental systems and techniques used to obtain the results presented in this thesis. Both Ultra High Vacuum and ambient STM systems are described in depth. The physical principles underlying such surface analysis probes as Low Energy Electron Diffraction, Auger Electron Spectroscopy, and Photoelectron spectroscopy are outlined, with the final sections discussing sample preparation and sulphur treatments.

3.1 UHV Systems

The preparation of well defined surfaces with negligible levels of contamination requires ambient pressures in the 10^{-10} Torr range. When pressures this low are achieved a number of hours are needed for a monolayer (a complete atomic layer) of contamination to adsorb on the sample surface. To achieve such Ultra High Vacuum (UHV) conditions a system of stainless steel vessels evacuated using suitable pumps must be utilised.

3.1.1 The Omicron UHV System.

The *Omicron* UHV STM system is a multi chamber construction consisting of an STM-, a surface analysis-, and a preparation-chamber with a fast entry load lock for introduction of samples from air. A detailed description of the STM chamber is given in Section 3.2. Figure 3.1 is a photograph of the entire system installed in Labor 5.13, *Physikalisch-Technische Bundesanstalt,* Braunschweig, Germany. The spherical main chamber measures 12" in diameter. An *Omicron* reverse view SPECTA LEED/AES optics is mounted on an 8" port at the front of the chamber. Two 4 $^1/_2$" ports inclined at right angles to each other serve as viewing windows, while a VSW manipulator mounted horizontally on a 6" flange allowed for translation of the sample in three orthogonal planes with rotation about the horizontal axis. This manipulator is equipped with an electron beam heater for high temperature sample annealing and a thermocouple to monitor sample temperature. As can be seen from the photograph, the *Omicron* system has a multiple port configuration for future installment of other surface analytical techniques (for example, X-Ray Photoelectron Spectroscopy). A $2^3/_4$" port connects the main chamber to the preparation chamber via an MDC sliding gate valve. Transfer of samples and STM tips from the preparation chamber to the main chamber and back is via a Fisons magnetically coupled Linear Transfer Mechanism (LTM).

In the preparation chamber, transfer to a VG manipulator mounted horizontally on a 6" flange allowed for resistive heating of the samples. (Electron beam irradiation and ion bombardment of samples is also possible via an electron and ion gun). Two 4 $^1/_2$" windows at the top of the chamber enabled a clear view of the sample both during transfer and annealing. The electrochemical sulphur cell was mounted on a $2^3/_4$" port at

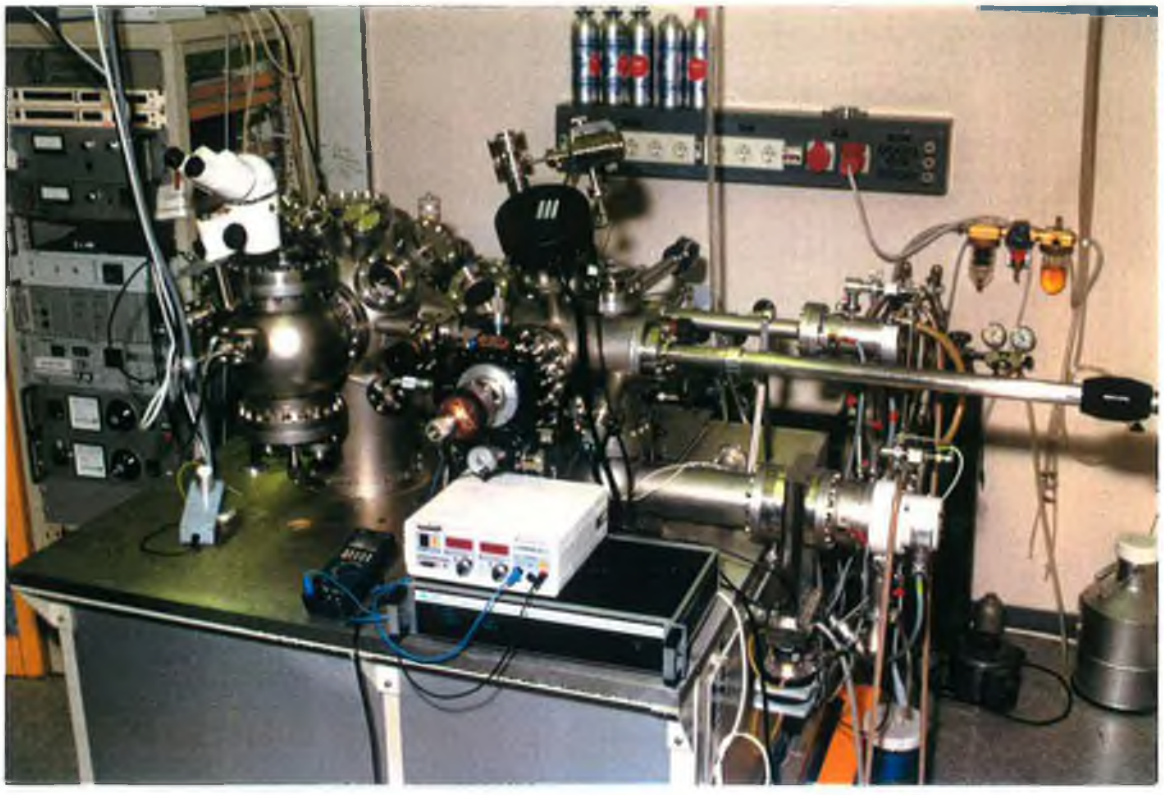

Fig 3.1 *The Omicron VakuumPhysik UHV STM system.*

the base of the chamber, inclined at a 45° angle. Also mounted on a 2 3/4" port at the top of the chamber is a Spectra Quadropole Mass Spectrometer (QMS). This was interfaced to a 486-based PC with hardware and software available, as standard, with the instrument. Within a Windows 3.1 environment it was possible to set up the multi-channel plate detector of this spectrometer for various masses and watch their evolution with time. This facility proved particularly useful during decapping of As capped GaAs samples (Section 3.7.2) as well as monitoring the partial pressure of S_2 during sulphur exposures (Section 3.8.2). Sample or tip transfer into the preparation chamber from air was via an MDC magnetically coupled linear transfer mechanism within the fast entry lock. After evacuating the lock to suitably low pressures an MDC gate valve between preparation chamber and entry lock was opened and the sample (or tip) transferred to the LTM in the preparation chamber. Pressures in both chambers were monitored by VSW ion gauges.

Roughing of the system was via a Balzers Turbo pump backed by a Balzers rotary pump. At suitably low pressures the ion pumps in both chambers were switched on. After baking of the system at 150°C for 12-15 hours, pressures in the 1×10^{-10} Torr range were obtained. Titanium sublimation pumps in both chambers provided additional

pumping. Samples were introduced to the preparation chamber after pumping of the load lock using another Balzers turbo pump.

3.1.2 VG ADES System - Daresbury SRS Beamline 6.1

The second UHV system used was a standard Vacuum Generators ADES 400 system with modifications to allow it to couple with the grazing incidence monochromator (GIM6) on beamline 6.1 at the Synchrotron Radiation Source at Daresbury, U.K. The system consists of a non-magnetic μ-metal main chamber in the form of a bell-jar to which a stainless steel preparation chamber is attached.

Measuring 14" in diameter and 36" in height the main chamber is mounted on a 17" base flange, just above which an 8" port leading to the pumping system is located. This chamber has two experimental working levels with an 8" top port on the chamber axis. The upper working level has seven 2 3/4" ports positioned radially around the chamber with an 8" port for LEED optics (a three grid Varian RFA system) opposite a 6" window on an axis parallel to the beam line and an 8" window at the front of the chamber. The lower working level contains eight 2 3/4" ports mounted radially around the chamber,a 6" viewing port and an 8" port to which the hemispherical analyser was attached. A load lock was attached via a 2 3/4" port and isolated from the main chamber via a MDC sliding gate valve for introduction of samples to UHV. A stainless steel carousel type sample holder capable of holding two samples was mounted on a Vacuum Generators LTM and used to transfer samples from the load lock to the main chamber and back. The electrochemical sulphur cell was also mounted at the lower level of the main chamber. A Vacuum Generators UMD20 universal manipulator located on the top 8" port allowed sample rotation about a vertical axis, azimuth rotation about an axis normal to the sample surface and movement in three orthogonal planes.

The load lock was pumped by a Balzers turbomolecular pump backed by an Edwards rotary pump with the main chamber pumped by both a Balzers turbomolecular pump (backed by an Edwards rotary pump) and a Varian ion pump. Further pumping was via Vacuum Generators LN_2 cold traps. Evacuation of the main chamber from atmosphere was via firstly, vane, sorption and the main chamber turbo pumps. At suitably low pressures the ion pump valve was opened. After baking the system at 180°C for 24 hours ultimate pressures of better than 7×10^{-11} mbar were achieved (monitored by Vacuum Generators ion gauges). A Vacuum Generators SX200 quadrupole mass spectrometer connected to the main chamber allowed both the detection of leaks and the monitoring of partial pressures of both As (during As decapping of samples - Section 3.7.2) and S (during deposition of sulphur - Section 3.8.2).

3.2 Omicron UHV STM

A schematic diagram of the STM chamber and photograph of the actual STM are illustrated in Figs 3.2 and 3.3 respectively. A linear drive mechanism (operated outside

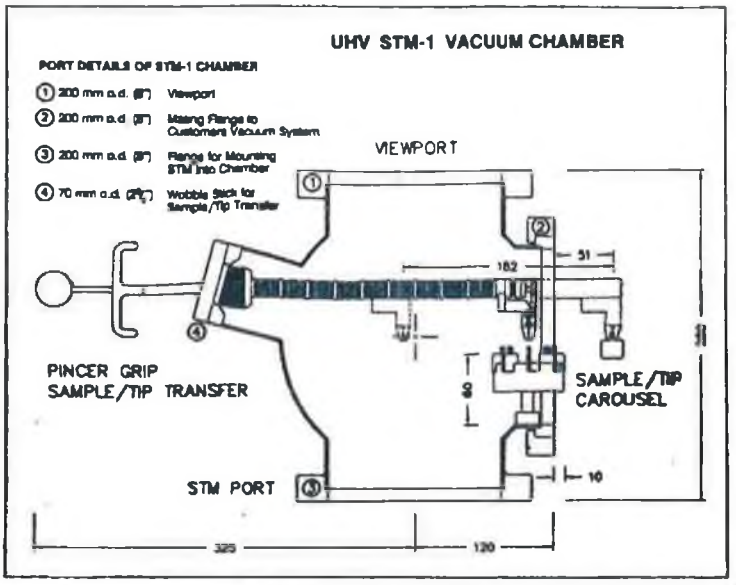

Fig 3.2 *A schematic diagram of the Omicron UHV STM chamber.*

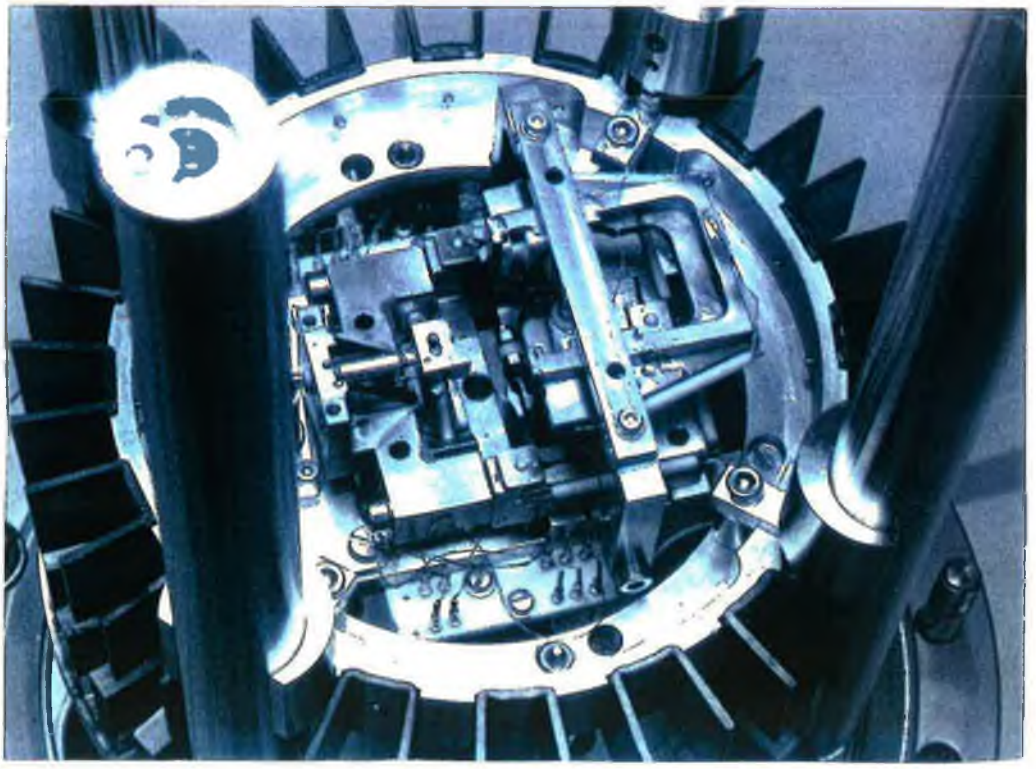

Fig 3.3 *Top view of the Omicron STM.*

UHV) moves the STM between its two levels of operation. The upper level is for sample/tip transfer where the STM unit is clamped in position. Sample and tip transfer to or from the STM is via a pincer-grip "wobble-stick". As can be seen from the schematic illustration of Fig. 3.5, the STM chamber contains an eight position sample/tip carousel from which both may be loaded into the STM. Due to the compatibility of the manipulators, transfer devices, carousel and STM as regards sample holder dimensions, it is also possible to load a sample directly into the STM from the main chamber manipulator.

Normal scanning operation of the STM is at the lower level. Here the STM is fully decoupled by a spring suspension system within the microscope supports and a circular array of magnets. This construction ensures elimination of mechanical vibrations down to 0.05 Å amplitude. Coarse sample to tip approach is by an XY stage which uses inertial drive piezoelectric elements. The sample is brought toward the tip while observed through the upper window using an optical microscope. Lateral positioning of 6mm in the X-axis is possible at this point. (For the semiconductors investigated in this work, the reflection of the tip in the mirror-like surface provided a useful guide to tip-sample separation). After coarse manual optical approach has achieved the optimal separation, an "auto-approach" is engaged. During this stage, one forward step of inertial drive coarse approach (adjustable from 500 to 2000 Å) is followed by a slow forward ramp of the tip. If during this slow ramp no tunnelling current is detected, the tip is retracted to the ramp start position and another forward step of coarse approach carried out. This process is repeated until tunnelling current is detected, at which point the forward ramp is stopped and the feedback loop activated. The tip is held within a ceramic holder fixed to the "apex" of a tripod, or triple tube, scanner arrangement. These three individual piezo elements are connected to a UHV pre-amplifier situated only 25mm from the tip.

STM data acquisition - both imaging and CITS spectroscopy - and parameter setting is via a Hewlett Packard HP300 graphics workstation interfaced through an IEEE488 BUS to a digital/analog control unit. Bias voltage and tunnelling current are adjustable within ranges of +10 to -10 V and 0-50nA respectively. Typically, scan step sizes of 1-2 Å were used in the course of this work - however, a minimum step size of 0.1 Å is possible. Maximum possible image area is 2000x2000 $Å^2$. All tips used were NaOH AC etched tungsten. During scanning all turbo pumps were switched off to keep noise levels at a minimum.

3.3 The Nanoscope II Air STM

The Nanoscope II consists of three major components - the actual microscope head and base unit, the control unit and the computer workstation, as illustrated schematically in Fig 3.4. The STM "head" consists of a piezoelectric tube scanner encased in a stainless steel surround with a mounted pre-amp. Coarse adjust screws on the base

enable the tip position above the sample to be adjusted, with a stepper motor controlling a fine approach screw at the back of the head.

Both the raster scan and the feedback loop are controlled by a Digital Signal Processor (DSP) in the workstation. This DSP passes Z and/or current data to the 80386 CPU and graphics processor in the workstation for display or storage. The feedback loop passes from the microscope through the control unit to the DSP and back again.

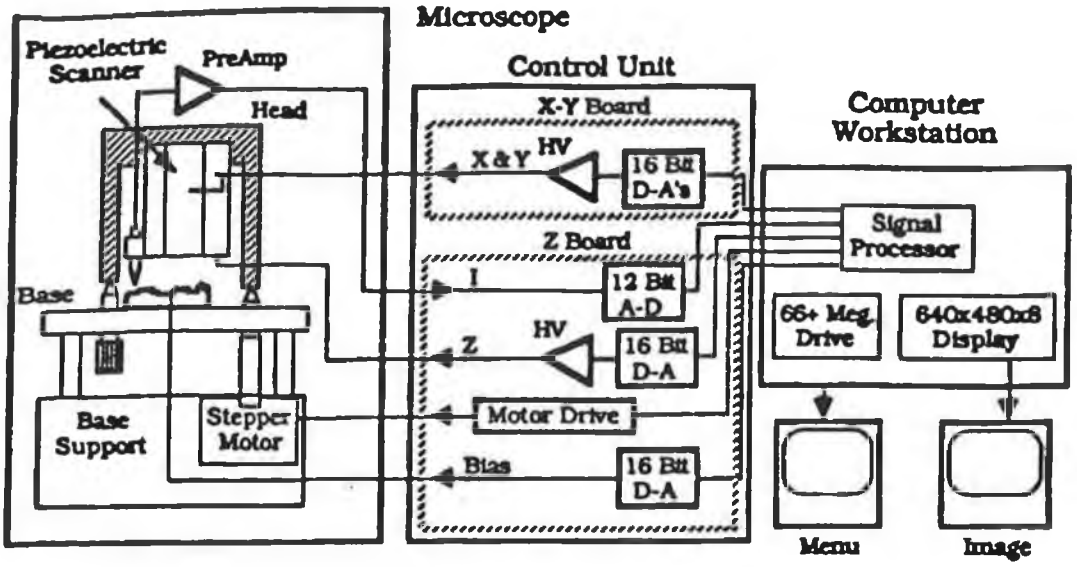

Fig 3.4 *A schematic diagram of the Nanoscope II air STM.*

The tunnelling current from the microscope enters the control unit and is sampled at a 63 KHz rate, converted to a digital binary representation and transmitted over a flat ribbon cable to the DSP. The DSP then uses this value to calculate a new Z value which is transmitted back to the control unit where it is converted to an analogue signal, amplified with a high voltage amplifier and applied to the Z electrode of the piezoelectric scanner. Mounted on the front of the head is a 0.012" stainless steel tube and ceramic tip holder assembly that accomodates 0.010" "Nanotips" (either W or Pt-Ir) by "kinking" of the tip prior to insertion in the tube.

Acquisition of a tunnelling spectroscopy I(V) plot is possible by firstly setting the sample bias (V_{stab}) and tunnelling current and running the feedback loop. This establishes a tip-sample separation. The feedback loop is then disabled and the bias voltage (V_{bias}) ramped within preset limits. After the I(V) spectrum is taken the feedback loop is re-enabled. It should be stressed that, unlike the Omicron CITS method, the Nanoscope II acquires I(V) spectra at a single, pre-defined point, outside the normal scanning routine. By varying the initial stabilisation voltage while keeping the setpoint tunnelling current constant, it is possible to vary the tip-sample separation and so increase the dynamic range in the current measurement. Furthermore, variation of tip-

sample separation may influence the general form of the I(V) curve and enhance understanding of surface electronic properties. (This latter point is expanded on in more depth in Chapter 6).

3.4 Low Energy Electron Diffraction.

Low Energy Electron Diffraction (LEED)[1] is a standard analytical technique to check the crystallographic structure of both clean surfaces and adsorbed overlayers. A beam of electrons with a typical energy of 20-500 eV is incident on the sample surface. It follows from de Broglie's equation:

$$\lambda = h / mv \qquad (3.1)$$

that the wavelength of 100eV electrons is approximately 1Å. The diffraction of these waves by periodic crystal lattices is therefore to be expected. In the case of wave scattering at a periodic one-dimensional array, constructive interference occurs if the scattered waves from neighbouring points have path differences of multiples of the wavelength λ. If the primary wave strikes the surface at an incident angle ϑ_0, interference of the back-scattered waves occurs in directions ϑ, given by :

$$a(\mathrm{Sin}\vartheta - \mathrm{Sin}\vartheta_0) = n\lambda \qquad (3.2)$$

Here a is the distance between neighbouring scatterers and n denotes the order of diffraction. This is extendable to the two-dimensional case where each set of atomic rows (h, k) gives rise to a series of diffraction maxima (nh, nk) with varying order of diffraction n. As LEED experiments are usually performed with normal incidence of the primary electrons ($\vartheta_0 = 0$) then Eqn 3.1 can be written:

$$\mathrm{Sin}\vartheta = n\lambda d_{hk}^{-1} \approx n d_{hk}^{-1} \sqrt{150}\, U^{-1} \qquad (3.3)$$

where U is the electron energy in eV and d_{hk} is the spacing between atomic rows. The larger the unit cell the closer the first diffraction maxima will be to the surface normal. LEED studies allow the d_{hk} values, and thereby the geometry of the unit cell, to be determined. It is only possible to derive information on the arrangement of atoms within the unit cell by analysing the intensities of the diffraction maxima. To describe the formation of a LEED pattern in more depth it is first necessary to consider the *reciprocal lattice* .

3.4.1 The Reciprocal Lattice and Ewald Construction.

The formation of a LEED pattern is due to phase shifts by multiples of the wavelength λ between the back scattered electron waves from neighbouring lattice

points. Directions of the interference maxima are determined by the Bragg equation. We will be concerned only with this geometrical theory of LEED and not the kinematic theory that deals with the analysis of maxima intensities.

A two dimensional surface lattice represents the periodicity of the atoms in the surface layer. We define basis vectors **a1, a2** for a unit cell that is the smallest parallelogram from which the lattice may be constructed using translation operations. The complementary reciprocal lattice is defined by vectors **a1*, a2*** where **a1*** $\perp$ **a2** and **a2*** $\perp$ **a1**. Also :

$$\mathbf{a1.\ a1^*} = 1\ ;\ \mathbf{a2.\ a2^*} = 1 \tag{3.4}$$

Thus, for the corresponding scalar quantities a1, a1* for example :

$$a1.a1^* = (\text{Cos}\ (\pi / 2) - \gamma\ )^{-1} \tag{3.5}$$

where γ is the angle between a1 and a2. Therefore, from (3.5) :

$$a1^* = (a1\ \text{Sin}\ \gamma)^{-1} \tag{3.6}$$

Reciprocal lattice vectors **G** may now be defined as

$$\mathbf{G} = 2\pi(n_1\mathbf{a1^*} + n_2\mathbf{a2^*}) \tag{3.7}$$

Electrons with energy E are incident with a wave vector $\mathbf{k} = (\sqrt{2}mE)(h/2\pi)^{-1}$ on a surface and are scattered with a wave vector **k'**. For the Bragg condition to hold, the scattering vector

$$\mathbf{K}_{||} = \mathbf{k'}_{||} - \mathbf{k}_{||} \tag{3.8}$$

must equal a vector of the reciprocal lattice $\mathbf{G}_{||}$. The possible scattered beams (**k'**) may be obtained by use of the *Ewald Construction* . If we firstly attribute to every 2D reciprocal lattice point a rod normal to the surface, the **k'** beams may be obtained by the following. The incident wave vector **k** is positioned with its end at the origin of the reciprocal lattice and a sphere or radius **k** constructed. The condition $\mathbf{K}_{||} = \mathbf{G}_{||}$ is fulfilled for every point at which the sphere crosses a reciprocal lattice "rod" (Fig 3.5). In LEED experiments, the directions $\mathbf{K}_{||}$ of the scattered beams are given by the points where they intersect with a flourescent screen. *The observed diffraction pattern is a direct representation of the reciprocal lattice of the surface.*

It should be noted that if the surface periodicity is discontinuous with domains of mean diameter d < L (the coherence length of the electron beam) the spots are likely to be broadened. This is due to the superposition of electron waves scattered at different surface regions.

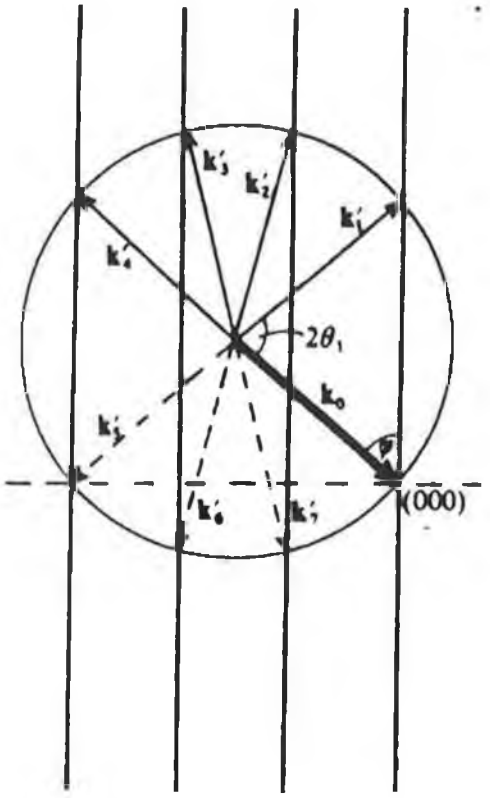

Fig.3.5 *The Ewald construction.*

3.4.2 The Omicron SpectaLEED

The LEED patterns observed in the experimental work for this thesis were acquired using either the rear-view Omicron SpectaLEED system or a Varian forward view LEED system. The rear-view LEED orientation eliminates the need for a second opposite viewport and also has the advantage that the sample manipulator does not obscure a large portion of the diffraction pattern. An internal retraction mechanism provides more space for manipulator movements in the main chamber.

A schematic diagram of the SpectaLEED principle of operation is illustrated in Fig. 3.6. The filament is enclosed within a Wehnelt cylinder and emits electrons when a current of approximately 1.3 A is passed through it. These electrons are collimated by a lens system (L1, L2, L3, L4) and finally leave the drift tube with the desired energy. In the drift tube the electrons traverse a field free region and will only be deflected by stray magnetic fields on their path to the sample. With the sample held at ground, normally incident electrons strike the surface generating back scattered electrons. As the first grid is also grounded, scattered electrons will not be deflected electrostatically. The second and third grids are at a negative potential whose magnitude is slightly smaller than the primary electron energy U and they therefore repel the inelastically scattered electrons. After passing the fourth grid (which is present to increase the energy resolution for AES

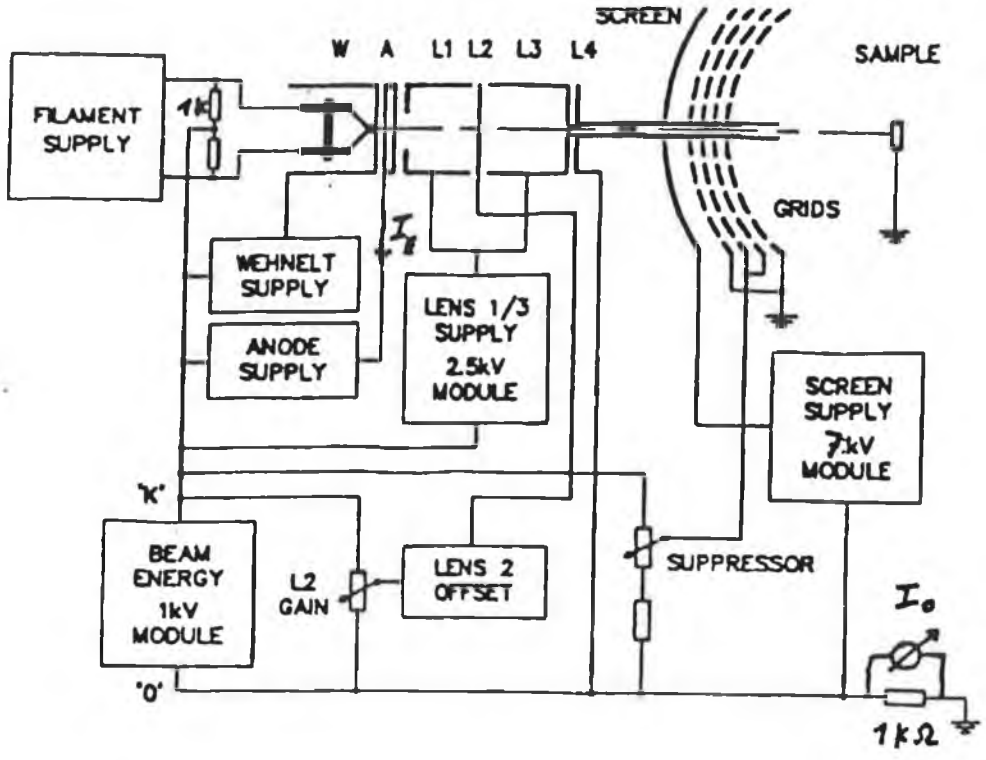

Fig 3.6 *Omicron SPECTALEED system schematic.*

- see next section - and is not present in the three grid Varian LEED system), scattered electrons are accelerated onto a fluorescent screen by a positive potential of 6 kV. The screen thus exhibits diffraction spots whose position is determined by the reciprocal lattice geometry as described in Section 3.4.1.

3.5 Auger Electron Spectroscopy

An atom which has been ionized in one of its core states may return to the ground state via one of two processes:

i) A higher level electron "falls" into the core hole with the subsequent emission of an X-ray photon, or,

ii) The core hole is filled by an outer electron but the energy is transmitted to another electron which leaves the atom with a characteristic kinetic energy.

This second process is termed the *Auger effect* [2] and is illustrated in Fig 3.7. X-ray emission is governed by selection rules for dipole radiation whereby the quantum number of orbital angular momentum must change by 1. On the other hand, the Auger process is not dependent on these selection rules and is a true radiationless process due to electrostatic interaction between the hole in an incomplete shell and the surrounding electrons. The transition probability is determined essentially by the Coulomb interaction. There is a strong energy dependence which reaches a maximum at 3-5 times the ionisation energy.

If the electronic states in a particular Auger process are deep-lying core-levels, the situation with a solid will be quite similar to that with free atoms, as these states will not

be strongly perturbed by chemical bond formation. If Auger electrons are emitted from the valence band, complications arise, especially if an adsorbate overlayer is present. In principle, any type of radiation with the ability to ionize inner shells of atoms may be used to excite Auger electrons. An electron beam is the standard source. Observation of Auger electrons with a kinetic energy around 1 KeV means an observation depth of about 15 Å. Typical escape depths are in the 5-20 Å range. Auger studies for this thesis were principally carried out using the Omicron SPECTA LEED/AES system. As described in Section 3.4.2, this system is a four grid Retarding Field Analyzer (RFA). Because of the small Auger signals, AES was carried out in the common derivative mode to suppress the effects of the large secondary electron background and highlight the Auger transitions.

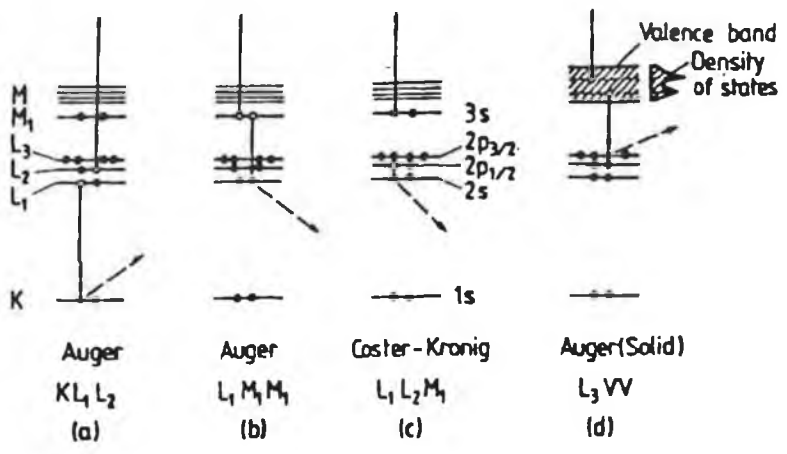

Fig 3.7 *The Auger process (from ref. 3) , (c) - the Coster-Kronig process, refers to a situation where the Auger electron arises from a transition between energy levels of the same shell.*

3. 6 Angle-Integrated Photoemission

Photoemission Spectroscopy performed with UV photons (UPS) or X-ray photons (XPS) is based on the photoelectric effect. The sample is irradiated by monochromatic photons which excite electrons from occupied to unoccupied states and thus into vacuum where they are detected by an analyser. The energy distribution curve (EDC) of the *photoelectrons* yields a qualitative image of the distribution of occupied states of the sample. Electrons that have lost "quasi-" continuous amounts of energy due to multiple scattering appear as a secondary electron background. Sharp peaks superimposed on this background correspond to kinetic energies of detected photoelectrons given by:

$$E_{kin} = h\upsilon - E_i - \phi \qquad (3.9)$$

where E_i is the binding energy of the initial state and ϕ the work function. All energies may be referred (in the case of a semiconductor) to the Fermi level of a metal layer, determined from the onset of photoelectron emission. (Both sample and reference metal layer must remain at ground, or a fixed potential). A typical EDC is illustrated in Fig.3.8.

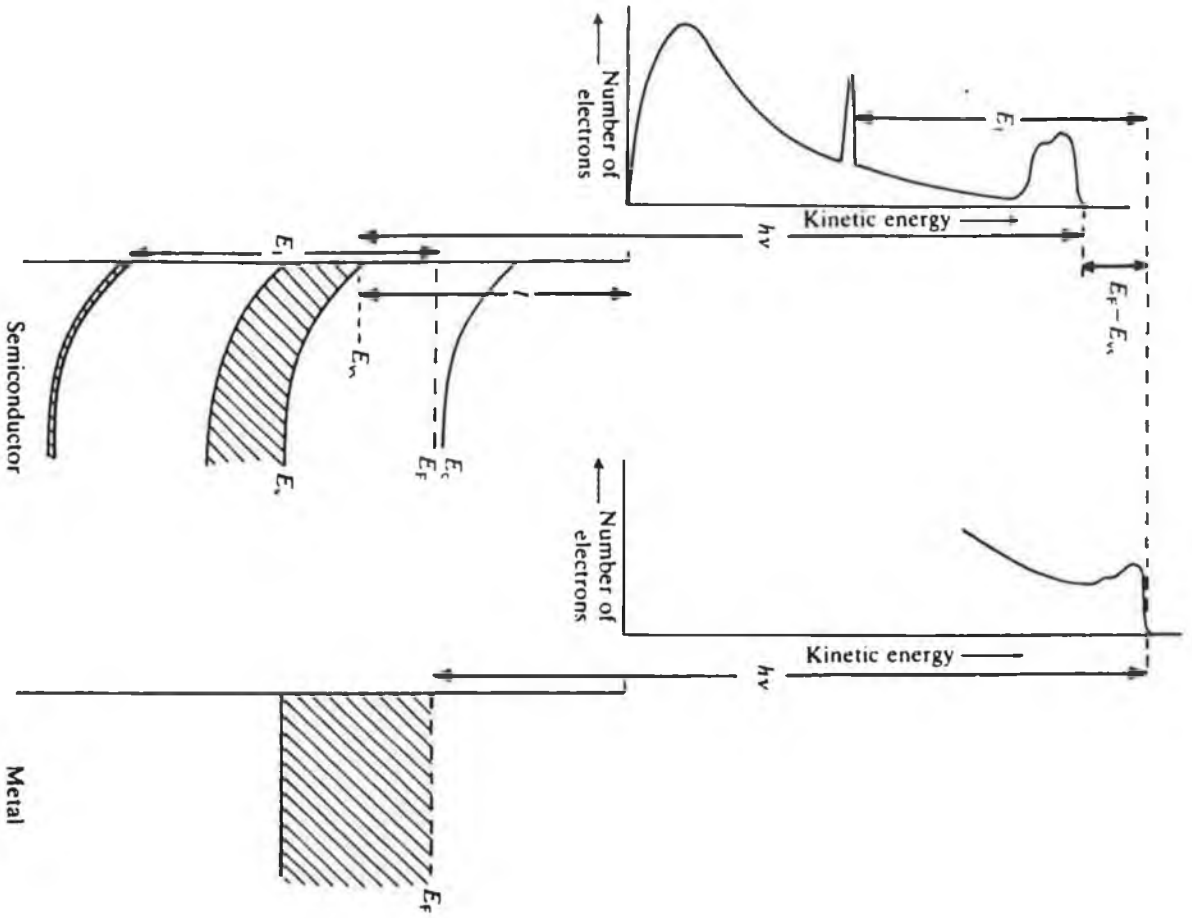

Fig 3.8 *Energy band diagrams for semiconductor and metal with corresponding EDC (From Ref. 4).*

Photoelectrons in the 20-100 eV kinetic energy range have path lengths comparable to the lattice spacing, so up to 30% of the total number of electrons in the spectra derive from the top layer of atoms.

The use of angle-integrating electron analysers gives integrated information about the distribution of electron energy states over a large region of reciprocal space. A determination of photoelectron wave-vector enables the dispersion of electronic bands (E(k)) for bulk and surface states to be determined. This can be achieved by means of an electron energy analyser with small angular aperture and the technique is known as *Angle Resolved Ultra-Violet Photoemission Spectroscopy (ARUPS)* .

A rigorous theoretical approach to photoemission requires a full quantum mechanical treatment of the process in which an electron is excited from an occupied state, leaves the solid and is detected at the analyser. Theoretical approaches such as this treat photoemission as a *one step process* [6]. In a solid, band gaps exist where there are no allowed electron states, whereas in the vacuum all states are allowed free electron states. Wave functions of the total system, vacuum plus solid, must fulfill existence conditions on both sides and will be connected by quantum mechanical conditions at the interface. For an electron with a short mean free path in the solid, the free electron wave (in the vacuum) couples to a damped, decaying wave. The coupling matrix element will thus vanish everywhere except near the surface due to the limited spatial overlap of the wavefunctions. A less accurate but more instructive approach to the above is the *three-step model* [7] in which the photoemission process is separated into three independent parts:

i) Optical excitation of an electron from an initial into a final state;
ii) Propogation of this excited electron to the surface/vacuum "interface";
iii) Emission of the electron from the solid into the vacuum with conservation of $k_{||}$;

These three steps are, in reality, not independent of each other but this treatment leads to a simple factorisation of the corresponding probabilities in the photoemission yield.

The optical excitation of an electron is described by the Golden rule[8] transition probability dependent, principally, on :

$$|< f,k \,|H|\, i,k>|^2 \qquad (3.10)$$

where i, k > and f, k > are Bloch states with negligible change in wavevector k. The perturbation operator, H, is given by the momentum operator and the vector potential A of the incident electromagnetic wave:

$$H = e/2m \,(A\cdot p + p\cdot A) \qquad (3.11)$$

This transition probability is more commonly referred to as the *photoionisation cross section* for a particular state of a particular element. It has been shown by Cooper[9] that

the photoionisation cross section for a particular level is highly energy dependent and may pass through a *"Cooper minimum"* .

The exact value of the binding energy measured for a given state depends on its chemical environment. Core level states will exhibit shifts in binding energy due to an altered chemical state of the element. The energy of an electron in a core level is determined by the attractive potential of the nuclei and a screening potential due to the repulsive Coulombic interaction of the other electrons. A change in the chemical environment of a particular atom involves a spatial rearrangement of its valence electrons. The change in binding energy and therefore the chemical shift ΔE_i experienced by an atom i in two different compounds A and B with valence charges q_i^A and q_i^B, respectively, can be expressed :

$$\Delta E_i^{A,B} = k\,(q_i^A - q_i^B) + (V_i^A - V_i^B) \qquad (3.10)$$

where k is a coupling constant which relates the interaction between the core and valence electrons and V_i is the Madelung potential. The first term on the right-hand side of equation 3.10 takes account of the fact that a decrease in valence electron density on atom i is accompanied by an increase in binding energy. The second term is a measure of the potential due to the other atoms which surround atom i. For most solids both terms are of the same order of magnitude and partially cancel, with the result that values of chemical shifts tend to be of the order of a few eV or less. The most appropriate approach to the consideration of chemical shifts is to compare the electron states of an N electron system with those of the (N-1) electron system left after photoemission. For a solid, N is very large and the (N-1) system will negligibly differ from the N system.

Nowadays *Synchrotron Radiation* has come to play a vital role in photoemission spectroscopy. A synchrotron yields a continuous spectrum of radiation extending from the far infra-red to the hard X-ray regime with the cut off energy dependent on the acceleration energy. Use of UV and X-ray monochromators provide an adjustable spectral source. Further advantages of synchrotron radiation other than photon energy tunability are its 100% polarisation in the plane of the ring (not utilised in these experiments), its high degree of collimation and stability and the availability of high photon fluxes. For the photoemission experiments detailed in Chapter 5, the synchrotron radiation was rendered monochromatic by a grazing incidence monochromator constructed at Daresbury Laboratory[10]. One of the principle features of the design is that only two reflections are required to monochromate the radiation. A 1200 l/mm blazed grating (to an angle of 1.89^o) manufactured by Tayside Optical Technology is used. The concave mirror occupies a fixed position along the lower line and the grating is simply rotated to scan wavelength.

A VSW HA100 Hemispherical Analyser was used to measure the energy distribution of electrons emitted from the sample surface. The analyser operates by electrostatically

focussing incoming electrons in such a way that only those within a certain range E_o + ΔE reach the detector (a channeltron electron multiplier). The *pass energy*, E_o, is defined by the balance between centripetal force and the electrostatic force of the field due to a voltage applied between two metallic hemispheres. In order to achieve a constant energy resolution ($\Delta E/ E_o$), the pass energy and thus the resolution can be held constant but the energy spectrum must be "shifted" through the analyzer energy window by variation of an acceleration or deceleration voltage before the analyser.

3.7 Sample Preparation

Detailed in the following sections are the procedures used to prepare samples for both ambient STM investigations and also *in situ* UHV studies (STM, LEED, AES, SXPS/UPS).

3.7.1 Flash Annealing of Silicon Surfaces

Both Si(111) and Si(100) wafers were cut from commercially available wafers (Wacker). After rinsing in acetone and ethanol, the samples were clamped into a tantalum holder and transferred into the UHV system. Following degassing at 400°C for, typically, 8 hours they were annealed a number of times to 900°C by electron beam irradiation and then cooled slowly. During the anneal the pressure was maintained in the 10^{-9} Torr range. This procedure resulted in large terraces, hundreds of angstroms wide, as imaged by STM with sharp LEED patterns. No oxygen or carbon signal was observed in AES spectra (above the detection limit of the system) with little adsorbate contamination visible in the STM images.

3.7.2 Arsenic Decapping

MBE grown GaAs epilayers, doped with Si to $1x10^{18}$ cm^{-3} and subsequently capped *in situ* with a protective arsenic layer were used for the S/GaAs investigations described in Chapter 5. These 2μm thick epilayers were grown on a GaAs(100) n^+ substrate[11] and stored in air for periods of time from 1 to 4 months. The samples were indium bonded to a tantalum sample holder and the As cap thermally desorbed in UHV to yield a clean GaAs surface. Earlier experiments indicated that use of Ta "wings" to hold GaAs(100) samples in place (as used for the Si samples) led to non-homogeneous removal of the As cap and the appearance of a range of reconstructions, as opposed to a single phase, across the surface.

For both the GaAs(100) and GaAs(111) surfaces examined, As desorption occured at temperatures in the 300-350°C range as monitored by mass spectrometry and the corresponding rise in chamber pressure. Depending on cap thickness, total pressures as high as $1x10^{-7}$ Torr were observed during decapping. The sample was held in the 300-350°C range while the partial pressures of As (75 amu) and As_2 (150 amu) first rose and then fell. After the pressure recovered and negligible levels of As and As_2 were present,

the sample was allowed cool to room temperature. Auger analysis was used to determine the cleanliness of the decapped samples. In a separate system (at Daresbury SRS), photoemission studies showed a large chemically shifted As oxide component which disappeared after removal of the cap. Clear (2x2) LEED patterns were observed for the GaAs(111) surfaces directly after decapping, whereas further annealing at various temperatures yielded the range of previously reported[12] reconstructions for the GaAs(100) surface.

As capped Si(111) samples were also investigated (Chapter 4) . Annealing of these samples to 450°C produced a sharp (1x1) LEED pattern with, again, no oxygen or carbon signal visible in the AES spectra.

3.7.3 Wet Chemical Treatment

The samples used for ambient oxidation and passivation studies detailed in Chapter 6 were cut from commercially available n-type GaAs(100) wafers with a doping concentration of $2x10^{18}$ cm^{-3} . Prior to passivation all samples were degreased and cleaned ultrasonically in de-ionised (DI) water, acetone and HPLC grade methanol. They were then placed in concentrated H_2SO_4 for 1 minute, etched in a room temperature H_2SO_4:H_2O_2:H_2O (5:1:1) solution for 3 minutes with continual stirring and then plunged immediately into one of the two passivating solutions described in the following section. An acidic etch such as that described should remove surface oxides and etch the GaAs substrate, leaving a residue of elemental As on the surface.

3.8 Sulphur Treatment

Two methods of sulphur treatment of semiconductor surfaces were used. For ambient STM studies aqueous sulphide solutions were employed, whereas a more precisely controlled flux of sulphur was achievable from a UHV compatible electrochemical sulphur cell. Both these sources of sulphur are described in the following sections.

3.8.1 Aqueous Sulphide Treatment

For P_2S_5 /$(NH_4)_2S$ and P_2S_5 /$(NH_4)_2S_x$ passivation, a procedure very similar to that of Dagata *et al.*[13] was followed. After solvent cleaning and etching of the sample it was plunged into one of two passivating solutions.These solutions differed only in the amount of excess sulphur they contained and were prepared as following:1g P_2S_5 was dissolved in 20 ml of either a $(NH_4)_2S$ or $(NH_4)_2S_x$ ($x \cong 2$) (having a 10% excess sulphur concentration) solution, 60 ml of water added and the solution stirred.After leaving the sample in the solution for 10 minutes it was then heated to 50^0 C for 10-15 minutes.Earlier preparations involved boiling this solution, however this results in a cloudy appearance and the sample surface becomes caked in a thick layer of amorphous

sulphur.After removal from the passivating solution the sample was given a brief methanol rinse (HPLC grade) and blown dry in nitrogen.

3.8.2 Electrochemical Sulphur Cell

The deposition of sulphur *in situ* using an electrochemical sulphur cell provided a novel "dry process" approach to sulphur treating semiconductor surfaces. The sulphur flux is generated by the decomposition of silver sulphide Ag_2S at temperatures of around 300°C, using the Pt/Ag/AgI/Ag_2S/Pt cell[14] illustrated schematically in Fig.3.9. The electrode array was prepared by fusing powders of silver, silver iodide and silver sulphide together with a sheet of platinum mesh in a KBr press under 1 tonne of pressure to form a cylinder of approximately 1cm in both length and diameter. A silver disc placed next to the fused silver powder provided electrical contact for the silver iodide cathode, while the platinum mesh made contact with the silver sulphide anode. The cell was then fitted tightly into a glass tube, one end of which had a 4 cm long capillary with a 5mm i.d. orifice through which the sulphur effused. External electrical contact to the anode and cathode was made via platinum leads. Sufficient pressure contact was maintained on the cell by means of a glass piston which was secured to the tube using steel springs. A sheet of stainless steel together with several windings of tungsten wire provided uniform heating of the electrolyte array when a current of 10 A was allowed to flow. The entire cell was mounted on a $2^3/_4$" flange providing a vacuum compatible sulphur source.

Silver sulphide coexisting with metallic silver at 200°C contains a large silver excess, whereas silver sulfide coexisiting with liquid sulphur at 200°C has a very nearly ideal stoichiometry. The chemical potentials and therefore the activities of both the silver and sulphur atoms in the silver sulphide vary with stoichiometry - changing the cell EMF changes the chemical potential and activity of sulphur in the silver sulphide and thus the gas phase pressure of sulphur over the cell. Furthermore, silver iodide is an ionic conductor and acts as a source or sink to the silver ions by transporting them from the silver sulphide to the silver. If an EMF is applied to the cell, current will flow through the cell as silver ions are removed from the silver sulphide until the stoichiometry has reached the point where the natural EMF of the cell is equal to the applied EMF. Sulphur vapour effusing from the orifice in the cell will cause an ionic current to flow, removing silver from the silver sulphide and maintaining the nonstoichiometry against the loss of sulphur. This current (typically 0.5 mA for the experiments detailed in this thesis) is then a direct measure of the sulphur flux effusing from the cell. Both Si(100) and Si(111) surfaces were exposed to this beam of sulphur for times ranging from 30 seconds to 2 minutes. GaAs(100) and GaAs(111)B surfaces were exposed to sulphur for, typically, five minutes. Auger studies revealed that a saturation coverage of sulphur was reached after the 5 minutes exposure.

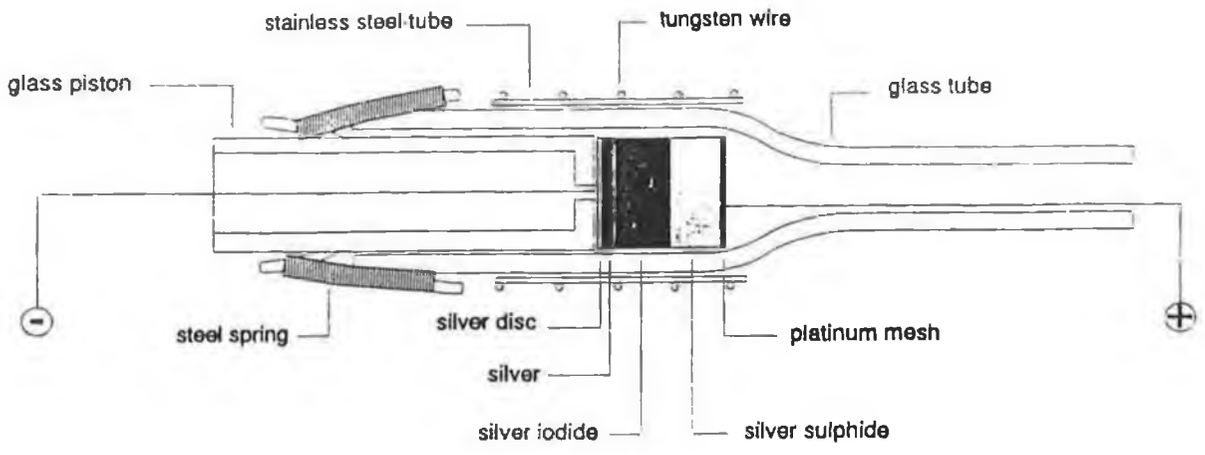

Fig 3.9 *Schematic representation of electrochemical sulphur cell. (From ref. 5)*

References

1. W. Ehrenberg, *Phil. Mag.* **18** 878 (1934)
2. P. Auger, *J. Phys. Radium* **6** 205 (1925)
3. H. Luth, *Surfaces and Interfaces of Solids,* (Springer Series in Surface Science, Vol. 15)
4. E. H. Rhoderick and R. H. Williams, *Metal-Semiconductor Contacts*, 2nd Ed. (Oxford Science Publications,1988)
5. L. Roberts, Ph.D. Thesis, Dublin City University (1993)
6. B. Feuerbacher, R. F. Willis, *J. Phys. C* **9** 169 (1976)
7. C. N. Berglund and W. E. Spicer, *Phys. Rev. A* **136** 1030 (1964)
8. D. P. Woodruff and T. A. Delchar, *Modern Techniques of Surface Science* , (Cambridge University Press, 1980)
9. J. W. Cooper, *Phys. Rev.* **128** 681 (1982)
10. M. R. Howells, D. Norman, G. P. Williams, and J. B. West, *J. Phys. E: Sci. Instrum* **11** 199 (1978)
11. The As/GaAs(100), As/GaAs(111) and As/Si(111) wafers were kindly provided by Dr. D. A . Wolff, University of Wales, Cardiff.
12. P. Drathen, W. Ranke and K. Jacobi, *Surf. Sci.* **77** L162 (1978)
13. J. A. Dagata, W. Tseng, J. Bennett, J. Schneir and H. H. Harary, *Appl. Phys. Lett.* **59** 3288 (1991)
14. W. Heegeman, K. H. Meister, E. Bechtold, and K. Hayek, *Surf. Sci.* **49** 161 (1975)

CHAPTER IV: A STUDY OF THE INTERACTION OF MOLECULAR SULPHUR WITH THE SILICON SURFACE

A description of the clean (111) and (100) silicon surfaces is followed by a discussion of the possibility of using a group VI atom, like sulphur, to passivate either surface. The reaction of sulphur with both Si(111) and Si(100) is then described and compared to the ideal As/Si(111) system.

4.1 The Clean Silicon Surface

An enormous research effort has been concentrated on silicon over the last thirty years or so due to both its practical importance in the semiconductor industry and a fundamental scientific interest in its elemental semiconductor properties. A group IV element, silicon forms tetrahedral sp^3 bonds and therefore displays a diamond-like structure. It still continues to dominate in all areas of solid state electronics except in optoelectronic and high frequency device technology where III-V semiconductors , due to their direct band gap and high electron mobility properties, are more commonly utilised. Both Si(111) and Si(100) surfaces can be prepared, without prior ion bombarding, by "flash-annealing" to temperatures in the 900-1100°C range (Chapter 3). The Si(111) surface thus exhibits a sharp (7x7) LEED pattern, whereas on the (100) surface one observes the appearance of a (2x1) reconstruction. Both the electronic and geometric structure of these reconstructions have been extensively investigated by STM and are described in the following sections.

4.1.1 The Structure of The Si(111)-7x7 Reconstruction

The (7x7) reconstruction of the Si(111) surface is one of the more complicated structures encountered in surface science to date. Since its first observation[1] it has been the subject of intense theoretical and experimental research with the *Dimer-Adatom-Stacking Fault (DAS)* model proposed by Takayanagi *et al.*[2] now currently accepted. The first STM studies of the (7x7) reconstruction by Binnig *et al.*[3] certainly played a major role in the elucidation of this structure.

A schematic diagram of the 7x7 as proposed by Takayanagi *et al.*[2] is illustrated in Fig. 4.1. Fig 4.2(i) is a typical STM empty state image and Fig 4.2(ii) a filled state image acquired simultaneously of the same area using the Omicron UHV STM. As with all STM images presented in this thesis, the data is rendered as a grey scale with lighter shades representing "higher" points. The maxima apparent in both STM images may be directly associated with the 12 top layer atoms (*adatoms*) in the DAS structure. These adatoms are each bonded to three second layer atoms, thereby eliminating three dangling bonds while introducing a new one. The two triangular sub-units of adatoms are surrounded by silicon dimers and rendered inequivalent by a stacking fault in the left sub-unit. Finally, at the corners of the unit cell there are silicon vacancies. As a result of

this complex reconstruction, from the 49 original silicon surface dangling bonds only 19 survive in the 7x7 unit cell. Six are located on the second layer, triply co-ordinated silicon atoms - the *rest atoms* . Twelve are on the adatoms and the final dangling bond is located at the atom on the bottom of the corner vacancy or, as more usually described, *corner hole.*

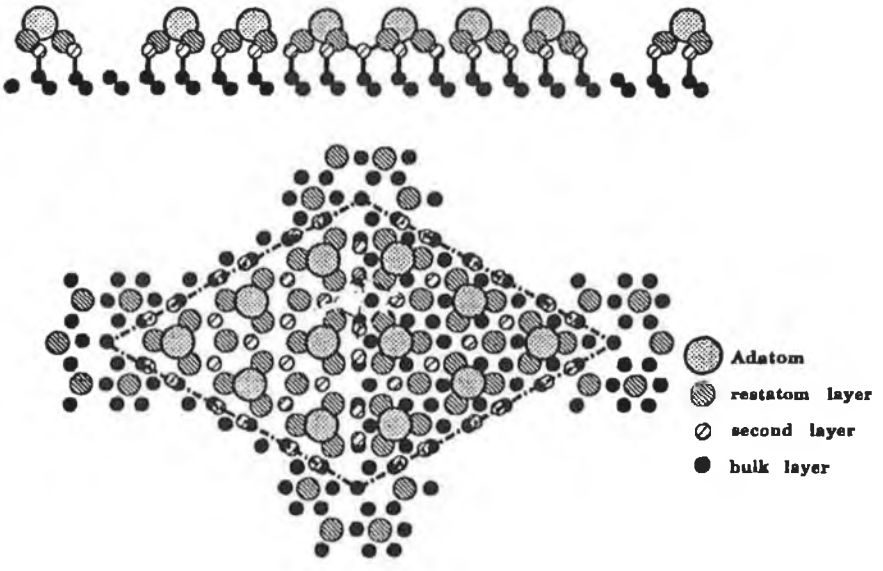

Fig 4.1 *The DAS model of the Si(111)-7x7 reconstruction. (From Ref. 3)*

While tunnelling from filled states (Fig 4.2(ii)) the asymmetry in the unit cell due to the stacking fault is immediately apparent. Chou *et al.*[4] studied the electronic structure of stacking faults in silicon and found that the fault introduces a new state at 0.1 eV above the valence band edge and dispersing into the valence band. This state contributes tunnel current to the tip when the sample is negative, making the stacking fault half of the cell appear higher than the other half. Furthermore, as the adatom dangling bond states lie closest to the Fermi level they are the most prominent feature in the tunnelling image. This is due to the fact that the tunnelling barrier is greater for states further removed from E_F, increasing by nearly an order of magnitude for each electron volt. The main conclusion to be drawn from STM studies of the Si(111)-7x7 reconstruction is that the mixture of geometric and electronic effects necessitates careful interpretation of the tunnelling images.

4.1.2 Si(100) - The (2x1) Surface

For the unreconstructed Si(111) surface, each surface atom will have one dangling bond. However, on the Si(100) surface - due to a termination of the bulk lattice in a different direction - there are two dangling bonds per surface atom. The bulk terminated, unreconstructed surface is shown in Fig 4.3. LEED studies[5] revealed that the (100) surface forms a (2x1) reconstruction. It is now accepted that this reconstruction involves

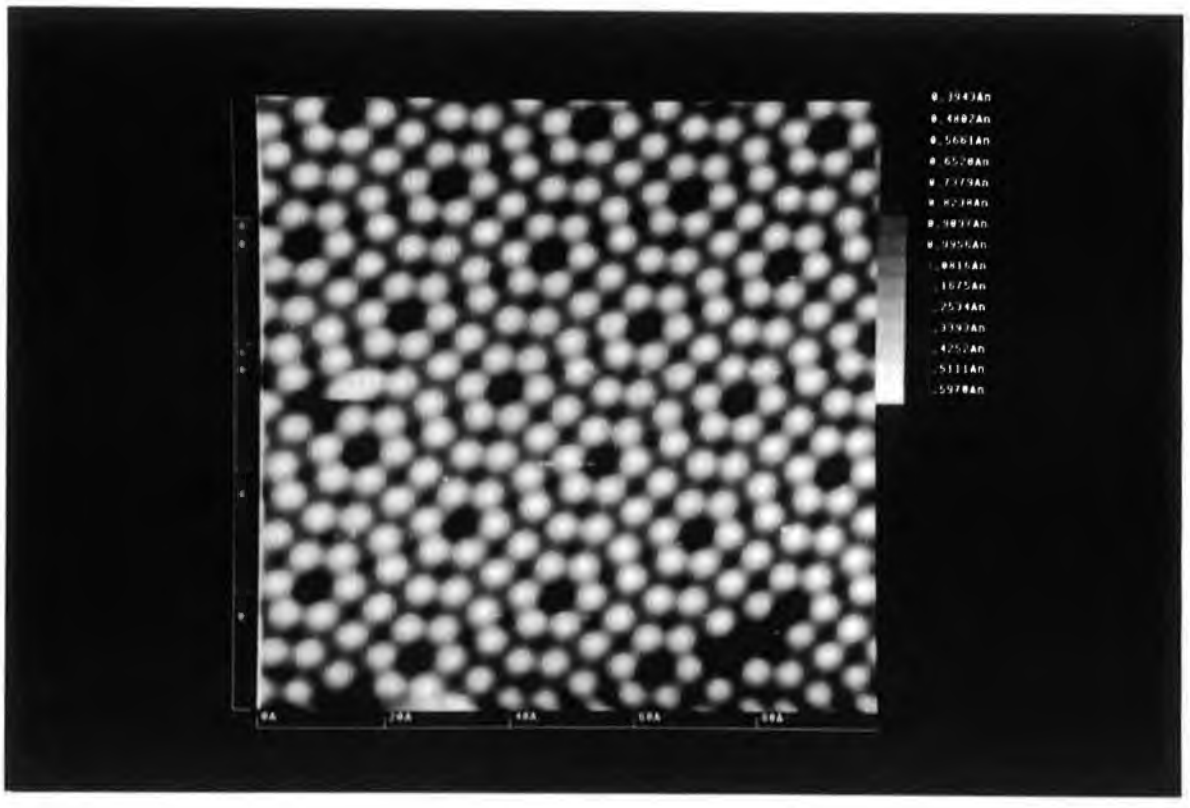

(i)

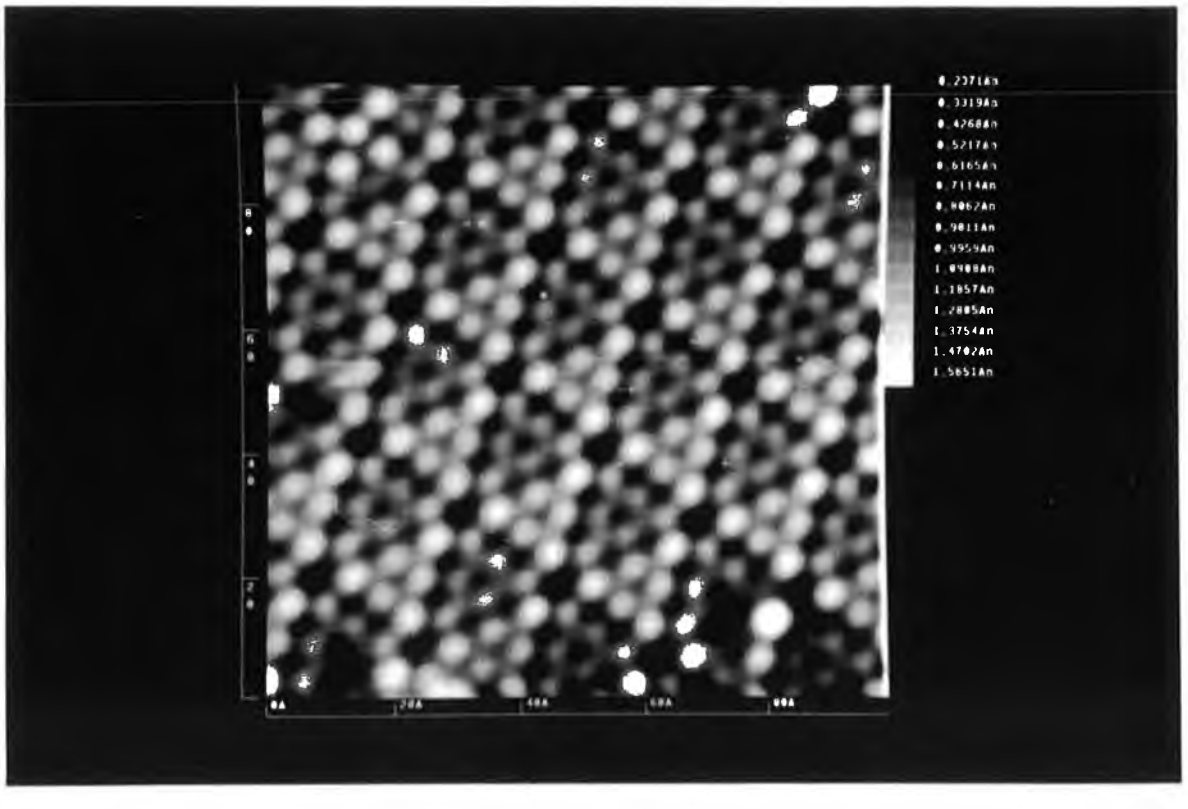

(ii)

Fig 4.2 (i) *An empty state image of the Si(111)-7x7 surface (V=-2V, I=1 nA)* **(ii)** *A filled state image (V=2V, I=1nA) of the same area acquired simultaneously.*

alternate rows of surface atoms moving together (without breaking bonds) to form rows of surface dimers as also illustrated in Fig 4.3. Half the surface dangling bonds are thereby eliminated, with one remaining dangling bond located at the ends of the dimers. These interact and form π bonding and π^* antibonding states. The two remaining electrons will occupy the π level. It is possible for these dimers also to buckle - such buckled dimers are visible in STM images at room temperature near defects. In fact it is thought that, at room temperature, the STM captures an average representation of fluctuating dimers switching between buckling extremes. An elongated symmetric protrusion centred over the dimer results. Wolkow[6] has shown that on cooling to 120K, the number of buckled dimers increased at the expense of symmetric appearing dimers. He concluded that only bistable dimers could account for this observation.

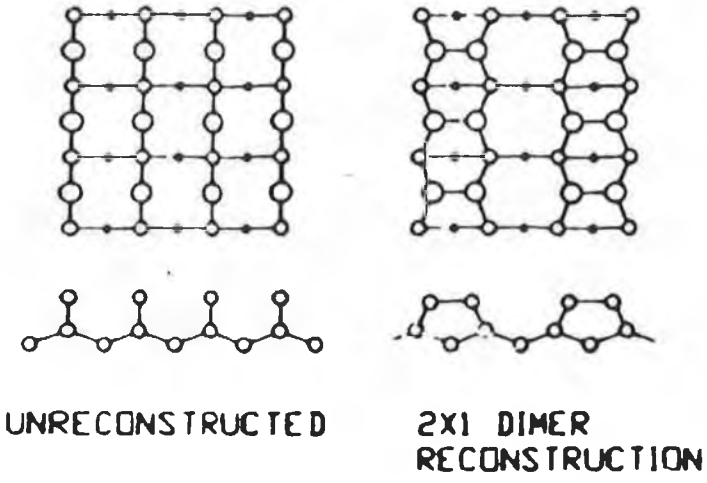

Fig 4.3 *The bulk terminated Si(100) surface and the (2x1) dimer row reconstruction.*

Dimers that are buckled due to their proximity to a defect, or naturally settle at room temperature in a buckled configuration, undergo a transfer of charge from the lower atom to the upper atom. A filled state image will show the charge densities due to the upper buckled dimer atoms. Both symmetric and buckled dimers are clearly visible in the STM image of Fig 4.4 (a). It should also be noted that on traversing a single atomic step on the Si(100) surface the dimer bond orientation, and thus the dimer row direction, rotates by 90°. This is easily visible in STM images (Fig 4.4 (b)) and gives rise to a two domain (2x1) LEED pattern.

4.2 Sulphur as a Silicon Surface Passivant?

As detailed in Chapter 2, sulphur passivation of III-V semiconductors has received a great deal of attention over the last number of years. Passivation of the Si(111) and Si(100) surfaces is readily achievable using arsenic as the passivating species. As the (111) surface has one dangling bond per surface atom, arsenic atoms are accomodated by replacing the outermost atoms in the silicon surface thus forming a (1x1) configuration and saturating three dangling bonds per adsorbed atom. A more in-depth description of

the As/Si(111) system is given in Section 4.5 below. On the Si(100) surface both Uhrberg*et al.*[7] and Bringans *et al.*[8] have determined that the three covalent bonds per arsenic adsorbate atom are accounted for by two bonds to the (100) surface and one As-As dimer bond.

Kaxiras [9] has suggested that as the Si(100) surface has two dangling bonds per atom, an investigation of the possibility of passivation of this surface with a group VI element (which tends to form two covalent bonds) would prove useful. He notes, firstly, that the most important aspect of surface restoration (i. e. the creation of an ideal (1x1) bulk termination) is the valence difference between the substrate and adsorbate[10]. In the ideal situation all surface dangling bonds are eliminated when the adsorbate atom replaces the bulk terminated plane. Such an atom he terms a valence-mending adsorbate (VMA). However, this adsorbate must exist in a bulk phase with the same local bonding geometry as the the restored surface. Therefore sulphur, tending to form twofold co-ordinated structures, is unlikely to restore the three-fold co-ordinated Si(111) surface. Surface stress, furthermore, plays a large role in determining whether the chosen adsorbate will restore the surface. If the covalent radii and bond angles of the adsorbate and silicon surface atoms are similar this is likely to lead to an increased stability. Finally, chemical reactivity must be taken into account. Using these criteria Kaxiras suggested[10] that both S and Se appear promising as VMA's on Si(100). They tend to form structures with twofold co-ordination and their average bond length is close to that of bulk silicon (though much closer in the case of Se than in the case of S). The S-Si bond energy is also larger than that of the Si-Si bond[11] which is more likely to lead to the formation of volatile Si_nS_m molecules rather than a stable S:Si(100) phase. In conclusion, Kaxiras states that both chemical reactivity and induced stress would tend to inhibit the formation of S:Si(100) as opposed to Se:Si(100).

Kruger and Pollmann[12] have concluded from *ab-initio* calculations of S adsorption on Si surfaces, that S adatoms are adsorbed in bridge positions above the surface in sites very close to the lattice positions of the continued bulk lattice to form S:Si(100)-(1x1). This is in contrast to the results of Kaxiras and, as will be seen in section 4.3, our STM and LEED data. Interestingly, Kaxiras has extended his work on the Se:Si(100) system to include first principles calculations on the structure of an ideal (1x1) phase with the silicon surface dangling bonds saturated by monolayer selenium coverage. This was shown to give rise to a surface state with large dispersion spanning the entire silicon band gap[9].

In the following sections, STM,LEED and AES results on the reaction of sulphur with both the Si(100) and Si(111) surfaces are described. No ideal S termination was found on either surface. The STM results, however, bear a remarkable similarity to similar studies of the reaction, and subsequent desorption of oxygen from the Si surface. As the Si-O bond length is much shorter than the Si-Si bond length and the Si-O bond is energetically much stronger, a stable O overlayer does not form on Si[10]. For this

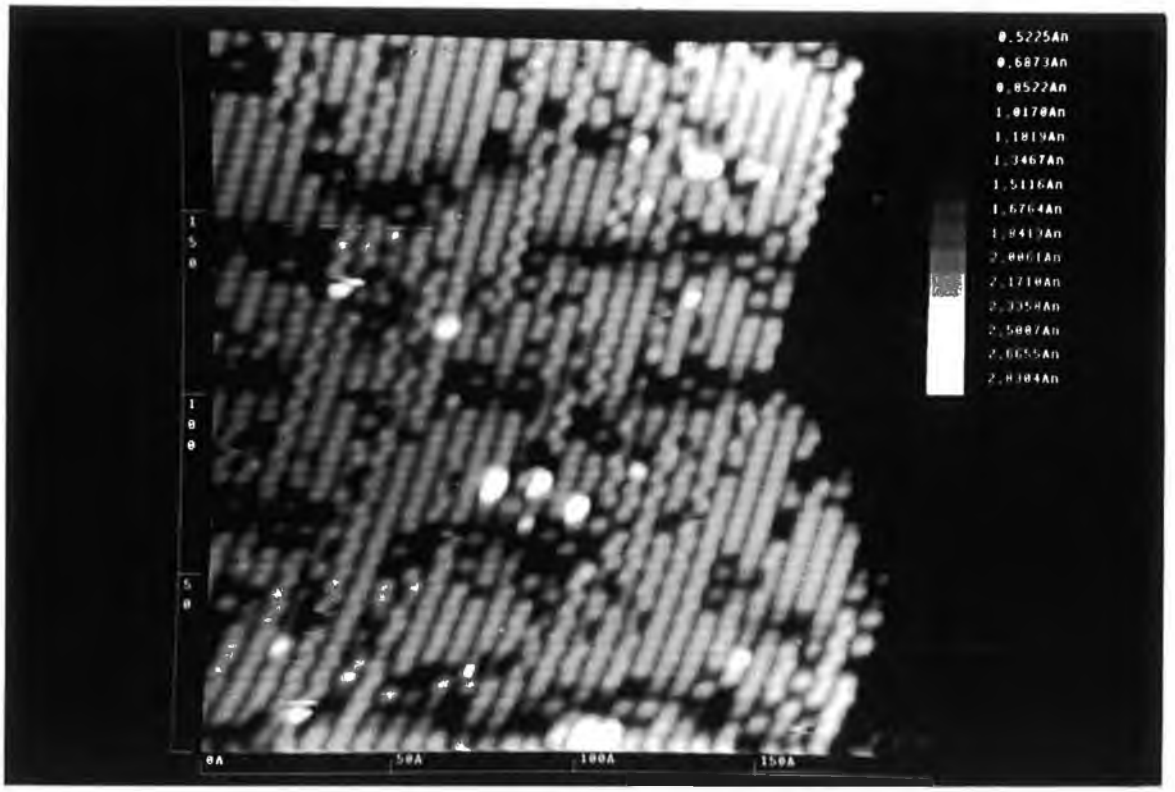

(a)

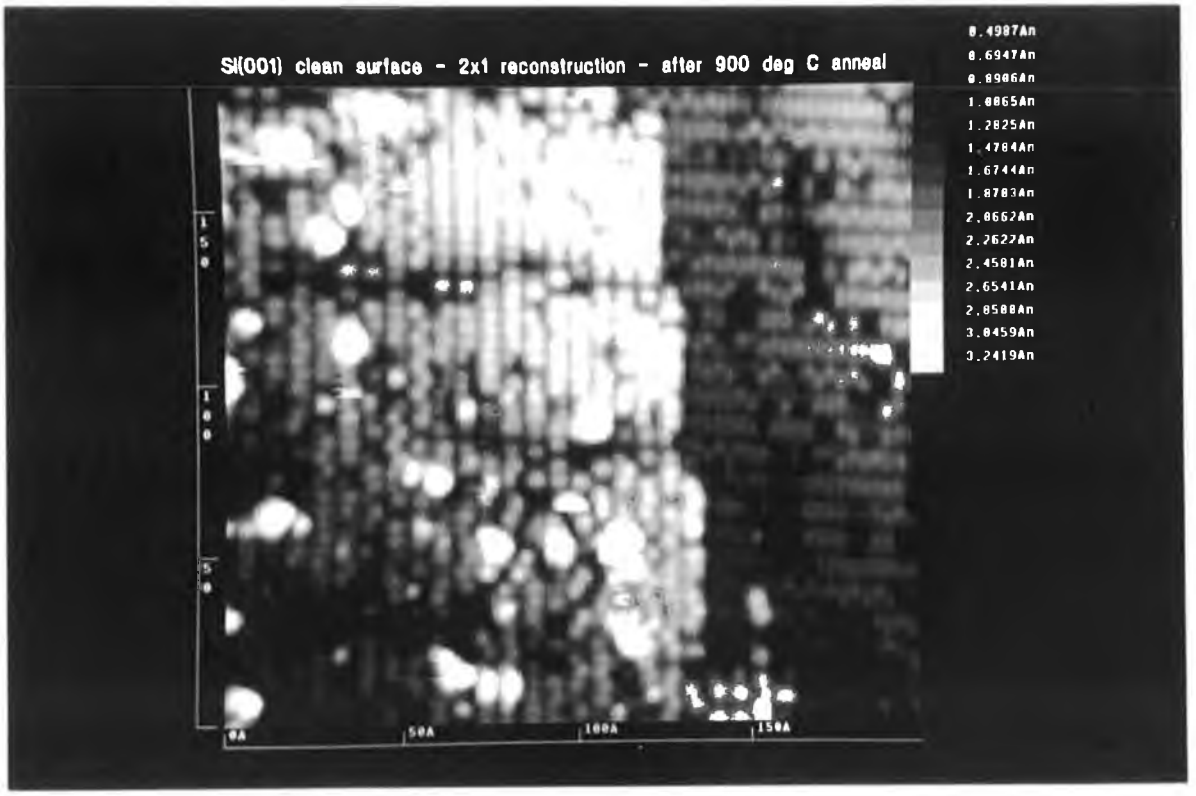

(b)

Fig 4.4 (a) *The Si(100) 2x1 reconstruction as imaged by STM* **(b)** *An image with an atomic step visible showing the rotation of the dimer rows from upper to lower terrace. (V=2V, I=1nA for both images)*

reason, STM studies of the oxidation of the Si surface have principally focussed on the initial (sub-monolayer) stages of adsorption. At very low coverages preferential sites for initial adsorption on Si(111)[13] and Si(100)[14] have been identified. Johnson *et al.*[15] have recently studied the decomposition and desorption of ultrathin oxide layers on Si(100) using STM, with Seiple *et al.*[16] having investigated elevated temperature oxidation and etching of the Si(111) surface. As will be described in the following sections, these groups' results regarding desorption of O from the Si surface are in very good agreement with our data on S desorption.

4.3 A Sulphur Induced c(4x4) Reconstruction of the Si(100) Surface

A c(4x4) reconstruction of the Si(100) surface has been reported by a number of authors from both LEED and recently published STM studies. Wang *et al.*[17] induced the c(4x4) reconstruction by thermally annealing the Si(100)-2x1 surface at 580-630°C for several minutes in UHV. Both Kato *et al.*[18] and Ide and Mizutani[19] have reported that the c(4x4) formed following exposure of the Si(100) surface to hydrogen and annealing in the 570-690°C range. Pandey[20] has proposed a π-bonded defect model for Si(100) reconstruction as an alternative to the buckled dimer model. By removal of a surface dimer, a defect is created. The removal generates a broken bond on each of the four second layer atoms to which the removed dimer was originally bonded. These sub-surface broken bonds can thus be completely eliminated by dimerisation, as shown schematically in Fig.4.5. The most energetically favourable defect density was suggested to be 25%. Ihara *et al.* [21] have proposed a further dimer defect on the basis of molecular dynamics simulations using a local pseudopotential. Their calculations predict the occurence of a metastable dimer state existing beneath the surface - an *interstital* dimer. The bond length of this dimer was seen to be longer than that of the surface dimer.

Wang *et al.*[17] proposed a modified π-bonded defect model for the c(4x4) reconstruction they observed, with defects distributed in a long range ordered form. Kato *et al.*[18] reproducibly formed the c(4x4) structure after high hydrogen exposure with subsequent annealing and suggested that the only essential difference between their results and those of Wang *et al.*[17] was the manner in which the excess of missing dimer defects were created. They also proposed the model of Wang *et al.*[17] for the c(4x4) structure they observed. Ide and Mizutani[19] have used STM to study the c(4x4) surface, again after hydrogen exposure. A comparison of filled- and empty-state images indicated the existence of a single dimer on the top layer in the c(4x4) unit cell. Uhrberg *et al.*[22] have similarly used STM to investigate the atomic structure of this metastable c(4x4) phase, created through hydrogen adsorption and annealing. First principles total energy calculations, in conjunction with their filled and empty state images, led them to propose a mixed ad-dimer model consisting of buckled dimers oriented parallel to the original dimer rows and symmetric dimers along the original (2x1) dimer rows. A schematic

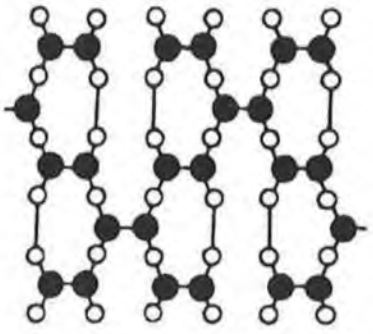

Fig 4.5 *π- bonded defect model of Si(100) reconstruction as proposed by Pandey (From Ref. 20). Filled circles represent the first layer atoms and open circles represent the second layer atoms.*

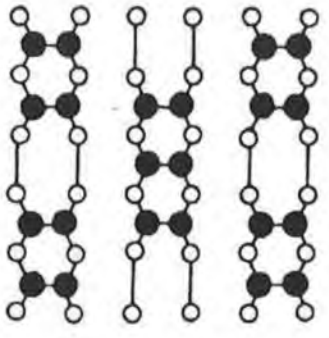

Fig 4.6 *Modified π-bonded defect model for the c(4x4) reconstruction as proposed by Wang et al. (From Ref. 16)*

illustration of this c(4x4) model is displayed in Fig 4.7. In the experimental study presented here, the appearance of a c(4x4) reconstruction on the Si(100) surface followed the thermal desorption of an adsorbed sulphur layer deposited *in situ.*

As described, Kaxiras' work [9,10] on sulphur as a silicon surface passivant or restorant suggests that such an ideal termination on the Si(100) surface is energetically unfavourable. A photoemission core-level study of the adsorption of molecular sulphur on the Si(100) surface was carried out by Weser *et al.*[23]. They reported that for room temperature adsorption, the sulphur bonded to the surface atoms with the surface retaining the (2x1) reconstruction with no evidence of additional spots related to an ordered overlayer. These results indicated that unlike the adsorption of sulphur on Ge(100) system where an ordered (1x1) bulk termination was found to occur by the same group[24], the adsorption of sulphur on Si(100) did not restore the silicon surface. When the adsorption process was studied at 200°C they found evidence from the presence of higher oxidation states that sulphur was penetrating into the bulk.

A clean Si(100)-2x1 surface was prepared and exposed to molecular sulphur as described in Chapter 3. The sulphur covered surface was subsequently annealed to

325°C over a 15 minute period with an equivalent time for cooling which helped to minimize thermal drift of the piezoelectric elements of the STM. The LEED pattern for the sulphur covered surface is shown in Fig.4.8(a). The (2x1) reconstruction spots are clearly visible, the only difference noted from the clean surface is an increase in background intensity. As described above, this behaviour was also noted by Weser *et al.*[23]

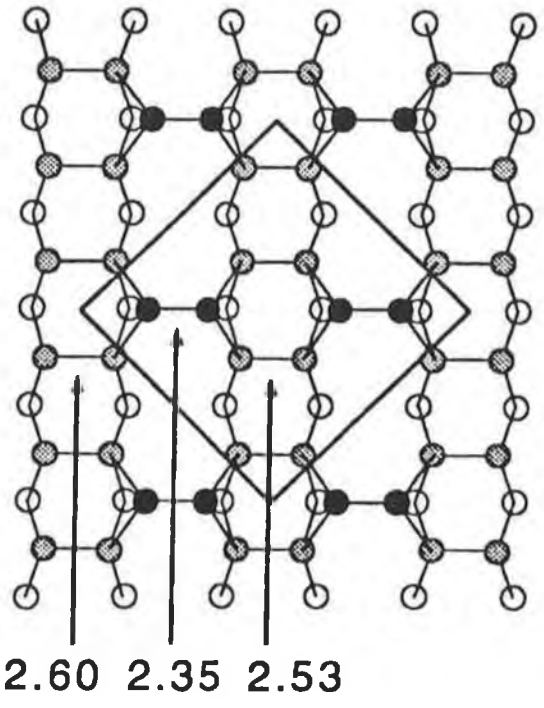

Fig 4.7 *Mixed ad-dimer model of Uhrberg et al. (From Ref. 22). Solid circles highlight the surface atoms.*

An estimate of the sulphur coverage from the attenuation of the Si (90 eV) Auger line, with respect to the signal for the clean surface, would indicate an approximate thickness of 1-2 monolayers. The fact that there appears to be no structural rearrangement following sulphur adsorption suggests that interaction between the sulphur and silicon surface at room temperature is weak. (This contrasts quite strongly with the adsorption of sulphur on GaAs(100) and GaAs(111) surfaces, as discussed in the following chapter). The STM image of the sulphur-covered surface illustrated in Fig 4.8(b) reveals the presence of an overlayer with a high density of vacancies. The distance between adjacent maxima in the tunnelling image is dependent on the direction of measurement. This distance, when measured along the direction of the underlying dimer rows, indicates a separation of 4-5 Å, while the distance perpendicular to this amounts to 7-8 Å. From this we deduce that the sulphur adsorbs preferentially along dimer rows. From these results it is quite evident that, for room temperature adsorption, there is no ideal (1x1) sulphur-terminated reconstruction. By investigating the variations in the intensity of the sulphur (152 eV) Auger line across the surface it was established that the

sulphur coverage was homogeneous, again in good agreement with the observation of Weser *et al.*[23]. The results of the *ab-initio* calculations of Kruger and Pollmann[12] led the authors to suggest that differences in their results (the formation of a stable S:Si(100)-(1x1) phase) and those of Weser *et al.*[23] were due to the S deposition procedure of the latter group (an electrochemical sulphur cell, of similar design to that used in this study).

After annealing of the sulphur covered surface Auger spectra taken at different positions on the surface revealed either no sulphur signal or a very small signal just above the detection limit of the system used (approximately 0. 1 ML coverage). This suggests that most of the sulphur was desorbed during the annealing cycle with a small amount remaining on the surface or diffusing into the crystal as reported by Weser *et al.*[23] for adsorption at 200°C. Fig 4.9 illustrates the sharp c(4x4) LEED pattern observed for the annealed surface. There were no changes in this pattern across the entire surface; therefore, we do not believe that sulphur directly contributes to the c(4x4) reconstruction, but rather that it is an adsorbate-induced structure involving only silicon atoms. As noted by Wang *et al.*[17], all the (2x1) LEED spots coincide with the integral and half-order spots of the c(4x4) reconstruction;therefore the c(4x4) can co-exist as domains on the (2x1) structure. The filled- and empty-state images of the c(4x4) surface illustrated in Figs 4.10(a) and 4.10(b), respectively, clearly show an ordering of features along the original dimer row direction. As in the images presented by Uhrberg *et al.*[22], the brightest features in Fig 4.10(a) outline the c(4x4) periodicity; however, the presence of these features is not necessary for the surface to exhibit this symmetry. From a comparison of the filled- and empty-state images of these features in Figs 4.10(a) and 4.10(b) we attribute them to symmetric dimers along the original (2x1) dimer rows, in agreement with the proposal of Uhrberg *et al.*[22]. On the right-hand side of Fig.4.10(a), (2x1) dimer rows can be observed (indicated by the A arrow) which are seen to split in the empty state image in Fig.4.10(b). This splitting along the (2x1) dimer rows is identical to the splitting of the brightest feature observed in the c(4x4) region of the surface confirming that this is indeed a symmetric dimer. A comparison between the height of these dimers in the c(4x4) pattern with the dimers along the (2x1) dimer rows indicates that they are at the same height. We believe that these "high dimers" in the c(4x4) pattern are the same as the feature resolved by Ide and Mizutani[19].

Areas of the surface in Fig 4.10 (b) are visible (indicated by the B arrow) where this "high dimer" is absent and there is an underlying pattern consisting of protrusions alternatively spaced by approximately 10 Å and 6 Å along the rows. This can be more clearly seen for the filled state of Fig.4.11 which allows the detailed structure of these underlying features to be more clearly resolved. It is also apparent that the "high dimer" is only ever observed in the 10 Å spacing along the original dimer rows. Uhrberg *et al.*[22] have similarly observed this variation in spacing between such neighbouring features which creates the c(4x4) symmetry. They attribute these protrusions to buckled, parallel

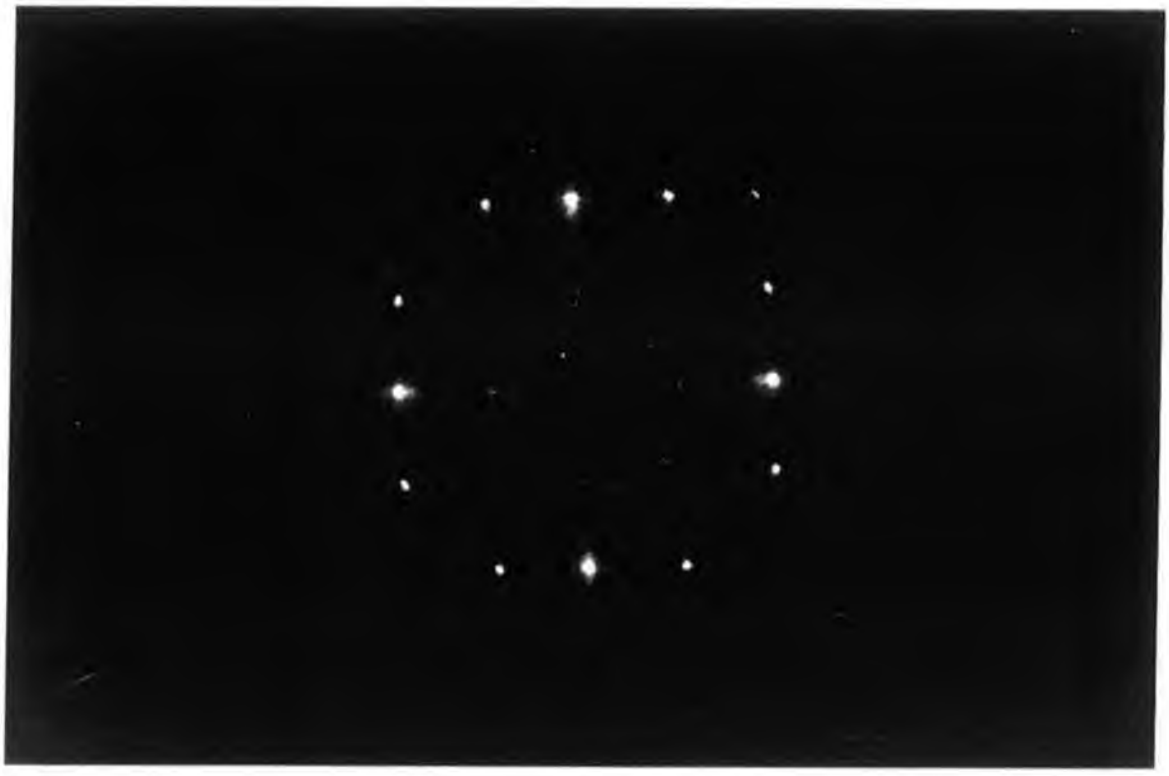

(a)

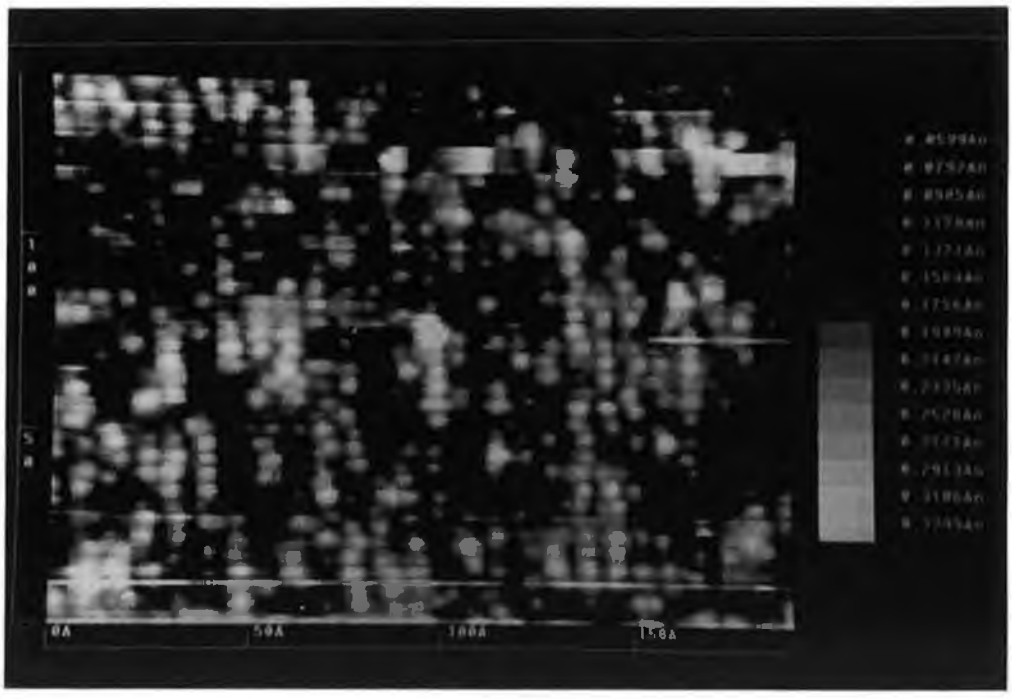

(b)

Fig 4.8 (a) *The (2x1) LEED pattern (EP = 41eV) and* (b)*the STM image observed for the sulphur-covered surface.*

ad-dimers in their "mixed ad-dimer" model. As discussed earlier, for silicon dimers, such buckling has been shown to give rise to charge transfer from the "down" to "up" atom resulting in the filled state image corresponding to predominant tunnelling from the "up" atom[25]. Conversely, the empty-state image should be dominated by tunnelling from the "down" atom. However, a detailed comparison between the empty state image in Fig.4.10(b) and the filled state image of Fig.4.11 reveals a direct registry between the periodicity of these underlying features in both images. Unfortunately, due to degraded resolution in the filled-state image of Fig.4.10(a), it was not possible to observe the detail of the underlying structure for a direct comparison with Fig.4.10(b). Nevertheless, since we can use the position of the symmetric "high dimer" as a reference point in both filled- and empty-state images, it is possible to confirm that there is no shift in registry between the positions of the underlying features, within experimental error. This is inconsistent with these features originating from buckled dimers since there should be a shift in registry between the filled- and empty-state images resulting in an inversion in the positions of the alternative "long-short" spacings along the dimer rows. It is therefore

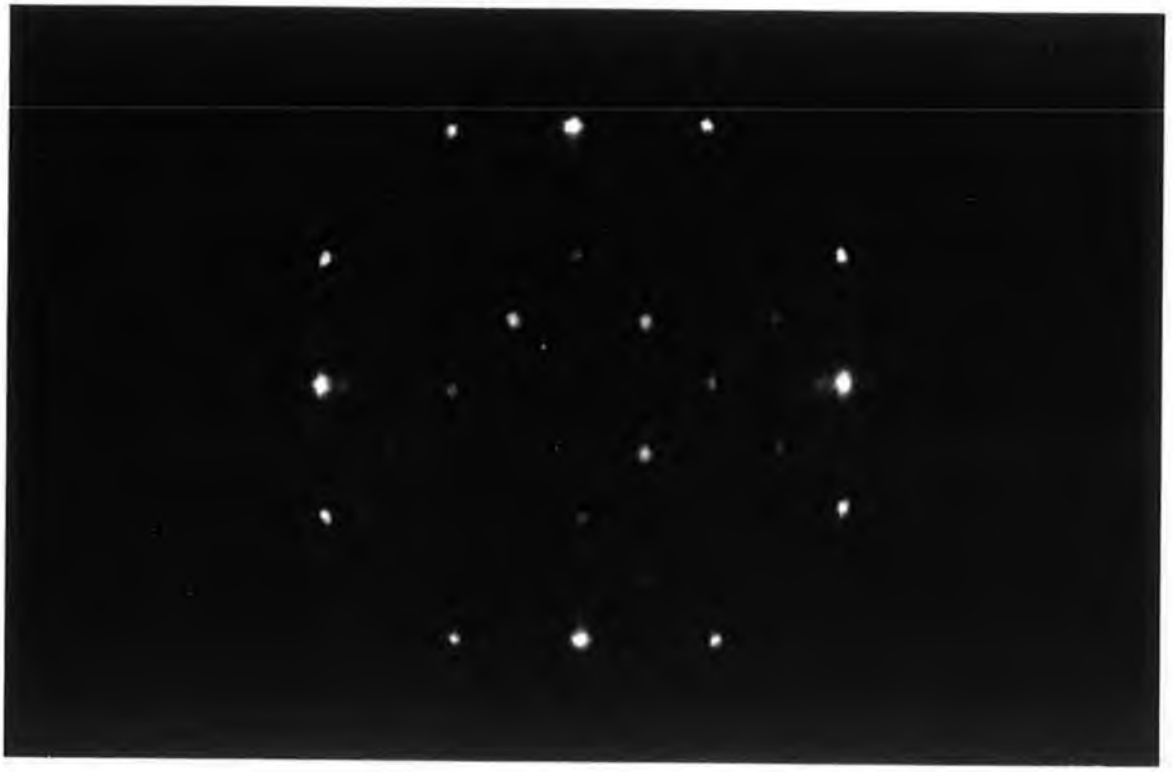

Fig 4.9 *The c(4x4) LEED pattern observed for the annealed silicon surface (EP = 66 eV).*

proposed that these protrusions consist of dimers which have an increase in the degree of π-bonding between the dangling bond states resulting from an increased degree of planarity of the c(4x4) structure. This would explain the narrowing in the width of the underlying dimer feature with respect to the high-dimer in the filled-state image and the inability to resolve the splitting in the empty state image of these underlying features. The increase in planarity of the c(4x4) structure, as first outlined by Pandey[20], is due to the presence of a high number (between 25% and 50%) of missing dimer defects.

The differences in the interpretation of the STM images presented in this work to those of Uhrberg *et al.*[22] can be attributed to the ability, in this study, to individually resolve protrusions in both filled- and empty-state images which are in direct registry. A schematic model of the c(4x4) reconstruction consistent with the experimental observations is presented in Fig.4.12(a) with the unit cell outlined. However, a model which satisfactorily accounts for the above experimental observations must be able to explain the identical alternating periodicity observed in both the filled- and empty-state images. A possible surface reconstruction consistent with this experimental observation would consist of alternate missing dimers and interstitial dimers resulting in a non-uniform spacing of the remaining surface dimers as illustrated schematically in Fig.4.12 (b). This structure would be a composite of missing dimer defects as described by Pandey[20] , alternating with interstitial dimers as proposed by Ihara *et al.*[21] along the original dimer rows and would not require the presence of the "high dimer" in order to reproduce the c(4x4) surface reconstruction observed .

Johnson *et al.*[15] have observed, with STM, a c(4x4) reconstruction of the Si(100) surface after thermal desorption of a monolayer oxide coverage. Although the model proposed by this group for the c(4x4) reconstruction is inconsistent with our results, it is interesting to note that O and S desorption from the Si(100) surface results in very similar behaviour. As detailed in Section 4.2, both the Si-S and Si-O bond energies are incompatible with surface restoration and the desorbing species creating defects in the surface layer are most likely SiO and Si_nS_m molecules respectively. A very recent study of Ar-ion bombarded Si(001) surfaces by STM[26] has also reported the appearance of a c(4x4) reconstruction. A model for this reconstruction was proposed whereby buckled dimers are arranged in anti-phase with missing dimer rows located between every other dimer line. This model, however, was based solely on empty state imaging and is also inconsistent with the STM images discussed above. What is interesting about that study is the appearance of the c(4x4) reconstruction due to the creation of defects caused by Ar-ion bombardment. In section 4.4, defect creation due to sulphur desorption from the Si(111)-7x7 surface is found to cause structures that have also been seen to occur on the 7x7 surface after bombardment with Xe ions at elevated temperatures[27]. Unlike previous studies[16-19], the appearance of the c(4x4) phase occured at a desorption temperature of 325°C, much lower than the 600-700°C anneal needed to create this reconstruction after hydrogen exposure. Furthermore, the observation that above a temperature of 700°C the

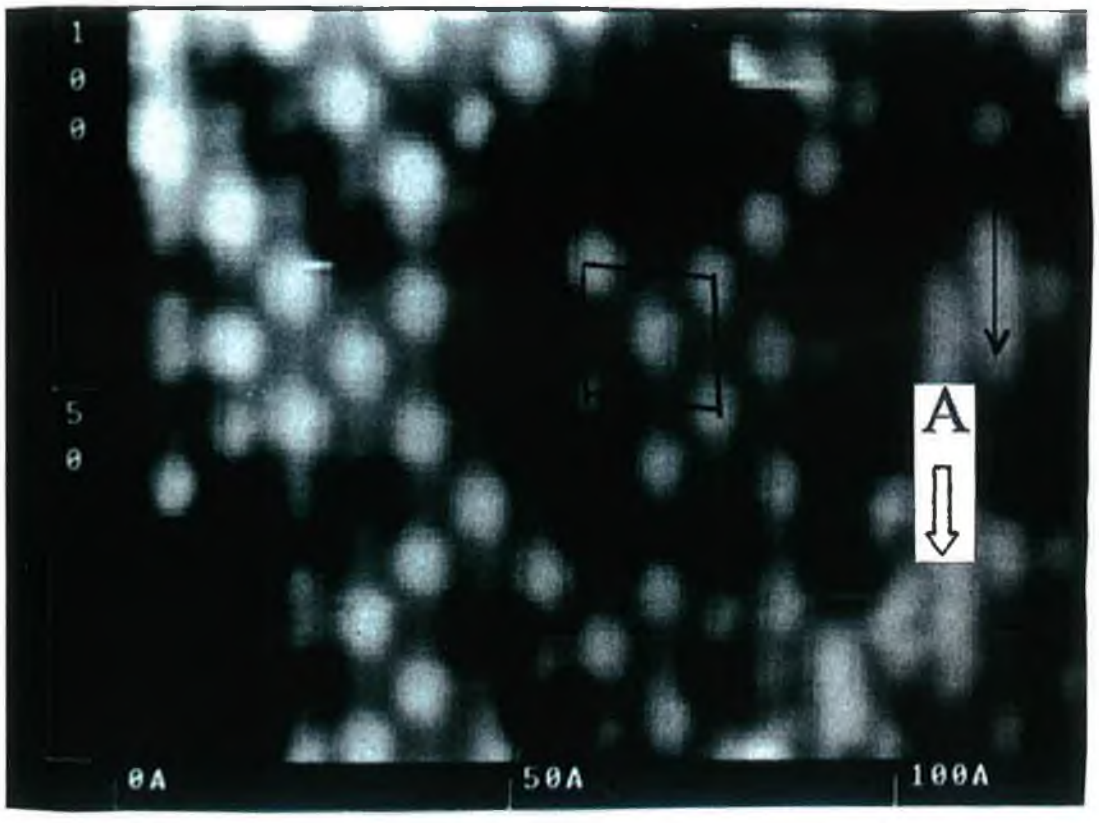

(a)

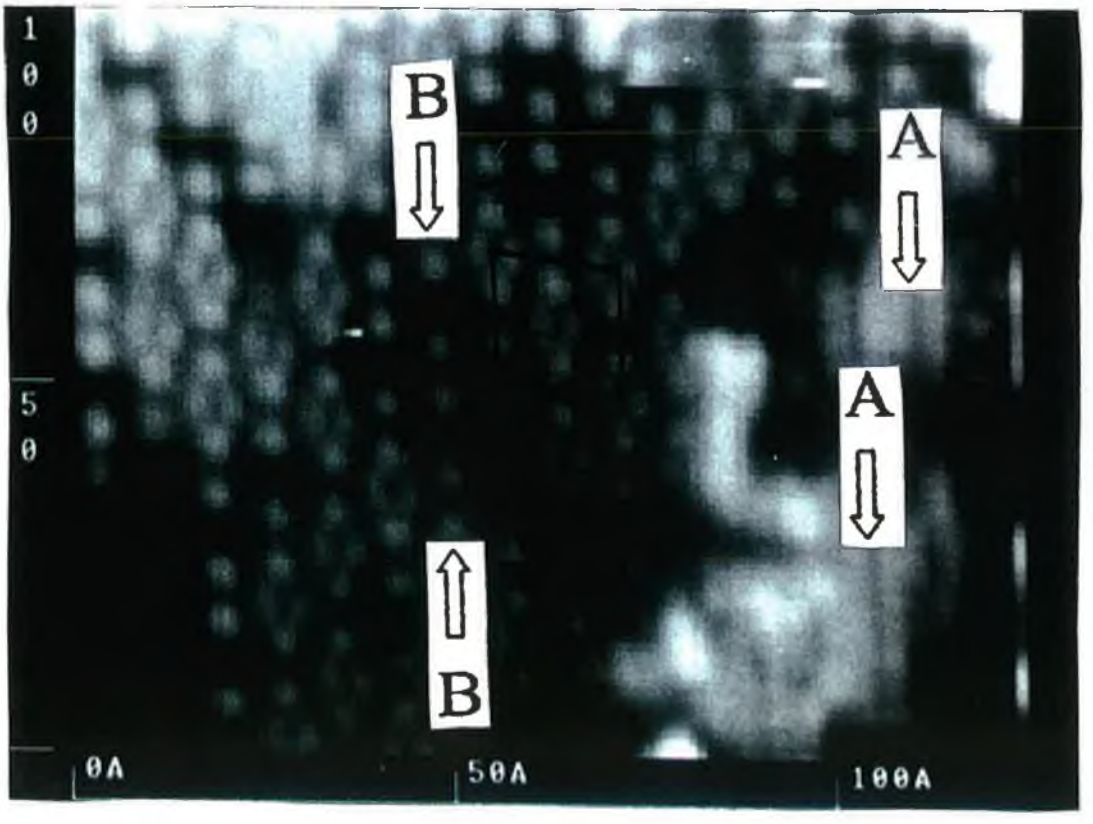

(b)

Fig 4. 10 *A filled-* **(a)** *and empty-* **(b)** *state image of the same surface region acquired simultaneously, showing the c(4x4) structure coexisting with (2x1) dimer rows on the right indicated by the A arrows. The B arrows indicate a region of the surface with no "high dimers" present.*

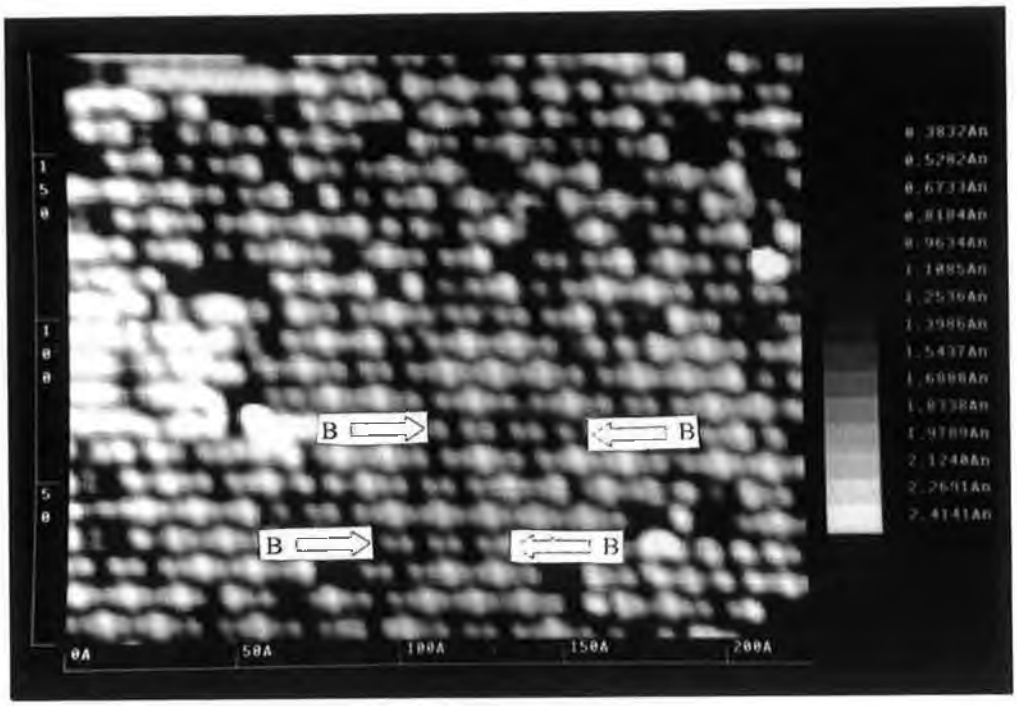

Fig 4.11 *A high resolution filled state image of the c(4x4) surface. The B arrows indicate dimer rows without "high dimers" present.*

c(4x4) surface transformed irreversibly to the (2x1) reconstruction is close to the 730°C temperature determined by Uhrberg *et al.* [22] for this transition.

Again, from a comparison with earlier studies, it is proposed that the c(4x4) surface reconstruction as described occurs as a result of defects created in the silicon surface region as a result of sulphur desorption. The creation of volatile Si_nS_m molecules as described by Kaxiras[10] could well be a possible source of surface defects as indeed would the penetration of sulphur into silicon at elevated temperatures as reported by Weser *et al.* [22]

4.3 Vacancy Creation on the Si(111)-(7x7) Surface due to Sulphur Desorption

The interaction of group VI elements other than oxygen with the silicon surface has received little attention other than the work of Kaxiras[9,10] and Weser *et al.* [23] detailed in the previous section. A brief overview of some research, using STM, directed at understanding the mechanism of oxygen induced etching and defect creation on the Si(111)-(7x7) surface will act as a broad overview of the reaction of a group VI species with this surface. The similarity of the oxygen and sulphur reactions with Si(111), as detailed later in this section serves to strengthen the validity of citing this work.

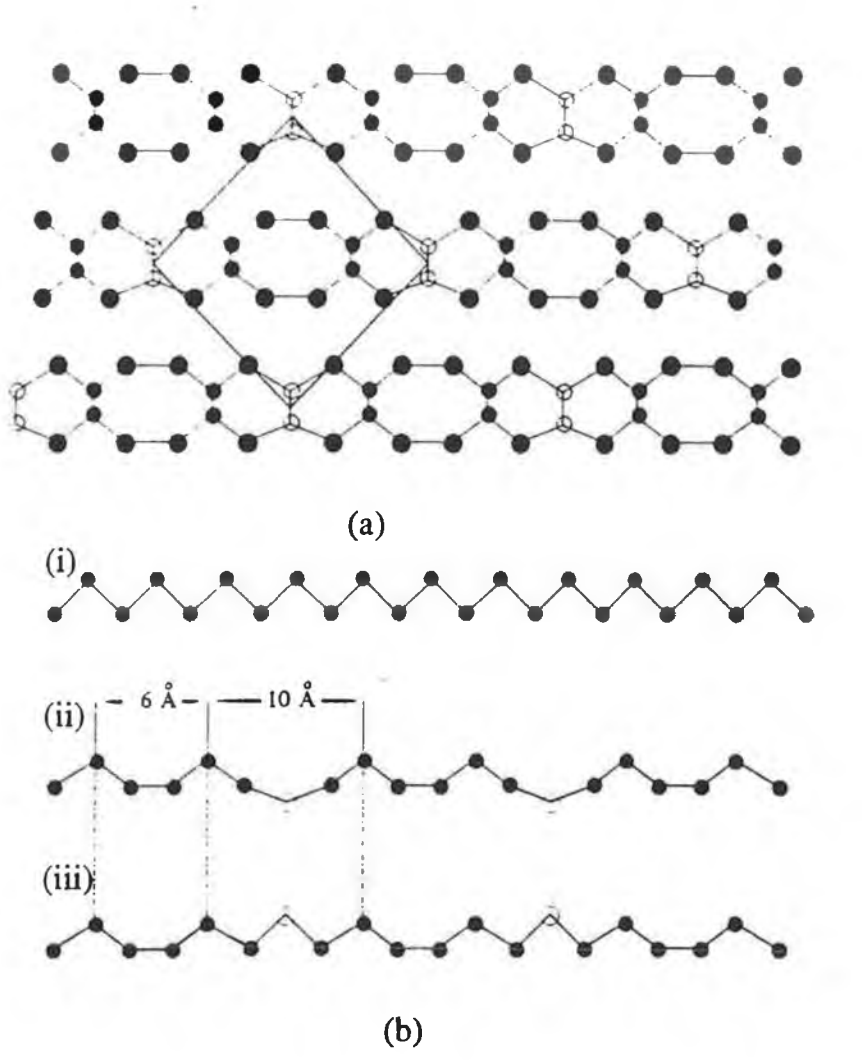

Fig.4.12 (**a**) *Proposed structural model of the c(4x4) surface, with open circles representing the possible sites of "high dimers", solid circles representing the dimers along the original (2x1) dimer rows and shaded circles representing the second layer atoms.* (**b**) *Section (i) original dimer rows ; section (ii) missing dimers interspaced with interstitial dimers ; and section (iii) missing dimers interspaced with "high dimers"*

Feltz *et al.* [28] have used *in situ* STM imaging to investigate high temperature oxygen induced etching of the Si(111)-(7x7) surface. They demonstrated that during the reaction at temperatures around 700°C, the initial etching process was via a step flow mechanism in the top silicon layer. At later stages the appearance of monolayer deep holes nucleating at structural imperfections in the surface layer was noted. These observations were thus explained by a vacancy coalescence mechanism where vacancy creation was due to desorption of a silicon oxide species. A comparable study of the initial oxidation of the Si(111)-(7x7) surface at elevated temperatures (400°C - 600°C) by Seiple *et al.* [16] also

demonstrated an oxygen induced etching process with the creation of surface holes and step edge retraction due to the coalescence of vacancies. The newly exposed surfaces often reconstructed into metastable 5x5 or 9x9 structures as well as the stable 7x7 structure.

A recent STM study of the thermal desorption of ultrathin oxide layers from the Si(100) surface by Johnson *et al.* [15] has shown that this process produces a high degree of pitting and a more ragged appearance to step edges. The authors concluded that the desorption of oxygen causes a redistribution of surface silicon atoms. Mobile Si atoms, not directly involved in SiO desorption, are trapped at terrace edges or under remaining oxide patches. Bedrossian and Klitsner[27] have observed similar vacancy coalescence and step retraction for sputter induced vacancies due to Xe ion bombardment. Furthermore they have determined that vacancy mediated sputtering can also lead to the appearance of surface regions containing a variety of local metastable reconstructions but no long range order. A number of metastable reconstructions other than the equilibrium 7x7 have been observed on the laser annealed Si(111) surface by Becker *et al.*[29]

A Si(111)-7x7 surface was prepared and exposed to a beam of molecular sulphur as detailed in Chapter 3. From the STM image of the sulphur covered surface illustrated in Fig 4.13(a) it is clear that no ordered termination of the 7x7 surface is present. A saturation coverage was not reached with any exposure - in this particular image the thickness of the sulphur overlayer, as determined from AES studies, is approximately 1.5 monolayers. LEED studies indicated that the surface retained a (7x7) diffraction pattern, with visibly weakened spot intensity and an increase in diffuse background as illustrated in Fig 4.13(b). This suggests that the interaction between the Si(111) surface and sulphur at room temperature is not strong enough to induce a structural rearangement of the silicon surface as was similarly observed for the S-Si(100) system at room temperature. Imaging at negative bias polarity (filled states) was unstable with no reproducible images formed. It is possible to see in a number of places the (7x7) unit cell corner holes. From their position we can deduce that there is no preferential adsorption on either the faulted or unfaulted half of the unit cell at this coverage.

After annealing of the sulphur covered sample at 375°C, the STM images reveal the presence of a number of monolayer deep holes in the otherwise well ordered 7x7 surface. It should be noted that the presence of sulphur could not be detected on the annealed surfaces above the detection limit of the AES system used (approximately 0.1 monolayer). In figure 4.14(a) monolayer deep holes are clearly visible with Fig 4.14(b) illustrating the presence of the 7x7 reconstruction at the bottom of a surface hole. Seiple *et al.*[16] have observed the occurence of similar behaviour after oxidation of the Si(111)-7x7 surface at 500°C, as have Bedrossian and Klitsner[30] following the bombardment of the Si(111)-7x7 surface with 225 eV Xenon ions at elevated temperatures. Both groups conclude that the depressions in the surface are due to coalescence of mobile vacancies created due to SiO desorption at low oxygen exposure[16], and ion sputtering[27],

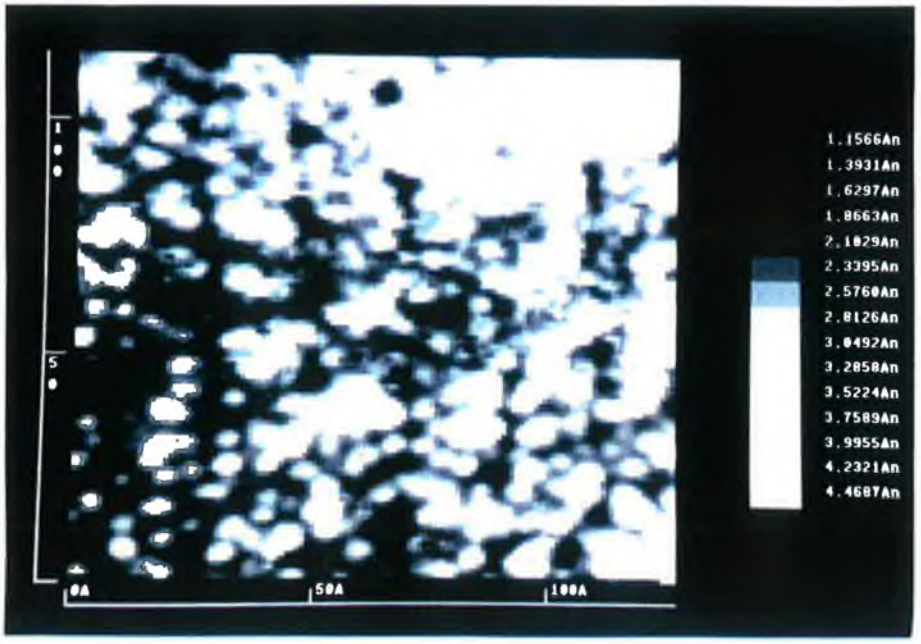

(a)

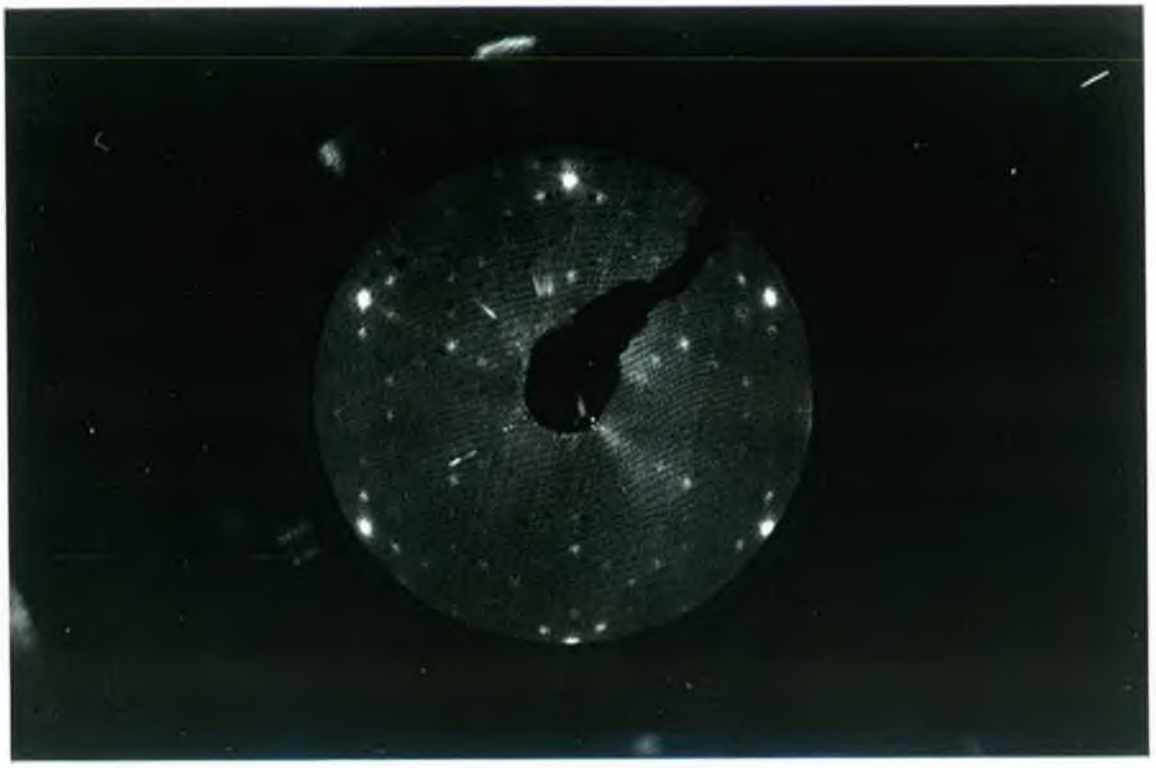

(b)

Fig 4.13 (**a**) *STM image of the Si/Si(111) surface (V=+2V, I=0.5nA)* (**b**) *Corresponding LEED pattern*

respectively. Desorption of a SiO species exposing a new silicon layer, which is, in turn, 7x7 reconstructed has also been described in some detail by Feltz *et al.* [28]. Their data demonstrates the important role that surface diffusion plays in the reaction process. However they cite two possible diffusing ad-particles - mobile vacancies in the topmost silicon layer or mobile oxygen adatoms - with the latter suggestion described as being less likely. The progress of the oxygen etching reaction was found in that work to be dependent on the mobility of the vacancies (or oxygen adatoms), the density of defects in the 7x7 structure and the terrace size. If a low defect density existed and/or the vacancy or oxygen adatom mobility was high then the diffusing species could reach the nearest step edge - i. e. the etching would occur via a step flow mechanism. With a high defect density or large terrace size Feltz *et al.* propose that mobile vacancies or oxygen adatoms could cluster forming monolayer deep pits.

In the present study it is suggested that the desorption of a sulphur overlayer is a further process that leads to the creation of random vacancies which, at the thermal desorption temperature, are sufficiently mobile to coalesce and create holes in the silicon surface layer. Interestingly, the dendritic forms of step edges seen to occur at lower sample temperatures (and corresponding lower vacancy mobility) during oxygen induced Si(111)-7x7 etching by Feltz *et al.*[28] were not observed in the course of this work. This would suggest that the terrace width on the clean surface was sufficiently large over the majority of the surface to cause mobile vacancies to preferentially coalesce and form holes rather than reach step edges. As in the case of the Si(100) surface, due to the S-Si bond energy being greater in magnitude than that of the Si-Si bond, Si_nS_m molecules are likely to be formed. Annealing of the sulphur covered sample may thus lead to an etching of the silicon surface. An etching of silicon has been observed by Holm[30] during silicon sulphide based vapour phase growth where he stresses that the most important factor for vapor phase transport efficiency is the difference in partial pressures of SiS_2 and S_2, depending on temperature and pressure[31]. However, the creation of monolayer deep holes was not observed after sulphur desorption from the Si(001) surface. This may relate to a difference in activation energy for Si diffusion on Si(111) and Si(001) surfaces. Values of 0.2 to 1.6 eV have been determined for activation energy in the case of silicon diffusion on Si(111) surfaces[32], whereas Brocks *et al.*[33] have found a value of 0.6 eV for diffusion parallel to the dimer rows on the Si(001) surface and a value of 1.0 eV for diffusion perpendicular to the rows.

Following the creation of a large number of surface defects, the remaining surface atoms may not exhibit the 7x7 reconstruction, but instead remain largely disordered or reconstruct into other local metastable structures. This appears to be particularly noticeable at step or hole edges as can be clearly seen in Fig.4.15(a). A small area of c(4x2) reconstruction appears within a surface region exhibiting no long range order close to a step edge. More distant from the edge the undisturbed 7x7 periodicity is clearly observed. In this image we believe that the local randomness of the surface structure has

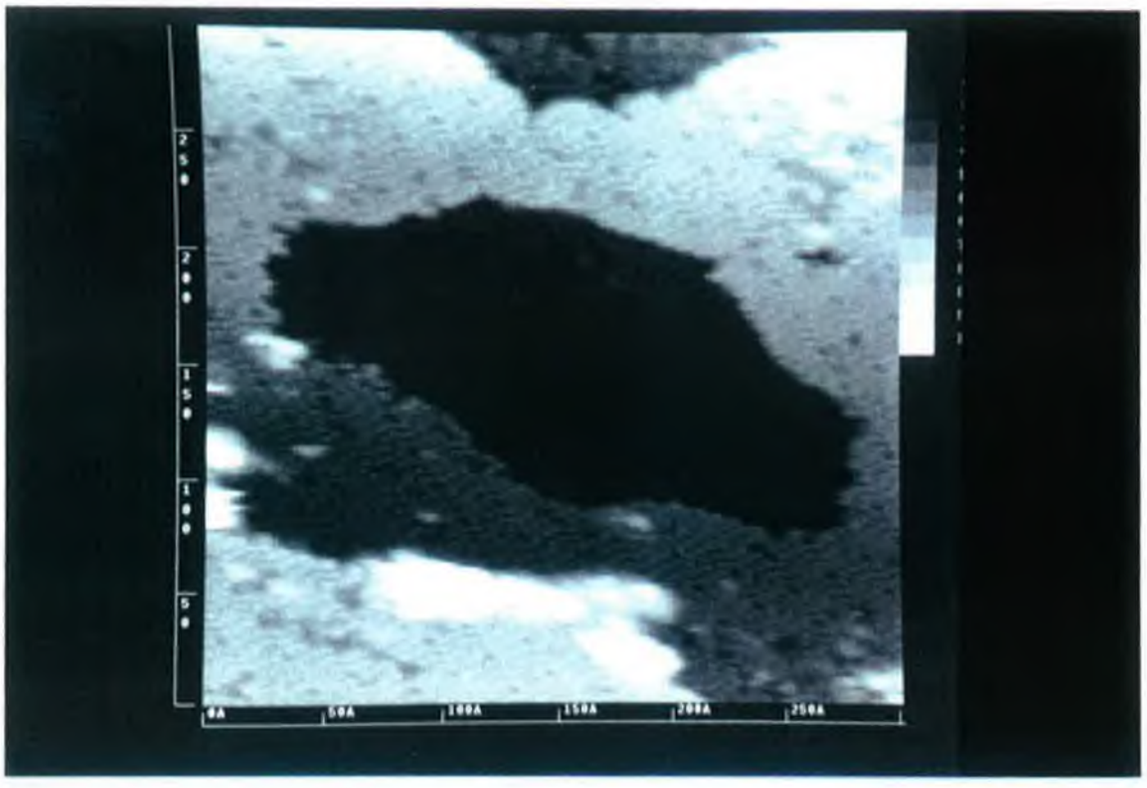

(a)

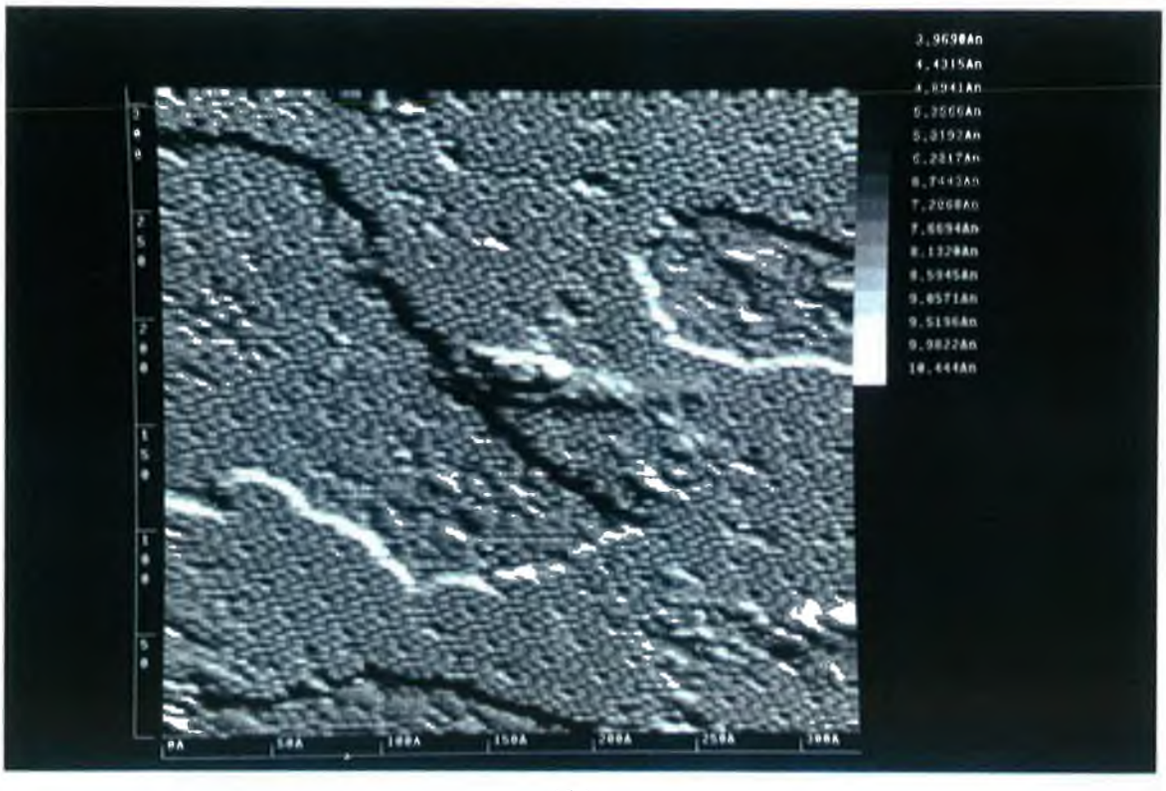

(b)

Fig 4.14 (a) *Monolayer deep holes in Si(111) surface after sulphur desorption* **(b)** *Presence of 7x7 reconstruction at bottom of surface hole (first order differentiated image to enhance contrast).*

been caused by the coalescence of mobile vacancies. Furthermore, very small areas of the $(\sqrt{3}x\sqrt{3})R30^{\circ}$ reconstruction have also been observed in the course of this work, most often at the lower surface of a step or hole edge - as illustrated in Fig. 4.15(b). Both the c(4x2) and $(\sqrt{3}x\sqrt{3})R30^{\circ}$ reconstructions have previously been observed on the laser annealed Si(111) surface[29], and attributed to close packed adatom surfaces with each adatom populating a closed triangular double site, following the work of Northrup[34]. Although the $(\sqrt{3}x\sqrt{3})R30^{\circ}$ reconstruction has also been attributed to boron dopant segregation at the Si(111) surface[35], we have not observed this structure on clean Si(111) samples from the same wafer without prior sulphur desorption and therefore believe that the $(\sqrt{3}x\sqrt{3})R30^{\circ}$ reconstruction observed is a silicon adatom structure.

Finally, the appearance of a (5x5) reconstruction was also observed following sulphur desorption. Feenstra and Lutz[36] have performed an STM and Scanning Tunnelling Spectroscopy (STS) study of the 5x5 reconstruction prepared via annealing of the cleaved Si(111) surface at 320°C. The structure of the (5x5) surface was found to be consistent with the DAS model, with the asymmetry between the unit cell triangular sub-units readily apparent in filled state images. Fig 4.16 illustrates the (5x5) reconstruction observed after sulphur desorption. The 6, as opposed to 12 in the 7x7 reconstruction, unit cell adatoms are clearly visible. During STM investigations of low temperature epitaxial growth of silicon, Köhler *et al.*[37] imaged the (5x5) after growth at 520°C noting that previous electron diffraction work[38] had reported a disappearance of this structure when the substrate temperature during deposition exceeded 520°C. The (5x5) phase observed in this study may again be attributed to reconstruction (at the sulphur desorbing temperature of 375°C) of surface material following creation and coalescence of a large number of vacancy defects. Seiple *et al.*[16] have similarly explained the appearance of the 5x5 structure during studies of the elevated temperature oxidation of Si(111) in terms of vacancy coalescence exposing new surface material which may thus undergo reconstruction.

4.5 The Arsenic Passivated Si(111) Surface - A Comparison with Sulphur Termination

In the preceding sections the non-ideal termination of both the Si(100) and Si(111) surfaces with sulphur has been described. An ideal system - the As:Si(111) (1x1) bulk termination is now discussed for comparison.

A series of core level and ultra-violet photoemission experiments on the <111> faces of Si and Ge (see, for example, refs 39 and 40) has determined that a termination of these semiconductors with a monolayer of arsenic results in the formation of a (1x1) surface and decreased chemical reactivity. The As atoms bond to three equivalent Si (or Ge) atoms in the surface layer (replacing the original top layer Si atoms) and put their remaining two electrons into a lone-pair state. This occupies a filled band and eliminates the Si dangling bond states. It should be

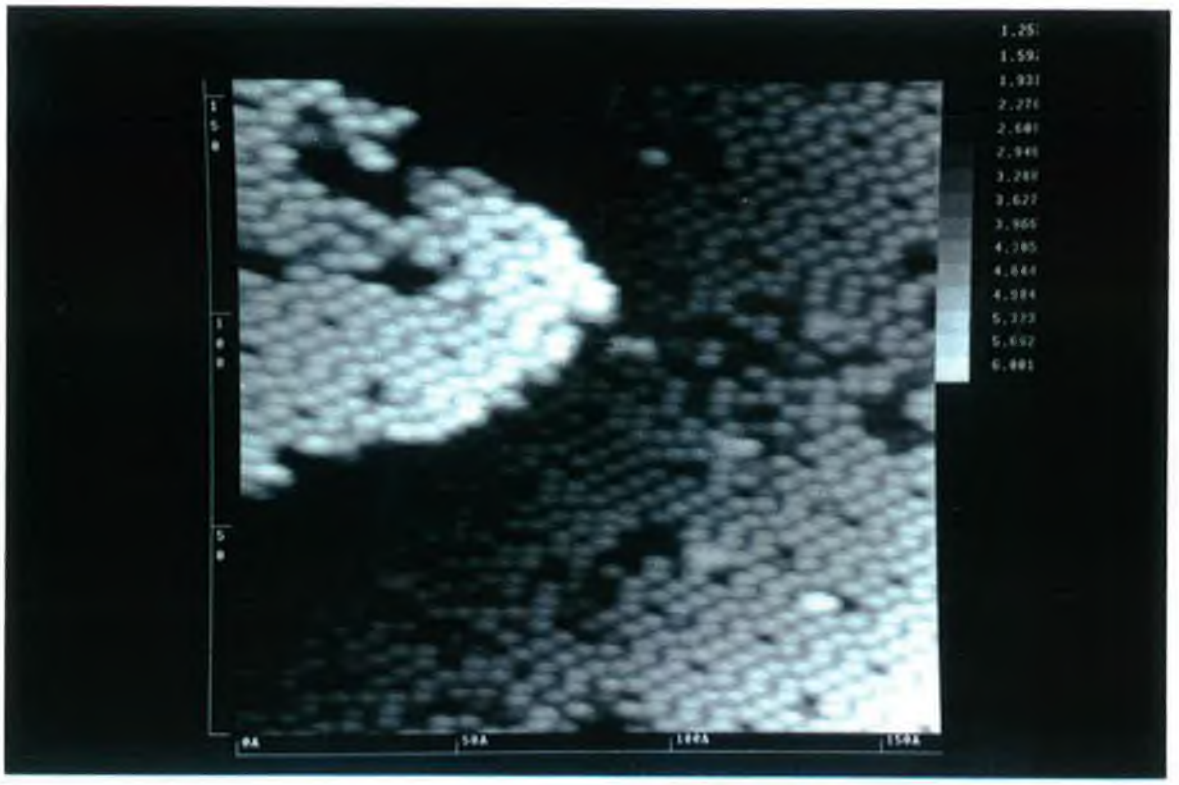

(a)

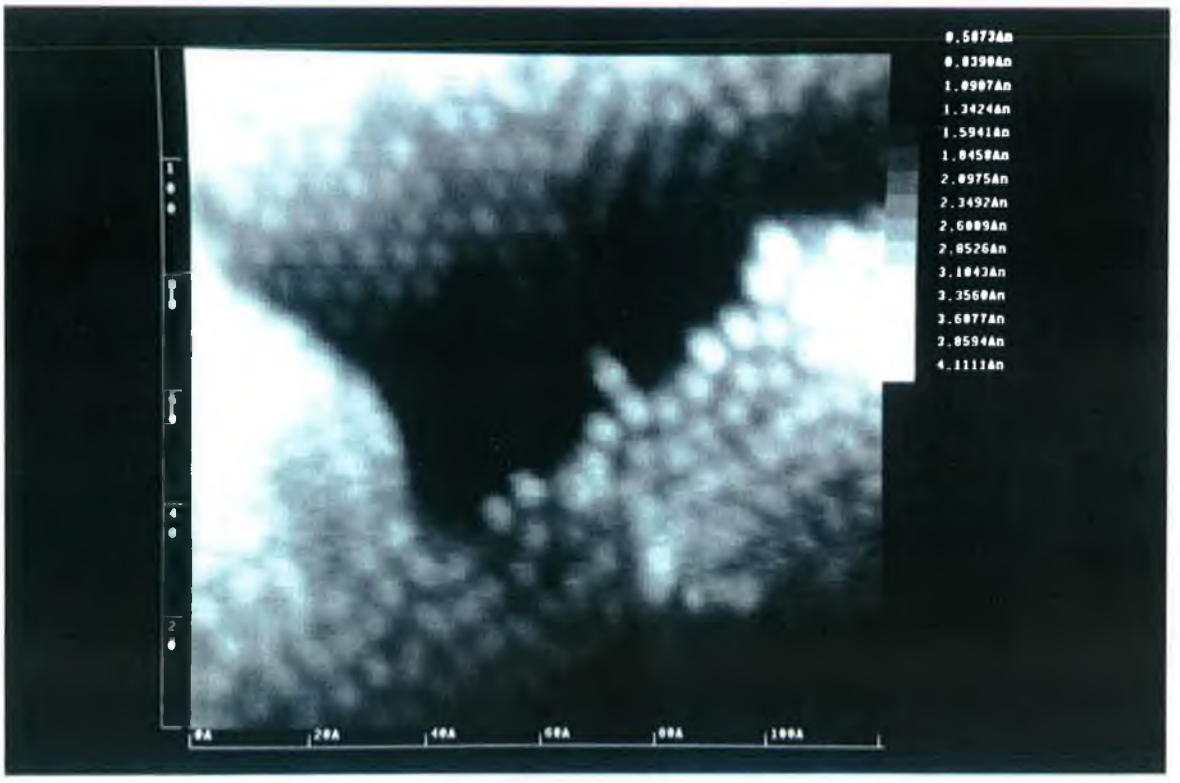

(b)

Fig 4.15 (a) *Area of surface after sulphur desorption exhibiting large degree of disorder;* **(b)** *Small region of the* $(\sqrt{3}x\sqrt{3})R30^{o}$ *reconstruction.*

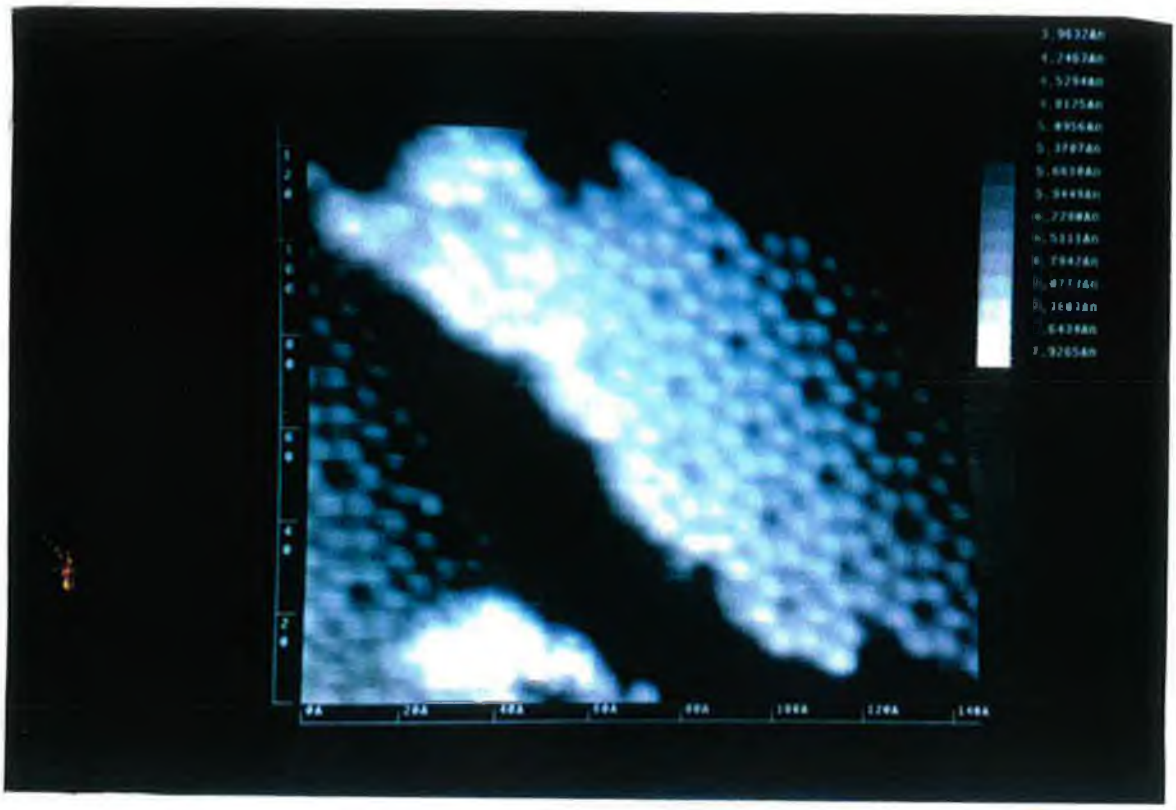

Fig 4.16 *The (5x5) reconstruction observed after sulphur desorption*

stressed that the As atoms occupy bulk sites and do not adsorb on the surface. Uhrberg *et al.*[40] have shown that the As:Si(111) (1x1) surface is almost unaffected (i. e. little change in the lone-pair surface state photoemission) by exposure to controlled amounts of oxygen, air and hydrogen, even with exposures as high as 10^7 and 10^{11} Langmuirs (L) of oxygen and air. This should be compared with the Si(111) surface where at 15 L oxygen exposure all dangling bond surface state emission was removed. The As:Si(111) (1x1) surface discussed in the following differs in one main respect from previous studies[7,8]. There, in all cases, creation of the Si(111)-7x7 surface was followed by exposure to an As_4 flux, *in situ*, with the sample held at temperatures in the 700°C range or flashed to 1050°C and allowed to cool. In this work, As capped Si(111) wafers were decapped, as described in Chapter 3, after having been left in air for some months. LEED analysis at 83 eV revealed a sharp (1x1) pattern as shown in Fig.4.17.

A corresponding STM image of the surface, taken at a bias voltage of 0. 5V and 100 pA tunnelling current, is shown in Fig.4.18 with the distance between the protrusions in the image being 3.8 Å -the silicon bulk (111) surface lattice spacing. The decrease in density of states from the Si(111)-7x7 surface forces a decrease in the demanded tunnelling current to the 100 pA value, as noted by Becker *et al.*[7] . At a 0.5 V bias a corrugation amplitude of 0.1 Å was observed, also in good agreement with the STM images of that group. The ideal (1x1) restoration of the Si(111) surface is readily apparent from figures 4.17 and 4.18 and is in sharp contrast to the overlayers observed after sulphur deposition on the Si(111) surface or the etching of the surface that occurs with annealing the sulphur covered surface.

Fig 4.17 *The (1x1) LEED pattern observed after decapping the As:Si(111) sample at 450°C.*

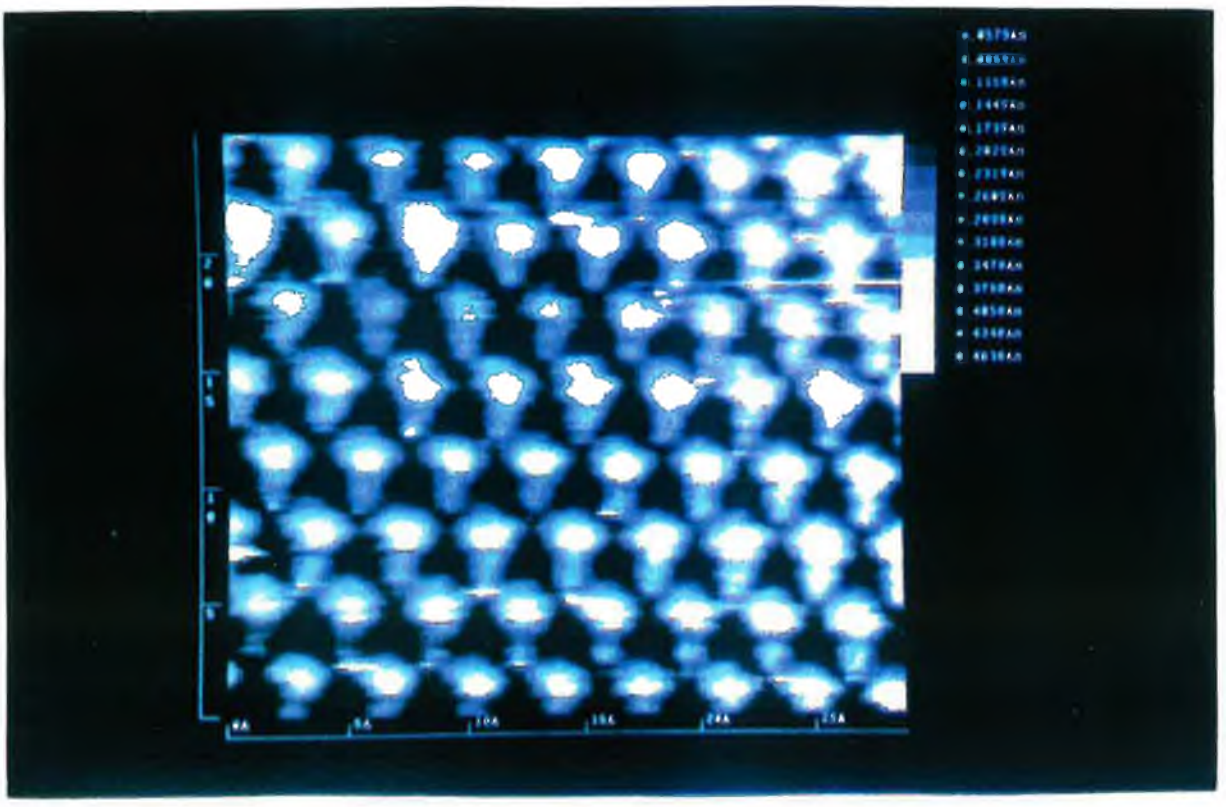

Fig 4.18 *STM image of the As:Si(111) surface (V=+0. 5V, I=100 pA)*

4.6 Summary

The reported results are the first in depth STM study of the interaction of sulphur with the silicon surface. Our study would suggest that sulphur cannot ideally terminate either the Si(100) or Si(111) surface and therefore cannot be considered as a useful surface passivant (unlike, for example, As). On thermal desorption of the sulphur overlayer, defect creation is observed to occur on both Si surfaces. The appearance of the c(4x4) reconstruction on the Si(100) surface at 325°C is significantly lower than has been previously reported for either the H-[22] or O-induced[15] c(4x4) structure. Similarly, the monolayer etching mechanism observed for sulphur desorption from the Si(111)-7x7 surface occured at a much lower temperature than oxygen induced etching[16]. Therefore, the nature of sulphur interaction with both the Si(100) and Si(111) is characterised by lower temperature reactions than oxygen. This is not surprising considering the volatility of Si_nS_m molecules as described by Kaxiras[10].

On both surfaces, the new reconstructions observed after sulphur desorption may be explained by vacancy creation in the original silicon surface reconstruction. Differences in the diffusion energy for a Si atom on Si(100) and Si(111) surfaces are reflected in the fact that the (7x7) surface has very long range order while the (2x1) structure is much more localised. This difference in diffusion energies may also be used to explain the monolayer etching mechanism that was observed *only* on Si(111) surfaces.

References

1. R. E. Schlier and H. E. Farnsworth, *J. Chem. Phys.* **30** 917 (1959)
2. K. Takayanagi, Y. Tanishiro, M. Takahashi and S. Takahashi, *Journ. Vac. Sci. Technol. A* **3** 1502 (1985)
3. G. Binnig, H. Rohrer, C. Gerber and E. Weibel, *Phys. Rev. Lett.* **50** 120 (1983)
4. M. Y. Chou, S. G. Louie, and M. I. Cohen, *Proceedings of the 17th International Conference on the Physics of Semiconductors,* Ed. D. J. Chadi and W. A. Harrison, (New York:Springer) (1982)
5. S. Y. Tong and A. L. Maldondo, *Surf. Sci.* **78** 459 (1978)
6. R. A. Wolkow, *Phys. Rev. Lett.* **68** 2636 (1992)
7. R. S. Becker, B. S. Swatrzentruber, J. S. Vickers, and M. S. Hybertsen, *Phys. Rev. Lett.* **60** 166 (1988)
8. M. Copel, R. M. Tromp, and U. K. Köhler, *Phys. Rev B* **37** 10756
9. E. Kaxiras, *Mat. Res. Soc. Symp. Proc.* **193** 143 (1990)
10. E. Kaxiras, *Phys. Rev. B.* **43** 6824 (1991)
11. W. A. Harrison, *Electronic Structure and the Properties of Solids: The Nature of the Chemical Bond* (W. H. Freeman, San Francisco, 1980)
12. P. Krueger and J. Pollmann, *Phys. Rev. B* **47** 1898 (1993)
13. Ph. Avouris, I-. W. Lyo, and F. Bozso, *Journ. Vac. Sci. Technol. B* **9** 424 (1991)
14. D. Cahill and Ph. Avouris, *Appl. Phys. Lett.* **60** 326 (1991)
15. K. E. Johnson, P. K. Wu, M. Sander and T. Engel, *Surf. Sci.* **290** 213 (1993)
16. J. Seiple, J. Pecquet, Z. Meng and J. P. Pelz
17. H. Wang, R. Lin and X. Wang, *Phys. Rev. B.* **36** 7712 (1987)
18. K. Kato, T. Ide, T. Nishimori and T. Ichinokawa, *Surf. Sci.* **207** 177 (1988)
19. T. Ide and T. Mizutani, *Phys. Rev. B.* **45** 1447 (1992)
20. K. C. Pandey, in *Proceedings of the Seventh International Conference on the Physics of Semiconductors*, edited by J. D. Chadi and W. A. Harrison (Springer - Verlag, New York, 1985) p55
21. S. Ihara, S. L. Ho, T. Uda and M. Hirao, *Phys. Rev. Lett.* **65** 1909 (1990)
22. R. I. G. Uhrberg, J. E. Northrup, D. K. Biegelsen, R. D. Bringans and L. E. Swartz, *Phys. Rev. B.* **46** 10251 (1992)
23. T. Weser, A. Bogen, B. Konrad, R. D. Schnell, C. A. Schug and W. Steinmann, in *Proceedings of the Eighteenth International Conference on the Physics of Semiconductors,* edited by O. Engstrom (World Scientific, Singapore, 1987)
24. T. Weser, A. Bogen, B. Konrad, R. D. Schnell, C. A. Schug and W. Steinmann, *Phys. Rev. B.* **35** 8184 (1987)
25. R. M. Tromp, R. J. Hamers, and J. E. Demuth, *Science* **234** 324 (1986)
26. K. Uesugi, T. Yao, T. Sato, T. Sueyoshi and M. Iwatsuki, *Appl. Phys. Lett.* **62** 1600 (1993)

References

1. R. E. Schlier and H. E. Farnsworth, *J. Chem. Phys.* **30** 917 (1959)
2. K. Takayanagi, Y. Tanishiro, M. Takahashi and S. Takahashi, *Journ. Vac. Sci. Technol. A* **3** 1502 (1985)
3. G. Binnig, H. Rohrer, C. Gerber and E. Weibel, *Phys. Rev. Lett.* **50** 120 (1983)
4. M. Y. Chou, S. G. Louie, and M. I. Cohen, *Proceedings of the 17th International Conference on the Physics of Semiconductors,* Ed. D. J. Chadi and W. A. Harrison, (New York:Springer) (1982)
5. S. Y. Tong and A. L. Maldondo, *Surf. Sci.* **78** 459 (1978)
6. R. A. Wolkow, *Phys. Rev. Lett.* **68** 2636 (1992)
7. R. S. Becker, B. S. Swatrzentruber, J. S. Vickers, and M. S. Hybertsen, *Phys. Rev. Lett.* **60** 166 (1988)
8. M. Copel, R. M. Tromp, and U. K. Köhler, *Phys. Rev B* **37** 10756
9. E. Kaxiras, *Mat. Res. Soc. Symp. Proc.* **193** 143 (1990)
10. E. Kaxiras, *Phys. Rev. B.* **43** 6824 (1991)
11. W. A. Harrison, *Electronic Structure and the Properties of Solids: The Nature of the Chemical Bond* (W. H. Freeman, San Francisco, 1980)
12. P. Krueger and J. Pollmann, *Phys. Rev. B* **47** 1898 (1993)
13. Ph. Avouris, I-. W. Lyo, and F. Bozso, *Journ. Vac. Sci. Technol. B* **9** 424 (1991)
14. D. Cahill and Ph. Avouris, *Appl. Phys. Lett.* **60** 326 (1991)
15. K. E. Johnson, P. K. Wu, M. Sander and T. Engel, *Surf. Sci.* **290** 213 (1993)
16. J. Seiple, J. Pecquet, Z. Meng and J. P. Pelz
17. H. Wang, R. Lin and X. Wang, *Phys. Rev. B.* **36** 7712 (1987)
18. K. Kato, T. Ide, T. Nishimori and T. Ichinokawa, *Surf. Sci.* **207** 177 (1988)
19. T. Ide and T. Mizutani, *Phys. Rev. B.* **45** 1447 (1992)
20. K. C. Pandey, in *Proceedings of the Seventh International Conference on the Physics of Semiconductors*, edited by J. D. Chadi and W. A. Harrison (Springer - Verlag, New York, 1985) p55
21. S. Ihara, S. L. Ho, T. Uda and M. Hirao, *Phys. Rev. Lett.* **65** 1909 (1990)
22. R. I. G. Uhrberg, J. E. Northrup, D. K. Biegelsen, R. D. Bringans and L. E. Swartz, *Phys. Rev. B.* **46** 10251 (1992)
23. T. Weser, A. Bogen, B. Konrad, R. D. Schnell, C. A. Schug and W. Steinmann, in *Proceedings of the Eighteenth International Conference on the Physics of Semiconductors,* edited by O. Engstrom (World Scientific, Singapore, 1987)
24. T. Weser, A. Bogen, B. Konrad, R. D. Schnell, C. A. Schug and W. Steinmann, *Phys. Rev. B.* **35** 8184 (1987)
25. R. M. Tromp, R. J. Hamers, and J. E. Demuth, *Science* **234** 324 (1986)
26. K. Uesugi, T. Yao, T. Sato, T. Sueyoshi and M. Iwatsuki, *Appl. Phys. Lett.* **62** 1600 (1993)

27. P. Bedrossian and T. Klitsner, *Phys. Rev. B* **44** 13783 (1991)
28. A.Feltz, U. Memmert and J. Behm, *Chem. Phys. Lett.* **192** 271 (1991)
29. R. S. Becker, A. Golovchenko, G. S. Higashi and B. S. Swartzentruber, *Phys. Rev. Lett.* **57** 1020 (1986)
30. C. Holm, L. Koenders, private communication.
31. C. Holm and E. Sirtl, *Journ. Cryst. Growth.* **54** 253 (1981)
32. F. Allen and E. Kasper in *Silicon Molecular Beam Epitaxy*, edited by E. Kasper and J. C. Bean (CRC Press, Boca Raton, FL, 1988), Vol. I, p.65 and references therein.
33. G. Brocks, P. J. Kelly and R. Car, *Phys. Rev. Lett.* **66** 1729 (1991)
34. J. Northrup, *Bull. Am. Phys. Soc.* **31** 584 (1986)
35. P. Bedrossian, R. D. Meade, K. Mortensen, D. M. Chen, J. A. Golovchenko and D. Vanderbilt, *Phys. Rev. Lett.* **63** 1257 (1989)
36. R. M. Feenstra and M. A. Lutz, *Journ. Vac. Sci. Technol. B* **9** 716 (1991)
37. U. Köhler, J. E. Demuth and R. J. Hamers, *Journ. Vac. Sci. Technol. A* **7** 2860 (1989)
38. M. Horn, Ph.D. Thesis, Universitat Hannover (1988)
39. M. A. Olmstead, R. D. Bringans, R. I. G. Uhrberg, and R. Z. Bachrach, *Phys. Rev. B* **34** 6041 (1986)
40. R. I. G. Uhrberg, R. D. Bringans, M. A. Olmstead, and R. Z. Bachrach, *Phys. Rev. B* **35** 3945 (1987)
41. Y.J. Chabal, G. S. Higashi, K. Raghavachari, and V. A. Burrows, *Journ. Vac. Sci. Technol. A* **7** 2104 (1989)
42. G. S. Higashi, Y. J. Chabal, G. W. Trucks, and K. Raghavachari, *Appl. Phys. Lett.* **56** 656 (1990)

CHAPTER V : IN SITU SULPHUR ADSORPTION ON DECAPPED GaAs(100) AND GaAs(111)B SURFACES

Previous studies on the reaction of S with GaAs surfaces have mainly concentrated on aqueous sulphide and H_2S treatments (as detailed in Chapter 2). We present STM, LEED, AES, and PES results on the in situ interaction of S (from an electrochemical cell) with GaAs(100)-c(2x8), (4x6) and (4x1), and GaAs(111)B-(2x2) surfaces. Use of As capped GaAs samples enabled a characterisation of the initial surface, prior to S deposition. A number of possible structural models for the S treated surfaces are outlined.

5.1 Atomic and Electronic Structure of Reconstructed GaAs(100) Surfaces.

GaAs is of the *zincblende* structure with bonding that is best described as being mixed ionic and covalent in character. The 4s and 4p valence electrons contribute eight electrons per GaAs bond - three from Ga and five from As - with the difference in electronegativity of the two elements leading to charge transfer from Ga to As. As will be described in the following sections, this electronegativity difference has been used by Pashley[1] as the basis of an "electron counting" rule which can be used to explain the various reconstructions observed on the GaAs(100) surface[2]. Indeed,the reconstructions of most III-V semiconductor surfaces have shown to be consistent with restrictions imposed by this rule. Most STM studies to date of the GaAs surface have concentrated on the (110) face which is easily prepared by cleavage. For this surface, as was detailed in Chapter 1, the ionic character of the surface bonds leads to the possibility of selectively STM imaging either Ga (empty) or As (filled) states. While GaAs(110) surfaces exhibit a (1x1) relaxed structure, the other low index surfaces display a variety of reconstructions dependent on their method of preparation.

The (100) surface of GaAs is interesting not only from a fundamental scientific viewpoint but also due to it being the principal substrate for epitaxial growth and the fabrication of both MIS devices and low dimensional quantum structures. An unreconstructed As-rich surface would consist of a (1x1) structure of As atoms bonded to two Ga atoms in the underlying layer, with two partially filled dangling bonds oriented parallel to [110], as illustrated in Fig.5.1(a). As for the Si(100) surface, dimerisation of these surface atoms leads to a substantial unit cell energy minimisation. Furthermore, Pashley[1] has shown that the stable surfaces of III-V semiconductors correspond to structures in which the number of group III dangling bond states is as close as possible to the number of group V dangling bond states. The high energy Ga dangling bond states donate their electrons to the As dangling bond states which are degenerate in energy with the bulk valence bands, leaving no occupied states in the band gap which could induce

other reconstructions. This rule ensures that the surface is as close as possible to being non-metallic, non-polar and metastable.

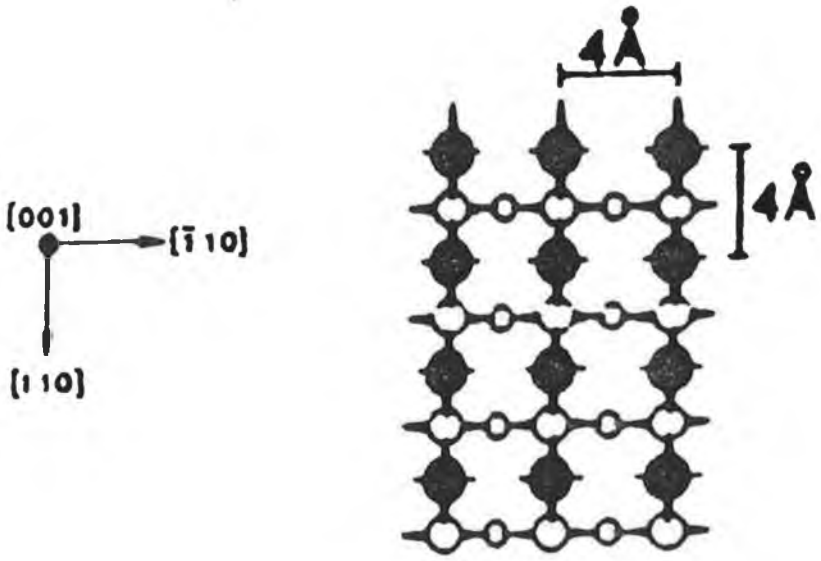

Fig 5.1 *The bulk-terminated, unreconstructed GaAs(100) surface.(From ref 8). Solid circles represent top layer As atoms.*

For the specific case of a completely dimerised GaAs(100)As - 2x1 surface, the As-As bond contains two electrons with each As atom contributing one electron. As in the bulk, every bond with an underlying Ga atom requires a contribution of 5/4 electron from the As atom. (In bulk GaAs, each As atom makes four bonds with its Ga nearest neighbours. As arsenic has five valence electrons it contributes 5/4 electron to each bond). Therefore, every surface As atom has 5-5/4-5/4-1 or 3/2 electrons in its dangling bond orbital. Thus, the As dangling bond orbital is only partially full resulting in a metallic, unstable (2x1) termination which is not observed experimentally on the GaAs(100) surface.

Instead of this complete (2x1) structure, GaAs(100) exhibits a wide range of surface reconstructions depending on surface preparation and the resultant ratio of As to Ga. In order of decreasing As/Ga concentration - during growth or after growth and annealing - c(4x4), c(2x8)/(2x4), (1x6)/(2x6), (4x6) and c(8x2)/(4x2) reconstructions are observed. A (4x1) reconstruction is also consistently observed and has been described as a disordered c(8x2) phase[3]. These different surface reconstructions have been studied using, for example, LEED and AES[4,5], UPS[6,7] and STM[3,8]. However, doubt about the precise composition of the various surface structures still remains. Core-level photoemission studies of MBE grown GaAs(100) surfaces by both Katnani *et al.* [9] and Veen *et al.*[10] determined that the c(4x4) surface was terminated in more than a monolayer of As. Structures with one, two and three dimers in c(4x4) arrays atop a complete As layer have been subsequently proposed[11]. The STM images of Biegelsen *et*

al.[3] of this reconstruction were consistent with a topmost layer consisting of three As dimers.

The first high resolution STM images of the c(2x8)/(2x4) reconstruction of the As-rich GaAs(100) surface were presented by Pashley *et al.*[8]. As for the samples used in the studies to be described in sections 5.2 and 5.3, the Kowalczyk *et al.*[12] technique of capping the sample with a thick As film before removal from the MBE system was used. Inside the STM's UHV system, the sample was "decapped" by thermally desorbing the protective As layer at a temperature of 370°C. Subsequent annealing of the sample at 450°C resulted in the appearance of a c(2x8) LEED pattern. The STM images showed that the composition of the (2x4) unit cells is consistent with a model of three As dimers and a missing dimer, arranged to give domains of either (2x4) or c(2x8) periodicity (Fig.5.2) (The AP and IP symbols refer to anti-phase and in-phase boundaries, with K1, K2 and K3 referring to kink sites. All these features were observed by Pashley *et al.*[8] in their STM study). Considering the three dimer/one missing dimer model in terms of the electron counting rule, the elimination of one out of every four dimers of the (2x1) structure described previously creates four Ga dangling bonds. By making these

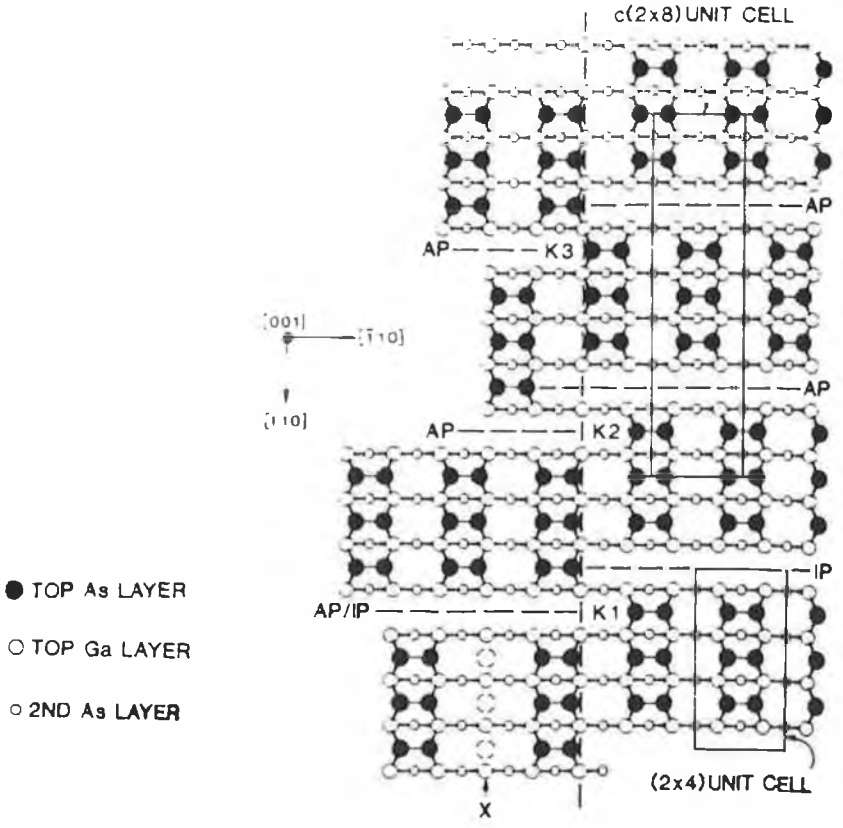

Fig 5.2 *The GaAs(100)-c(2x8) reconstruction. (From ref. 8)*

dangling bonds empty, the three excess electrons (3/4 from each dangling bond) can saturate the lone pair states of the three As dimers in the unit cell and provide charge balance for the (2x4) structure. Total energy calculations carried out by Chadi[13] also showed that a unit cell with three As dimers and one missing dimer is energetically the most favourable for the (2x4) surface but is almost degenerate in energy with a structure

that contains only two dimers per unit cell, with compensatory dimerisation of the exposed second layer Ga atoms[14]. Indeed, the two missing dimer unit cell has been consistently observed in STM images of the c(2x8) reconstruction[3,15,16]. The presence of either the 1 or 2 missing dimer unit cell is critically dependent on the precise surface stoichiometry which is, itself, a function of annealing temperature[14].

Synchrotron Radiation soft XPS (SR SXPS) was used to characterise decapped GaAs(100) surfaces by Spindt *et al.*[17]. They observed the attenuation of a chemically shifted component at higher binding energy (BE) (relative to the bulk As-Ga peak) in the As 3d spectrum after annealing at 450°C. This was attributed to a removal of As atoms bonded primarily to the underlying As layer. LeLay *et al.*[18] similarly observed the attenuation of this "excess As" component at 450°C. In both cases, another component shifted to lower BE was observed in the As 3d spectra due to the As dimers terminating the c(2x8) surface, as first proposed by Ludeke *et al* [19].

The first atomic resolution images of both the (2x6) and c(8x2) reconstructions were presented by Biegelsen *et al.*[3] A (2x6) surface was prepared by annealing a c(2x8) sample at 600°C for 5 minutes. STM data indicated that the surface unit cell (as illustrated in Fig. 5.3) consisted of two As dimers and four missing dimers stacked along the (x6) direction. Considerable disorder in the (2x) direction was present which corresponded with streaking of the 1/2 and 1/3 order spots in the observed (1x6) LEED pattern. A (4x6) surface was prepared, by the same group, by annealing the (2x6) surface at 670°C. The LEED pattern then consisted of a superposition of (4x1) and (4x6) domains. STM imaging found a coexistence of (2x6) and (4x1) phases with the latter being described as disordered c(8x2).

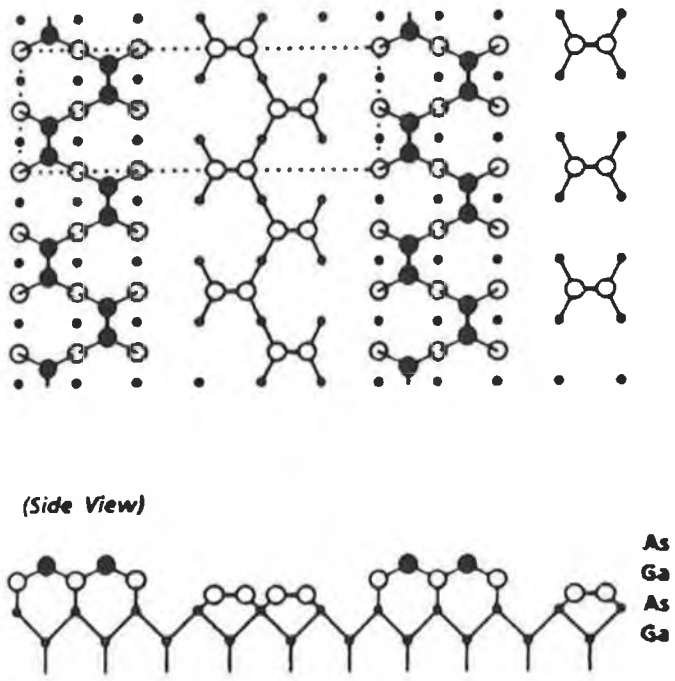

Fig 5.3 *The model for the (2x6) reconstruction proposed by Biegelsen et al. (From ref.3)*

After annealing at 690°C, Biegelsen *et al.* obtained images of the c(8x2) reconstruction, but with very poor resolution. (The degradation in resolution was attributed to Ga transfer to the tip). They proposed a missing Ga dimer model, with the c(8x2) periodicity consisting of an ordered array of (4x2) subunits. Each (4x2) unit cell consists of two adjacent Ga dimers and two missing dimers. Frankel *et al.*[20] have suggested a missing Ga dimer model for the c(8x2) reconstruction, analogous to the missing As dimer model for the c(2x8) surface (Fig.5.2).

As mentioned previously, the *precise stoichiometry* of the various GaAs(100) surface reconstructions is, at present, not fully understood and doubt remains to their exact atomic structure. The first attempt at a systematic determination of the composition of the individual (100) phases - prepared by MBE growth - was by Drathen *et al.*[4] A quantitative evaluation of As coverage for each reconstruction was performed using the layer attenuation model of Ranke and Jacobi[21] and a calibration measurement on a cleaved GaAs(110) surface. The height ratio of the low energy Auger peaks I_{As}(31eV): I_{Ga}(55eV) was taken as a measure of the surface content. All coverages were referred to a coverage value of $\theta_{As} = 0.5$ corresponding to the peak height ratio of the cleaved (110) sample. Their study concluded that the reconstructions are ordered from highest As surface content to lowest with increasing annealing temperature. The c(2x8),(4x6) and c(8x2) surfaces were found to have an As content of 0.61, 0.27 and 0.22 respectively. Although qualitative agreement was reached with an earlier study[5] regarding the sequence of appearance of the GaAs(100) reconstructions as a function of annealing temperature, large discrepancies were observed in the respective Auger peak height ratios. This discrepancy may arise from differences in background and valence band changes. (The As 31eV Auger line contains a valence band contribution that is not present in the As 39 eV peak[22], therefore the latter peak height is a more stringent measure of surface As *concentration*). Other attempts[23,24] to quantify the As/Ga surface ratio have similarly proved inconclusive, with widely differing values reported. Indeed, as stated by Skala *et al.*[25], surface Ga concentrations for the c(8x2) reconstruction ranging from 0.48 to greater than 1.0 have been reported.

Until recently it has been assumed that no As-Ga intermixing in the (100) planes occurs. Using high resolution Medium Energy Ion Scattering (MEIS), Falta *et al.*[26] have proposed that all GaAs(100) surface reconstructions are more Ga rich than previously predicted. They support this proposal in terms of Coulombic repulsion between As lone pair orbitals, which leads to As replacement by Ga in the first and second layers. It is interesting to note, however, that this group find that the c(2x8) two missing dimer unit cell observed in a number of STM studies[3,15,16] does not agree with their experimental data. Again, this may be attributed to differences in surface stoichiometry due to the precise surface preparation procedure used.

An SR SXPS study by Vitomirov *et al.*[27] determined that the intensity ratio I (As 3d) : I (Ga 3d) for the c(8x2) reconstruction almost equalled the lowest value obtained for the

c(2x8) reconstruction. Skala *et al.*[25], in a very recent STM study of the c(8x2) reconstruction propose a model (Fig.5.4) consisting of equal numbers of As and Ga dimers oriented perpendicularly to each other. Filled- and empty-state STM images were found to be entirely consistent with this model. Furthermore, the electron counting rule is satisfied leading to no net charge imbalance on the surface. The authors cite previous STM observations[3,15,16] showing that the most As depleted c(2x8) reconstruction has a surface As concentration of 0.5. This, coupled with the results of Vitomirov *et al.*[27], led them to suggest that the As concentration of the c(8x2) phase is also 0.5 - a natural consequence of their unit cell model. From high resolution SR core level spectroscopy results, LeLay *et al.*[18] tentatively assigned the two surface components in their c(8x2) surface Ga 3d spectra of 570°C annealed GaAs(100) to inequivalent dimers in the unit cell model of Frankel *et al* [20]. The As 3d surface component observed was assigned to the threefold co-ordinated second layer As next to the missing row of Ga dimers. A similar decomposition of core level spectra of the c(8x2) surface was shown by Vitormirov *et al.*[27]. They also found that the Fermi level position for the c(8x2) reconstruction was 0.1 eV closer to the VBM (for n-type sample) than for the c(2x8) reconstruction. LeLay *et al.*[18], however, found that the Fermi level was consistently pinned mid-gap for all reconstructions.

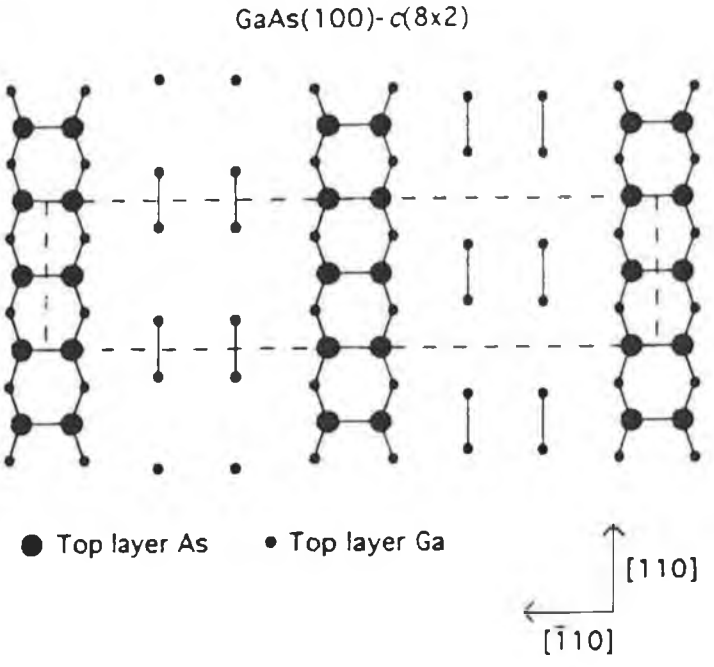

Fig 5.4 *The GaAs(100)-c(8x2) surface model of Skala et al.(From Ref. 25)*

The question of the exact nature of Fermi level pinning on the reconstructed GaAs(100) surface is also not fully resolved. Brillson *et al.*[28] reported "unpinned" Schottky barrier formation on decapped GaAs(100) surfaces with barrier heights over a wide (0.75 eV) range. It was suggested that the surface reconstruction formed after 580°C annealing served as an insulating layer which prevented Metal Induced Gap States (MIGS) from pinning the GaAs at mid-gap. However, in an extensive study of electronic structure and Al and Au Schottky barrier formation on identically prepared GaAs(100) surfaces, Spindt *et al.*[17] did not observe this large variation in barrier height. A comprehensive comparison of their results with those of Brillson *et al.*[28] led the authors to conclude that surface photovoltaic effects were solely responsible for the apparent "unpinned" Fermi level. STM studies have shown that as the Si doping level of MBE grown GaAs is increased, an increasing number of "kinks" form in the missing dimer rows of the c(2x8) reconstruction[29]. Spatially resolved tunnelling spectroscopy measurements by Pashley *et al.*[30] have indicated that negative charge resides at the kink sites (which act as surface acceptors) with the Fermi level being pinned mid-gap by states extending from the band edges. These studies have been extended to Be doped (p-type) samples[31] where no kink sites and, therefore, no donor states are observed. As a result, the Fermi level position for p doped GaAs(100) samples is controlled only by intrinsic defects such as steps and missing unit cells. For their p-type samples this group measured a Fermi level position of $E_v + (0.15 \pm 0.1$ eV).

In conclusion, from the degree of disagreement between various groups using a wide range of surface sensitive probes, it is evident that both the atomic and electronic structure of the GaAs(100) surface reconstructions is not fully understood. The precise surface stoichiometry (As/Ga ratio) of these reconstructions is still a subject of debate. A lack of structural models for the clean surface phases consistent with all the experimental data of course complicates the analysis of adsorbates on these surfaces. Conversely, the chemical reaction of the adsorbate with the surface may prove helpful in the characterisation of a particular reconstruction. This chapter details STM, SRPES, AES and LEED studies of the interaction of sulphur with the GaAs(100) and GaAs(111)B surfaces where an electrochemical cell was used for sulphur deposition. Unlike studies of aqueous sulphide treated samples (Chapter 2), this method of *in situ* treatment enables the GaAs surface to be characterised before sulphur adsorption.

5.2 An STM and Photoelectron Core-Level Spectroscopy Investigation of the Sulphur Treated GaAs(100) Surface.

As detailed extensively in Chapter 2, dramatic photoluminescene enhancement and an unpinning of the Fermi level have been reported for aqueous sulphide treated GaAs surfaces. This suggests a considerable reduction in surface state density. There are several reports on the characterisation of these S-treated surfaces using photoemission spectroscopy (see Chapter 2). However, some of these reports are inconsistent

concerning the structure and bonding formed, probably due to differences in sample preparation methods and experimental conditions. Indeed, although it is now widely accepted that both S-As and S-Ga bonds form at the sulphide treated surface, poor resolution in early photoemission experiments (and also the use of much less surface sensitive XPS)[32] precluded the observation of a S-Ga bonding state. It was therefore - wrongly - concluded that only As sulphides were present. We have attempted a more systematic study using reconstructed GaAs(100) surfaces to aid understanding of the surface modification induced by sulphur adsorption. The thermal decapping of As/GaAs(100) and As/GaAs(111)B surfaces combined with *in situ* sulphur adsorption using an electrochemical cell aids considerably the characterisation of the S treated surfaces.

SXPS measurements using SR were performed at beam line 6.1 at Daresbury Synchrotron Radiation Source, U. K. (Chapter 3). The photon energy chosen for As and Ga 3d core level analysis was 100 eV, providing maximum surface sensitivity with near identical escape depths for the photoelectrons[18]. Overall instrumental resolution at 100eV was 0.25-0.3 eV. The n-type (Si doped to $2x10^{18}$ cm^{-3}) As capped GaAs samples were indium bonded to a Mo sample holder before introduction to the UHV system. This ensured homogeneous removal of the As film during thermal desorption - as mentioned in Chapter 3. After decapping, the sample was annealed to 450°C for 5 minutes. This resulted in the appearance of a clear c(2x8) LEED pattern.

The photoelectron spectra were curve fitted by assuming the *Voigt* profile - a Lorentzian convolved with a Gaussian line shape - using a non-linear least squares fitting routine[33]. The Gaussian broadening accounts for the instrumental resolution and also any broadening due to disorder and potential variations (non-homogeneous band-bending) across the surface. Spindt *et al.*[17] note that such surface potential variation may not necessarily be Gaussian but they also have used that approximation in their curve-fitting. The Lorentzian shape is the natural broadening due to the finite lifetime of the core hole. The core-level decomposition parameters used for the clean GaAs(100)-c(2x8) surface are shown in Table 5.I and are within the range of previously reported values[17,18,27,28]. For both the Ga and As 3d core levels the Gaussian width is considerably larger than the instrumental resolution. Room temperature phonon broadening contributes to this increase in the Full Width at Half Maximum (FWHM).

	As 3d	**Ga 3d**
Gaussian FWHM	0.49 eV	0.42 eV
Lorentzian width	0.13 eV	0.18 eV
Branching ratio	0.66	0.65
Spin Orbit Splitting	0.69 eV	0.45 eV

Table 5.I *The fitting parameters for the clean GaAs(100)-c(2x8) surface.*

Figure 5.5 shows the results of the curve fitting procedure applied to the As 3d spectrum for (i) the clean c(2x8) surface and (ii) the clean (4x1) surface. Three components in the fit were necessary to obtain the minimum χ^2 for the c(2x8) surface. The core level spectrum consists of the bulk As-Ga component and two surface core level components shifted by 0.61 ± 0.02 eV and 0.40 ± 0.02 eV to higher and lower binding energy (BE) respectively. A number of previous studies[17,18,27] have identified the higher BE component as being due to excess As atoms (remaining from the decapping procedure) bonded primarily to other As atoms. Further evidence that this is the case is visible in the As 3d spectrum of the (4x1) surface (Fig 5.5(ii)). At the higher annealing temperature needed to form this reconstruction, the excess As desorbs and the component at higher BE is absent from the spectrum. Ludeke *et al.* [19] were the first to identify the low BE component with the As dimers terminating the c(2x8) surface. For the (4x1) surface, the lower BE component shifts to 0.49 ± 0.02 eV, consistent with the results of Vitomirov *et al.* [27].

For the Ga 3d spectra (Figs 5.6 (i) and (ii)), three components are necessary in both cases to achieve a good fit of the experimental data. The two surface components in the c(2x8) spectrum are shifted by 0.42 ± 0.02 eV and -0.30 ± 0.02 eV relative binding energy. Ga also exhibited two surface components in the spectra of LeLay *et al.* [18] for the decapped c(2x8) surface which were not observed on the MBE grown surface. However, the authors did not comment on the origin of the surface components. Two surface core level shifted components are incompatible with a surface reconstruction consisting of only a three As dimer/one missing dimer unit cell for the c(2x8) surface as described in Section 5.1. For that unit cell,*all* Ga surface atoms are threefold co-ordinated and this should give rise to only one surface component in the core level spectra. If the surface consists of : i) the two dimer/two missing dimer phase, or ii) a mixture of both phases, then dimerisation of underlying Ga as described by Farrell and Palmström[14] will give rise to another component. Interestingly, Vitomirov *et al.*[27] did not observe this second component in their studies of decapped GaAs(100) surfaces. This suggests that, in their case, the three As dimer/missing dimer unit cell was dominant across the surface.

For the (4x1) reconstructed surface (a disordered c(8x2) phase[3]), the magnitude of the surface component at lower relative binding energy in the Ga 3d spectrum increases with respect to that of the c(2x8) surface. This has also been observed in the data of LeLay *et al.*[17]. That group identified the two surface components for the c(8x2) surface as being due to inequivalent dimers in the unit cell. Assuming the model of Frankel *et al.*[20], one dimer in which Ga is bonded to four fold co-ordinated As in the second layer is surrounded by two dimers in which Ga is bonded to three fold co-ordinated second layer As. Vitormirov *et al.*[27] observed that the relative binding energies and emission intensities of the surface shifted components are extremely sensitive to variations in the thermal desorption procedure and note variations of as much as 0.1 eV in the binding

energies from sample to sample. It should be stressed that our AES analysis of the (4x1) surface yielded an I_{As}(31eV): I_{Ga}(55eV) ratio of 3:1. This is the ratio measured by Drathen *et al.* [4] for the c(2x8) surface corresponding, in their data, to an As coverage of 0.5 ML. Furthermore, Bachrach *et al.*[23], from angle-integrated PES measurements, also estimated an As coverage of 0.5 for the c(8x2) surface.

Fig. 5.7(i) illustrates a filled state STM image of the (4x1) surface taken with a sample bias voltage of -2V and a tunnelling current of 1nA. (Empty state images taken with voltages between +2V and +3V displayed much poorer resolution). Dimer rows are the most prominent feature of this image. (The large variations in contrast along the rows are most likely a tip effect). A "zoom" of an area of Fig.5.7(i) is illustrated in Fig.5.7(ii). As discussed in the previous section, Skala *et al.*[25] has proposed a model for the c(8x2) unit cell consisting of two As and two Ga dimers. Uninterrupted rows of As dimers are separated by two rows containing Ga dimers, oriented perpendicularly to the As dimers. The model therefore directly implies a surface As concentration of 0.5 ML. Nodes along the centre of the rows are resolved, albeit with poor resolution, in a number of places in Fig. 5.7(ii). This node in the dimer rows has also been observed in high resolution images of the c(2x8) reconstruction[16]. For both the c(2x8) and c(8x2)/(4x1) phases the node can be associated with the higher energy of the filled As lone pair states relative to the As-As dimer bond. Fig. 5.8 is an image of the coexistence of (2x6) and (4x1) reconstructions on a different sample surface. As also suggested by both Biegelsen *et al.* [3] and Skala *et al.*[25], we believe it is this mixture of phases that gives rise to a (4x6) LEED pattern. Our images of the (2x6) phase are in excellent agreement with those of Biegelsen *et al.*[3] discussed earlier (Fig. 5.3). A large amount of surface disorder, probably due to randomly bonded As, is evident near the boundary of the two phases.

Tunnelling spectroscopy (I(V)) characteristics for the c(2x8) surface have been previously published[34]. Acquisition of such I(V) spectra is possible by opening the feedback loop and ramping the sample voltage while measuring the tunnelling current. The characteristic reproduced in Fig. 5.9 was taken over the dimer rows of the (4x1) reconstruction. Current observed at negative sample bias is due to tunnelling from filled states (valence band states, if no surface states are present in the band gap). In this case, filled states are due to the As lone pair orbitals. Strangely, I(V) spectra taken over the Ga dimer rows were identical to that of Fig.5.9. This effect was explained by Gallagher *et al.*[34] for the c(2x8) surface by proposing that during spectroscopic measurements the tip couples strongly only with the As lone pair orbitals, even when positioned over the missing dimer rows. As the current observed at positive sample bias is much smaller than for negative bias, achieving atomic resolution in empty state images within the voltage range measured will be very difficult. Indeed, Skala *et al.*[25] required a bias of +3.4 V to acquire well resolved empty state images in their recent STM study of the c(8x2) surface.The most important observation from our measurements is that the I(V) spectra for the (4x1) surface were almost identical to those for the (2x6) surface (not

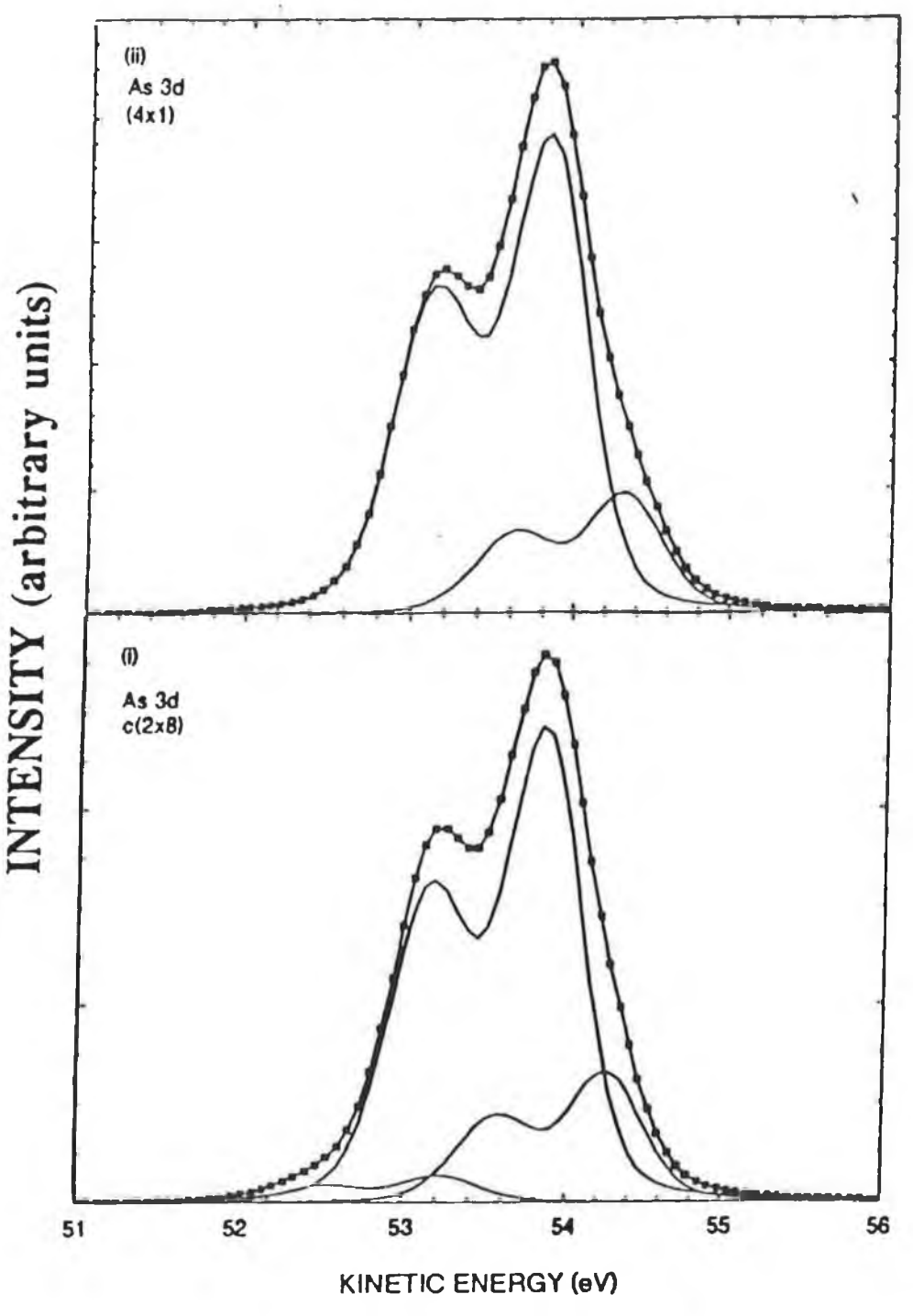

Fig 5.5 *Results of the curve fitting procedure applied to the As 3d spectrum of,* **(i)** *the clean c(2x8), and,* **(ii)** *the clean (4x1) GaAs(100) surfaces.*

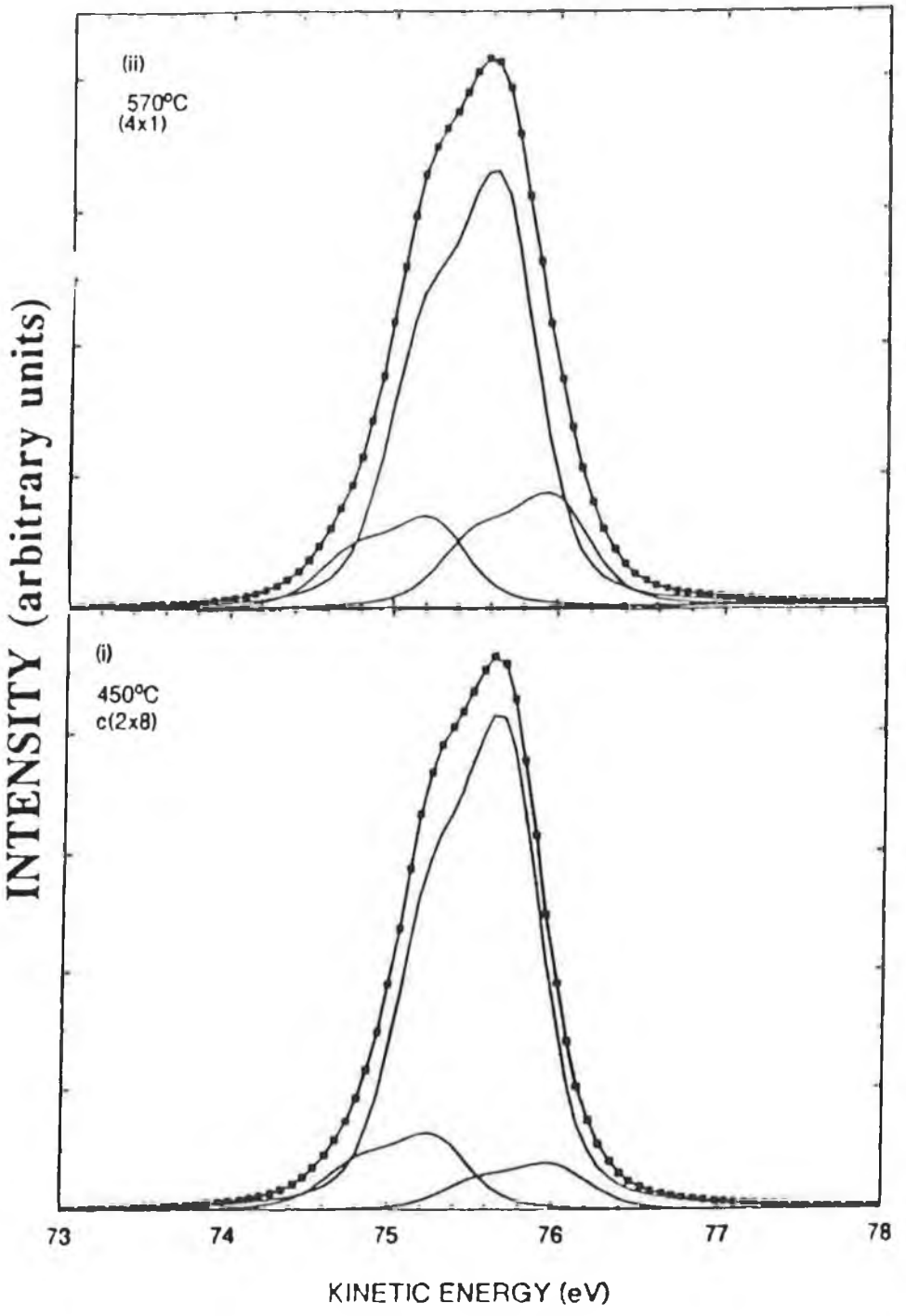

Fig 5.6 *Results of the curve fitting procedure applied to the Ga 3d spectrum of,* **(i)** *the clean c(2x8), and,* **(ii)** *the clean (4x1) GaAs(100) surfaces.*

reproduced) and also the c(2x8) spectra of Gallagher *et al.*[34]. In all cases the Fermi level position - 0V in the spectra - is pinned near the centre of the band gap. On the GaAs(100) surface, the surface states that cause the pinning have been found to reside not mid-gap, but instead at the valence and conduction band edges. Very high dynamic range (possible by moving the tip closer to the surface during a spectroscopic scan) is essential to observe these states[35], but this is not a feature of the spectrum of Fig. 5.9. As will be discussed in depth in the following chapter, Feenstra and Stroscio[36] have observed dopant-derived states in the I(V) spectra of cleaved (unpinned) GaAs(110) surfaces. These states serve to remove the appearance of the band gap in tunnelling spectroscopy characteristics. Band bending due to surface states (either intrinsic or extrinsic) "pinches off" these dopant states, with the band gap of ≈ 1.4 eV visible in Fig.5.9. Valence band spectra of both the c(2x8) and (4x1) surfaces are reproduced in Fig.5.10. Similar to the spectra of Spindt *et al.*[17], there is only a slight difference between the two. This correlates well with the similarity of the tunnelling spectroscopy characteristics and is a strong indication that the electronic density of states and thus the Fermi level position of the c(2x8) surface is not dramatically different from the (4x1) surface. Measurements of the position of the VBM with reference to the Fermi level of a Ta metal foil in contact with the sample, confirmed that the semiconductor Fermi level was pinned mid-gap for all reconstructions.

One question regarding the photoemission data for the clean (4x1)/c(8x2) surface remains to be answered. For the Ga 3d spectra, two surface components are required to achieve a good fit to the data in both our results and many other groups'[17,18,27]. If the model of the c(8x2) reconstruction proposed by Skala *et al.*[25] is correct, all surface Ga is dimerised and thus in the same bonding orientation. Therefore, only one surface component should be sufficient to fit the data. The reason for this discrepancy is at present unclear but may again be due to an existence of slightly differing unit cells across the surface. As the (4x1) phase is said to consist of disordered c(8x2) unit cells, this proposal may be plausible. A second explanation is in terms of the MEIS data of Falta*et al.*[26] where intermixing of Ga and As in the uppermost atomic layer was proposed. Unfortunately, it is not possible to identify the exact origin of both Ga 3d surface components with our photoemission data while remaining consistent with the c(8x2) model of Skala *et al.*[25] that provides the best explanation of our STM and AES data.

A c(2x8) surface was exposed to a sulphur flux from an electrochemical cell (described in Chapter 3) operated at a current of 0.5 mA for 5 minutes. The results of this exposure, with subsequent annealing at 250°C,350°C and 550°C on both the As and Ga 3d core levels are displayed in figures 5.11 and 5.12 respectively. Room temperature adsorption of sulphur (Fig 5.11(i)) leads to the disappearance of the As 3d low BE surface component with two very broad components appearing at 1.1eV and 1.7 eV higher BE. A smaller magnitude broadened component exhibiting a chemical shift of 0.5 eV to higher binding energy appears in the Ga 3d spectrum (Fig.5.12(i)). This 0.5 eV

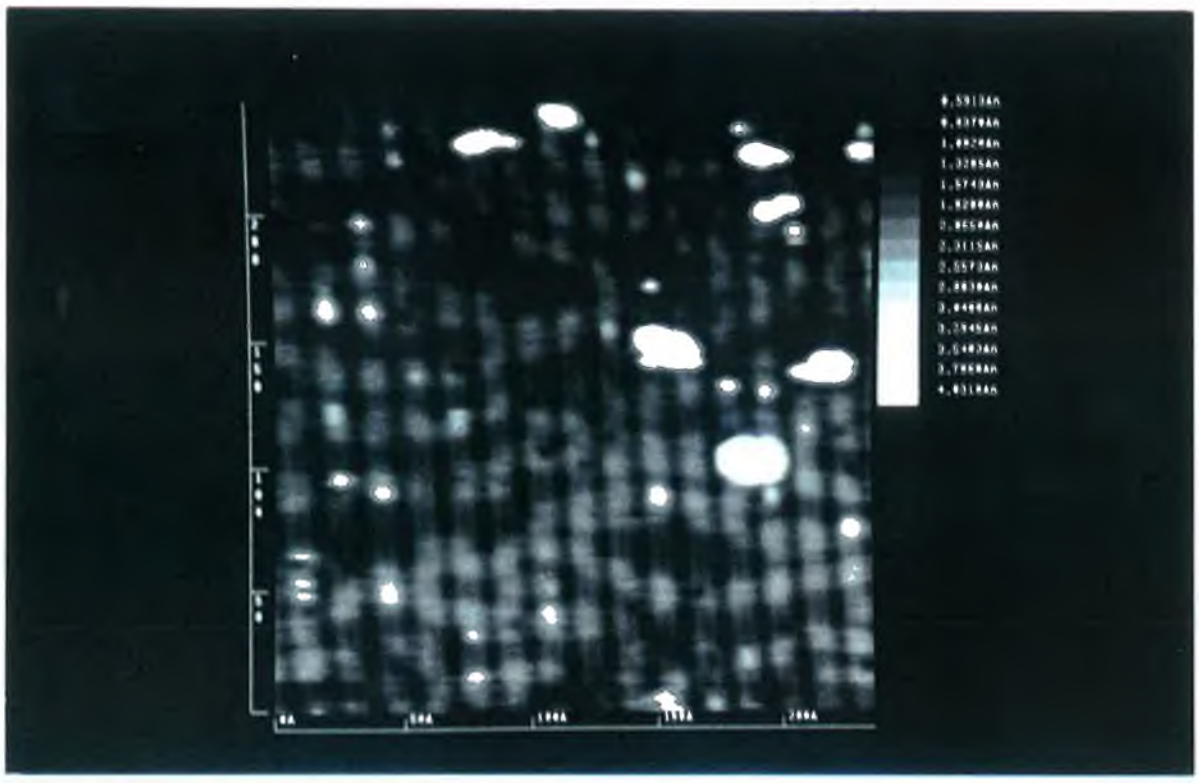

(i)

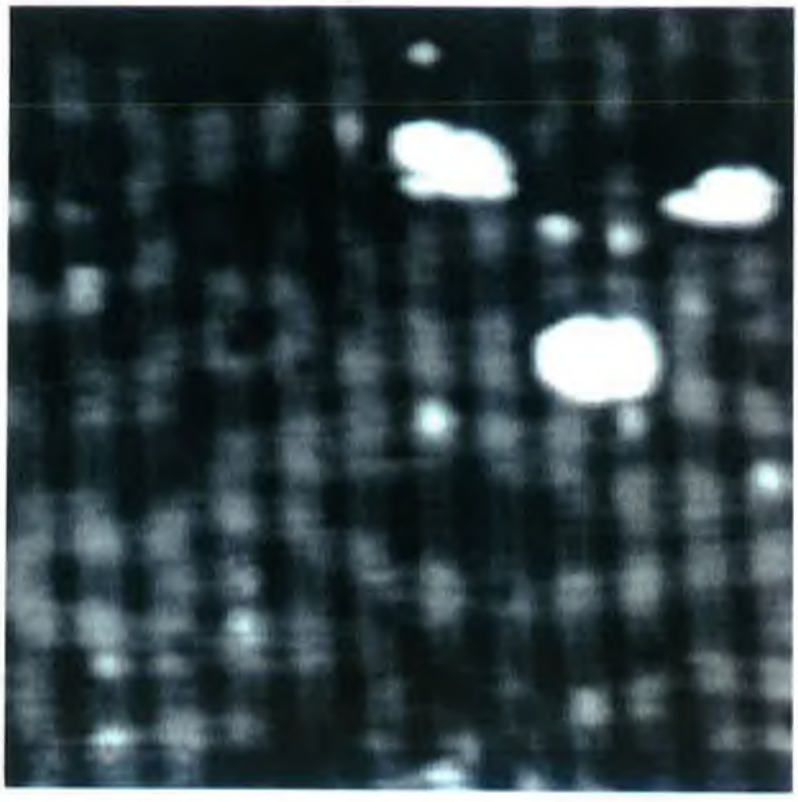

(ii)

Fig 5.7(i) *The GaAs(100)-c(8x2) surface reconstruction imaged with a bias of 2V and a tunnelling current of 1 nA;* **(ii)** *a "zoom" of fig. 5.7(i) with nodes in the dimer rows resolved in places.*

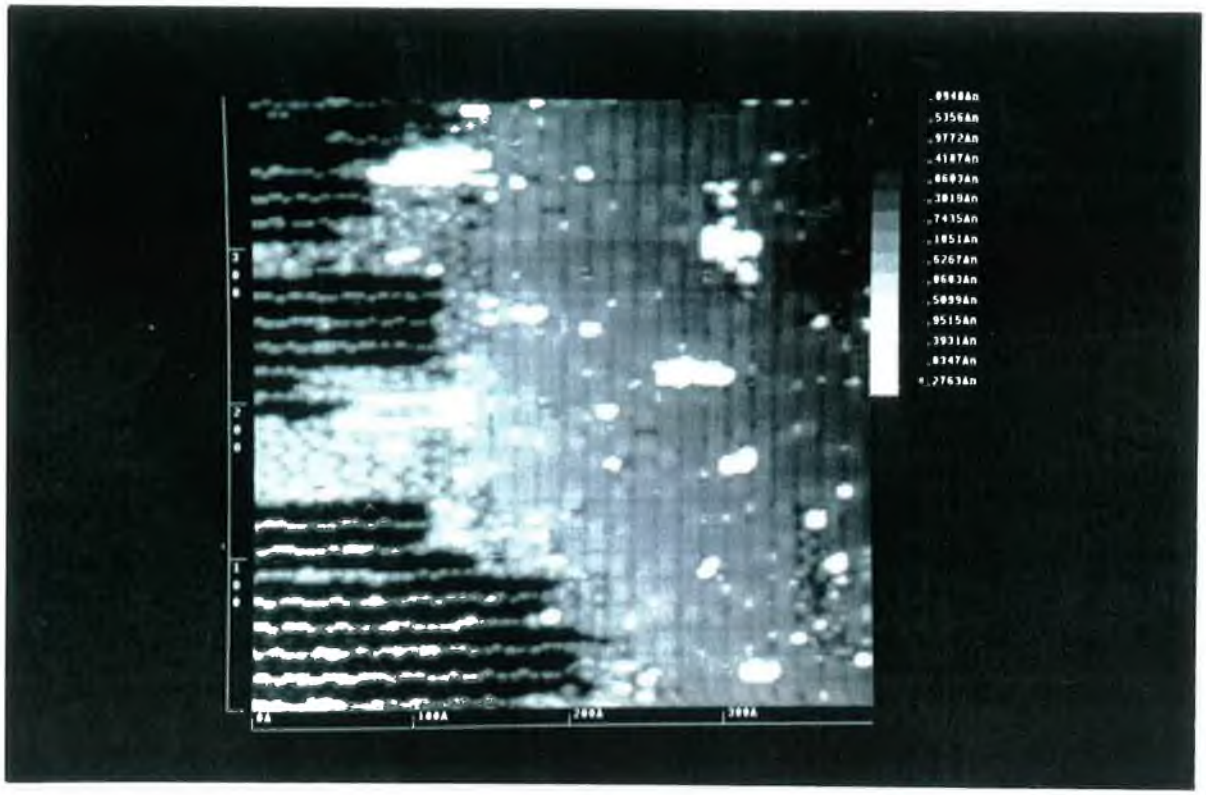

Fig. 5.8 *A coexistence of (2x6) and (4x1) phases. A large amount of disorder is visible near the boundary of the phases.*

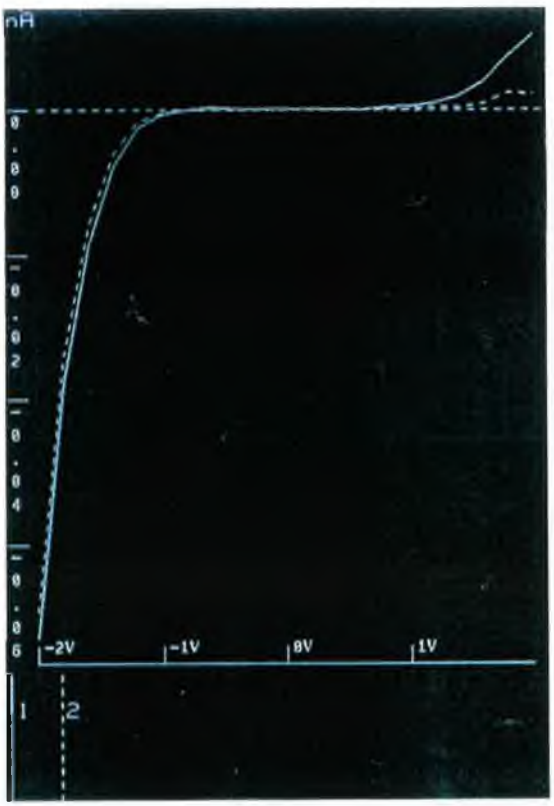

Fig 5.9 *Tunnelling spectroscopy characteristic of the GaAs(100)- (4x1) surface.*

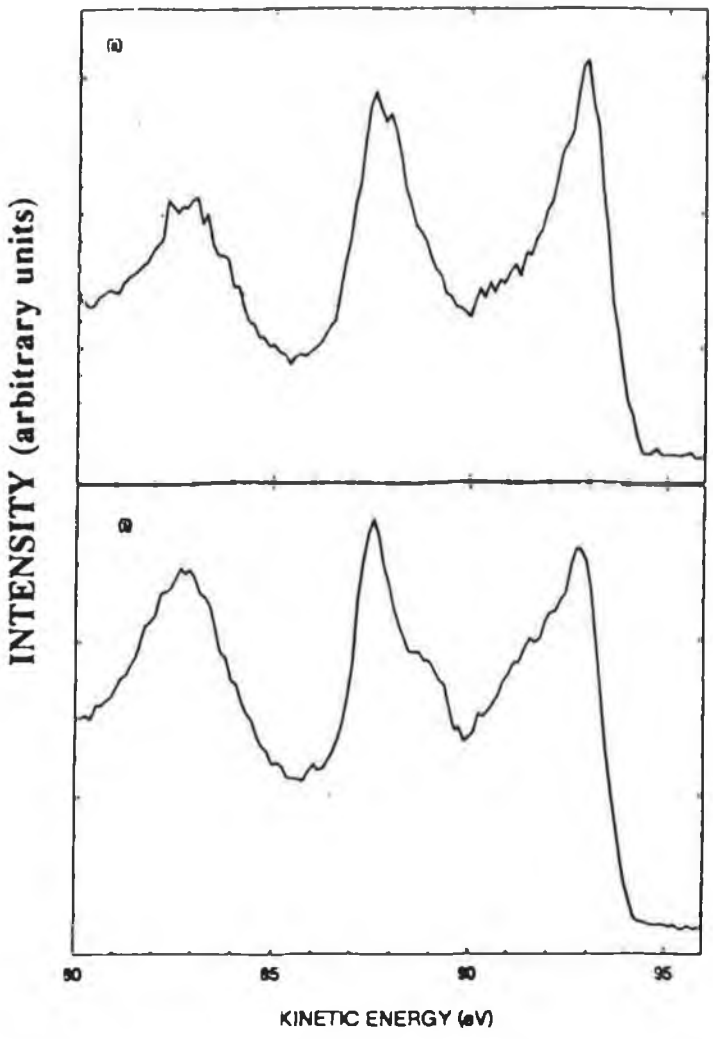

Fig 5.10 *Valence band photoemission spectra for,* (**i**)*the c(2x8), and,* (**ii**)*the (4x1) surfaces.*

shift is in good agreement with the 0.55eV value determined by Spindt *et al.*[37] for the $(NH_4)_2S$ treated surface. Like Spindt *et al.*[37], we find no evidence of a second S-Ga component as was observed by Sugahara *et al.*[38] for $(NH_4)_2S_x$ treated surfaces. Both the etching rate and excess sulphur concentration of this latter solution were proposed as the origin of the second Ga-S bonding component. Further experiments by that group[38], using an electrochemical cell to expose chemically cleaned GaAs(100) samples to S at elevated temperatures have found only one Ga-S peak at 0.6 eV higher BE. Interestingly, in common with all other groups, we have observed a larger chemical shift for the As-S bond than for the Ga-S bond. This may seem strange considering the electronegativity difference of S and Ga is larger than that of S and As. However, Hirayama *et al.*[39] have noted that when S bonds to As the electron charge is transferred from As to S. This is "opposite" to the direction of charge transfer in the Ga-As bond and results in a large chemical shift.

Although it is possible to fit the As 3d spectrum of Fig.5.11(i) with a single much higher intensity broad peak due to sulphur, it was found that after annealing to 250°C the component at 1.7eV disappears while there is little change in the component at 1.1 eV.

Furthermore, for RT S adsorption on both the (4x6) and (4x1) surfaces, the magnitude of the 1.7 eV component is severely attenuated with respect to that on the c(2x8) surface. This suggests that this component is related to the excess As concentration on the GaAs surface. The randomly bonded excess As remaining from the cap may react with the adsorbed sulphur forming a volatile arsenic sulphide compound that desorbs at relatively low temperatures. Similar observations were made by Roberts *et al.*[40] in an earlier study of the *in situ* reaction of sulphur with the decapped GaAs(100) surface. Spindt *et al.*[37], in a UPS study of the $(NH_4)_2S$ treated GaAs(100) surface also observed a very broad chemically shifted component at 1.7 eV higher relative binding energy. The magnitude of the relative binding energy of this shift is a further indication of arsenic sulphide compound formation. Significant disorder in the overlayer contributes to the severe broadening of both the chemically shifted components. The very high diffuse background of the (1x1) LEED pattern (Fig.5.13) observed for this surface and STM imaging confirmed this high degree of disorder. For RT exposure of a GaAs(100)-(4x1) surface to sulphur, it was found that the S(152eV) Auger line displayed large variations across the surface. Attempts to follow the adsoption of sulphur on the surface in terms of a Bier's law attenuation law were not successful, strongly suggesting that sulphur does not follow a layer-by layer growth mechanism for RT adsorption.

While the As 3d chemically shifted component at 1.7 eV disappears after a 250°C anneal (Fig. 5.11(ii)), there is an increase in the magnitude of the chemically shifted component in the Ga 3d spectrum. This removal of the 1.7 eV chemically shifted component in the As 3d spectrum was similarly observed by Spindt *et al.*[37] after annealing at 250°C. In a study of temperature dependent changes on $(NH_4)_2S_x$ treated GaAs(100),GaAs(111)A and GaAs(111)B surfaces, Scimeca *et al.*[41] have found that the intensity of the Ga-S bond increases at the expense of the As-S intensity as the sample is annealed. After annealing at 350°C, figures 5.11(iii) and 5.12(iii), the higher BE component in the As 3d spectrum is completely removed while there is a significant increase in the Ga-S intensity. That Ga-S bonds become dominant after annealing in the 350°C range was previously noted by both Oigawa *et al.*[38] and Sugahara *et al.*[42] from SR PES studies of aqueous sulphide treated surfaces. This suggests a higher stability of Ga-S bonds over As-S bonds which is likely considering their respective heats of formation and their relative bond energies as calculated by Ohno[43].

Considerable reduction in the diffuse background of the (1x1) LEED pattern occurs as the S exposed GaAs(100) surface is annealed from RT to 350°C. At 250°C, a clear (1x1) pattern is visible. A RHEED and XPS study[38] of $(NH_4)_2S_x$ etched GaAs(100) surfaces also described the appearance of a (1x1) RHEED pattern after RT treatment which was attributed to S bridge bonded to underlying Ga atoms. However, the $(NH_4)_2S_x$ passivated GaAs(100) surface has shown no observable LEED pattern to date, suggesting the formation of an amorphous S compound overlayer. This contrasts with the highly stable LEED pattern observed on the $(NH_4)_2S_x$ treated InP(100) surface

which persisted even after three days exposure to air[44]. High resolution XPS studies showed that the sulphur-induced InP(100)-(1x1) surface is terminated by S which bonds only to In. Based on these studies, Tao *et al.*[44] have suggested that S occupies the bridge site of phosphorous vacancies - i.e. a sulphur-phosphorous exchange reaction occurs. From the As 3d core-level spectra of Figs 5.11(i) - (iii), it is evident that for the (1x1) LEED pattern observed in our studies, a single bulk component is insufficient to fit the spectrum. Therefore, in our case, the (1x1) phase can not solely be due to S bridge bonded to underlying Ga. As suggested recently by Berkovits and Paget[45], the (1x1) pattern is most likely due to an amorphous sulphur layer which covers the surface, saturating dangling bonds and thereby preventing the formation of dimers. The (1x1) LEED pattern observed can therefore be attributed to the bulk terminated GaAs pattern which is observed through the disordered sulphur overlayer. STM imaging of the (100) surface after RT adsorption of sulfur confirmed the presence of this disordered overlayer (Fig. 5.14). Massies *et al.*[46] found that for room temperature H_2S treatment of the GaAs(100)-c(2x8) and (4x1) surfaces adsorption is non-dissociative leading to a disordered overlayer and a (1x1) LEED pattern. However, we still observe a very clear 1x1) LEED pattern after annealing at 350°C where no S-As component is visible in the core level spectrum of Fig.5.8(iii). Indeed, a surface shifted component at 0.47 ± 0.02 eV appears towards lower BE, within the energy range of a similar low BE surface component which appears on both the (4x1) and (4x6) surfaces. It may be possible that there exists a minimum activation energy for the formation of As dimers on the (100) surface which is not achieved by annealing at 350°C. However, this is only a very tentative suggestion and the exact origin of the (1x1) phase at 350°C is not understood.

After annealing at 550°C the (1x1) LEED pattern changes to a (2x1) pattern (Fig. 5.15).(A gradual sharpening of the 1/2 order spots occurs in the 350°C-500°C range). This sulphur induced reconstruction was first observed by Massies*et al.*[46] after H_2S treatment of the c(2x8) surface at 700 K and has been more recently observed in both RHEED[39] and other LEED[47] studies. AES studies by Massies *et al.*[46] suggested that for H_2S exposure at elevated temperatures, S exchanges with As in the surface layer producing the (2x1) phase. Estimates of the sulphur coverage from the attenuation of the Ga(55 eV) Auger line, by that group, ranged from 0.7 - 1.0 monolayer. Again, the suggestion that there is a surface sulphur -arsenic exchange reaction leading to the (2x1) phase is inconsistent with our photoemission data. There is very little observable difference between the As 3d spectrum of the (2x1) surface (Fig.5.11(iv)) and that of the clean (4x1) surface (Fig.5.5(ii)) which results after annealing at 570°C. (Annealing at 570°C is accompanied by the disappearance of the S 2p photoemission and S 152 eV Auger peaks. Changes in the S 2p spectrum as a function of annealing temperature are described later in this section).

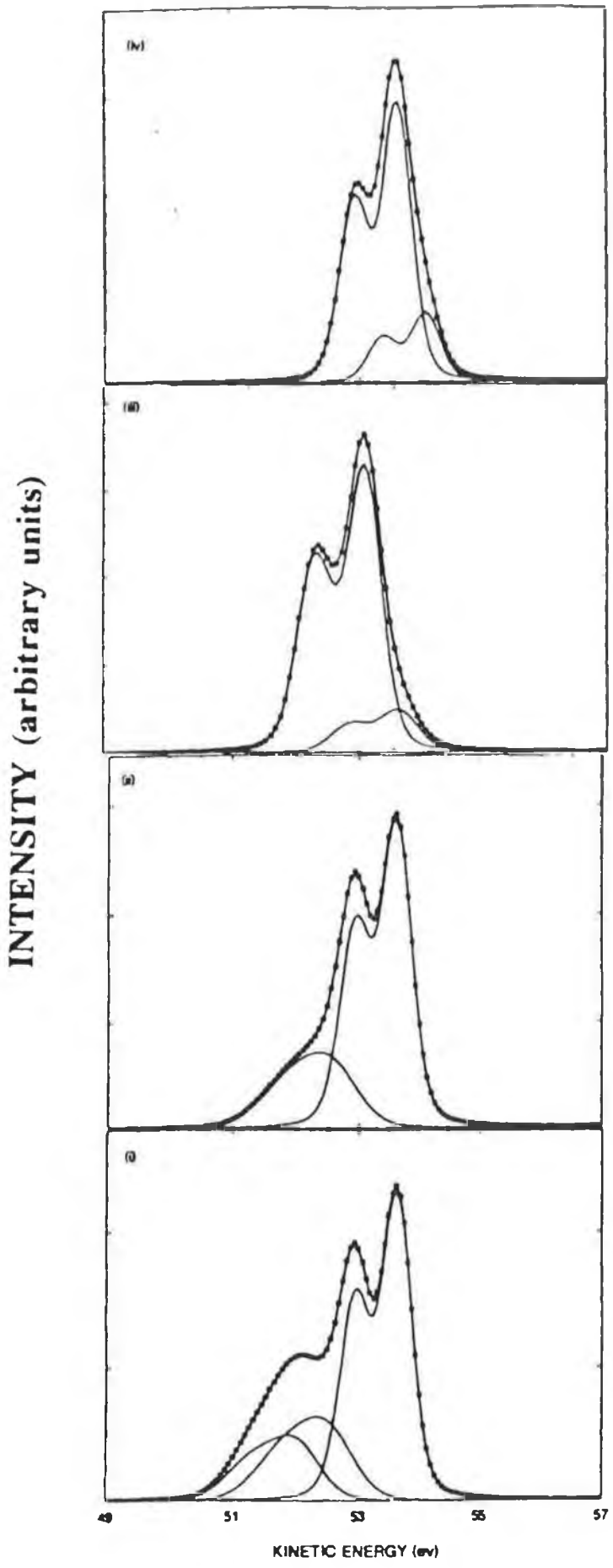

Fig 5.11 *As 3d spectra for the sulphur exposed and annealed c(2x8) surface. (i) RT adsorption, (ii) 250°C, (iii) 350°C, and (iv) 550°C,*

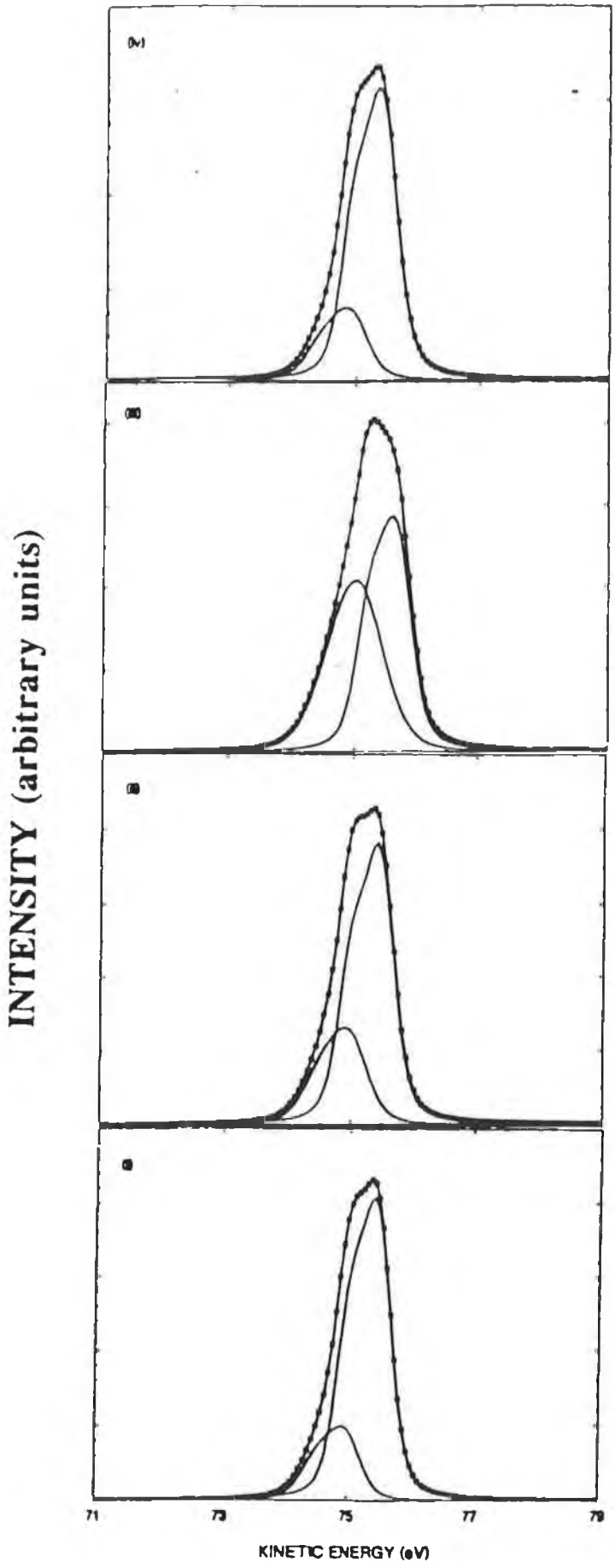

Fig 5.12 *Ga 3d spectra for the sulphur exposed and annealed c(2x8) surface. (i) RT adsorption, (ii) 250°C, (iii) 350°C, and (iv) 550°C,*

Fig 5.13 *(1x1) LEED pattern observed after room temperature S adsorption on the GaAs(100)-c(2x8) surface.*

As stressed previously, an As-S surface exchange will lead to the As 3d spectrum consisting of only a bulk component. Indeed, this is the case for the Se induced GaAs(100)-(2x1) reconstruction as investigated by Takatani *et al.*[48]. As for the sulphur treated c(2x8), (4x6) and (4x1) surfaces investigated in the present study, all Se stabilised surfaces showed a (2x1) reconstruction irrespective of the initial clean surface reconstruction. The As 3d peak for the Se/GaAs(100)-2x1 surface was fitted with a single component of bulk GaAs. Similarly, Gallet and Hollinger[49] find only a single P (bulk) component for the S treated InP(100) surface whereas the In peak exhibits a sulphur induced chemically shifted component. An exchange reaction was once more proposed to occur between P and S. That group, however, make the important point that for a (2x1) surface unit cell with a monolayer of sulphur dimers, a charge imbalance problem occurs. (This can be easily determined by use of simple electron counting arguments). They suggest that the existence of both S-S and P-P dimers with the same surface concentration is the only arrangement that will lead to an electrically neutral surface.

Filled state STM images of the S induced (2x1) surface are shown in Fig.5.16, taken with a bias of -2V and a tunnelling current of 1nA. Attempts at imaging this surface at positive bias (i.e. empty state imaging) were unsuccessful, with considerable feedback loop instability. The dimer rows, running in the (110) direction and with an 8 Å period,

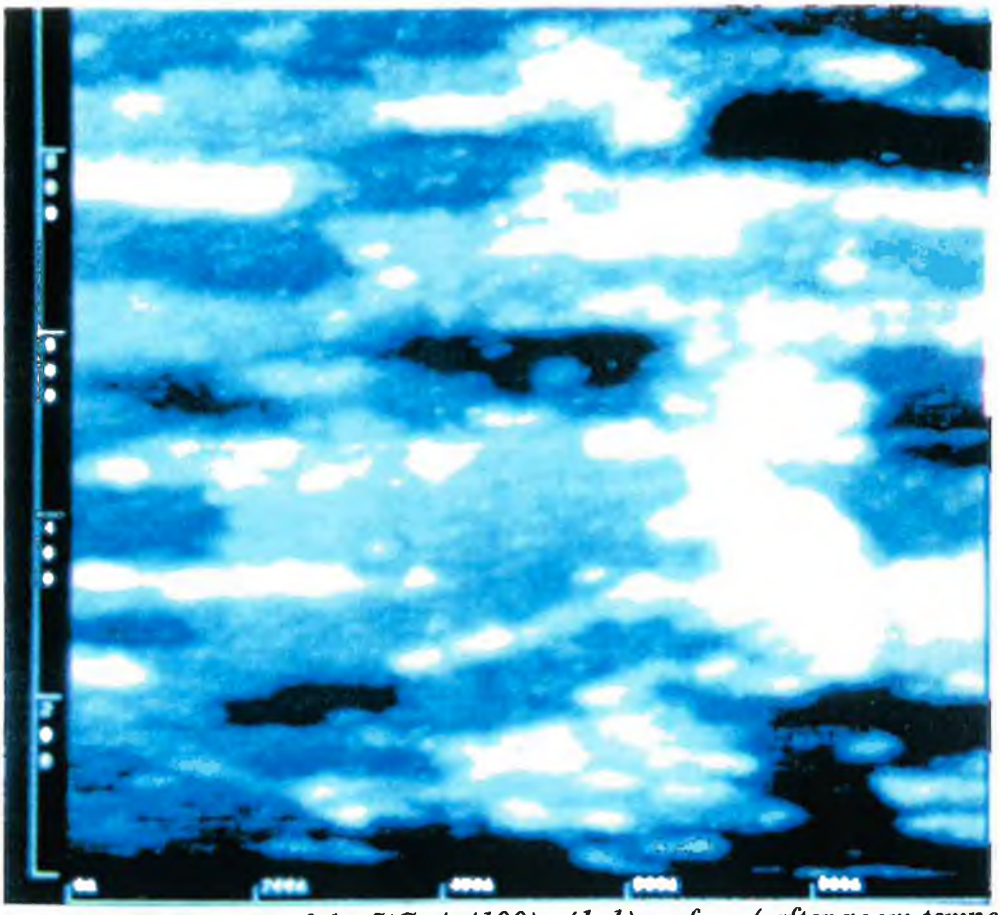

Fig 5.14 *An STM image of the S/GaAs(100) - (1x1) surface (after room temperature S adsorption).*

Fig 5.15 *The S/GaAs(100) - (2x1) LEED pattern formed after annealing above 350°C*

are clearly visible. A fair degree of disorder is present across the surface as a whole, with small islands clearly visible. These islands could have a number of sources. It is possible that they are excess As remaining from the decapping procedure bound to S, excess S remaining after annealing or, perhaps, As that has diffused to the surface as a result of a bulk S-As exchange as described below. A number of factors lead us to believe that the dimer rows consist of both As and S dimers. At no stage in the annealing process, and particularly for the (2x1) surface, is a bulk component sufficient to fit the As 3d peak. There is, furthermore, little change in the As 3d spectra for the (2x1) and clean (4x1) surfaces. An AES analysis of both the (2x1) and (4x1) surfaces yielded an average $I_{Ga}(2x1):I_{Ga}(4x1)$ ratio of 0.77. (Here it should be stressed that for the (2x1) surface the S (152eV) Auger peak intensity was homogeneous across the surface). Using the layer model of Ranke and Jacobi[21], as also applied by Massies *et al.*[46] to measurements on the H_2S exposed surface, the coverage (θ) of the adsorbed sulphur is given by:

$$\theta d = -\lambda_s \ln (I_{Ga}(2x1) / I_{Ga}(4x1)) \qquad (5.1)$$

where d is the thickness of a monolayer and λ_s is the escape depth for Auger electrons for a transition occuring on the substrate atoms. Using an escape depth of 5-10 Å and a value for d of 2.3 Å (according to the data of Massies *et al.* [46]), we find a sulfur coverage, θ=0.56 - 1 ML. At the lower limit, a half monolayer S coverage is in good agreement with that predicted by the electron counting rule for an electrically neutral S/GaAs(100) surface. Sulphur satisfies its back-bonding to the underlying Ga atoms in the same way as As, i.e. by contributing 1.25 electron to each bond[43]. This means that each S atom in an S-S dimer has an excess of 6-(1.25)-(1.25)-1 or 2.5 electrons.This extra 0.5 electron per S atom (or 1 electron per S dimer) can fully compensate the 1 electron deficit of each As-As dimer. This means that all surface atoms are in a closed shell environment with all dangling bond orbitals full. These filled dangling bond orbitals will thus lie in the VB, rendering the surface chemically inert[15].

Assuming that there is little difference in the unit cell structure of the (4x1) and c(8x2) surfaces, and accepting the proposal of Skala *et al.*[25] that the surface As concentration of the c(8x2) surface is 0.5, one possible surface structure for the S induced GaAs(100)-(2x1) phase consists of equal numbers of As and S dimers. For this model, we must assume that the As and S dimers have approximately the same scattering probability as LEED does not distinguish between them. The inability to stably tunnel at positive sample bias is a further indication of a closed shell environment for each atom. One other point to make regarding the STM image is that it is not possible to resolve a node in any of the dimer rows as was possible for the (4x1) surface. For the fully filled S and As orbitals of the (2x1) surface, Coulombic repulsion due to their spatial proximity is likely to make observation of this node unlikely. The filled state charge density is

therefore more spatially localised over the dimer. Further evidence that the (2x1) surface is terminated in both As-As and S-S dimers was provided by the Reflectance Anisotropy (RA) studies of Berkovits and Paget[45]. This group observed the appearance of a positive RA signal associated with the formation of S dimers after annealing an aqueous sulphide treated surface above 440°C. The As dimer signal (of the same polarity) was however still present in the RA spectrum of the annealed surface. After complete desorption of S by annealing at 585°C, both As and Ga dimer signals (with opposite polarity due to their orientation) were present in the RA spectrum.

The possible geometries for the (2x1) sulphur terminated GaAs(100) surface suggested by Ren and Chiang[50] are inconsistent with our results. Three of these geometries involved the bridging of As dimers with either a sulphur atom or sulphur dimer. As is evident from our core level spectra, the (2x1) surface exhibits only S-Ga bonding. Ren and Chiang[50] proposed one further geometry whereby an S atom replaced an As atom in a S dimer. Both the absence of As-S bonding and AES results determining that As is not lost from the (4x1) surface as a result of the formation of the (2x1) structure would again argue strongly against this geometry.

All previous studies of the reaction of aqueous sulphides with the GaAs(100) surface have noted a 0.2-0.3 eV Fermi level shift towards the CBM (n-type samples) when compared with the untreated surface. This shift only occurred after annealing in the 350°C-400°C range and was attributed to the formation of Ga-S bonds. Annealing of chemically etched GaAs(100) samples at 550°C in a sulphur flux from an electrochemical cell also led to a decrease in band bending by 0.2-0.3 eV[38]. For the c(2x8) surface we observe a 0.2 eV shift of the Fermi level position towards a flat band condition *after room temperature adsorption*. No change in the Fermi level position was noted during subsequent annealing until, at 570°C, sulphur is completely desorbed and a return of the Fermi level to its original position occurs. Interestingly, for both the (4x6) and (4x1) surfaces the situation is quite different. After RT adsorption the same shift of 0.2 eV is observed, however after annealing to 500°C the Fermi level position is 0.4 and 0.5 eV closer to the CBM than for the respective clean surfaces. In both cases a (2x1) LEED pattern, of similar quality to that described for S adsorption on the c(2x8) surface, was observed. The As 3d core level spectra for both (2x1) surfaces were qualitatively similar, but the chemically shifted component in the Ga 3d spectrum was increased in magnitude. This Fermi level movement suggests a possible alternative interaction between sulfur and the GaAs surface. The lower the initial decapping temperature and, thus, the more As rich the starting surface, the greater the degree to which As-S compound formation occurs. When heated, this As sulphide desorbs removing sulfur from the surface. On annealing this surface further, the As dimers reform along with sulfur dimer formation, but band bending hasn't been reduced to any significant extent. On the (4x1) starting surface, there is less As for compound formation so more sulfur can bond to the surface Ga atoms resulting in a better unpinning of the surface. This model would suggest that

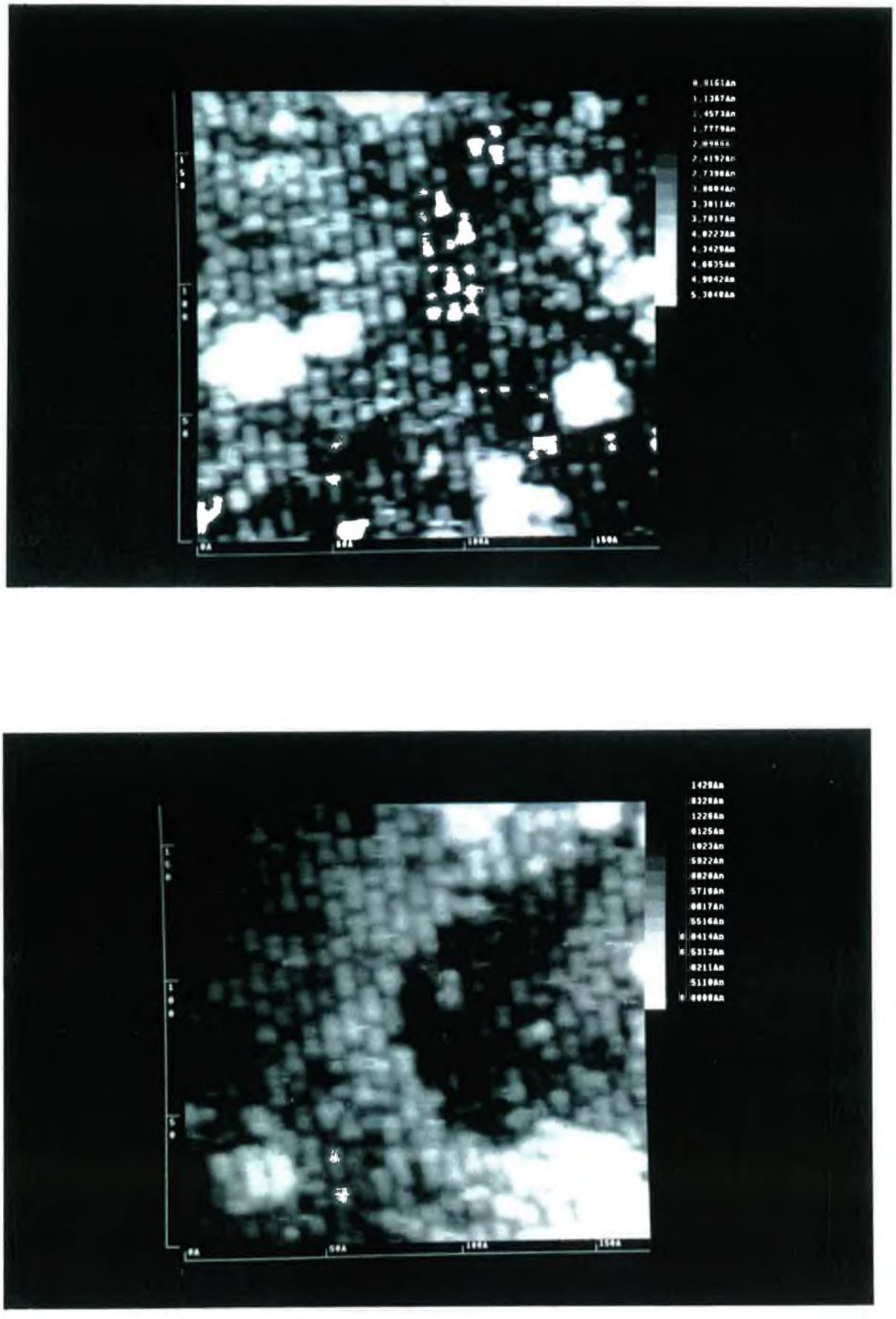

Fig 5.16 *Filled state STM images of the S/GaAs(100)-(2x1) surface. An atomic step, 2.8 Å high, is visible in the lower image.*

the less As dimers there are on the 2x1 surface, the better the Fermi level unpinning. It does not explain why the sulfur atoms dimerise nor is it consistent with the electron counting model. However, although the electron counting model explains the various reconstructions of the GaAs(100) surface, it does not account for the Fermi level pinning on these surfaces. From our experimental observations the sulphur doesn't cause a large shift in the Fermi level position unless the starting composition is (4x1), therefore it is not clear how important the electron counting model is in explaining Fermi level pinning, although it is undoubtedly invaluable in providing surface structural models.

From the results detailed above we have outlined two possible models for the (2x1) surface reconstruction. However both ignore one significant observation which is evident from the photoemission data. Spectra of the S 2p core level ($h\upsilon$=190 ev) taken at 250°C,350°C and 550°C consistently exhibit two components (Fig.5.17(i)-(iii)). This is inconsistent with there being only one S-Ga bond configuration. Non-linear least-squares fitting of the S 2p spectra showed a Lorentzian width of 0.21± 0.02 eV, a spin orbit splitting of 1.18 ± 0.03 eV, an energy separation of the two peaks of 0.85 ± 0.03 eV and a branching ratio of 0.46 ± 0.03. This final value is close to the ratio of the degeneracy (2J+1) of the $2p_{1/2}$ and $2p_{3/2}$ levels. As the annealing temperature is increased the Gaussian FWHM of the S 2p peaks decreases from 0.85 eV (1x1 LEED pattern) to 0.74 eV (2x1 LEED pattern). This trend, along with the temperature dependent attenuation of the peak at lower BE has also been found by Scimeca *et al.*[51] for the Se treated GaAs(100) surface. They propose a model whereby Se exchanges with As up to four atomic layers into the GaAs crystal. This diffusion into the bulk GaAs is likely to occur for sulphur too, considering the negligible difference in the covalent radii of S and Se, explaining the presence of the two S 2p components (surface and bulk) while there are only Ga-S bonds evident from the As and Ga 3d core-levels. An angle resolved core-level study of the Se treated (100) surface by Maeda *et al.*[52] has identified the component at lower BE with the surface bonded Se while the higher BE component was found to be due to four-fold co-ordinated (bulk) Se. Oshima *et al.*[53] have proposed a model for the $(NH_4)_2S_x$ passivated GaAs(100) surface where a full monolayer of S terminates the surface and more sulphur exchanges with As in the third layer. The temperature dependent attenuation of the lower BE component relative to the higher BE component in the S 2p spectra of Fig.5.17 is an indication of sulphur penetrating into the bulk crystal as a function of annealing temperature. The X-Ray Photoelectron Diffraction data of Gallet and Hollinger[49] from the annealed $(NH_4)_2S_x$ treated InP(100) surface has further indicated that the reaction of S with InP is not limited to the first atomic layer but extends to a number of layers below the surface. They suggest also that the out-diffusion of P (after exchange with S in the bulk) may play an important role in the process. It is not possible to tell whether out-diffusion of As plays a significant role during the annealing of the S covered GaAs(100) surface described here.

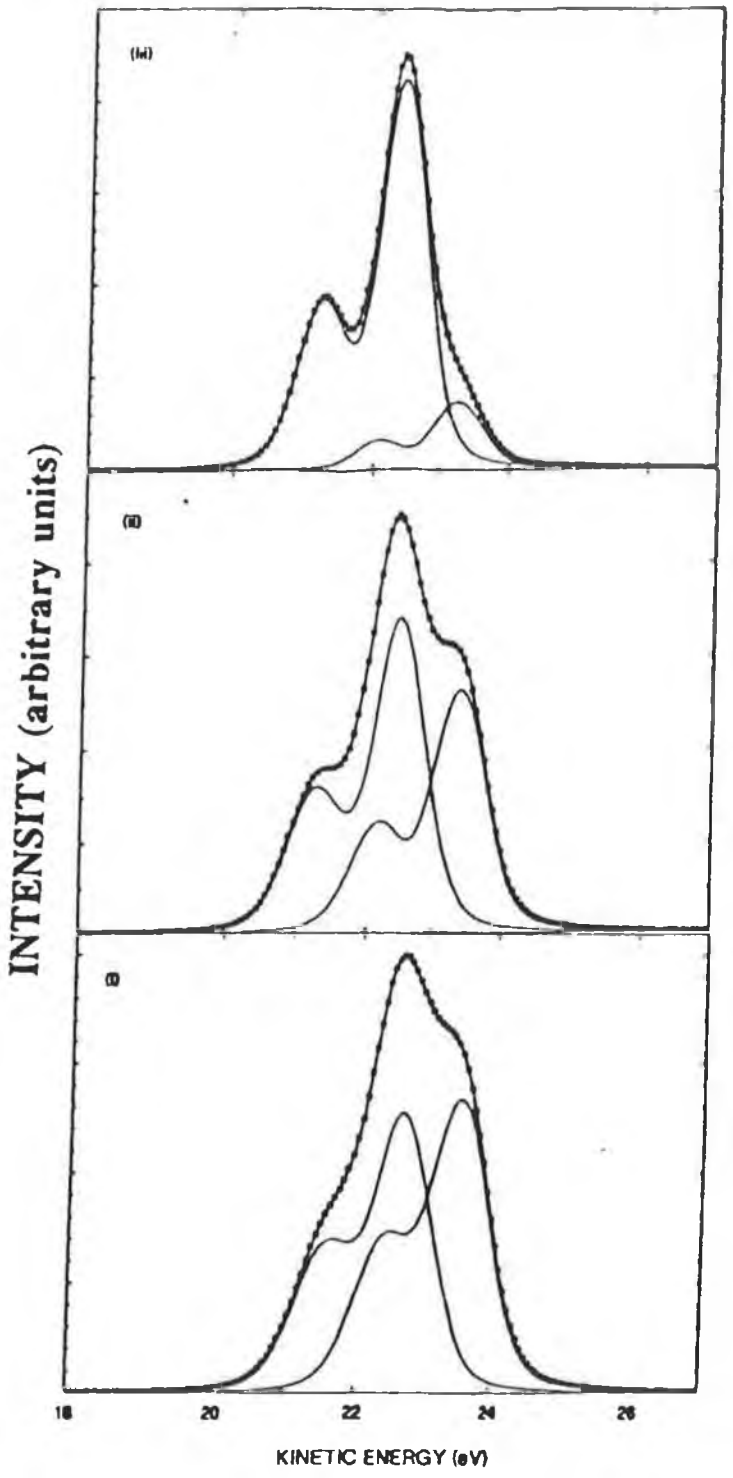

Fig 5.17 *S 2p core level photoelectron spectra for the sulfur treated GaAs(100) surface after annealing at (i) 250°C, (ii) 350°C and, (iii) 550°C*

In summary, the interactions between S and the GaAs(100) surface are complex and at present we cannot be sure of the significance of S penetrating into the surface layers as regards Fermi level position and can only speculate as to the exact composition of the (2x1) dimer rows. Significantly, we have not observed the replacement of all surface As with S as has been suggested previously and has been observed on the Se treated (100) surface. The observations that at 570°C the sulphur is totally desorbed (from both AES and SR PES data) and that the Fermi level moves back to its initial mid-gap position suggest that the sulfur hasn't penetrated too far into the surface which would cause surface doping. Similar behaviour has been reported for the Se/GaAs(100) reactions. Furthermore, the fact that it is possible to obtain almost flat band conditions on the sulphur treated surface by following the correct surface preparation procedure is significant for the potential technological applications of this surface.

5.3 The GaAs(111)B Surface : The As Trimer Model

Throughout the previous sections the "electron counting" rule has been employed to determine the extent of charge neutrality of various reconstructed surfaces. The driving force behind III-V semiconductor surface reconstruction is the minimisation of mid-gap dangling bond states by filling group V and emptying group III dangling bonds. Biegelsen *et al.*[54] have shown that the (2x2) reconstruction of the GaAs(111)B surface is also consistent with this "autocompensation". (For compound semiconductors, there are two inequivalent (111) faces. For GaAs the B face is As terminated). STM images of MBE grown samples acquired by that group strongly supported a model where As atoms are involved in trimer structures, arranged in a (2x2) symmetry, atop a full As layer (Fig.5.18).

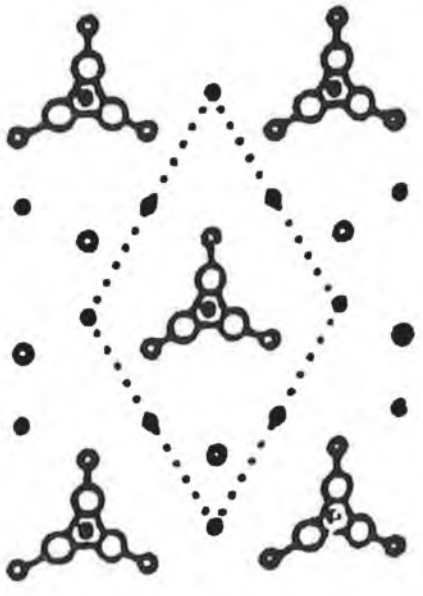

Fig.5.18 *The trimer model of the As rich GaAs(111)B surface as proposed by Biegelesen et al. (From ref 54) (Large open circles represent chemisorbed As trimer atoms, small open circles first layer As, and filled circles second layer Ga).*

A consideration of this model in terms of the electron counting rule also indicates that, as for the (100) surface reconstructions, all As dangling bonds are filled while all Ga dangling bonds are empty. For the (2x2) unit cell, three of the four second layer As atoms are four-fold coordinated (bonded to three underlying Ga atoms and one As atom in the topmost layer). The fractional electron charge due to each of these three atoms is thus 5-1.25-1.25-1.25-1 = 0.25. All As trimer atoms are three-fold co-ordinated (to other As atoms) and therefore each atom has 5-1-1-1=2 electrons which are accomodated in fully occupied lone pair orbitals. One second layer three-fold coordinated As atom remains, which has a dangling bond containing 1.25 electrons. The excess 0.25 electron of each of the three four-fold co-ordinated second layer As atoms can thus saturate this dangling bond, leading to a situation where all As dangling bonds are filled.

Fig 5.19 illustrates STM images (V_{bias} = 3V, I_t = 50pA) of the decapped GaAs(111)B surface prepared as described in Chapter 3. As these are the first images of the decapped surface obtained it is interesting to note that the surface quality is comparable to that of the MBE grown surface. This is not the case for the (100) surface where decapped samples exhibit a higher degree of disorder. A number of surface stacking faults are visible which were also observed in the images of Biegelsen *et al* [54]. Much lower currents (<100 pA) were required to stably image the (111)B surface as compared to the (100) surface suggesting a lower density of surface states for the former. Images acquired at negative bias displayed much poorer resolution.

The inability to acquire adequate resolution filled-state images in the present study (and also in another very recent study of the decapped GaAs(111)B surface[54(a)]) may be explained by examining the tunnelling spectroscopy characteristics of Fig 5.20(ii). With respect to the image of Fig 5.20(i), I(V) curve (1) was taken above an As trimer on a well ordered region of the surface. Here it is evident that the majority of the tunnelling current occurs *into unoccupied states* of the sample. From the GaAs(111)B electronic surface structure, as discussed above, tunnelling into unfilled surface states should occur through empty Ga dangling bonds. As this would result in the observation of a (1x1) and not a (2x2) periodicity in the STM images, one possible explanation for the current flowing at positive sample bias is that it is due to unoccupied *anti-bonding* states of the As trimer. As, to the best of our knowledge, no band structure calculation or inverse PES experiment results have been published for the GaAs(111)B-(2x2) surface, we cannot determine the plausibility of this suggestion at the present time. Above a region where defects occur, as observed on the right hand side of Fig.5.20(i), I(V) characteristics typical of spectrum 2 were acquired. Here, the situation is reversed and much more current arising from filled state density occurs. It is proposed that the defect area represents missing As trimers with a corresponding exposure of underlying As dangling bond orbitals. Unfortunately, lack of dynamic range in the spectroscopy measurements (due to a very low tunnelling current of 50 pA) means that the position of

the band edges can not be accurately measured, and therefore, an estimation of the Fermi level position is not possible.

It is interesting to compare these STM images and tunnelling spectroscopy results with the As and Ga 3d core-level spectra obtained from a similarly decapped GaAs(111)B exhibiting a (2x2) LEED pattern. As for the GaAs(100) surface, a photon energy of 100eV was used to investigate both core levels. The fitting parameters for the clean surface are given in Table 5.II.Three components are necessary to provide a good fit for the As 3d peak (Fig.5.21(i)) - the bulk As-Ga component and two surface core level shifted (SCLS) components S1 and S2. The component shifted to relative higher BE (S1) suggests that the As atoms responsible for this component are chemisorbed on the

	As 3d	**Ga 3d**
Gaussian FWHM	0.48 eV	0.37 eV
Lorentzian width	0.13 eV	0.20 eV
Branching ratio	0.66	0.70
Spin Orbit Splitting	0.70 eV	0.45 eV
BE shift of S1	0.51 eV	
BE shift of S2	- 0.56 eV	

Table 5.II *The fitting parameters for the clean GaAs(111)B - (2x2) surface.*

surface, like the excess As component on the (100) surface, forming As-As bonds and giving rise to the (2x2) symmetry.

It is possible that excess (randomly bonded) As remaining from the cap may also contribute to the intensity of S1 but little evidence of undesorbed As was found in STM images over 1000x1000 $Å^2$ areas of the surface. The surface component shifted to lower BE in the As 3d spectrum (S2) can be attributed to the bulk terminating surface As atoms, i.e. the remaining As atom (not involved in the trimer structure) in the (2x2) unit cell of Fig.5.18 which has gained electron density. Further evidence that the (111)B surface is terminated in more than a monolayer of As was evident from AES spectra where an As (31 eV) : Ga (55 eV) ratio of 4.5 was found, in good agreement with the results of Ranke and Jacobi[55].

As found previously by Katnani *et al.*[9] and Ranke and Jacobi[56], the Ga 3d peak (Fig.5.21(ii)) can be fitted with a single spin orbit doublet. This is a clear indication that, for the GaAs(111)B surface, all Ga is in a four-fold or bulk-coordinated environment which is consistent with the model of Biegelsen *et al.*[54] (Fig 5.18) described above.

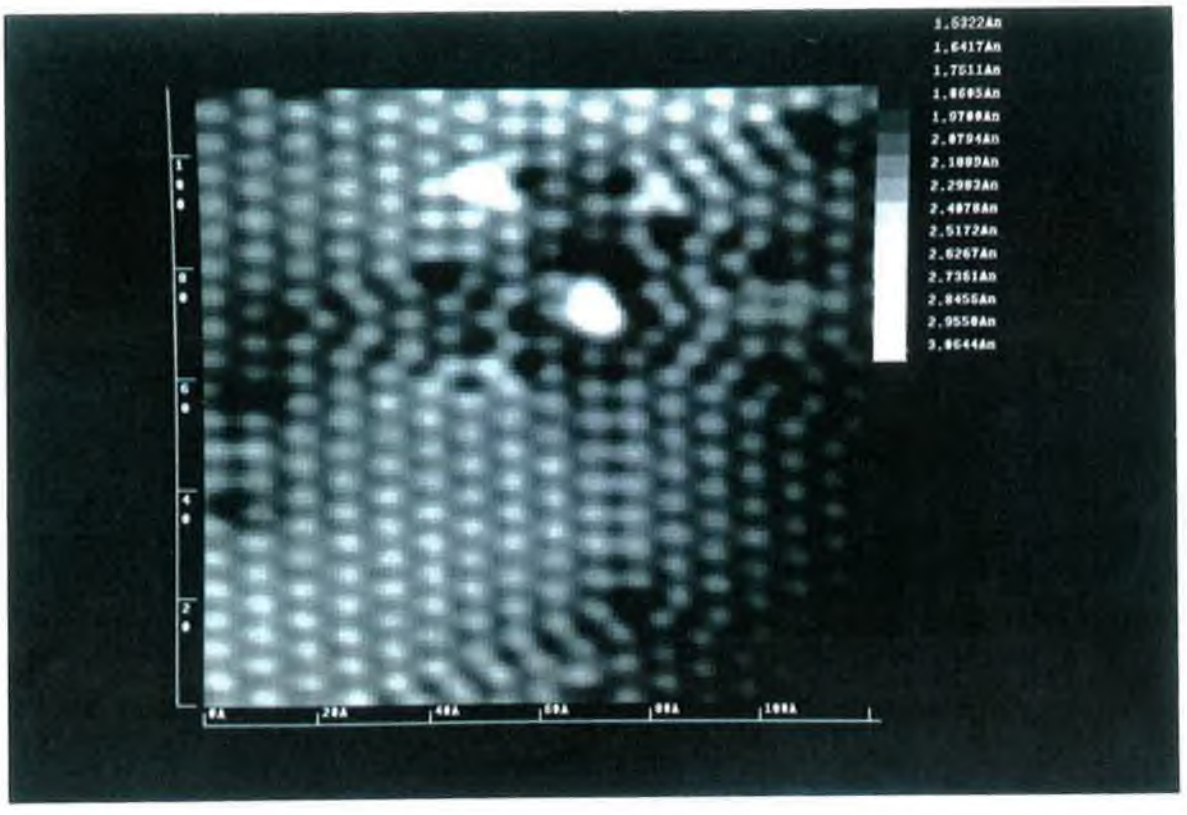

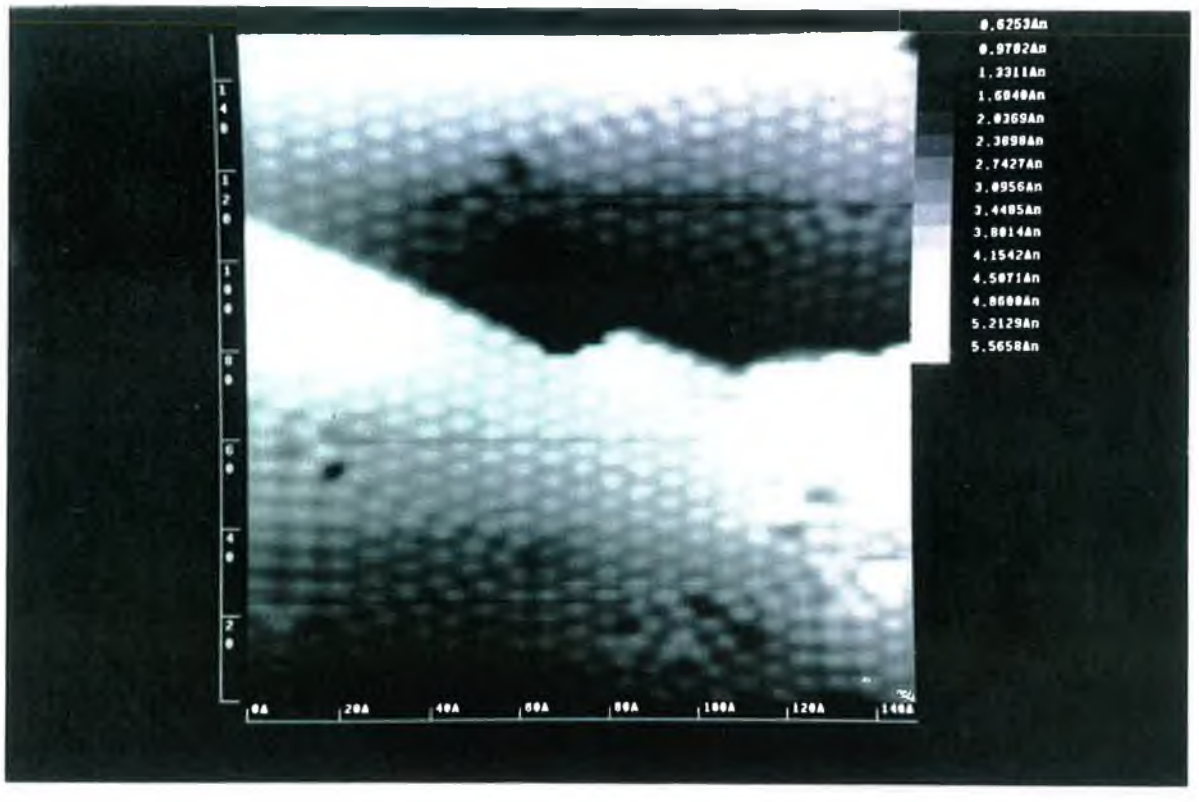

Fig 5.19 *STM images of the (2x2) reconstruction of the decapped GaAs(111)B surface (a single atomic step is visible in the lower image).*

(i)

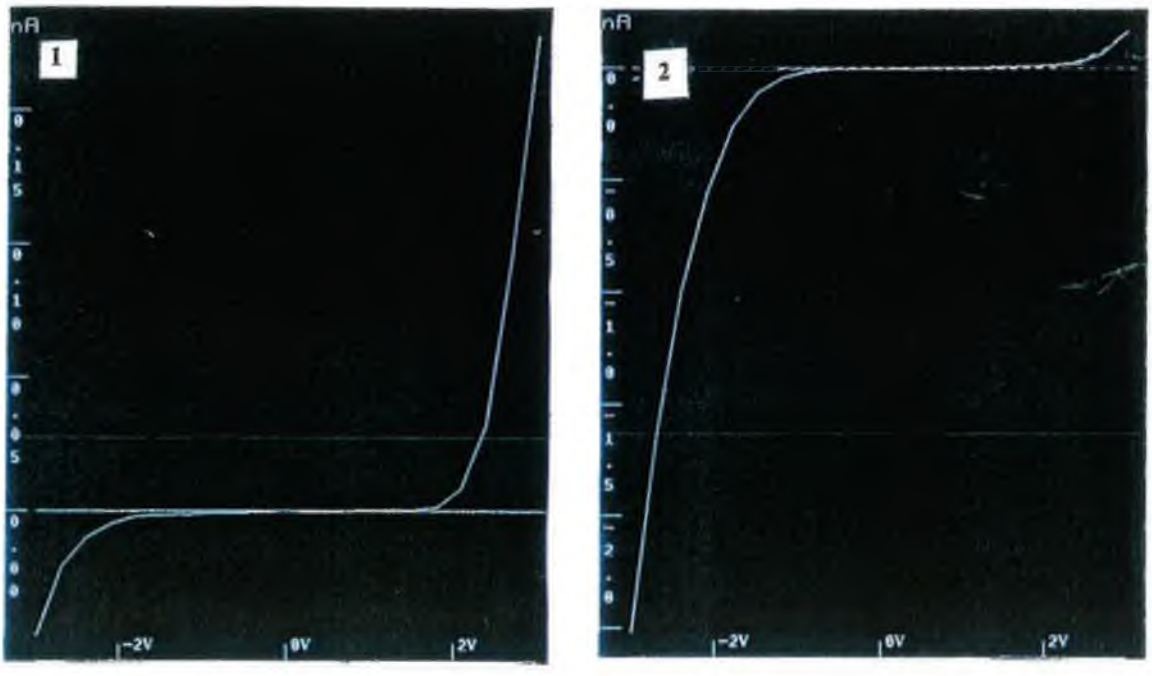

(ii)

Fig. 5.20 **(i)** *A region of the (2x2) surface where an area containing surface defects is visible,* **(ii)** *tunnelling spectroscopy characteristics taken over a (2x2) region (1), and over the defect area (2).*

5.4 Surface Structure and Chemical Bonding of S Treated GaAs(111)B Surfaces.

Although extensive work has been carried out on the passivation of GaAs(100) surfaces with a variety of aqueous sulphides (Chapter 2), relatively few groups have investigated a similar passivation of GaAs(111) surfaces. Sugiyama *et al.* (72) have used Soft X-Ray Standing Waves to determine the structure of $(NH_4)_2S_x$ treated GaAs(111)A and (111)B samples. They found that for the (111)A surface, sulphur atoms bond on top of first layer Ga atoms whereas sulphur atoms exchange with first layer As atoms and bond to three underlying Ga atoms for the (111)B surface. These results were consistent with a first principles study of sulphur passivation of GaAs by Ohno[43]. As the coordination number of sulphur therefore varies from 1 (GaAs(111)A) to 3 (GaAs(111)B) the desorption temperature for sulphur from the (111)B surface should be greater. This was confirmed by Scimeca *et al.*[41]. Oshima *et al.*[53] have found, using an identical sulphide treatment, a sulphur coverage for the (111)B surface greater than unity, suggesting that, as for the (100) surface, sulphur is present at the third layer. Only one previous study has attempted to describe the reaction of sulphur with an *in situ* prepared GaAs(111)B surface[56]. However, H_2S gas was used in that study whose decomposition at the surface is likely to create arsine (AsH_3) and complicate the analysis of the reaction of sulphur.

Fig 5.22 illustrates the changes in the As 3d core level after (i) RT exposure to sulphur and subsequent annealing at (ii) 250°C, and, (iii) 450°C. The most striking result of RT exposure is that both surface components S1 and S2 of the clean spectrum are required in order to obtain a good fit. Although there is an attenuation and a broadening of the S1 component (FWHM=0.51 eV) little change in intensity is observed for the S2 component. However this latter component undergoes a shift of 0.07 eV towards higher BE as compared to the clean surface. A fourth very broad component (FWHM = 0.56 eV) shifted to 1.2 eV higher binding energy also appears. The Ga 3d spectrum (Fig.5.23(i)) exhibits a small intensity (< 8% of the bulk component) chemically shifted component after RT S adsorption. The magnitude of the chemical shift is 0.5 eV which is in good agreement with that observed for the (100) surface. The small intensity of the reacted component is not surprising considering the predominance of As in the topmost layer of the (111)B surface. An STM image of the surface after RT S adsorption is illustrated in Fig. 5.24. Although atomic steps are visible, the surface is covered with large amorphous clusters. For the S covered (111)B surface, as found for the (100) surface, stable images were possible only at negative bias suggesting a considerable increase in the density of filled states. The changes in the As 3d spectrum observed after RT S adsorption are quite similar to those observed by Ranke and Jacobi[56] for adsorption of H_2S on the GaAs(111)B-(2x2) surface. They also observed preferential adsorption on As atoms without a reduction of the S2 surface core level shift (SCLS) intensity. The STM images indicate that a large fraction of the surface after room

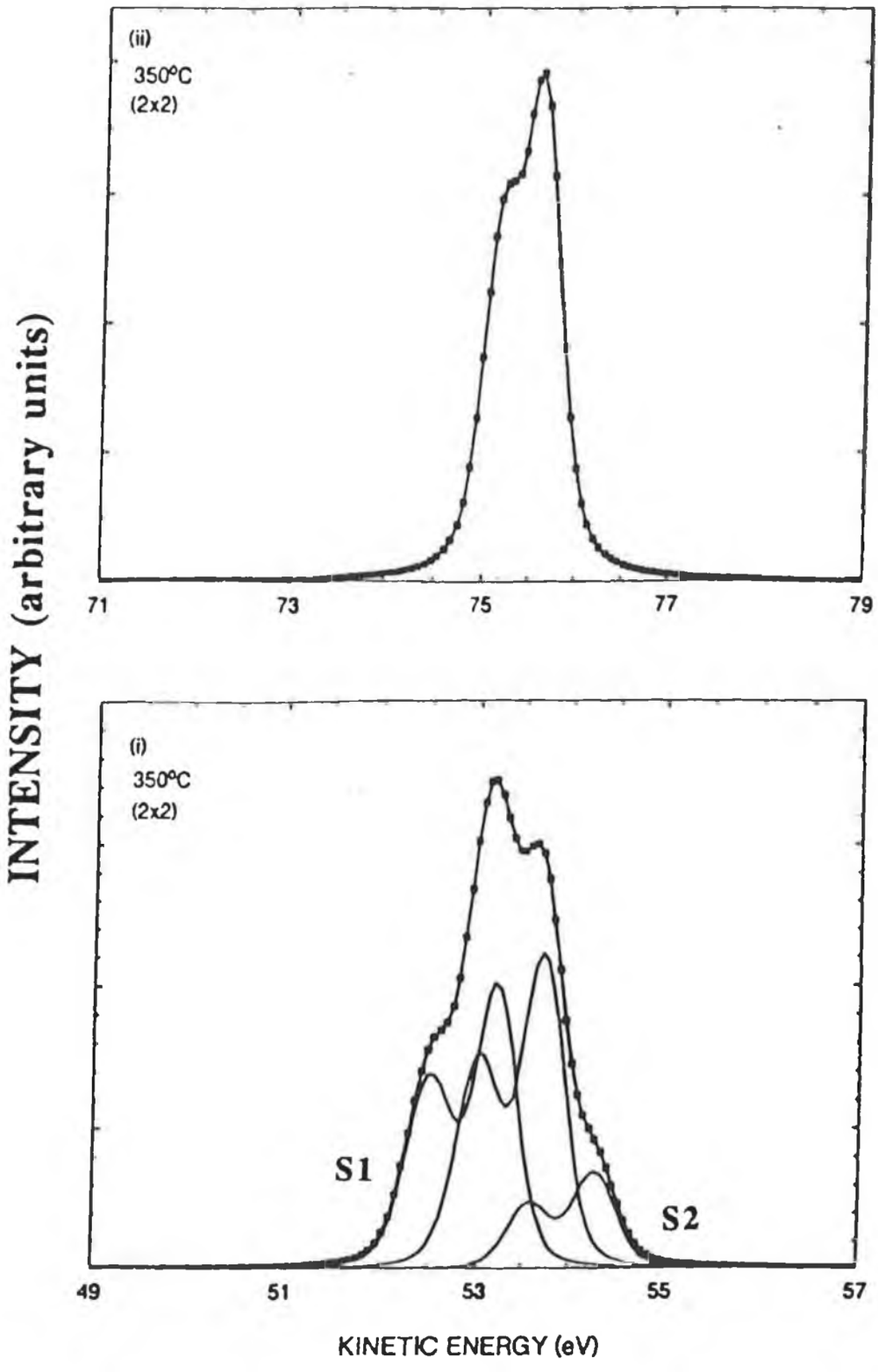

Fig 5.21 **(i)** *As 3d, and,* **(ii)***Ga 3d photoelectron core level spectra for the clean GaAs(111)B-(2x2) surface.*

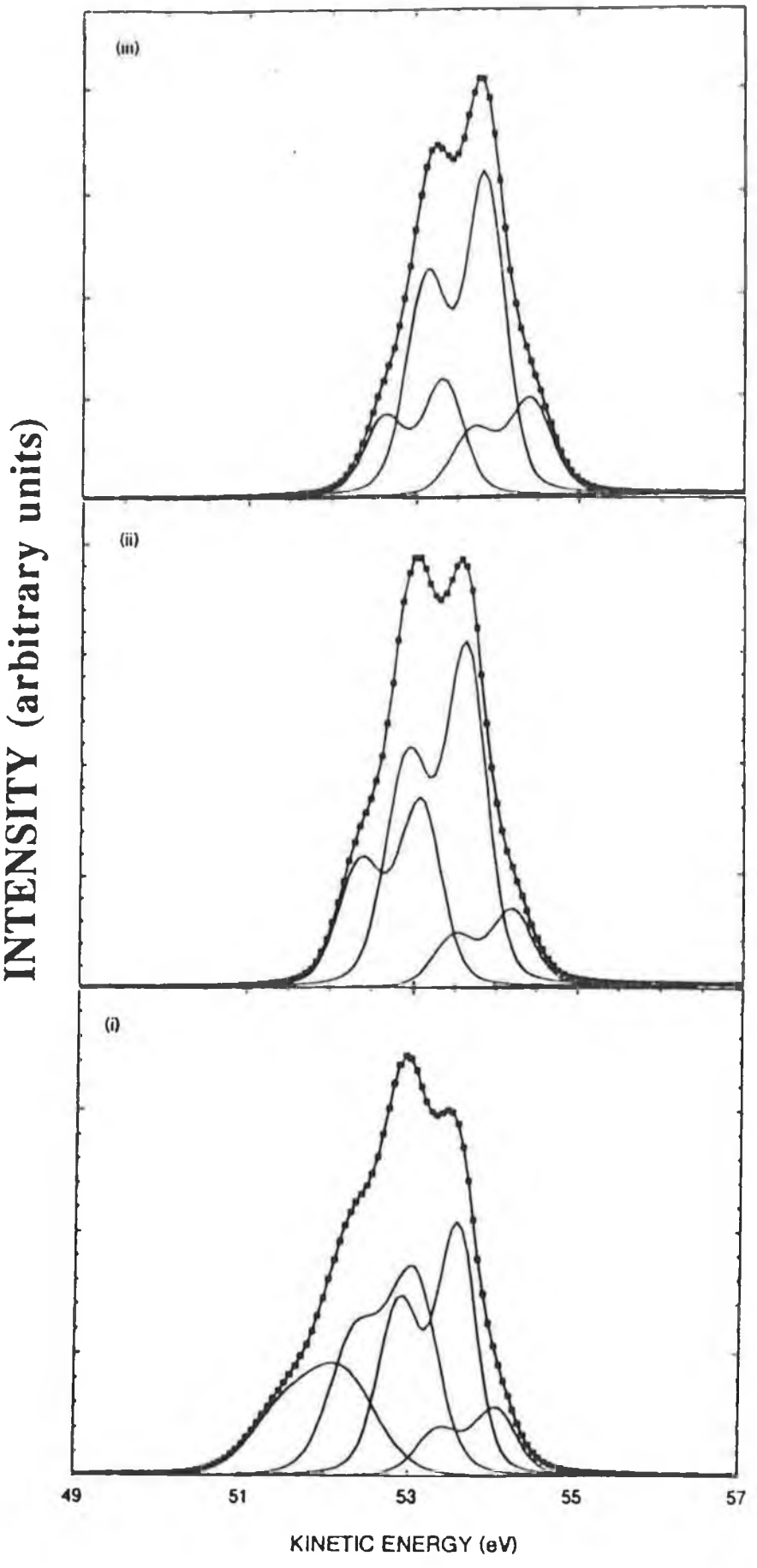

Fig 5.22 *As 3d core-level spectra after* **(i)** *room temperature adsorption of sulfur,* **(ii)** *annealing to 250°C, and,* **(iii)** *annealing to 450°C.*

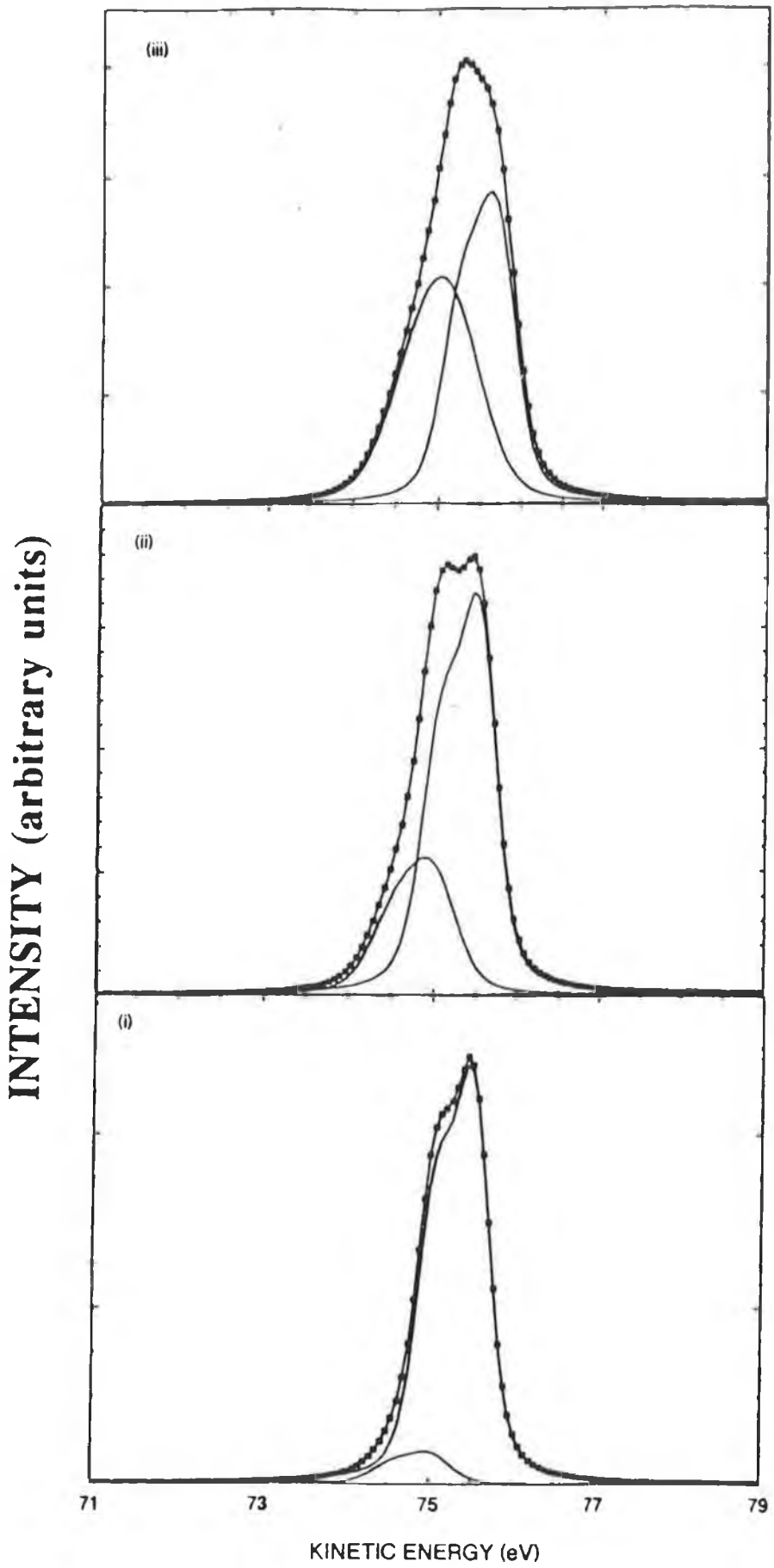

Fig 5.23 *Ga 3d core-level spectra after* **(i)***room temperature adsorption of sulfur,* **(ii)** *annealing to 250°C, and,* **(iii)** *annealing to 450°C.*

temperature S adsorption is covered by islands or clusters (The LEED pattern for this surface was (1x1) with a high diffuse background). The most plausible explanation for these results is that S adsorption induces a coalescence of surface As and that the clusters observed in the images are due to both elemental As and As sulphide. On annealing at 250°C, Fig 5.22(ii), the broad surface component at 1.2 eV higher BE in the As 3d

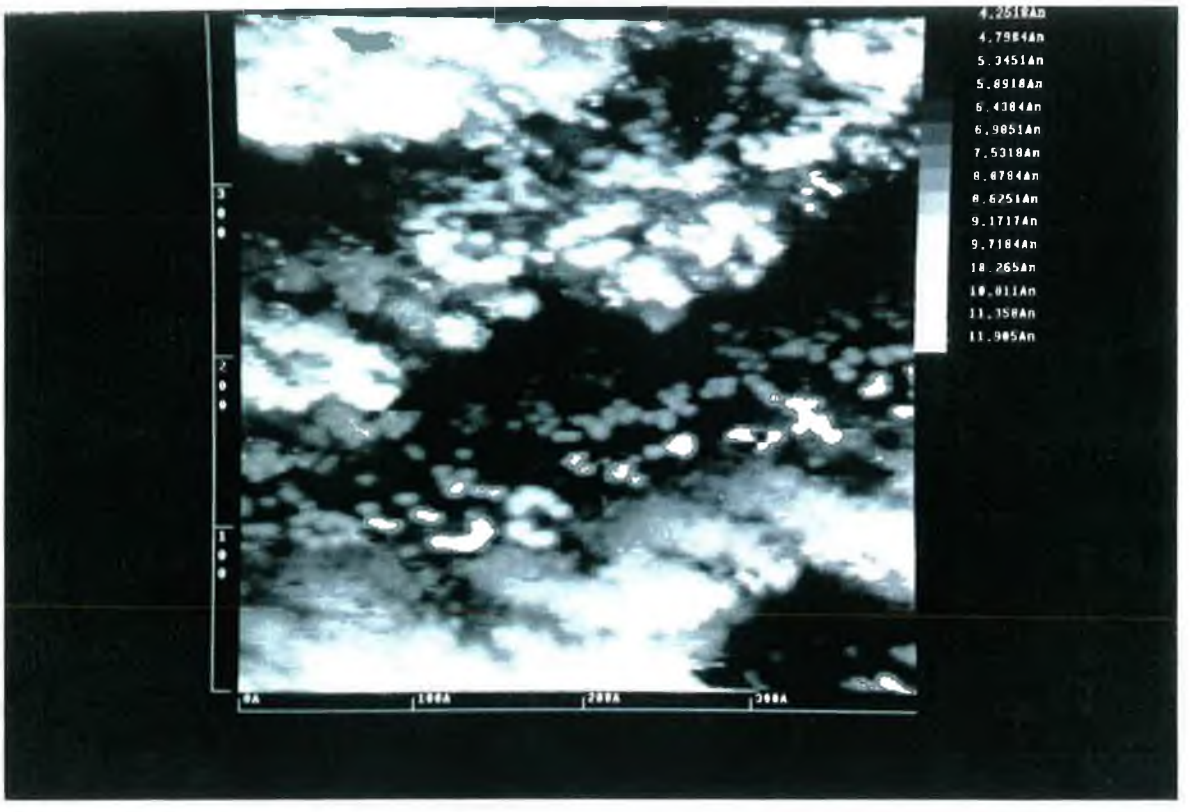

Fig 5.24 *STM image of the S/GaAs(111)B-(1x1) surface after room temperature S deposition.*

spectrum disappears indicating the removal of As sulphides. This is accompanied by a marked decrease in intensity of the S1 component, which is further attenuated on annealing at 450°C. As suggested by Ranke and Jacobi[56] for H_2S adsorption, the reaction of S may lead to a weakening of the accumulated As bonding to the substrate, which thus leads to As desorption at lower temperatures.

The evolution of the Ga 3d core-level (Figs.5.23 (i)-(iii)) with annealing is similar to that observed for the (100) surface, with an observed increase in the magnitude of the chemically shifted component. That S preferentially bonds with Ga on the GaAs(111)B surface as the annealing temperature is raised has been similarly noted by Scimeca *et al* [41]. This group found no evidence from their particular measurements of the S 2p core level for S diffusion into the bulk. We find changes in the S 2p spectrum qualitatively

similar to those of the (100) surface as the annealing temperature is raised, suggesting again that diffusion of S into the bulk plays an important role.

STM images of the surface also show important temperature dependent changes. Fig.5.25 illustrates images that are typical of those acquired after annealing at (i) 350°C, and, (ii) 550°C. The annealed S/GaAs(111)B surface, although exhibiting a clear (1x1) LEED pattern (Fig.5.26), displays no long range order. A high density of clusters is still present on the surface annealed at 350°C that we believe is due to agglomerated As. The small areas of (1x1) reconstruction that are visible are most likely due to both As and S bonded to the underlying Ga, as is suggested by the core-level spectra. Further annealing to 550°C, where the As-As component was found to be removed from the As 3d peak, leads to a removal of the clusters and the surface adopting the appearance of Fig.5.25(ii). Here, again, the LEED pattern consisted of clear (1x1) dots. The calculations of Fan *et al.*[57] from I(V) LEED measurements on a Bi-induced (1x1) structure of the Si(100) surface also indicated that the Bi adatoms did not have long range ordered structures but that they stabilised the (1x1) structure of the Si surface. This group also observed a sharp (1x1) LEED pattern for the Bi/Si(100) surface and found that it was most likely that the valence electrons of the Bi atoms were saturating the dangling bonds of the surface Si atoms. The existence of the disordered overlayer was argued to be related to the charge transfer between Bi atoms and the Si surface. Due to the large electronegativity difference existing between S and Ga, strong S-Ga interaction may prevent the formation of an ordered overlayer as was analogously suggested for the Bi-Si interaction. As for the S/GaAs(100) -(2x1) surface however, the As 3d peak for the (1x1) surface can never at any stage in the annealing process be fitted with a single bulk component. Therefore, it is likely that both S and As exist in the topmost layer of the (1x1) reconstruction.

The behaviour of the Fermi level position as a function of sulphur deposition and annealing was dramatically different from that observed on the (100) surface. For the clean (2x2) surface we found E_F approximately 0.3 eV from the conduction band minimum (CBM). For the doping level of the particular samples used ($2x10^{18}$ cm^{-3}) we would expect the Fermi level to be approximately 0.05 eV above the CBM - i.e. the semiconductor is degenerate. The residual band bending may be due to a small surface density of "missing trimer" defects, as was illustrated in Fig.5.20. On RT adsorption of sulphur, there is an approximate 0.1 eV shift of the Fermi level towards the CBM, with no change in this position as the surface is annealed to 500°C (the (1x1) LEED pattern becomes increasingly sharper). We did not observe S desorption from the GaAs(111)B surface for temperatures up to 580°C, consistent with the results of Scimeca *et al.* [41]. As that group has suggested, the three-fold co-ordination of S atoms on the (111)B surface leads to a much higher desorption temperature (≈ 620°C) than that observed on the GaAs(100) surface.

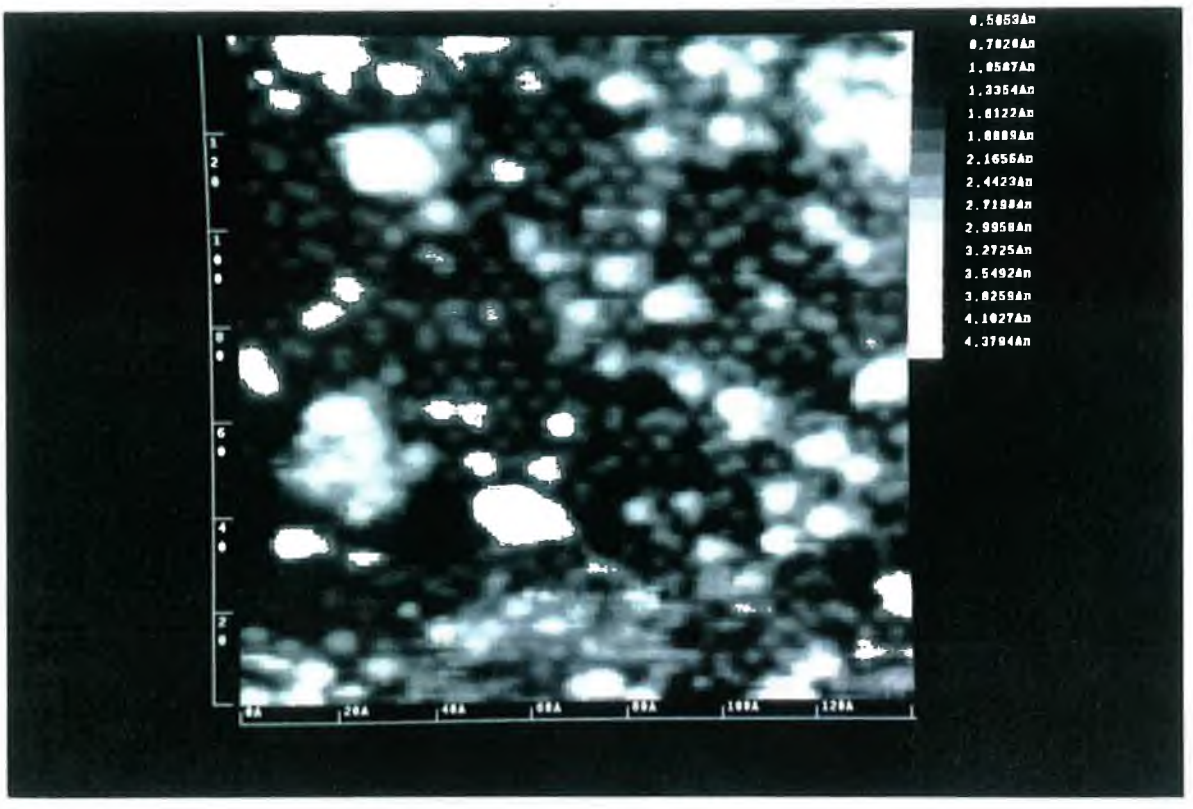

(i)

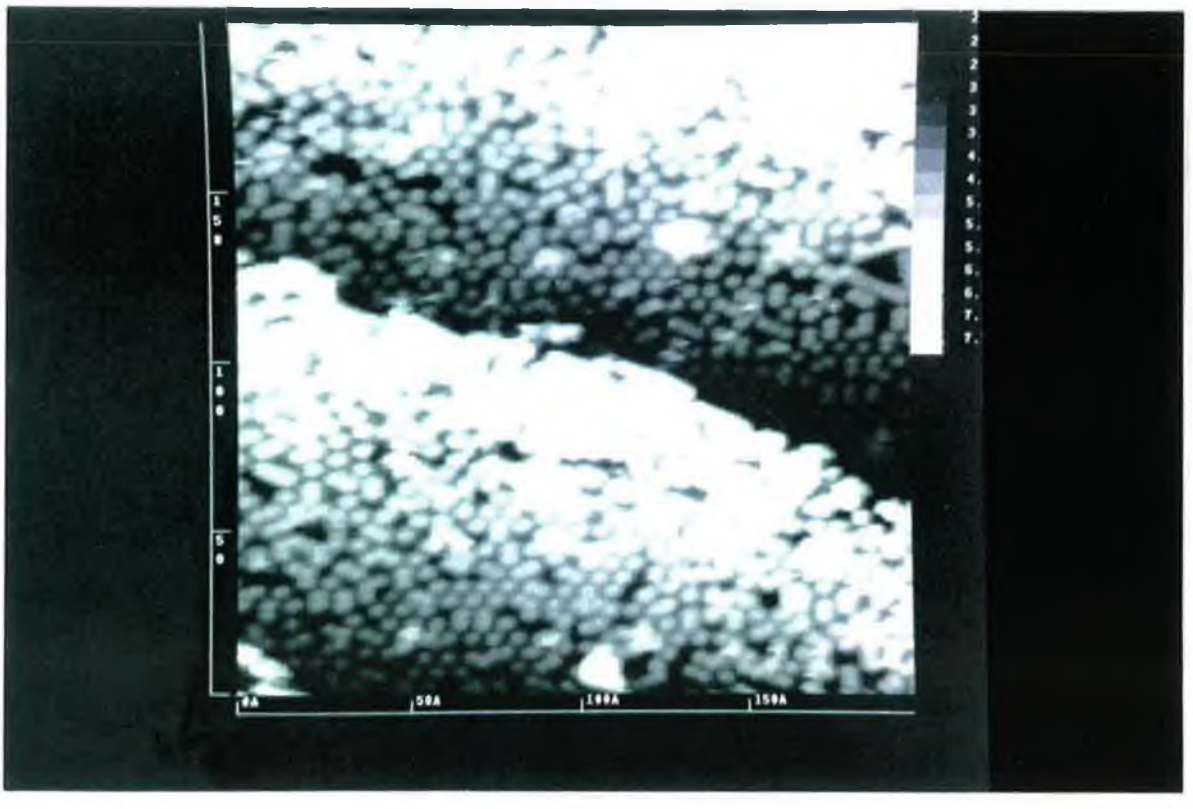

(ii)

Fig 5.25 *STM images of the S/GaAs(111)B - (1x1) surface after annealing at* **(i)** *350°C, and,* **(ii)** *550°C*

Fig 5.26 *The (1x1) LEED pattern observed for the S/GaAs(111)B surface after annealing at 350°C.*

5.5 Summary

We have presented the first STM data on the interaction of molecular sulphur with the decapped GaAs(100) and GaAs(111)B surfaces. For the clean decapped GaAs(100)-(4x1) surface our STM images are most consistent with the c(8x2) model recently proposed by Skala *et al* [25]. Images of the coexistence of the (2x6) and (4x1) surface phases have been obtained and tunnelling spectroscopy measurements indicate that the Fermi level is pinned mid-gap for both reconstructions. Decapped GaAs(111)B surfaces exhibited a (2x2) reconstruction, with our STM images being in good agreement with the trimer model proposed by Biegelsen *et al.* [54]. It was suggested that the ability to obtain high resolution images of this surface at positive sample bias may be due to tunnelling into anti-bonding states due to As-As bonding within the As trimer.

The images of the S-treated surfaces were found to provide a good measure of surface atomic structure and periodicity, however information on the density of surface electronic states and chemical bonding was limited using STM alone. SXPS was therefore also employed to further understanding of the bonding states present at the S treated surfaces. Furthermore, unlike the majority of previous studies, we used As capped GaAs(100) and GaAs(111)B samples prepared by thermally desorbing the protective As film *in situ*. This provided an oxide- and carbon-free, well ordered surface

on which to investigate the reaction of sulphur deposited from an electrochemical cell. We have found consistent differences between our results on both GaAs surfaces and those of previous studies using aqueous sulphide treatments and chemically etched GaAs samples. The (1x1) phase observed in RHEED studies of the aqueous sulphide treated GaAs(100) surface after annealing in vacuum was found to be due to an amorphous S overlayer saturating surface dangling bonds, and not solely due to S bridge bonded to Ga, as previously proposed[39]. Similarly, we have found no evidence for an S overlayer displaying long range order on the (111)B surface, even though a clear (1x1) LEED pattern was visible.

For both the Se/GaAs(100)-(2x1)[48] and S/InP(100)-(2x1)[49] surfaces, a single bulk component has been found to be sufficient to fit the P 2p or As 3d photoelectron core-level spectrum. This was not the case for our As 3d spectra of the S/GaAs(100)-(2x1) and S/GaAs(111)B-(1x1) surfaces, suggesting that a complete exchange of As and S does not occur. For the (2x1) surface we have suggested a possible surface structure consisting of both As and S dimers consistent with both our experimental results and the electron counting model. S 2p spectra of both surfaces indicated that diffusion of sulfur into the bulk GaAs crystal may also occur. A more detailed analysis of this S penetration would be possible using the X-Ray Photoelectron Diffraction (XPD) technique, as has been applied to S treated InP(100) surfaces[49].

Only for the GaAs(100)-(4x1) S-treated surface, after annealing, have we observed a large shift of the Fermi level position with respect to its (pinned) position on the clean surface. This may be due to the greater number of Ga-S bonds that form on this surface. Little variation in Fermi level position is noted for the GaAs(111)B surface after S deposition and annealing. The ability to obtain an almost flat band condition on the GaAs(100) surface after *in situ* S deposition has not previously been observed and is an important result in terms of the technological applications of the GaAs(100) surface.

References

1. M. D. Pashley, *Phys. Rev. B* **40** 10481 (1989)
2. D. J. Chadi, in *The Structure of Surfaces III* (Springer Series in Surface Sciences, Vol. 24, edited by S. Y. Tong, M. A. Van Hove, K. Takayanagi , and X. D. Xie, Springer-Verlag, Berlin, Heidelberg) (1991)
3. D. K. Biegelsen, R. D. Bringans, J. E. Northrup, and L. E. Swartz, *Phys. Rev. B* **41** 5701 (1990)
4. P. Drathen, W. Ranke and K. Jacobi, *Surf. Sci.* **77** L162 (1978)
5. A. J. Van Bommel, J. E. Crombeen, and T. G. J. van Oirschot, *Surf. Sci.* **72** 95 (1978)
6. P. K. Larsen, J. F. van der Veen, A. Mazur, J. Pollmann, J. H. Neave, and B. A. Joyce, *Phys. Rev. B* **26** 3222 (1982)
7. P. K. Larsen, J. H. Neave, J. F. van der Veen, P. J. Dobson, and B. A. Joyce, *Phys. Rev. B* **27** 4966 (1983)
8. M. D. Pashley, K. W. Haberern, W. Friday, J. M. Woodall, and P. D. Kirchner, *Phys. Rev. Lett.* **60** 2176 (1988)
9. A. D. Katnani, H. W. Sang,Jr., P. Chiaradia, and R. S. Bauer, *Journ. Vac. Sci. Technol. B* **3** 608 (1985)
10. J. F. van der Veen, P. K. Larsen, J. H. Neave, and B. A. Joyce, *Solid State Comm.* **49** 659 (1984)
11. M. Sauvage - Simkin, R. Pinchaux, J. Massies, P. Calverie, N. Jedrecy, J. Bonnet, and I. K. Robinson, *Phys. Rev. Lett.* **62** 563 1989
12. S. P. Kowalczyk, D. L. Miller, J. R. Waldrop, P. G. Newman, and R. W. Grant, *Journ. Vac. Sci. Technol.* **19** 255 (1981)
13. D. J. Chadi, *Journ. Vac. Sci. Technol. A* **5** 834 (1987)
14. H. H. Farrell and C. J. Palmström, *Journ. Vac. Sci. Technol. B* **8** 903 (1990)
15. M. D. Pashley, K. W. Haberern, and J. J. Ganes, *Surf. Sci.* **267** 153 (1992)
16. V. Bressler - Hill, M. Wassermeier, K. Pond, R. Maboudian, G. A. D. Briggs, P. M. Petroff, and W. H. Weinburg, *Journ. Vac. Sci. Technol. B* **10** 1881 (1992)
17. C. J. Spindt, M. Yamada, P. L. Meissner, K. E. Miyano, T. Kendelwicz, A. Herrera - Gomez,W. E. Spicer, and A. J. Arko, *Phys. Rev. B* **45** 11108 (1992)
18. G. LeLay, D. Mao, A. Kahn, Y. Hiuv, and G. Margaritondo, *Phys. Rev. B* **43** 14301 (1991)
19. R. Ludeke, T. C. Chiang, and D. E. Eastman, *Physica* **117B-118B** 819 (1983)
20. D. J. Frankel, C. Yu, J. P. Harbison, and H. H. Farrell, *Journ. Vac. Sci. Technol. B* **5** 113 (1987)
21. W. Ranke and K. Jacobi, *Surf. Sci.* **63** 33 (1977)
22. W. Blömacher, Diplomarbeit, Universitat Duisberg (1988); L.Koenders, private communication.

23. R. Z. Bachrach, R. S. Bauer, P. Chiaradia, and G. V. Hansson, *Journ. Vac. Sci. Technol.* **18** 797 (1981)
24. I. Kamiya, D. E. Aspnes, L. T. Florez, and J. P. Harbison, *Phys. Rev B* **46** 15894 (1992)
25. S. L. Skala, J. S. Hubacek, J. R. Tucker, J. W. Lyding, S. T. Chou, and K. -Y. Cheng, *Phys. Rev. B* **48** 9138 (1993)
26. J. Falta, R. M. Tromp, M. Copel, G. D. Petit, and P.D. Kirchener, *Phys. Rev. Lett.* **69** 3068 (1992)
27. I. M. Vitomirov, A. D. Raisanen, A. C. Finnefrock, R. E. Viturro, L. J. Brillson, P. D. Kirchner, G. D. Petit, and J. M. Woodall, *Journ. Vac. Sci. Technol. B* **10** 1898 (1992)
28. L. J. Brillson, R. E. Vituorro, C. Mailihot, J. L. Shaw, N. Tache, J. McKinley, G. Margaritondo, J. M. Woodall, P. D. Kirchner, G. D. Petit, and S. L. Wright, *Journ. Vac. Sci. Technol. B* **6** 1263 (1988)
29. M. D. Pashley and K. W. Haberern, *Phys. Rev. Lett.* **67** 2697 (1991)
30. M. D. Pashley, K. W. Haberern, and R. M. Feenstra, *Journ. Vac. Sci. Technol. B* **10** 1874 (1992)
31. M. D. Pashley, K. W. Haberern, R. M. Feenstra, and P. D. Kirchner, *Phys. Rev. B* **48** 4612 (1993)
32. C. J. Sandroff, M. S. Hedge, L. A. Farrow, C. C. Chang, and J. P. Harbison, *Appl. Phys. Lett.* **54** 362 (1989)
33. The PC based curve-fitting software was written by Dr. A. A. Cafolla,Dept. of Physics, Dublin City University
34. M. L. Gallagher, R. H. Prince, and R. F. Willis, *Surf. Sci.* **275** 31 (1992)
35. R. M. Feenstra, *Phys. Rev. Lett.* **63** 1412 (1989)
36. R. M. Feenstra and J. A. Stroscio, *Journ. Vac. Sci. Technol. B* **5** 923 (1987)
37. C. J. Spindt, D. Liu, K. Miyano, P. L. Meissner, T. T. Chiang, T. Kendelewicz, I. Lindau, and W. E. Spicer, *Appl. Phys. Lett.* **55** 861 (1989)
38. H. Sugahara, M. Oshima, R. Klauser, H. Oigawa, and Y. Nannichi, *Surf. Sci.* **242** 335 (1991)
39. H. Hirayama, Y. Matsumoto, H. Oigawa, and Y. Nannichi, *Appl. Phys. Lett.* **54** 2565 (1989)
40. L. Roberts, G. Hughes, B. Fennema, and M. Carbery, *Journ. Vac. Sci. Technol. B* **10** 1862 (1992)
41. T. Scimeca Y. Watanabe, R. Berrigan, and M. Oshima, *Phys. Rev. B* **46** 10201 (1992)
42. H. Oigawa, J. Fan, Y. Nannichi, H. Sugahara, and M. Oshima, *Jpn. Journ. Appl. Phys.* **30** L322 (1991)
43. T. Ohno, *Phys. Rev. B* **44** 6306 (1991)
44. Y. Tao, A. Yelon, E. Sacher, Z. H. Lu, and M. J. Graham, *Appl. Phys. Lett.* **60**

2669 (1992)
45. V. L. Berkovits and D. Paget, *Appl. Phys. Lett.* **61** 1835 (1992)
46. J. Massies, F. Dezaly, and N. T. Linh, *Journ. Vac. Sci. Technol.* **17** 1134 (1980)
47. X. -S. Wang, K. W. Self, R. Maboudian, C. Huang, V. Bressler-Hill, and W. H. Weinburg, *Journ. Vac. Sci. Technol. A* **11** 1089 (1993)
48. S. Takatani, T. Kikawa, and M. Nakazawa, *Phys. Rev. B.* **45** 8498 (1992)
49. D. Gallet and G. Hollinger, *Appl. Phys. Lett.* **62** 982 (1993)
50. S. -F. Ren and Y. -C. Chiang, *Phys. Rev. B* **41** 7705 (1990)
51. T. Scimeca, Y. Watanabe, F. Maeda, R. Berrigan, and M. Oshima, *Appl. Phys. Lett.* **62** 1667 (1993)
52. F. Maeda, Y. Watanabe, T. Scimeca, and M. Oshima, *Phys. Rev. B* **48** 4056 (1993)
53. M. Oshima, T. Scimeca, Y. Watanabe, H. Oigawa, and Y. Nannichi, *Jpn. Journ. Appl. Phys.* **32** 518 (1993)
54. D. K. Biegelsen, R. D. Bringans, J. E. Northrup, and L. -E. Swartz, *Phys. Rev. Lett.* **65** 452 (1990)
54(a). J. Thornton, IRC in Surface Science, Liverpool University
55. W. Ranke and K. Jacobi, *Prog. Surf. Sci.* **10** 1 (1981) and references therein
56. W. Ranke, J. Finster, and H. J. Kuhr, *Surf. Sci.* **187** 112 (1987)
57. W. C. Fan, N. J. Wu, and A. Ignatiev, *Phys. Rev. B* **45** 14167 (1992)

CHAPTER VI: AN AMBIENT STM INVESTIGATION OF AQUEOUS SULPHIDE PASSIVATED GaAs(100) SURFACES

Ambient Scanning Tunnelling Microscopy imaging has been used to study the oxidation of GaAs(100) surfaces which have been passivated in aqueous $P_2S_5/(NH_4)_2S$ and $P_2S_5/(NH_4)_2S_x$ solutions. An analysis of tunnelling spectroscopy curves from passivated surfaces in terms of planar Metal-Insulator-Semiconductor (MIS) theory is presented and compared to spectroscopy data from the chemically etched surface.

6. 1 Time Resolved Native Oxide Growth Observation

As detailed extensively in Chapter 2, the modification of the electronic properties of GaAs surfaces due to treatment with aqueous ammonium sulphide solutions has been the subject of considerable investigation of late. These treatments represent an alternative, albeit less precisely controlled, method of passivation as compared to the *in situ* sulphur deposition described in the previous chapter.

After etching, GaAs(100) surface oxides are removed leaving excess As. Subsequent exposure of the surface to air leads to oxide regrowth. Extensive XPS studies have been carried out on the growth of these native oxides (see, for example, ref 1). Following the initial chemisorption of a layer of oxygen, bulk-like oxides form (mainly Ga_2O_3 and As_2O_3) disrupting the surface structure. It is the formation of these stable oxides on passivated, homogeneous GaAs(100) surfaces that is investigated in this study. The three-dimensional, high resolution imaging capabilities of the STM can monitor, in real time, changes in chemical and electronic surface structure. An STM image of a surface contains information on both the surface topography and local electrical conductivity. The presence of poorly conducting oxide regions on a perfectly "flat" surface appear as variations in the surface topography due to the movement of the STM tip towards the surface in order to maintain a constant tunnelling current. Therefore, variations in peak-to-valley (P-V) and root mean square (RMS) roughness of these surfaces as a function of passivation procedure provide a critical - although convoluted - assessment of the surface topography, and its chemical and electrical uniformity[2]. The reduction of surface state density reported for sulphur treated GaAs surfaces[3] contrasts heavily with the disruptive nature of semiconductor surface oxidation which results in an increase in surface state density.

In this study, the ambient oxidation of GaAs(100) surfaces passivated in both $P_2S_5/(NH_4)_2S$ and $P_2S_5/(NH_4)_2S_x$ solutions is investigated by STM over $3x3\mu m^2$ areas. Consistent differences were found in both initial P-V and RMS roughness values of these surfaces and significantly different rates of oxidation were observed. The chemical composition of the passivated surfaces was determined by AES and the role of phosphorous in the passivation treatment was investigated. The effect of the scanning electric field of the STM on the oxidation process is discussed. STM tunnelling

spectroscopy characteristics for the passivated and unpassivated surfaces are discussed in Sections 6.2 and 6.3 with nanolithographic patterning of the passivated surface briefly discussed in Section 6.4.

Images of the chemically etched unpassivated surface, $P_2S_5/(NH_4)_2S$ and $P_2S_5/(NH_4)_2S_x$ treated surfaces (prepared as described in Chapter 3) after 15 min exposure to air are shown in Figs 6.1 (a) - (c), respectively. The corresponding RMS roughness values (R_{app}) over representative $1\mu m^2$ areas are 8nm for the unpassivated surface and 0.4 and 0.3 nm for the $P_2S_5/(NH_4)_2S$ and $P_2S_5/(NH_4)_2S_x$ treated surfaces respectively. This method of using apparent roughness parameters to characterise the passivated surface has previously been employed by Dagata *et al.*[2], and the 0.4 nm value noted for the surface treated in the $P_2S_5/(NH_4)_2S$ solution is in excellent agreement with the value determined by that group for a similar treatment. Slightly lower roughness parameters were consistently obtained on the $P_2S_5/(NH_4)_2S_x$ treated surfaces. All the images displayed in Fig.6.1 were captured after a single scan. AES spectra of both these passivated surfaces revealed the presence of sulphur and phosphorus. As outlined above, the STM image is a convolution of the surface topography and the chemical homogeneity of the surface. The surface oxidation of GaAs leads to the physical disruption of the surface by the formation of stoichiometric oxides which in turn contribute to the chemical inhomogeneity which affects local conductivity. Therefore, we believe that it is reasonable to consider the apparent surface roughness as a relative measure of the extent of surface oxidation rather than simply reflecting the surface topography. Both of the passivating solutions substantially reduce the topographical and chemical inhomogeneities apparent on the unpassivated surface.

All passivated surfaces investigated in this study had a final methanol rinse prior to being blown dry with nitrogen. Using DI water as opposed to methanol as the final rinse yielded surfaces comparable to Fig 6.1(a). This behaviour was also observed by Richter and Hartnagel[4], who found by XPS measurements that a final water rinse produced a surface much like the unpassivated surface with a large oxygen content in both the As and Ga 2p photoemission peaks. Wang *et al.*[5] also noted that the PL intensity of the $P_2S_5/(NH_4)_2S/S_x$ treated surface, having undergone this final water rinse, decreased to that of the unpassivated surface.

In order to determine whether the final water rinse altered the chemical composition of the passivated surfaces, we compared the AES spectra of surfaces rinsed in both DI water and methanol. These spectra revealed that a final water rinse removed phosphorus from the surface while the methanol rinsed surface had phosphorus present. This removal of phosphorus by a final water rinse was also reported by Wang *et al.*[5] and more recently, Wang *et al.*[6]. XPS studies, carried out by the former group, of P_2S_5 treated surfaces indicated that the phosphorus was not bonded to the Ga or As surface atoms but involved only in S-P and P-O bonding configurations. These observations

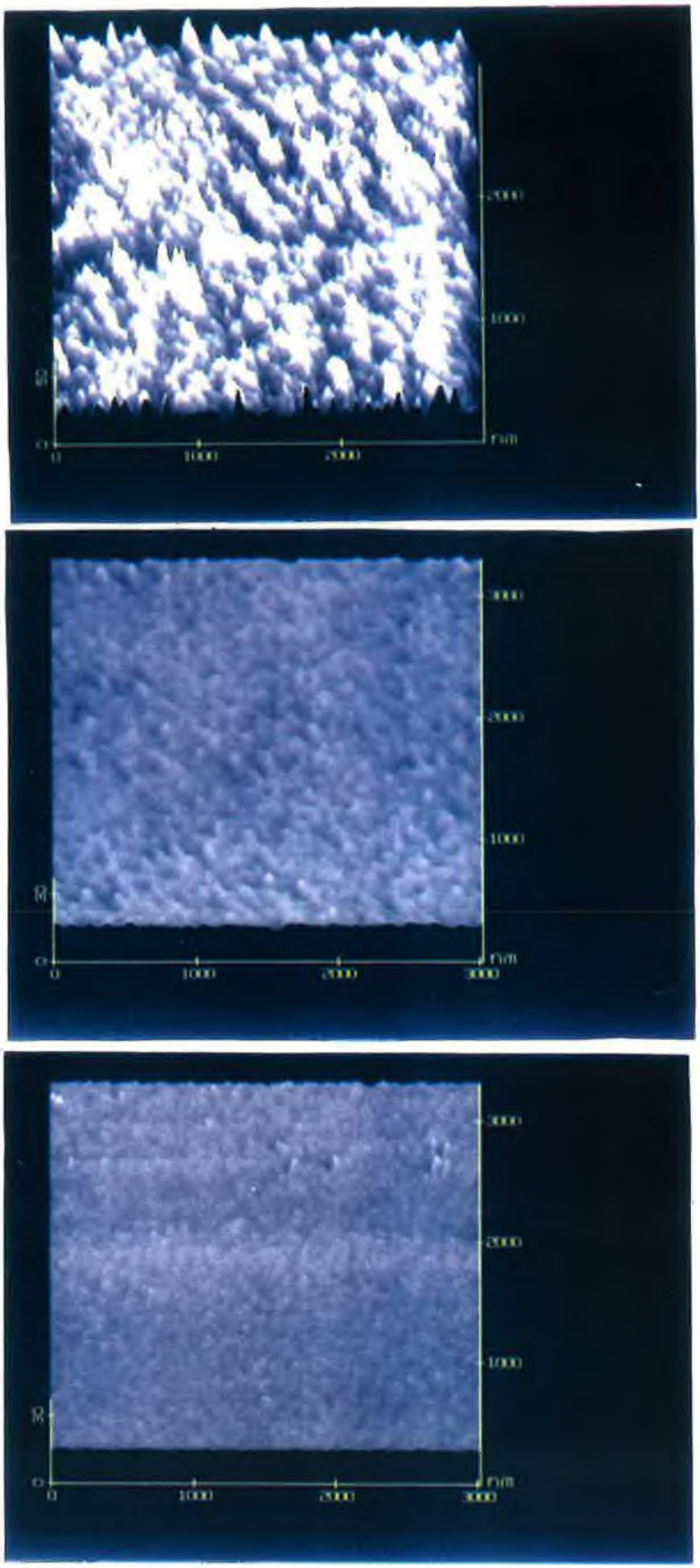

Fig 6.1 *STM images over 3x3 μm² areas of the (a) chemically etched, (b) $P_2S_5/(NH_4)_2S$ passivated and, (c) $P_2S_5/(NH_4)_2S_x$ treated GaAs(100) surface after 15 minutes exposure to air.*

would thus support the idea that the phosphorous is involved in the passivation mechanism by chemically reacting with adsorbed oxygen to form an oxide which is thermodynamically stable with respect to Ga or As oxides as previously proposed by Lee *et al.*[7]. Therefore, it would appear that the phosphorus plays a key role in stabilising the passivated surface against oxidation.

One further sulphur treatment was applied to the GaAs(100) surface. After solvent cleaning and chemically etching as before, the sample was placed in a solution of $(NH_4)_2S_x$ overnight and then blown dry with nitrogen and placed in vacuum as described by Hirayama *et al.*[8]. Auger spectra revealed a sulphur signal on this surface which was considerably larger than that found for samples passivated in either of the P_2S_5 based treatments. Attempts to image this surface by STM after removal from vacuum were not successful due to excessively noisy and unstable tunnelling images. We speculate that this is due to presence of loosely bound sulphur layers on the surface. These layers, under the influence of the scanning electric field are likely to cause STM image instability. We have found that by heating of the $(NH_4)_2S_x$ solution to 50°C and reducing the time the sample is left in the solution to 10 minutes, that stable images on this sulphur passivated surface are possible, however initial roughness values are substantially larger than those found on surfaces passivated in the P_2S_5 containing solutions. Throughout these studies we have observed that STM images of different areas across the passivated surfaces display a large spread in the roughness values. Some isolated regions were found to have roughnesses as high as 5 times that of the surface as a whole. Wang *et al.*[5] have also reported that the passivation across the surface was by no means uniform, observing a 40% variation in PL intensity from different areas. In an attempt to make the passivation treatment more uniform, they subsequently used a $(NH_4)_2S$ rinse as their final preparation step, however our experience of surfaces rinsed in this manner is that they are incompatible with STM imaging

The ambient oxidation of these passivated surfaces as a function of time was investigated by monitoring changes in the apparent surface roughness with the STM under two sets of conditions. Firstly, the passivated surface was scanned once a day over a period of eight days to monitor changes in surface profile and secondly, a 3x3 μm^2 area was scanned continuously to monitor the local oxide growth within the scanned area. The observation that continual STM scanning of the passivated surfaces caused a rapid increase in the local oxidation rate dictated such an approach. In order to study the rate of native oxide growth, the exposure of the passivated surface to repeated scanning was minimised. Graphs plotting the change in surface roughness for both passivating solutions over an 8 day period are shown in Fig. 6.2. These results should be compared with the fact that surface roughness values of 40-50nm (p-v) were routinely obtained for the unpassivated surface one hour after etching. Both surfaces exhibit similar trends, but it is apparent that the $P_2S_5/(NH_4)_2S_x$ treated sample oxidises at a much slower rate. This becomes increasingly obvious following prolonged exposure to air with the

$P_2S_5/(NH_4)_2S_x$ passivated surface displaying surface roughness values one third those of the $P_2S_5/(NH_4)_2S$ treated surface after eight days. These passivating treatments clearly inhibit the native oxide growth to a very significant extent. The difference between the two passivating solutions from our studies is purely quantitative with the $P_2S_5/(NH_4)_2S_x$ solution producing a surface which is more resistive to ambient oxidation. Our results support the proposal made by Nannichi *et al.*[9] that the additional reactive sulphur component in the $P_2S_5/(NH_4)_2S_x$ solution, which etches the GaAs surface, ensures the complete removal of any residual surface oxides following the initial acidic etch.

The changes in surface profile resulting from the oxidation of a passivated surface which was scanned continuously were spatially analyzed. Figure 6.3 illustrates the formation and growth of oxide islands on $P_2S_5/(NH_4)_2S_x$ passivated surfaces over a 24 minute scanning period. There is a 4 minute time lapse present from image to image, this being the time needed to collect STM data for one image at a scan rate of 1.3 Hz. It can be clearly seen that oxide growth is via the formation of nucleation centres dispersed

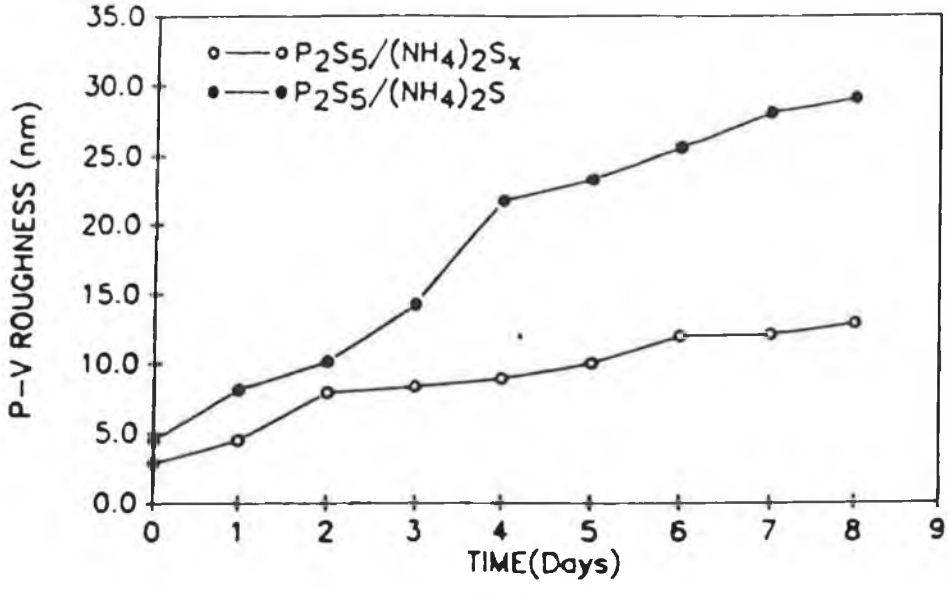

Fig 6.2 *Surface roughness (P-V) plotted as a function of time (in days) for both the $P_2S_5/(NH_4)_2S_x$ (open circles) and $P_2S_5/(NH_4)_2S$ (closed circles) treated surfaces using a single STM scan to monitor oxide growth.*

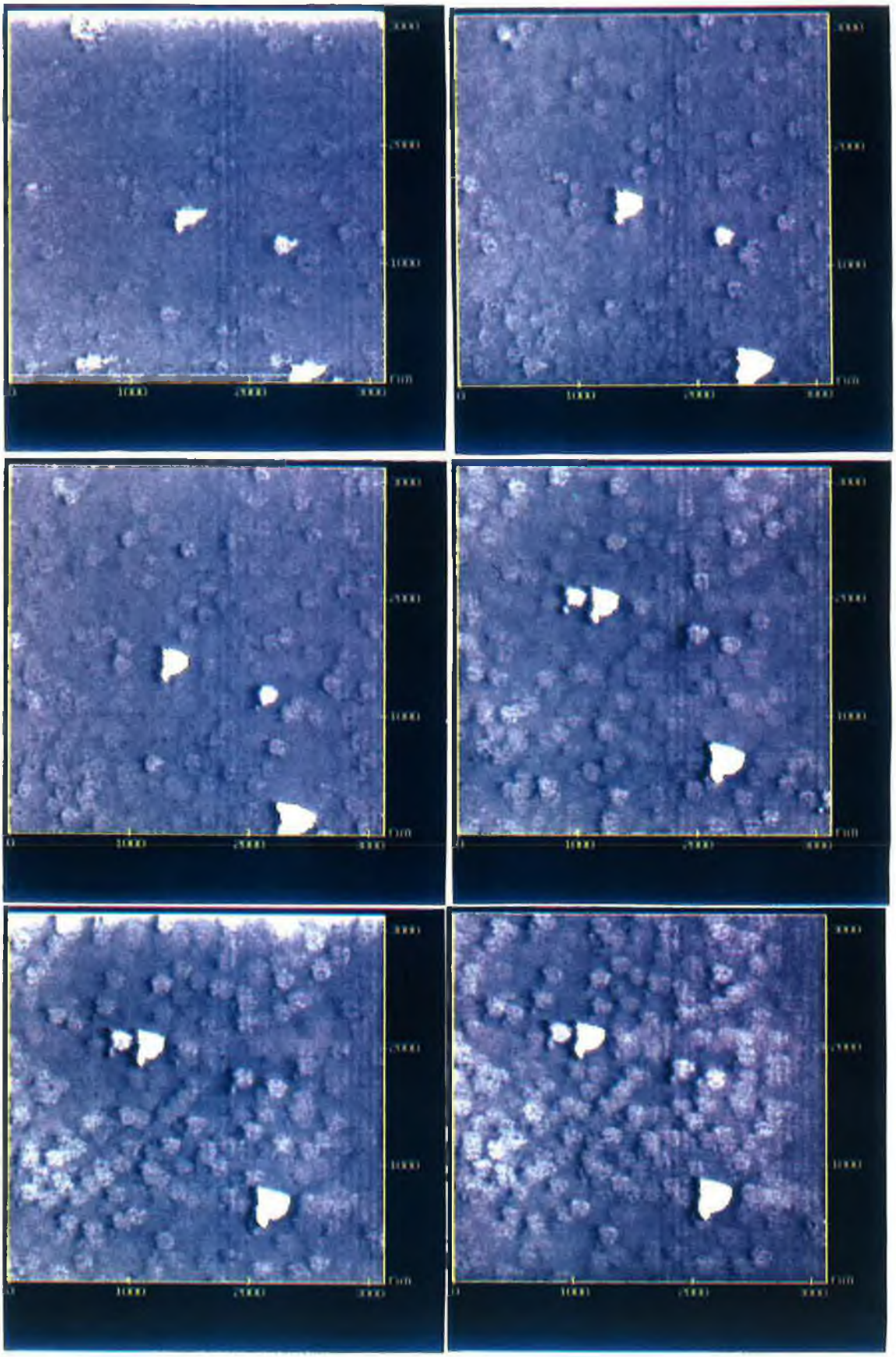

Fig 6.3 *Oxide growth across a 5 x 5 μm^2 area of the $P_2S_5/(NH_4)_2S_x$ treated GaAs(100) surface over a continual scanning period of 24 min.(The largest islands were formed by tip-sample bias pulsing, as discussed in Section 5.4, and serve to locate the same surface area - images are sequential from top left to bottom right of figure)*

across the semiconductor surface which grow and coalesce. It has been suggested in an STM study of imaging multi-quantum well structures in air[10], that surface oxidation may be accelerated by the tunnelling current. In order to investigate this effect on GaAs, a $P_2S_5/(NH_4)_2S_x$ passivated surface was scanned over a 3x3 μm^2 area continuously for one hour. By then increasing the scan area to 10x10 μm^2 area it was possible to note the effects of prolonged scanning on the oxidation process. In Fig.6.4, the continuously scanned area in the centre is quite dramatically oxidised when compared to the surrounding surface (scanned twice). STS characteristics (detailed in section 6.3.2) within the roughened area, revealed a change from those of the clean surface. The enhanced roughening of the surface is dependent on both the tunnelling current/bias voltage combination and, surprisingly, the scan rate used. By raising the tunnelling current to 5nA (thus reducing the tip-sample separation) , the bias voltage to -4.5 V (from -3.8 V) and maintaining the scan rate constant (1.3 Hz), areas such as that observed in Fig. 6.4 may be created. However, there is also a practically linear dependence of oxidation rate on scan rate up to a value of 19 Hz, above which no further increase occurred. Dependence on tunnel current and bias voltage strongly suggests that the accelerated oxide growth is due to the scanning electric field of the STM.

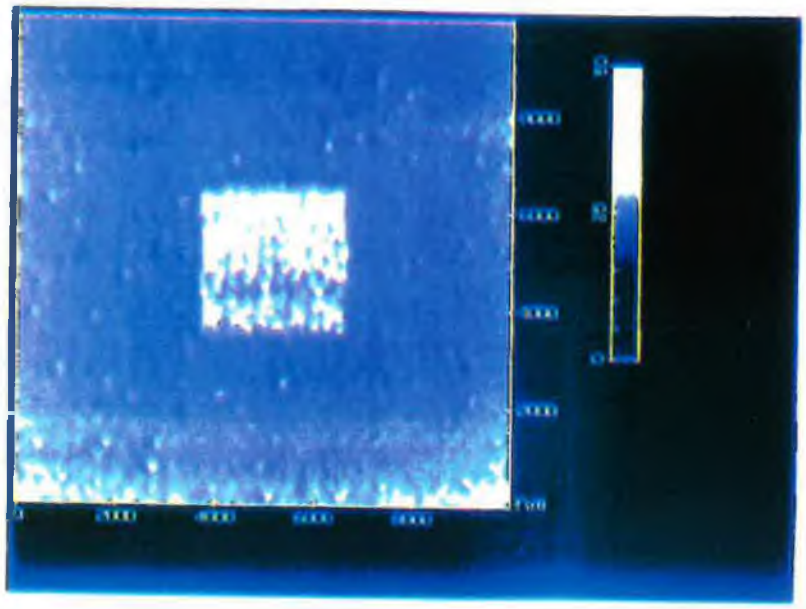

Fig 6.4 *The effect of continual STM scanning on a 3x3 μm^2 region of the passivated surface within a 10x10 μm^2 area.*

Figure 6.5 illustrates the change in surface roughness as a function of scanning time up to one hour. We propose that the initial rapid change in surface roughness corresponds to the electric field of the STM disrupting the surface passivating layer resulting in the field enhanced oxidation of the underlying surface. This is followed by a more gradual increase in surface roughness reflecting the subsequent slower rate of surface oxidation. Previous studies of the ambient oxidation of GaAs have also reported an initial rapid oxidation phase followed by a much slower logarithmic growth rate[11]. The fact that little difference in the profile of the roughness curves was observed for the two passivating solutions supports the idea that the electric field strongly disrupts the passivating layer. The relative improvement in resistance to ambient oxidation observed for the $P_2S_5/(NH_4)_2S_x$ treated surface is therefore lost due to the magnitude of the electric field effect. There is a significant difference in the general shape of the oxide islands that form on continuously scanned surfaces as opposed to those scanned only once. This is immediately apparent when the images of Fig. 6.1 and Fig. 6.3 are compared. While we do not have a satisfactory explanation for this observation it is possibly that the STM's scanning electric field not only causes an increased oxidation rate but also influences the spatial distribution of the products of the oxygen-substrate reaction.

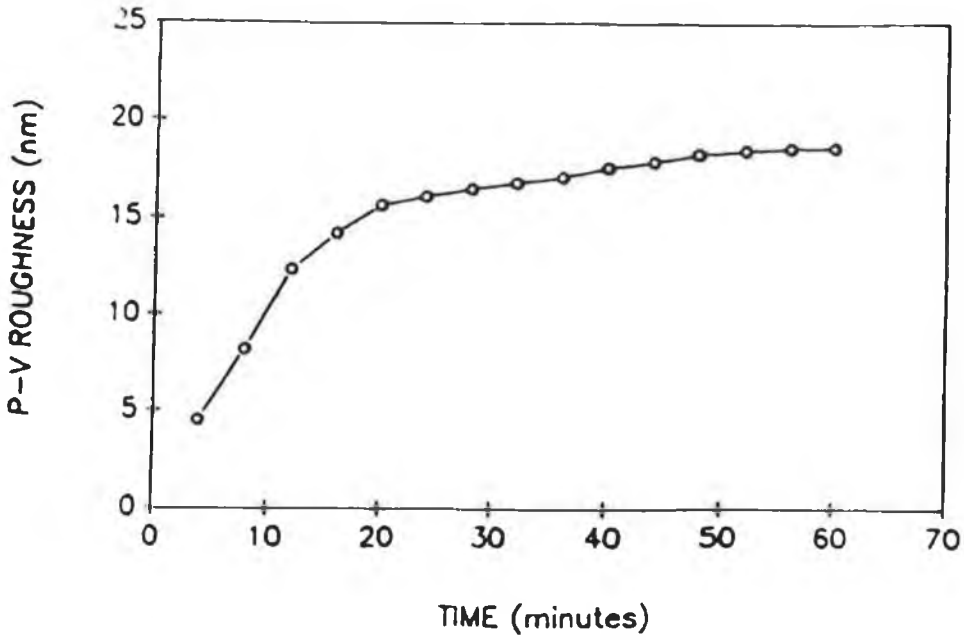

Fig 6.5 *Surface apparent roughness plotted as a function of scanning time.*

Finally, no LEED patterns were observed on any of the passivated GaAs surfaces detailed in this study. This contrasts with the room temperature (1x1) LEED pattern and conversion of this pattern to a (2x1) structure after annealing above 350°C observed for the sulphur treated GaAs(100) surfaces described in the previous chapter. Furthermore, LEED studies of $(NH_4)_2S_x$ passivated InP(100) surfaces indicated the formation of a (1x1) LEED pattern after room temperature treatment[12], as also observed by Tao *et al.*[13]. These observations strongly suggest that no ideal sulphur termination of the GaAs(100) surface results from using the $P_2S_5/(NH_4)_2S_x$ treatments as described.

6.2 Ambient Tunnelling Spectroscopy of Etched and Passivated GaAs(100) Surfaces.

As described in Chapter 5, STS is an important complementary technique to STM as it probes local electronic state density aiding STM image interpretation. In section 6.3, planar Metal-Insulator-Semiconductor (MIS) theory is applied to ambient STS spectra obtained on passivated GaAs(100) surfaces. Before presenting this analysis, however, it is necessary to detail, in some depth, previous UHV STS results obtained by Feenstra and Stroscio[14] on the cleaved GaAs(110) surface. This is due to the I(V) characteristics of the passivated GaAs(100) surface bearing a close similarity to the I(V) characteristics of the (unpinned) GaAs(110) surface cleaved in UHV.

6.2.1 Tunnelling Spectroscopy of the Oxygen-GaAs(110) System: The Model of Feenstra and Stroscio.

In Fig.6.6, STS I(V) data from the n-type GaAs(110) surface, obtained by Feenstra and Stroscio[14] in UHV, is displayed. Referring to the energy diagram in the inset three contributions to the measured tunnelling current may be noted. (Importantly, the data is displayed on a logarithmic scale; high dynamic range is essential in tunnelling current measurement). The three contributions are labelled V; tunnelling from valence band states, C; tunnelling into (empty) conduction band states and D; tunnelling from occupied dopant states in the conduction band. For the dopant concentration used in their study ($1x10^{18}\,cm^{-3}$), Feenstra and Stroscio[14] note that, at room temperature, almost all of the dopant impurities are ionized leading to the band of dopant states within the conduction band. These dopant states play an important role in the spectroscopy, as they remove the region of near-zero conductivity (the band gap) that would be expected in the I(V) spectrum for a semiconductor with a band gap of 1.4 eV.

Theoretical calculations of the I(V) spectra were found to agree with experiment only when tunnelling through the (tip-induced) space charge (depletion) region of the semiconductor was included. Band-bending in the semiconductor was evaluated by integrating Poisson's equation through the semiconductor to compute the electrostatic potential and, thus, the position of the energy bands. Transmission through the tip-

induced space charge region was then calculated. For a space charge region in depletion the potential is parabolic and the transmission coefficient is given by[14] :

$$\exp \{ -w (2\alpha m\phi)^{1/2} h^{-1} \} \qquad (6.1)$$

where α is the effective mass and ϕ the surface barrier height. The width of the depletion region is given by:

$$w = (2\varepsilon_s\phi (Ne)^{-1})^{1/2} \qquad (6.2)$$

where $\varepsilon_s = 12.9\varepsilon_o$ is the semiconductor dielectric constant and N is the doping concentration. For surface band bending of < 0.4 eV, Feenstra and Stroscio found that the transmission through the space charge region is sufficiently large (due to a sufficiently narrow depletion region width) for dopant state derived tunnelling current to be observed in the I(V) spectrum. This ability to tunnel through the space charge region indicates, that at sufficiently low voltages, all of the tunnelling current is due to bulk dopant states - i.e. a region spatially inside the GaAs crystal is probed[14].

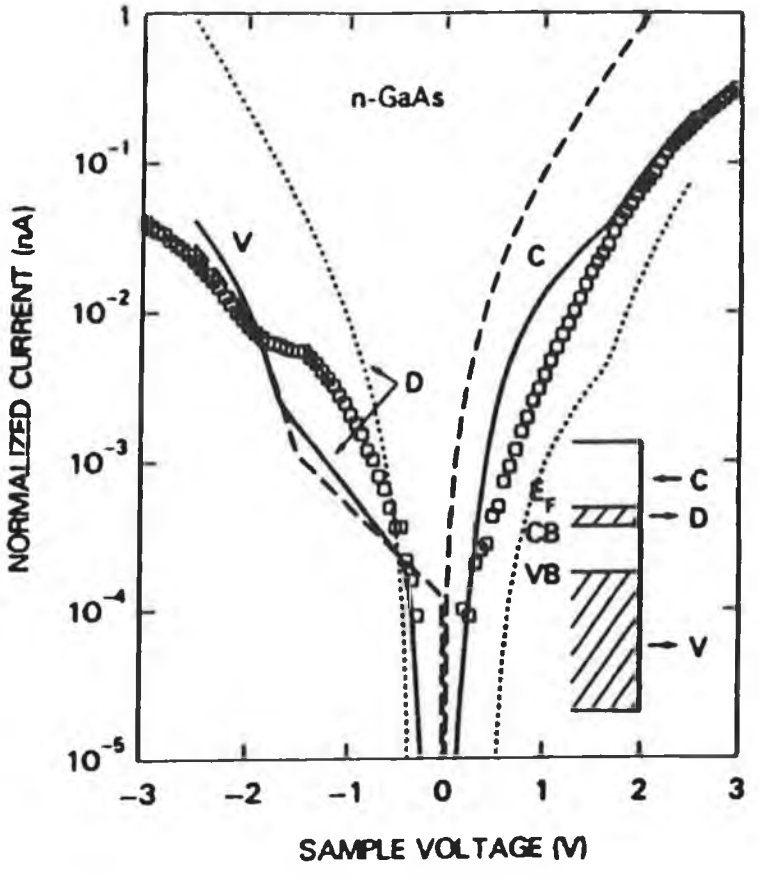

Fig 6.6 *Tunnelling Spectroscopy characteristic for the n-type GaAs(110) surface with schematic energy band diagrams.(From ref .14)*

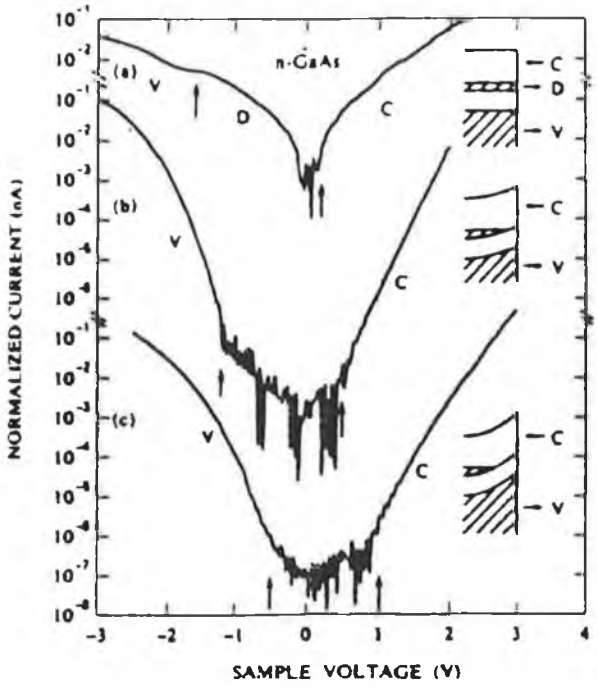

Fig 6.7 *Normalised tunnelling spectroscopy I(V) characteristics for (a) the clean n-GaAs(110) surface, (b) with $3x10^3$ L exposure to Oxygen, (c) with $5x10^4$ L exposure top oxygen (From ref. 15)*

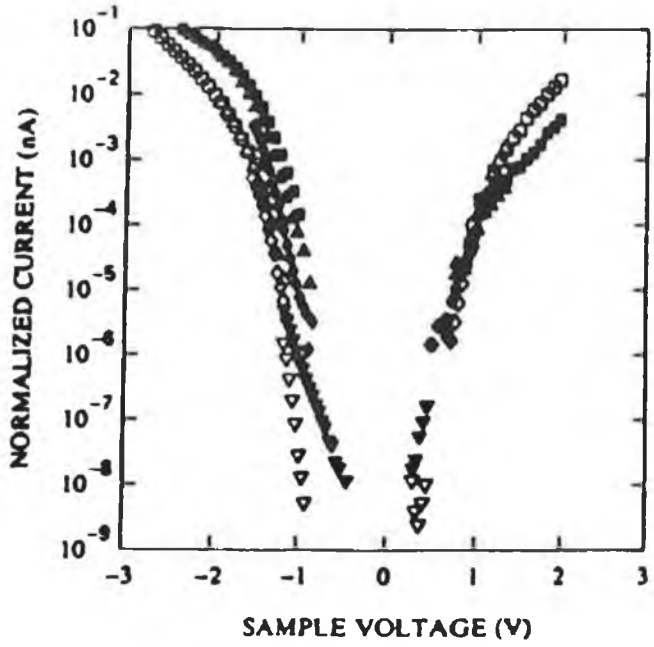

Fig 6.8 *I(V) characteristic taken on an oxygen adsorbate (solid symbols) and off the adsorbate (open symbols) on the n-GaAs(110) surface.(From ref .15)*

Fig 6.7 illustrates normalised I(V) curves for oxygen adsorbed on n-GaAs(110), again taken from the work of Stroscio and Feenstra[15]. Fig 6.7(a) is the clean spectrum reproduced. The surface Fermi level corresponds to 0V on the plot and, as expected for a heavily doped n-type semiconductor, lies close to the conduction band edge. When oxygen is adsorbed onto the surface the dopant state contribution to the tunnelling current disappears, forming a gap in the I(V) characteristic as shown in Fig.6.7(b) and 6.7(c).

Stroscio and Feenstra associated the formation of this gap with surface state induced band bending in the semiconductor which effectively attenuates or "pinches off" the dopant state component of the measured tunnelling current. At high oxygen exposures they found a larger shift in the surface Fermi level with it being pinned close to the valence band edge as observed in Fig 6.7(c). Not observed in Fig 6.7(c) is the increase in current between -1.0 and -0.5 eV that is present in spectra taken *on* an oxygen adsorbate, as opposed to near an oxygen adsorbate but on the GaAs surface (Fig. 6.7(c)). The acceptor state of the adsorbed oxygen was proposed to cause this increase in current within the band gap[15,16]. As observed in Fig.6.8, this current serves to reduce the measured band gap to $\approx$ 1.0 eV.

6.2.2 Reduction of Surface State Induced Band Bending on the Passivated GaAs(100) Surface.

The tunnelling spectroscopy characteristics reproduced in Fig.6.9 represent those of a $P_2S_5/(NH_4)_2S_x$ passivated and a chemically etched unpassivated GaAs(100) surface after 1 hour of exposure to air. These characteristics were obtained using Nanoscope II software (detailed in Chapter 3) with a stabilisation voltage of -700mV and a tunnelling current of 0.2 nA. From Fig 6.9 it is immediately apparent that there is a narrowing of the region of minimum conductivity (the band gap) when the passivated surface is compared to the unpassivated.

As also observed by Dagata and Tseng[17], this behaviour is consistent with the I(V) properties of the cleaved GaAs(110) surface oxidized in UHV, described in the previous section. For both the UHV and air environements surface oxidation leads to surface state induced band bending which significantly attenuates the contribution of dopant induced states in the semiconductor conduction band. The narrow band gap noted on the passivated surface is possibly due to either insufficient dynamic range in the tunnelling current measurement or residual surface defects causing a small degree of band bending. Evidence to strengthen the latter proposal came from comparable STS investigations on $P_2S_5/(NH_4)_2S_x$ passivated InP(100) surfaces which indicate that the narrow gap is reduced still further. This suggests a better passivation of InP(100) surfaces after $P_2S_5/(NH_4)_2S_x$ treatment with a more complete removal of residual oxides. For the etched surface a gap of $\approx$ 1.0 eV is present in the I(V) characteristic, in good agreement with the results of Dagata and Tseng[17]. Although this group did not investigate the Fermi

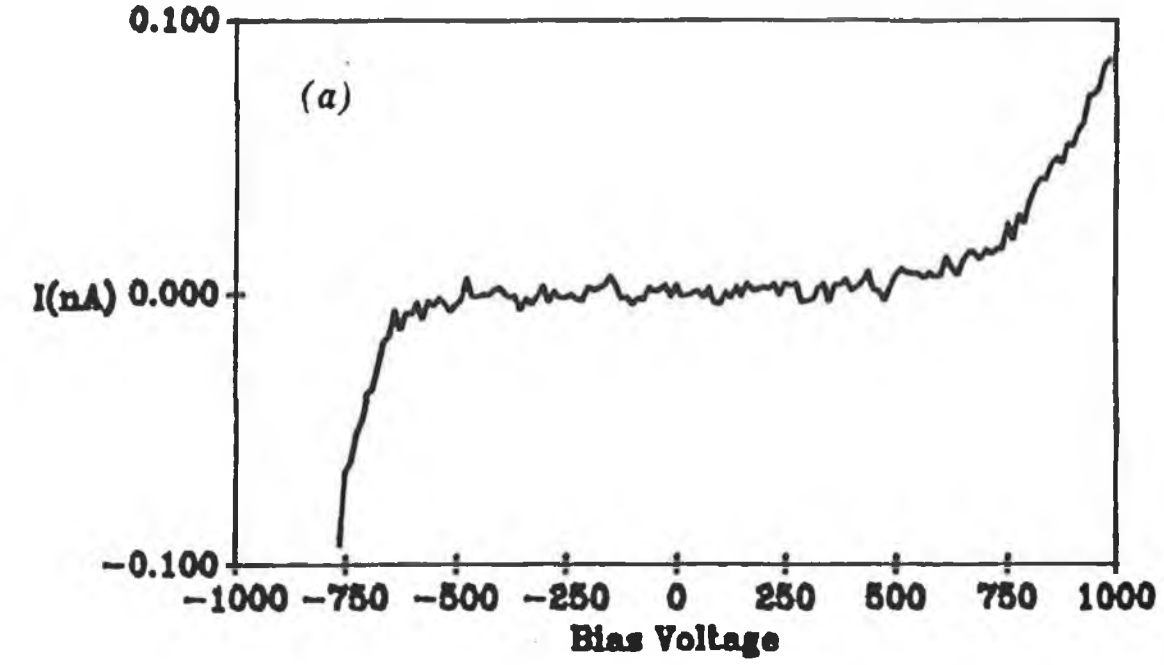

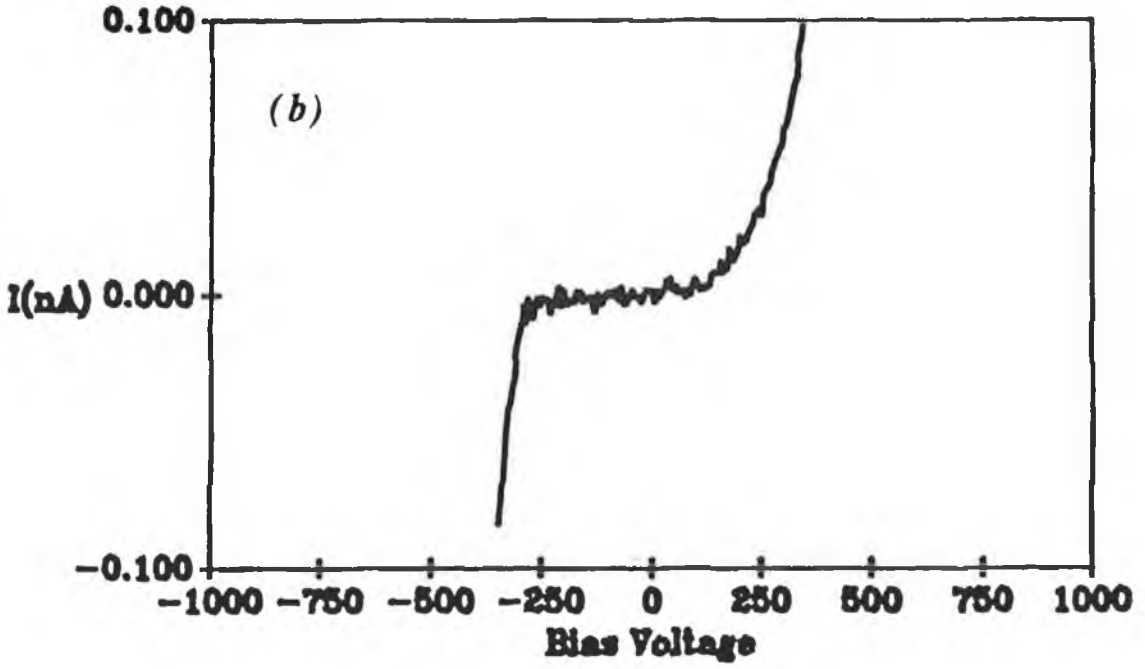

Fig 6.9 *Tunnelling spectroscopy characteristics of (a)the chemically etched,unpassivated and (b) the $P_2S_5/(NH_4)_2S_x$ passivated GaAs(100) surface.*

level position on their etched and passivated surfaces from tunnelling spectroscopy measurements, it is seen to be pinned mid-gap in the spectrum of Fig 6.9(a) for the similarly treated surfaces of this study. For the passivated surface E_F lies close to the conduction band edge as expected in the absence of a high density of surface states.

One further comparison should be made between the spectra of Fig. 6.9. Although the etched surface exhibits a far from symmetric curve (which only appears after exposure of the surface to air for longer periods of time (> 6 hours)), the conduction and valence band differential conductivities are slightly less than those of the passivated surface. This is a further indicator of chemical differences between the two surfaces and the formation of surface state density on the unpassivated surface.

6.3 Application of Planar Metal-Insulator-Semiconductor Theory to Ambient Scanning Tunnelling Spectroscopy

Metal-Insulator-Semiconductor (MIS) tunnel structures[18] are expected to show rectifying behaviour where the direction of rectification is dependent on the doping type. The forward characteristic of the tunnelling spectroscopy curve can be compared with MIS theory (assuming a thin tunnel transparent insulator). Although this theory strictly applies to the planar contact geometry, experiments by Kaiser *et al.*[19] on hydrogen passivated Si surfaces have shown that it accurately describes the current-voltage characteristics obtained using STM. Figure 6.10 shows the energy band diagram for a planar metal-vacuum-(n-type) semiconductor tunnel structure at zero bias. The difference between the tip work function and the semiconductor electron affinity results in the formation of a potential barrier. Conduction between the tip and the semiconductor involves thermionic emission of electrons over the barrier followed by tunnelling through the vacuum. The STM tip controls the barrier height through the field between tip and sample. By measuring MIS I(V) characteristics at different sample-tip separations a better understanding of current transport through passivated GaAs(100) interfaces may be obtained. The mechanism of acquisition of the I(V) characteristics at various tip-sample separations has been described in Chapter 3.

According to MIS theory, the forward branch of the I(V) characteristic is:

$$I=I_o \{ \exp [(q (V_o - V_B) / kT] - 1 \} \qquad (6.3)$$

where V_B is the total band bending in the semiconductor and V_o is the band bending in the absence of an external bias. The barrier height is described by:

$$V_B = V_o \{ ([(c+1)^2 - V/V_o]^{1/2}) - c \}^2 \qquad (6.4)$$

where:

$$c = (\varepsilon_s S)/ \varepsilon_i W_o \qquad (6.5)$$

Here ε_s and ε_i are the permittivities of the semiconductor and insulator respectively; S is the insulator thickness and W_o is the width of the depletion region at zero bias. Furthermore, Weimer *et al.* [20] note, that assuming no significant surface state density:

$$V_B(S,V) = V_o \left([1+(S/S_o)+V/V_o]^{1/2} - S/S_o \right)^2 \qquad (6.6)$$

An analysis of passivated GaAs(100) surface electronic properties was made by measuring a number of I(V) spectra at various tip-sample separations. These I(V) spectra are reproduced in Fig. 6.11 along with the calculated I(V) curves on a semi-log scale. For the calculated plots, the value of c governs the slope of the curve and V_o represents the deviation from linearity. The agreement between simple MIS theory and experiment is evidently very good. A barrier height (V_o) of 0.3 eV was required to obtain a good fit. However, it should be emphasised that, as for the tunnelling spectroscopy measurements of Bell *et al.*[21] on H-passivated Si(111) surfaces, the agreement between MIS theory and the experimental results is not very sensitive to variations in V_o between 0.2 and 0.4 eV. Nevertheless, the 0.3 eV value is significantly smaller than both the barrier height of unpassivated,pinned GaAs(100) surfaces and also the 1.1 eV value obtained by Berkovits *et al.*[22] for similar I(V) measurements on Na_2S passivated GaAs(100) surfaces. The low value of the barrier height is, however, consistent with a Fermi level position near the conduction band edge as observed in the spectra. Weimer *et al.*[20] note that there are two contributions to the tunnelling current at an unpinned semiconductor surface; *" widening the tip-sample gap exponentially suppresses tunnelling through the vacuum barrier while at the same time it exponentially enhances the number of free carriers capable of reaching the semiconductor surface"*. This dependence is evident in the I(V) spectra of Fig.6.11 where at smaller tip-sample separation values, an increased sensitivity of current to forward bias is noted. The variation is sensitivity is indicative of the fact that the Fermi level is not pinned and that band bending is increasing as a function of decreasing S. Our lack of sensitivity to the magnitude of the (tip-induced) band bending is most likely due to tunnelling through the space charge (barrier) region. Both the simple MIS model detailed above and the analysis of Weimer *et al.*[20], however, neglect any contribution to the tunnelling current from tunnelling through the space charge region, which, as discussed in the previous section, plays a major role in the I(V) spectra.

The theoretical spectra were fit to the experimental data by adjusting the values of I_o, a voltage independent constant and S. The value of S determines the shape of the spectrum and was 7.1, 8.2, 9.1 and 12.2 Å respectively for curves (a)-(d) in Fig 6.10.

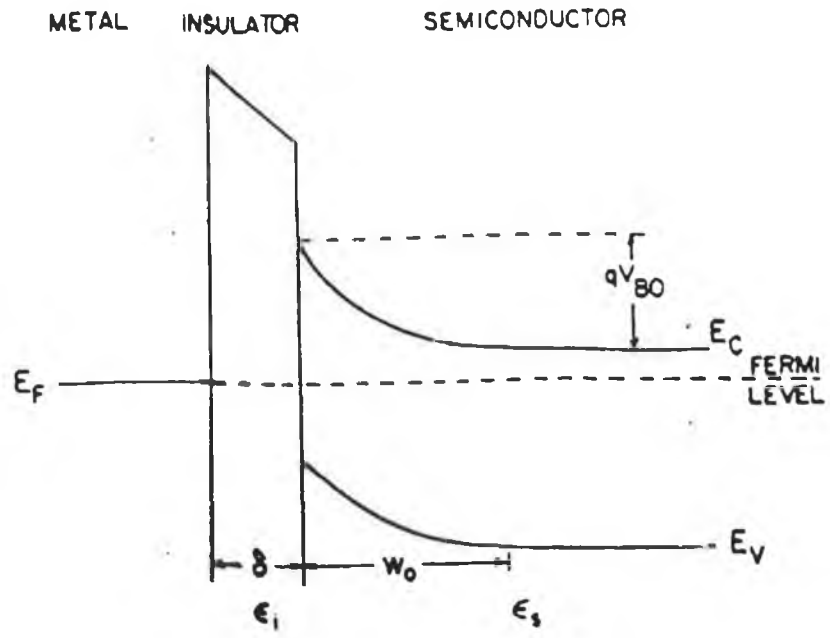

Fig 6.10 *Energy band diagram for a planar metal-vacuum-(n-type) semiconductor tunnel structure at zero bias. (From ref. 19)*

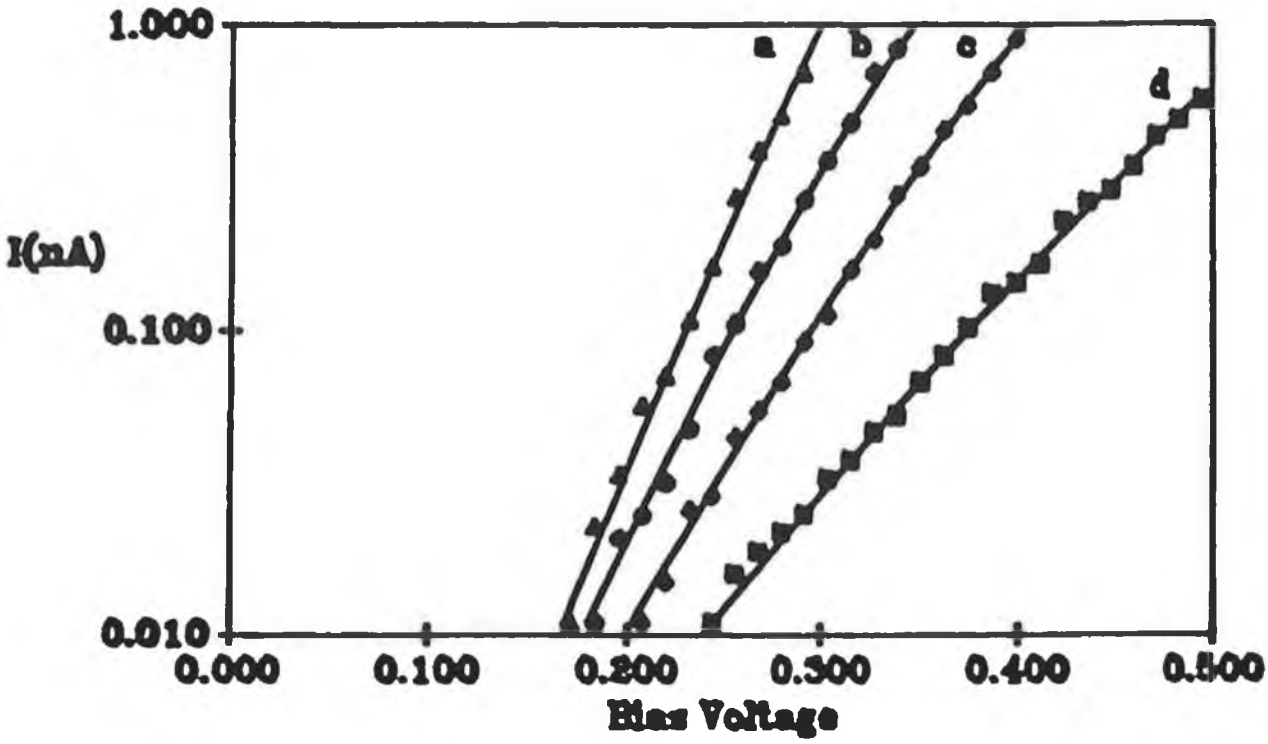

Fig 6.11 *Tunnelling spectroscopy I(V) spectra taken at various tip-sample separations on the passivated GaAs(100) surface. (a =7.1 Å, b=8.2 Å, c=9.1Å, and d=12.2 Å)*

These values are in good agreement with those of Kaiser*et al.*[19] on the (unpinned) H-passivated Si(111) surface. This group have also determined that the field at the sample due to a spherical tip is reduced in comparison to that for a planar electrode by only 3% for a 100Å tip. That the depletion region under the tip can be controlled by the tip-sample separation is a strong indication that a large decrease in the degree of Fermi level pinning on the GaAs surface occurs as a result of the passivation treatment.

6.4 Summary

The ambient oxidation of GaAs(100) surfaces treated with P_2S_5 / $(NH_4)_2S_x$ and P_2S_5 / $(NH_4)_2S$ solutions has been investigated by STM and tunnelling spectroscopy. Both treatments have shown to be capable of producing chemically uniform, physically flat surfaces which are resistant to ambient oxidation, with the P_2S_5 / $(NH_4)_2S_x$ treated surfaces displaying quantitatively enhanced passivation properties. The presence of phosphorous on the sulphur passivated surfaces appears to play a significant role in determining the initial surface roughness and the resistance of the surface to ambient oxidation. Continual scanning of a region of the passivated surface by STM, an increase in the bias voltage and tunnelling current above their normal scan values, and application of bias pulses, all result in a substantial increase in the local rate of oxide growth.

Tunnelling spectroscopy measurements have shown that the passivation reduces the surface state density to the extent that little band bending in the spectra is noted. Comparison of the I(V) plots with planar MIS theory indicates that the electronic surface quality of the passivated GaAs(100) surfaces investigated in this work approaches that of the (unpinned) H-passivated Si(111) surface. Tip-sample separation plays an important role in the tunnelling spectroscopy data, determining the sensitivity of the measured tunnelling current to the bias voltage. The sensitivity variation strongly suggests that the Fermi level is unpinned and that band bending is increasing as a function of decreasing tip-sample separation. Furthermore, to obtain a good fit of the experimental data to MIS theory, a barrier height of 0.3 eV was required. This value is in good agreement with that expected for a tungsten tip and an unpinned GaAs surface.

References

1. J. Massies and J. P. Contour, *Appl. Phys. Lett.* **46** 1150 (1989)
2. J. A. Dagata, W. Tseng, J.Bennett, J. Schneir, and H. H. Harary, *Appl. Phys. Lett.* **59** 3288 (1991)
3. See, for example, C. J. Sandroff, M. S. Hedge and C. C. Cjang, *Journ. Vac. Sci. Technol. B* **7** 841 (1989), and also Chapter 2 and references therein.
4. R. Richter and H. L. Hartnagel, *J. Electrochem. Soc.* **137** 2789 (1990)
5. Y. Wang, Y. Darici and P. H. Holloway, *J. Appl. Phys.* **71** 2746 (1992)
6. X. S. Wang, K. W. Self, R. Maboudian, C. Huang, V. Bressler-Hill and W. H. Weinburg, *Journ. Vac. Sci. Technol. A* **11** 1089 (1993)
7. H. H. Lee, R. J. Raciot, and S. H. Lee, *Appl. Phys. Lett.* **54** 724 (1989)
8. H. Hirayama, Y. Matsumoto, H. Oigawa, and Y. Nannichi, *Appl. Phys. Lett.* **54** 2565 (1989)
9. Y. Nannichi, J. Fan, H. Oigawa, and A. Koma, *Jpn. Journ. Appl. Phys.* **27** L2367 (1988)
10. I. Tanaka, T. Kato, S. Ohkuochi, and F. Osaka, *Journ. Vac. Sci. Technol. A* **8** 567 (1990)
11. F. Lukes, *Surf. Sci.* **30** 91 (1972)
12. B. Murphy, Dept. Of Physics, Dublin City University, private communication
13. Y. Tao, A. Yelon, E. Sacher, Z. H. Lu, and M. J. Graham, *Appl. Phys. Lett.* **60** 2269 (1992)
14. R. M. Feenstra and J. A. Stroscio, *Journ. Vac. Sci. Technol.B* **5** 923 (1987)
15. J. A. Stroscio and R. M. Feenstra, *J. Vac. Sci. Technol.B* **6** 1472 (1988)
16. C. Y. Su, I. Lindau, P. W. Chye, P. R. Skeath, and W. E. Spicer, *Phys. Rev. B* **25** 4045 (1982)
17. J. A. Dagata and W. Tseng, *Appl. Phys. Lett.* **62** 591 (1993)
18. S. M. Sze, *Physics of Semiconductor Devices*, 2nd Ed., (Wiley Pr. NY 1981)
19. W. J. Kaiser, L. D. Bell, M. H. Hecht, and F. J. Grunthaner, *Journ. Vac. Sci. Technol. A* **6** 519 (1988)
20. M. Weimer, J. Kramar, and J. D. Baldeschwieler, *Phys. Rev. B* **39** 5572 (1989)
21. L. D. Bell, W. J. Kaiser, M. H. Hecht, and F. J. Grunthaner, *Appl. Phys. Lett.* **52** 278 (1988)
22. V. L. Berkovits, L. F. Ivantson, I. V. Mararenko, T. V. L'Vora, R. V. Khasieva, and V. I. Safarov, *Sov. Phys. Semicond.* **25** 231 (1991)

CHAPTER VII: CONCLUSIONS AND SUGGESTIONS FOR FUTURE RESEARCH

A brief summary of the results presented in the previous chapters is given, with some suggestions for possible directions of future research.

Considerable effort, over the last number of years, has been applied to understanding the reaction of group VI elements with III-V semiconductor surfaces due to their action as surface passivants, as detailed in Chapters 2, 5 and 6. To the best of our knowledge, the results presented in Chapter 4 represent the first in-depth STM study of the reaction of sulfur with an elemental semiconductor.

No evidence for surface restoration due to an adsorbed S overlayer was found for either the Si(100)-(2x1) or Si(111)-(7x7) surface. It is, however, interesting to note that Weser *et al.* [1] have observed a (1x1) S termination of the Ge(100) surface using an electrochemical cell as the source of the sulfur flux. STM would be an ideal tool to study this system, with the ability to determine if the (1x1) phase is indeed due to an ordered monolayer, or simply a saturation of Ge dangling bonds by an amorphous S overlayer. The fact that little observable change occurs in either the Si(100)-(2x1) or Si(111)-(7x7) LEED pattern after sulfur deposition may be taken as an indication that a strong interaction between S and the Si surface, at room temperature, does not occur. Creation of surface vacancies occurs following the thermal desorption of sulfur, for both Si surfaces investigated. The monolayer etching mechanism that occurs on Si(111)-(7x7) surfaces after removal of the sulfur overlayer does not occur on the Si(100)-(2x1) surface and we accredit this to differences in the activation energy for diffusion of the respective surfaces. Minimum energy calculations might prove interesting if applied to the structural model for the c(4x4) reconstruction we have proposed - unfortunately, these calculations were not undertaken. A recent study[2] of the Si(100) surface has indicated that the interstitial dimer will induce states in the upper part of the surface band gap that would not be present for the missing dimer defect. Atomically resolved tunnelling spectroscopy measurements on the c(4x4) surface could then also help in determining if the c(4x4) structure does consist of both missing dimer and interstitial dimers, as seems most likely from our filled- and empty-state STM images.

The logical continuation of the S/Si research presented in Chapter 4 would be to investigate the reaction of other group VI elements (Se, Te) with the Si(100) and Si(111) surfaces. Kaxiras [3] has suggested that Si surface restoration with Se is more likely than with S. For an ideal, bulk-terminated (1x1) surface, as observed for the As/Si(111) system, *submonolayer* coverages of Se would enable the exact registry of the adsorbate with respect to the surface layer to be determined.

We have found that the model very recently proposed by Skala *et al.* [4] for the c(8x2) surface is most consistent with our STM images of the (4x1) surface. As described in

Chapter 5, a number of unresolved questions regarding both the precise structure and stoichiometry of the various GaAs(100) surface reconstructions, and the problem of Fermi level pinning. Our STM data on the interaction of S with both GaAs(100) and GaAs(111)B surfaces indicates that the (1x1) LEED pattern observed after RT adsorption on both surfaces is not due to an ordered sulfur monolayer. LEED I(V) measurements and dynamical calculations could provide further confirmation of this disorder. Auger and core-level photoelectron spectroscopy data indicate that the (2x1) reconstruction observed on the S treated and annealed GaAs(100) surface is due to both As and S dimers, in good agreement with the reflectance anisotropy measurements of Berkovits and Paget[5]. This proposal, while being consistent with both our experimental data and the electron counting rule, does not explain the larger Fermi level shift (0.5 eV) toward the conduction band minimum (CBM) observed for the sulfur treated (4x1) surface as compared to the c(2x8) surface (0.2 eV). We have suggested that the excess As coverage of the decapped surface may play an important role in the final Fermi level position of the subsequently S treated surface. The ability to obtain an almost flat band condition for the S-treated (4x1) surface is particularly important with regard to the technological applications of the GaAs(100) surface.

Sub-monolayer coverages of sulfur on both GaAs surfaces studied, with subsequent STM studies would considerably aid understanding of the S bonding sites, as registry with the clean surface reconstruction could be obtained. Repeated attempts to acquire atomically resolved tunnelling spectra on the S treated (100) and (111)B surfaces frustratingly failed to provide reproducible results. Such measurements, coupled with sub-monolayer S coverages, would enable differences in Fermi level position across the GaAs surface to be detected. Indeed, Pashley[6] has very recently performed similar measurements on the Se/GaAs(100)-(2x1) surface. Adsorption of metals on the sulfur passivated surfaces and subsequent determination of the Schottky barrier heights would, of course, be an informative experiment with regard to Fermi level unpinning.

For the clean GaAs(111)B-(2x2) surface, tunnelling has been found to occur predominantly into empty states of the sample, which seems strange considering that all As dangling bonds at the surface are filled and that Ga is four-fold coordinated. (A very recent STM study of the decapped GaAs(111)B surface has also found much higher resolution imaging at positive sample bias as opposed to negative sample bias[7]). The proposal that the current at positive sample bias is due to tunnelling into empty anti-bonding states of the sample is, of course, very tentative and would require a full band structure calculation or inverse photoemission results, not currently available, for confirmation. As the Fermi level for the clean surface is found close to the CBM it is nevertheless expected that tunnelling might occur through conduction band states. Very few studies, to date, have been attempted on either the GaAs(111)B or GaAs(111)A surfaces. STM and tunnelling spectroscopy investigations of sub-monolayer metal (Sb, Al) adsorption on these surfaces are planned.

Sulphur diffusion into the bulk GaAs crystal for (100) and (111)B samples has been observed through S 2p core-level spectra. X-Ray Photoelectron Diffraction (XPD) measurements could determine the extent to which this diffusion occurs.

A high resolution SR SXPS core-level study of the $P_2S_5/(NH_4)_2S_x$ passivated GaAs(100) surface detailed in Chapter 6 has not been attempted to date. That type of study might provide confirmation of the high reduction in surface state density that seems likely from our tunnelling spectroscopy measurements. It might also provide further information on the nature of the surface chemical bonds providing the passivation. UHV STM data on the *in situ* reaction of oxygen with these surfaces would prove interesting to compare with our ambient STM results.

References

1. T. Weser, A. Bogen, B. Konrad, R. D. Schnell, C. A. Schug, and W. Steinmann, *Phys. Rev. B* **35** 8184 (1987)
2. J. Wang, T. A. Arias, and J. D. Joannopoulus, *Phys. Rev B* **47** 10497 (1993)
3. E. Kaxiras, *Phys. Rev. B* **43** 6824 (1991)
4. S. L. Skala, J. S. Hubacek, J. R. Tucker, J. W. Lyding, S. T. Chou, and K. -Y. Cheng, *Phys. Rev. B* **48** 9138 (1993)
5. V. L. Berkovits and D. Paget, *Appl. Phys. Lett.* **61** 1835 (1992)
6. M. D. Pashley, *Abstracts of the 40th Symposium of the American Vacuum Society*, Orlando, FL, November 1993
7. J.Thornton, Interdisciplinary Research Centre in Surface Science, Liverpool, private communication.

APPENDIX

Refereed Publications:

Sulphur Induced c(4x4) Reconstruction of the Si(100) Surface Studied by Scanning Tunnelling Microscopy, P. Moriarty, L. Koenders, and G. Hughes, *Phys. Rev. B* **47** 15950 (1993)

Vacancy Creation on the Si(111)-(7x7) Surface due to Sulphur Desorption Studied by STM, L. Koenders, P. Moriarty, G. Hughes and O. Jusko, Accepted for publication, *Surf. Sci. Lett.*

Scanning Tunnelling Micrscopy Investigation of the Ambient Oxidation of Passivated GaAs(100) Surfaces, P. Moriarty, B. Murphy, and G. Hughes, *Journ. Vac. Sci. Technol. A* **11** 1099 (1993)

An Investigation of the Early Stages of Native Oxide Growth on Chemically Etched and Sulphur Treated GaAs(100) and InP(100) Surfaces by STM, P. Moriarty and G. Hughes, *Ultramicroscopy* **42-44** 956 (1992)

Other Publications not Directly Related to Thesis:

Atomic Resolved Material Displacement on Graphite Surfaces by STM, P. Moriarty and G. Hughes, *Appl. Phys. Lett.* **60** 2338 (1992)

Wave Function Imaging of the PbS(100) Surface by Scanning Tunneling Microscopy, A. R. H. F. Ettema, C. Haas, P. Moriarty and G. Hughes, *Surf. Sci.* **287/288** 1106 (1993)